ACCSCIENCE PUBLISHING

Brain & Heart

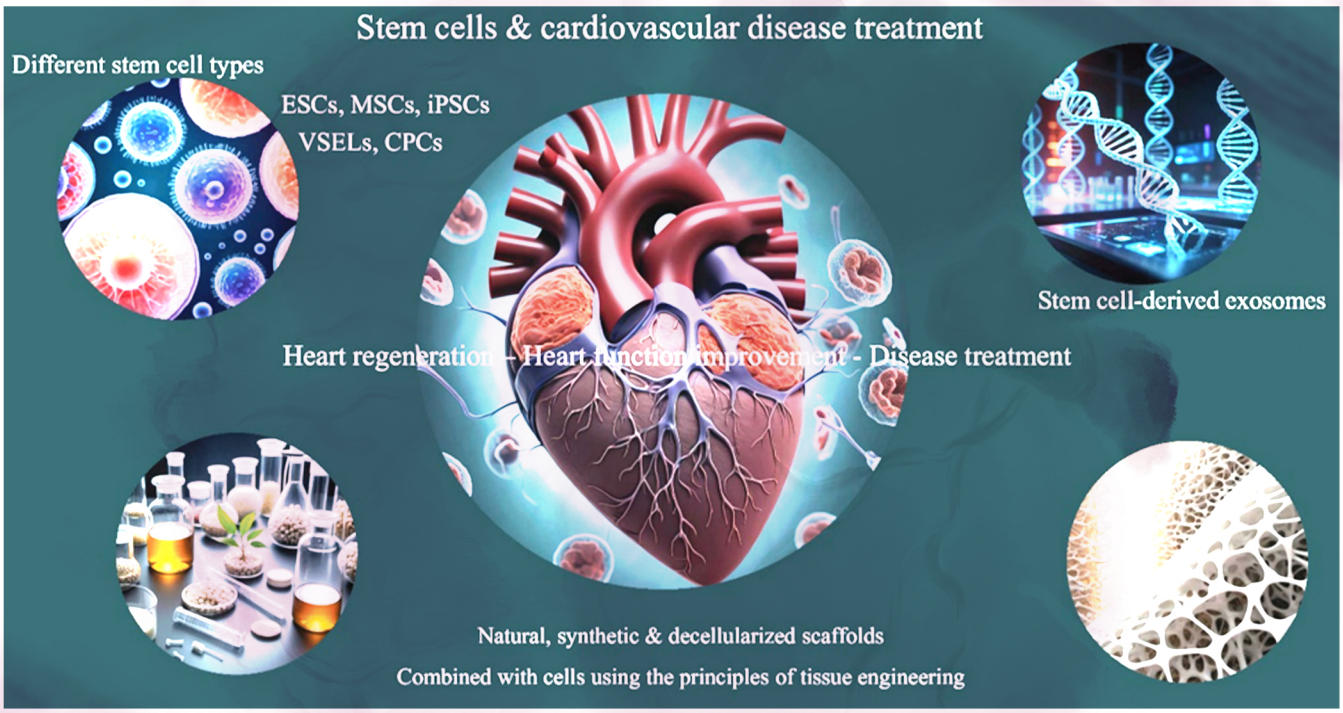

The future of cardiac care: How stem cells are revolutionizing cardiovascular disease treatment

ACCSCIENCE PUBLISHING
Volume 2 · Issue 4
November 2024
ISSN: 2972-4139 (Online)

Online ISSN: 2972-4139

Brain & Heart

Brain & Heart focuses on neurocardiology, a neurology and cardiology-based interdisciplinary subject that studies the circulatory mechanism of the human body, as well as the mechanisms of the interplay between the cardiovascular system and the nervous system.

The article types accepted by *Brain & Heart* include the following: original research article, review article, perspective article, case report, letter, editorial, and special feature article.

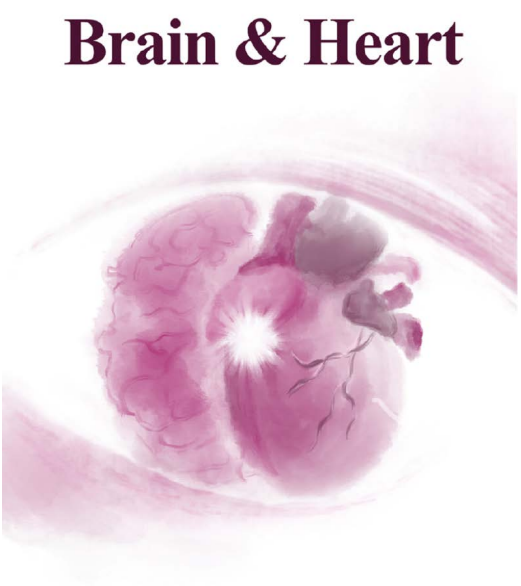

About the Publisher

AccScience Publishing is a publishing company based in Singapore. We publish a range of high-quality, open-access, peer-reviewed journals and books from a broad spectrum of disciplines.

Contact Us

Managing Editor
bh.office@accscience.sg

AccScience Publishing
8 Burn Road, #15-03 Trivex, Singapore 369977.

Volume 2 • Issue 4 • November 2024
ISSN 2972-4139 (online)

BRAIN & HEART

ACCSCIENCE PUBLISHING

Access Science Without Barriers

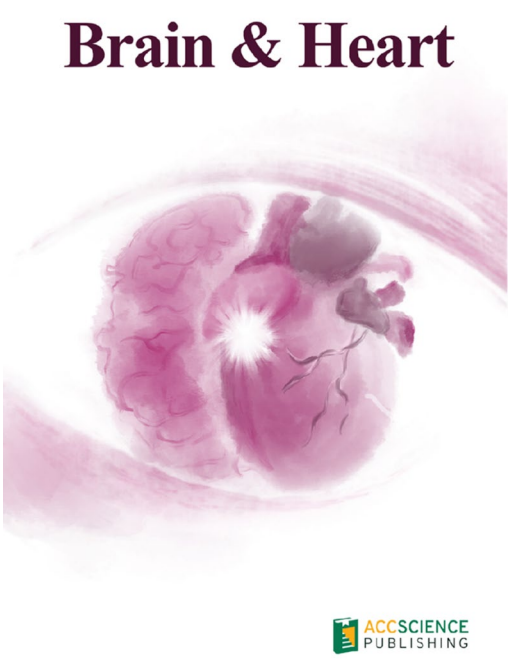

BRAIN & HEART

ISSN: 2972-4139 (online)

Editorial and Production Credits

Publisher: AccScience Publishing
Managing Editor: Naomi Li
Production Editor: Sharmila Velapasamy
Article Layout and Typeset: Sinjore Technologies (India)

For all advertising queries, contact bh.office@accscience.sg.

Supplementary file

Supplementary files of articles can be obtained at https://accscience.com/journal/BH/2/4.

Brain & Heart

Editorial Board

ACCSCIENCE PUBLISHING

Volume 2 | Issue 4 | November 2024 |

Brain & Heart

https://accscience.com/journal/BH

CONTENTS

ACCSCIENCE PUBLISHING

Brain & Heart

REVIEW ARTICLE

Characteristics and prognosis of patients with cardiac sarcoidosis presenting with atrioventricular block and ventricular arrhythmias

Caleb Carver[1]* and Raheel Ahmed[2]

[1]Department of Medicine, Gold Coast University Hospital, Southport, Queensland, Australia

[2]Department of Cardiology, Royal Brompton and Harefield Hospitals, London, United Kingdom

Abstract

Cardiac sarcoidosis (CS) may initially present with life-threatening arrhythmias such as atrioventricular block (AVB) and ventricular arrhythmia (VA), including ventricular tachycardia and ventricular fibrillation. Diagnosing CS is challenging due to subtle or absent findings in routine tests and the low sensitivity of the definitive diagnostic tool, endomyocardial biopsy. CS can also mimic other cardiac conditions such as dilated cardiomyopathy or arrhythmogenic right ventricular cardiomyopathy, and it may occur without any systemic involvement. Consequently, delays in presentation, accurate diagnosis, and initiation of appropriate treatment are frequent. Greater awareness of the condition could improve outcomes for patients with CS. Non-invasive advanced imaging techniques, such as 18F-fluorodeoxyglucose positron emission tomography and cardiac magnetic resonance imaging are essential for diagnosis, although they may not be accessible in all clinical settings. Management of arrhythmias in CS involves conventional therapies in the utilization of antiarrhythmics and non-pharmacological therapy (e.g., implantable devices), but with notable divergences in the use of immunosuppression and a preference for implantable cardioverter defibrillators over permanent pacemakers. This narrative review aimed to outline the clinical features of patients with CS presenting with AVB or VA and examine diagnostic investigations, imaging techniques, treatment approaches, and prognosis based on current research and international guidelines.

Keywords: Cardiac sarcoidosis; Sarcoidosis; Atrioventricular block; Ventricular tachycardia; Ventricular fibrillation; Sudden cardiac death

***Corresponding author:**
Caleb Carver
(calebcarver@yahoo.co.uk)

Citation: Carver C, Ahmed R. Characteristics and prognosis of patients with cardiac sarcoidosis presenting with atrioventricular block and ventricular arrhythmias. *Brain & Heart.* 2024;2(4):3515. doi: 10.36922/bh.3515

Received: April 27, 2024

Accepted: August 19, 2024

Published Online: October 8, 2024

1. Introduction

Sarcoidosis is a multisystem disease characterized by granuloma formation, inflammation, and subsequent scarring. Cardiac involvement is clinically evident in approximately 5% of cases, although imaging and postmortem studies have revealed that this may be an underestimation.[1,2] Cardiac sarcoidosis (CS) has a worse prognosis than other organ involvement, contributing to death in up to 85% of Japanese patients with sarcoidosis.[2] The manifestations of CS vary and include atrioventricular block (AVB), ventricular arrhythmias (VAs), left ventricular systolic dysfunction, and even sudden cardiac death,

with AVB and VA elevating the risk of sudden cardiac death. Most deaths from CS result from arrhythmias. CS is a heterogeneous disease, displaying varying severity and presentation across ethnicities. Prognosis is particularly poorer in Japanese patients than in those from Europe or the United States (US), with studies on Japanese patients often showing worse outcomes.[3] This ethnic variation is also observed in African American and White patients. A large-scale US study revealed a higher incidence of VAs and AVB in White patients than in African American patients but showed worse overall outcomes, including cardiogenic shock and mortality, in African Americans than in Whites.[4]

2. Review

2.1. Presentations of CS

CS can present in various forms, making diagnosis difficult. Autopsy data have revealed a high mortality rate associated with CS, with many cases remaining undiagnosed during the patient's lifetime.[5] In fact, sudden cardiac death (occurring within 24 h of symptom onset which often results in death at the scene or post-resuscitation without neurological recovery) may be the sole presentation in up to 14% of cases,[6] as observed in a large-scale Finnish study. However, most patients with asymptomatic CS, diagnosed through cardiac magnetic resonance (CMR) imaging, have been reported to follow a benign clinical course.[7]

CS may present as VAs, heart failure, or AVB, with heart failure increasing the risk of arrhythmia and hospitalizations.[8] The disease burden is high, with sarcoidosis posing a greater risk of heart failure development than known factors such as hypertension and coronary artery disease.[9] CS is also an important differential diagnosis for patients presenting with otherwise idiopathic ventricular tachycardia (VT). A case series showed that 12% of patients who underwent ablation for idiopathic VT were later diagnosed with arrhythmogenic CS, often in a delayed manner.[10] These patients were relatively young (average age: 51 years). Although two-thirds of the patients had extracardiac sarcoidosis at diagnosis, it was asymptomatic in all but two cases, as determined through 18F-fluorodeoxyglucose positron emission tomography (18F-FDG PET). The remaining one-third of the patients had isolated cardiac involvement. Similarly, a prospective study showed that 34% of patients with AVB of unknown origin were later diagnosed with CS.[11] Compared with patients with idiopathic AVB, those with CS-related AVB and aged <60 years had more adverse cardiac events (0/21 vs. 3/11, $p = 0.011$).[11] Likewise, Kandolin *et al.* found that over 25% of unexplained AVB cases in young and middle-aged adults were due to CS or giant cell myocarditis (GCM), both of which were associated with a high risk of adverse cardiac events.[12]

Diagnostic criteria for CS vary among expert societies. Key criteria and differences are detailed in Table 1, based on guidance from the Japanese Circulation Society (JCS, 2016),[13] the World Association for Sarcoidosis and Other Granulomatous Disorders (WASOG, 2014),[14] and the Heart Rhythm Society (HRS, 2014),[15] Notably, the JCS criteria are unique in not requiring positive histology for a definitive diagnosis. Common points among the criteria include advanced AVB and unexplained sustained VT, and the inclusion of extracardiac disease emphasizes the need for a multi-specialty evaluation when CS is suspected. However, the differences in diagnostic criteria lead to varied CS cohorts across different countries and centers, complicating the comparison of results, treatments, and outcomes due to a lack of standardization.

2.2. Pathophysiology of AVB and VA in CS

Although the exact cause of sarcoidosis remains unknown, the disease is characterized by the formation of granulomas in various tissues. Granulomas are clusters of cells surrounded by lymphocytes and plasma cells, including macrophages and often multinucleated giant cells, along with infiltrating T and B cells.[16,17] Granulomas are not unique to sarcoidosis; they can also occur in conditions such as giant cell arteritis, Crohn's disease, and granulomatosis with polyangiitis. They typically form in response to foreign bodies or specific infections such as tuberculosis.[17]

In CS, the myocardium is the most clinically significant site for granuloma formation, leading to inflammation and the development of non-conductive scar tissue. This results in the formation of re-entry circuits around the scarred areas.[18] However, it remains controversial whether active inflammation or subsequent scarring and fibrosis primarily induces the development of VAs.[17] Granulomas are formed in various locations, resulting in a wide range of VAs with different morphologies.[19] Conversely, AVBs typically occur when there is substantial involvement of the septum, impacting the His-Purkinje system.[20]

2.3. Distinguishing features of CS from other conditions presenting with AVB and VAs

Although echocardiography has a low sensitivity for diagnosing CS, thinning of the basal interventricular septum and/or regional wall motion abnormalities in a non-coronary distribution in patients with known extracardiac sarcoidosis is suggestive of cardiac involvement. Echocardiography can also provide cardiac function data that help determine the need for device implantation.

Table 1. Diagnostic criteria for CS as outlined by JCS, HRS, and WASOG[13-15]

JCS 2016	CS with systemic involvement Diagnosis confirmed histologically through endomyocardial biopsy OR *Major criteria** High-degree AVB or fatal VA LV contractile dysfunction ^{67}Ga citrate scintigraphy or 18F-FDG PET revealing abnormally high tracer accumulation in the heart LGE of the myocardium on CMR Basal thinning of ventricular septum or abnormal ventricular wall anatomy *Minor criteria* Abnormal ECG findings: VA, bundle branch block, axis deviation, abnormal Q waves Perfusion defect on perfusion scintigraphy Monocyte infiltration and moderate-to-severe myocardial interstitial fibrosis AND Granulomas found in other organs in addition to the heart OR Clinical findings suggestive of sarcoidosis in either the respiratory tract or eyes AND The presence of two of the following criteria • Bilateral hilar lymphadenopathy • Raised serum angiotensin-converting enzyme activity or lysozyme levels • High soluble interleukin-2 receptor levels • Significant tracer accumulation on ^{67}Ga citrate scintigraphy or 18F-FDG PET • High percentage of lymphocytes with a CD4/CD8 ratio of >3.5 in bronchoalveolar lavage fluid * *Where endomyocardial biopsy is negative, either two major or one major criterion and two or more minor criteria are required to make a diagnosis of CS*	Isolated CS Diagnosis confirmed histologically through endomyocardial biopsy OR ^{67}Ga citrate scintigraphy or 18F-FDG PET revealing abnormally high tracer accumulation in the heart AND three of the following High-degree AVB or fatal VA LV contractile dysfunction LGE of the myocardium on CMR Basal thinning of the ventricular septum or abnormal ventricular wall anatomy AND all of the following No clinical findings of sarcoidosis in organs other than the heart Chest CT showing no hilar lymphadenopathy or shadows along the lymphatic tracts ^{67}Ga scintigraphy or 18F-FDG PET revealing no abnormal tracer accumulation in organs other than the heart
HRS 2014	Diagnosis confirmed based on histological finding of non-caseating granulomas on endomyocardial biopsy Diagnosis of CS is probable if extracardiac sarcoidosis is confirmed and one or more of the following criteria are satisfied: Immunosuppressant-responsive cardiomyopathy or AVB Unexplained LVEF <40% Unexplained sustained VT or high-degree AVB Patchy FDG uptake on cardiac PET in a pattern consistent with that of CS LGE on CMR Positive gallium uptake in a pattern consistent with that of CS	
WASOG 2014	Granulomatous inflammation demonstrated in one other organ and one of the following criteria is satisfied: Treatment-responsive cardiomyopathy or AVB Reduced LVEF in the absence of other risk factors Spontaneous or inducible VT with no other risk factors Mobitz II or complete heart block Positive gallium uptake in a pattern consistent with that of CS LGE or T2 prolongation on CMR Defect on perfusion scintigraphy	

Abbreviations: 18F-FDG PET: 18-Fluorodeoxyglucose positron emission tomography; AVB: Atrioventricular block; CMR: Cardiac magnetic resonance imaging; CS: Cardiac sarcoidosis; CT: Computerized tomography; ECG: Electrocardiogram; HRS: Heart Rhythm Society; JCS: Japanese Circulation Society; LGE: Late gadolinium enhancement; LV: Left ventricle; LVEF: Left ventricular ejection fraction; VA: Ventricular arrhythmia; VT: Ventricular tachycardia; WASOG: World Association on Sarcoidosis and Other Granulomatous Disorders.

Furthermore, a reduced left ventricular ejection fraction (LVEF) is a significant independent risk factor for mortality.[21] Detection of echocardiographic findings at the initial presentation with AVB and VAs is associated with earlier diagnosis and treatment of CS.[10,13] Thinning of the basal septum is a major diagnostic criterion according to the JCS guidelines.[13]

A study by Di Stefano *et al.*[22] explored the use of left and right ventricular global longitudinal strain assessed through speckle-tracking echocardiography. They found a

significant difference between patients with early CS who had normal LVEF and right ventricular function (n = 23) and control patients without cardiac disease (n = 97). A left ventricular global longitudinal strain value of −16.3% had 82% sensitivity and 81% specificity for diagnosing CS.[22] The most common predictor of CS in patients with AVB and VAs is the presence of sarcoidosis in another organ system, with up to 99% of patients with CS having involvement of at least one other organ system.[5,11,23,24] The WASOG guidelines mandate the involvement of two organs for a CS diagnosis, based on clinical or histopathological evidence, making it crucial to assess for cardiac involvement in patients with extracardiac disease.

Notably, patients with CS are generally younger than those with AVB from other causes, as shown in studies referenced in Table 2; the average age of patients with CS in these studies ranged from 46 to 53 years. Differentiating CS from GCM, another granulomatous disease with similar presentations as CS and affecting a similar age group, poses a diagnostic challenge. The key differentiators include the presence of granulomas outside the heart and variations in endomyocardial biopsy findings.[25] A retrospective review in Finland reclassified 45 of 73 GCM diagnoses as CS based on biopsy and 18F-FDG PET results.[25] Endomyocardial biopsy has a low sensitivity due to patchy granuloma deposition within the heart, which may result in missed inflammation.[10] Therefore, detecting extracardiac granulomas using 18F-FDG PET is a less invasive method for distinguishing these diseases and should be considered before biopsy.[25] When extracardiac disease is not present, biopsy remains the primary diagnostic method despite its limitations.

2.4. CMR imaging and FDG PET findings in AVB versus VAs

CMR imaging and 18F-FDG PET are valuable for diagnosing CS. Late gadolinium enhancement (LGE) on CMR, indicating myocardial scarring and fibrosis, is a major diagnostic criterion according to JCS guidelines.[13] In contrast, 18F-FDG PET is effective in detecting active myocardial inflammation. Divakaran *et al.* showed that 18F-FDG PET has a high sensitivity (100%) for diagnosing CS but a relatively low overall specificity (33%). However, the presence of extracardiac uptake is pathognomonic, increasing the specificity of this method to 100% but reducing its sensitivity to 83%, highlighting the challenge of detecting isolated CS.[26] Additionally, 18F-FDG PET may play a prognostic role, with the extent of perfusion defects being a significant predictor of adverse events before and after immunosuppressive treatment.[27] Although LGE is commonly observed (ranging from 44% to 100%) in studies involving patients with confirmed CS,[10,23,28] direct comparisons between patients presenting with VAs versus AVB have not yet been reported. Notably, more severe disease is associated with a higher proportion of LGE, which is observed in 88% of patients with AVB and VT or LVEF <35% compared with 74% of patients with AVB alone.[28] LGE in the right ventricle is also linked to higher rates of sustained VT than LGE in other areas, although this finding is based on a small-scale retrospective study.[29] Newer T2 mapping sequences in CMR, in conjunction with LGE, can help differentiate active inflammation from fibrosis, improving both sensitivity and specificity of CMR.[30] The implication of T2 signal intensity on prognosis remains unclear.

3. Management strategies in AVB versus VAs

3.1. Corticosteroids and steroid-sparing agents

According to a study by Cheng *et al.* from the American Heart Association, the primary treatment for active CS is immunosuppression, with corticosteroids as the first-line therapy.[31] However, evidence supporting their use is limited, as no randomized controlled trials have been conducted. A retrospective cohort study of patients with CS presenting with AVB and LVEF >50% revealed that AVB completely resolved in 57% of patients treated with corticosteroids, suggesting that these factors play a role in preventing VAs.[32] These results are limited by the small sample size (n = 7; treated with corticosteroids), which may lead to an overestimation of the treatment effects.

A systematic review of corticosteroid use revealed that they may help improve AV conduction, with 47% of patients showing improvement when treated with steroids. The efficacy appears to decrease with worsening cardiac function at the start of treatment.[10,33] However, all studies reviewed had small sample sizes, and only a few of them assessed outcomes related to VAs. In a subsequent prospective study of patients with AVB and no extracardiac disease, corticosteroid therapy led to recovery of 1:1 conduction in only one of six patients after a mean follow-up of 21 ± 9 months and did not show improved outcomes.[11] Two of these six patients experienced adverse effects caused by the steroid treatment. The small sample size and single-center setting limit the study's power and comparability to other centers with different diagnostic criteria or ethnic profiles. This highlights the uncertainty regarding corticosteroid efficacy, particularly for VAs. No significant prognostic difference has been reported between high and moderate steroid doses,[34] but a large-scale randomized controlled trial (CHASM CS-RCT) is ongoing to investigate the effects of dosage and methotrexate augmentation on prognosis.

Table 2. Studies related to VAs and AVB in patients with CS

Author	Place of study	Type of study	No. of patients with AVB	No. of patients with VAs	Endpoints/outcomes	Key findings
Ekström *et al.* 2019[6]	Finland	Case Series	147	48	Endpoint event was death from any cause	Overall, 80% of deaths from CS were sudden cardiac death. AVB was the most common presentation, and the diagnosed patients showed a 5-year survival rate of 85%, which improved to 93% after receiving immunosuppressive therapy
Rosenthal *et al.* 2021[9]	USA	Prospective, multicenter cohort	58	152	Endpoint was diagnosis of either heart failure, AVB, VT, or death in patients with CS	Sarcoidosis is the strongest risk factor for the development of VT and AVB (no specific data available on prognosis after these presentations)
Hoogendoorn *et al.* 2020[10]	Netherlands	Case Series	4	10	Review of ejection fractions and clinical outcomes (death, hospitalization for heart failure, VT ablation) over time in early vs. late diagnosis of CS	Early diagnosis of CS and initiation of immunosuppressive therapy are critical to improving prognosis in patients referred for VT ablation with non-ischemic cardiomyopathy
Nery *et al.* 2014[11]	Canada	Prospective, single-center cohort	11	-	Diagnosis of CS in patients with second- or third-degree AVB and no history of sarcoidosis in another organ. Additional observed adverse events (heart failure, VT)	In patients presenting with AVB, patients with CS have more adverse clinical outcomes than those without
Cacoub *et al.* 2020[23]	France	Retrospective, single-center cohort	27	27	Assessed relapse-free survival, where relapse was defined as any new cardiac or non-cardiac symptom attributed to sarcoidosis by the patient's physician	High-degree AVB in patients with CS is associated with increased mortality. IV cyclophosphamide is associated with lower rates of cardiac relapse
Kaida *et al.* 2018[24]	Japan	Retrospective, single-center Cohort	15	-	Review of LVEF and brain natriuretic peptide levels over time in early vs. late CS diagnosis	Early diagnosis of CS in patients presenting with complete AVB significantly improves prognosis
Zhou *et al.* 2016[28]	USA	Retrospective single-center cohort	14	26	Primary endpoints were death and heart transplant. Recorded rates of reduced LVEF, VA, AVB	Lack of permanent pacemaker/ICD and age were significant predictors of mortality for patients with CS
Yodogawa *et al.* 2022[29]	Japan	Retrospective, single-center cohort	-	8	Evaluation of the location of LGE in patients with CS who presented with VAs	LGE in the RV free wall was associated with the development of VAs in patients with CS
Kato *et al.* 2003[32]	Japan	Retrospective single-center cohort	20	9 in follow-up period	Outcomes measured were death; improvement/ resolution of AVB; change in LVEF, VT, and side effects of corticosteroids	Corticosteroids are useful in the treatment of CS with AVB, leading to resolution in 57% of the patients. Steroids may also play a role in preventing VT
Sadek *et al.* 2013[33]	Japan, USA, Europe	Systematic Review	57	-	Outcomes examined were atrioventricular conduction, LVEF, VAs, and mortality	Corticosteroids can be effective for treating AVB, with 47.4% of the patients showing improvement. Not enough data to draw conclusions regarding VAs

(Cont'd...)

Table 2. ***(Continued)***

Author	Place of study	Type of study	No. of patients with AVB	No. of patients with VAs	Endpoints/outcomes	Key findings
Ahmed *et al.* 2023[36]	United Kingdom	Retrospective single-center cohort	2	3	Outcomes examined were findings on follow-up 18F-FDG PET and echocardiography, steroid maintenance dose, morbidity, and mortality	Infliximab was associated with a reduction in disease activity on follow-up 18F-FDG PET and an improvement of LVEF, with no significant arrhythmic events during follow-up. It was associated with an increased likelihood of infection
Mohsen *et al.* 2014[40]	USA	Retrospective single-center cohort	-	12	Recorded outcomes were death and delivery of ICD therapies	Glucocorticoid therapy did not prevent appropriate or inappropriate ICD shock delivery. No specific markers were associated with malignant VAs in CS
Nordenswan *et al.* 2018[41]	Finland	Case–control study	143	20 patients who presented with AVB	Endpoint was sudden cardiac death (fatal or aborted)	Patients with CS who presented with AVB have a high risk of sudden cardiac death. Patients presenting with AVB alone often had delayed diagnosis of CS and were most likely to require transplantation. Incidence of VT was 24% at 5 years after presentation
Mathijssen *et al.* 2022[44]	Netherlands	Retrospective single-center cohort	46	19	Primary outcome was appropriate ICD therapy delivery	Prior VA and right ventricular LGE were predictors of ICD therapy delivery, and low rates of inappropriate therapies were observed
Azoulay *et al.* 2020[45]	Japan, Europe, USA	Meta-analysis	Not stated	Not stated	Outcome measured was appropriate ICD therapy delivery	Age, male sex, LVEF, complete heart block, and ventricular pacing were associated with the delivery of appropriate ICD therapy
Jefic *et al.* 2009[47]	USA	Retrospective multicenter cohort	-	42	Endpoint was elimination of VA	VT ablation can be effective in eliminating or reducing VT burden in cases refractory to medical therapy
Siontis *et al.* 2022[48]	USA, Europe, Japan	Retrospective multicenter cohort	36	158	Immediate and short-term outcomes included procedural success, elimination of VT storm, and reduction in defibrillator shocks. The primary long-term outcome was the composite of VT recurrence, heart transplant, or death	Catheter ablation shown to be effective in treating medically resistant VT and reducing defibrillator shocks and recurrent VT storm
Muser *et al.* 2016[51]	USA	Retrospective single-center cohort	-	31	Long-term outcomes were VT-free survival, VT reduction, death, or heart transplant	Active inflammation at the time of ablation is associated with higher relapse rates, but VT ablation is overall effective in CS
Ahmed *et al.*[52]	United Kingdom	Retrospective single-center cohort	77	-	Endpoints were all-cause mortality, cardiac transplant, VA, or hospitalization for heart failure. Maintenance steroid dose and cardiac device upgrades and complications were evaluated	A late diagnosis of CS was associated with worse outcomes as well as a higher required steroid dose and a higher likelihood of requiring cardiac device upgrade

(Cont'd...)

Table 2. ***(Continued)***

Author	Place of study	Type of study	No. of patients with AVB	No. of patients with VAs	Endpoints/outcomes	Key findings
Nordenswan *et al.* 2018[53]	Finland	Case–control study	143	20 patients with AVB	Sudden cardiac death at presentation with VA	The risk of VA was high in patients initially presenting with AVB and remained higher if it was concomitant with VA or severe LVSD at the time of diagnosis
Takaya *et al.* 2015[54]	Japan	Retrospective single-center cohort	22	31 (including presentation with heart failure)	Endpoint was major adverse cardiac outcomes: cardiac death, VA, hospitalization for heart failure	Patients with AVB and VA have a similar mortality, although those with VAs may have a higher incidence of major adverse cardiac events

Abbreviations: 18F-FDG PET: 18 Fluorodeoxyglucose positron emission tomography; AVB: Atrioventricular block; CS: Cardiac sarcoidosis; ICD: Implantable cardioverter defibrillator; LGE: Late gadolinium enhancement; LVEF: Left ventricular ejection fraction; LVSD: Left ventricular systolic dysfunction; RV: Right ventricle; VA: Ventricular arrhythmia; VT: Ventricular tachycardia.

Steroid-sparing agents are commonly used as second-line treatments or adjuncts to corticosteroids. Among these, methotrexate is the most prominent and extensively studied. Although some reduction in myocardial inflammation has been observed with methotrexate through 18F-FDG PET, specific outcomes related to VAs and AVB have not been widely reported.[35] Infliximab use has been explored for cases refractory to second-line agents. A recent case series reported no major arrhythmic events (VA or AVB) in six patients over a mean follow-up period of 21.2 ± 15.5 months, and five of them had presented with VA or AVB at baseline. In addition, MRI during follow-up showed a reduction in FDG PET activity in all patients, indicating significant improvement in disease activity.[36] Larger, multicenter studies are warranted to further evaluate the efficacy of infliximab.

3.2. Implantable cardioverter defibrillator (ICD)

ICDs are considered as a Class 1 indication for VAs and a Class 2a indication for AVB, even if the AVB temporarily reverses. This recommendation is based on the high risk of future VAs, as outlined in Table 3.[15,37,38] Pacemaker indications, as specified by Glikson *et al.* in the 2021 ESC guidelines, primarily include complete heart block, Mobitz II heart block, Mobitz I with syncope or infranodal block, and symptomatic sinus node disease.[39] ICD implantation has been shown to significantly reduce mortality.[28] For example, Nery *et al.* reported that seven patients with CS underwent ICD implantation after initially presenting with AVB, with two of them subsequently receiving shocks for recurrent VT over an average follow-up period of 21 ± 9 months.11 Another retrospective study revealed that although 36.7% of patients received appropriate shocks, 30% received inappropriate shocks, and no significant predictors of such tachyarrhythmias were identified.[40] Owing partially to concurrent immunosuppression, patients with CS who undergo ICD implantation face a high risk of complications, including infections or lead fractures and dislodgement, affecting up to 15% of these patients.[41] In addition, an analysis by Kron *et al.* suggested that patients with isolated CS and ICDs had poorer outcomes than those with sarcoidosis involving other systems. This patient group had very high rates of VAs and appropriate shocks (69%) over 4 years.[42] However, selection bias may influence these findings, as isolated CS is less likely to be diagnosed or could be mistaken for other conditions, potentially leading to the diagnosis of only more severe cases. Factors associated with worse outcomes in this group include the presence of LGE on CMR, worsened New York Heart Association functional classification of heart failure, reduced LVEF, and comorbidities such as chronic kidney and lung diseases.[43]

Recent advancements in device leads and the increased use of home monitoring for device interrogation have led to lower rates of inappropriate shocks than those previously reported. For example, Mathijssen *et al.* recorded an inappropriate shock rate of 2.9%,[44] as shown in Figure 1 and Table 4. This study found that ICDs used for secondary prevention (class 1 indication) delivered appropriate therapy more frequently than those used for primary prevention (class 2A indication) over a median follow-up period of 2.8 years (82% vs. 19%), which aligns with international guidelines.[15,37,38] Predictors of appropriate therapy included prior VAs and RV LGE on CMR,[44] differing from a previous meta-analysis that identified younger age, male sex, lower LVEF, complete heart block, and ventricular pacing as significant predictors.[45] LGE in the RV has been linked to higher rates of sustained VT than that in other regions.[29] A meta-analysis assessing the risk of sudden cardiac death reported that positive LGE

Table 3. Indications for ICD implantation in patients with CS according to the 2014 HRS expert consensus,[15] the 2017 ACC/AHA/HRS statements,[38] and the 2022 ESC guidelines[39]

Class of recommendation	ICD recommendations in patients with CS		
	HRS expert consensus 2014	ACC/AHA/HRS statements 2017	ESC guideline 2022
1	Sustained VT, cardiac arrest, or LVEF<35% with expected survival of >1 year despite optimal medical therapy		
2a		LVEF >35% and evidence of scar on CMR/PET after resolution of inflammation with expected survival of >1 year	
2a	Syncope secondary to arrhythmia with LVEF >35%		
2a	Inducible sustained VA on EP study with LVEF >35% and expected survival >1 year	LVEF 35%–50% and minor LGE on CMR after resolution of inflammation with sustained monomorphic VT on EP study	
2a	Indication of permanent pacing and LVEF >35%		
2b	LVEF 36%–49% and/or RVEF <40% despite optimal medical therapy for heart failure and a period of immunosuppression		

Abbreviations: ACC: American College of Cardiology; AHA: American Heart Association; CMR: Cardiac magnetic resonance imaging; CS: Cardiac sarcoidosis; EP: Electrophysiology; ESC: European Society of Cardiology; HRS: Heart Rhythm Society; ICD: Implantable cardioverter defibrillator; PET: Positron emission tomography; LGE: Late gadolinium enhancement; LVEF: Left ventricular ejection fraction; RVEF: Right ventricular ejection fraction; VA: Ventricular arrhythmia; VT: Ventricular tachycardia.

Table 4. ICD indications in the studies referenced in Figure 1 (*n*=Number of patients)

Indication for ICD	Mohsen *et al.* (*n*=30)[40]	Mathijssen *et al.* (*n*=105)[44]
Ventricular arrhythmia	16	19
AVB/Bundle branch block	9	46
Others (reduced LVEF, syncope, sudden cardiac death)	5	40

Abbreviations: AVB: Atrioventricular block; ICD: Implantable cardioverter defibrillator; LVEF: Left ventricular ejection fraction.

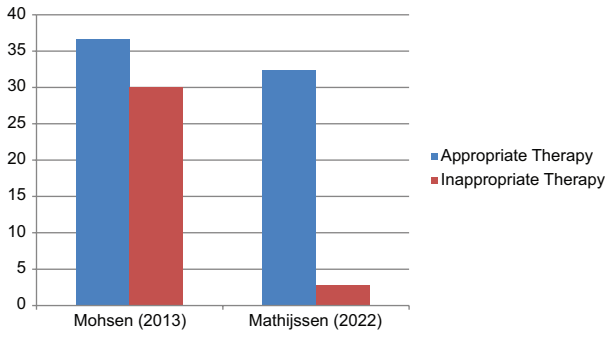

Figure 1. Comparison of appropriate and inappropriate implantable cardioverter defibrillator therapy administered over 9- and 8-year follow-up periods, respectively (x-axis = Percentage of patients receiving therapy). Figure created by author

and programmed electrical stimulation were associated with an 8.6- and 9-fold increased risk of VAs, respectively, and positive LGE and PET were correlated with a 6.8- and 3.4-fold increased risk of major adverse cardiac events, respectively.[46] Although no prospective randomized trials have evaluated ICD therapy specifically, its significance, despite the risks of complications and inappropriate therapy, was highlighted by Nordenswan *et al.*, who found a VA rate of 24.6% (n = 98) (sustained VT or sudden cardiac death) over 5 years using the Myocardial Inflammatory Diseases in Finland Study Group Registry.[41]

A challenge arises when a pacemaker is indicated and CS is suspected but not yet confirmed. Proceeding immediately to ICD implantation has the risk of inappropriate shocks but prevents the need for additional procedures, where a pacemaker is initially placed and later upgraded to an ICD. Temporary pacing may be used during diagnostic imaging, and clinical suspicion can help guide decision-making. At present, there are no established guidelines for such cases; therefore, treatment must be decided by the clinician on a case-by-case basis.

3.3. Antiarrhythmic drugs

Antiarrhythmic drugs are commonly used with an ICD to treat VAs, although their effectiveness has not been extensively studied. A multicenter prospective study on medical therapy for VAs recommended a stepwise approach: starting with an ICD alone, followed by the addition of an immunosuppressant and an antiarrhythmic drug, and finally using radiofrequency ablation. In this study, 12 of the 21 patients were managed with medical therapy alone, and 5 of the 9 patients who needed antiarrhythmics were prescribed amiodarone.[47] However, specific data on antiarrhythmic use for VAs in CS are limited. Sotalol and amiodarone are generally recommended because VAs in patients with CS often stem from re-entry or scar tissue, whereas beta blockers are suggested for their additional

benefit in heart failure. Class I antiarrhythmics, such as quinidine and flecainide, are typically avoided due to their potential to worsen arrhythmias in the presence of structural heart disease.[13,15]

3.4. Ablation

In cases refractory to medical therapy, catheter ablation might be considered. A multicenter retrospective study involving 158 patients showed that although CS has a high rate of VA recurrence after ablation, these rates are similar to those observed in other structural cardiomyopathies (46% vs. 40%).[48-50] Higher rates of VT recurrence were noted when active inflammation was present at the time of ablation, likely due to ongoing cycles of inflammation and scarring,[51] indicating that the timing of intervention affects prognosis in non-emergency cases. In addition, the induction of arrhythmia post-ablation in CS may not be associated with worse outcomes, such as VT recurrence, transplant, or death, unlike other cardiomyopathies.[45]

3.5. Prognosis

Hoogendoorn *et al.* investigated the impact of delayed diagnosis on the prognosis of patients with VAs. They compared patients diagnosed within 6 months of their initial presentation (n = 5) with those diagnosed after 6 months (n = 10), who had an average delay of 24 months. The later-diagnosed group had poorer outcomes, including reduced cardiac function, than the early-diagnosed group receiving immunosuppression, which showed generally stable function. This group also experienced more VT ablations, more hospitalizations for heart failure, and higher mortality (50% vs. 20%) over a mean follow-up period of 55 months.[10] Ahmed *et al.* also highlighted the importance of early diagnosis and initiation of immunosuppression in AVB cases. Their retrospective single-center review of 77 patients revealed that early diagnosis was linked to fewer device upgrades and lower maintenance steroid doses than delayed diagnosis over a mean follow-up period of 54.9 ± 45.3 months.[52] Delayed diagnosis has been associated with more severe LV dysfunction than early diagnosis, leading to a higher risk of hospitalization for heart failure, increased mortality, and a greater number of appropriate ICD therapies.[24,52] Despite this, the risk of sudden cardiac death remains high in patients with AVB, ranging from 9% to 14% over 5 years if AVB is the sole initial presentation and rising to 34% if AVB is accompanied with VAs.[53] Studies have consistently shown that the most common initial presentation of CS – (unexplained AVB)[6] – has worse outcomes, including a more severe clinical course, higher mortality, and increased risk of sudden cardiac death compared with other presentations or AVB in the absence of sarcoidosis.[11,23,41,53] Key findings are summarized in Table 2.

A long-term follow-up study revealed that one-third of patients who initially presented with VAs experienced a subsequent cardiac relapse. The relapse rate was similar to that of patients with second-degree AVB but significantly lower than that in patients with third-degree AVB (83%).[23] Using data from the Myocardial Inflammatory Diseases in Finland Study Group Registry, Nordenswan *et al.* evaluated the risk of major adverse cardiac events, such as death, transplantation, and life-threatening tachyarrhythmias, based on the initial presentation with AVB versus AVB accompanied with VAs and/or severe LV systolic dysfunction. Over a median follow-up period of 2.8 years, 24% of patients with AVB ± non-severe LV systolic dysfunction experienced an event, whereas this rate was more than double (56%) in those with AVB and VAs or severe LV systolic dysfunction at diagnosis, indicating a higher risk of further arrhythmias or recurrence when VAs are present at diagnosis.[53]

A Japanese study evaluated 53 patients with CS who initially presented with either AVB or VAs (n = 22 vs. n = 31), evaluating major adverse cardiac events over a 36-month follow-up period. This study reported that AVB was associated with a better composite endpoint than VT and/or heart failure (log-rank test, P = 0.046), largely due to fewer hospitalizations for heart failure. The mortality rates were similar between the two groups.[54]

Isolated AVB often remains undiagnosed for extended periods, with average delays in diagnosis ranging from 8 to 18 months, which has significant prognostic implications.[24,53] The frequent occurrence of unexplained second- and third-degree heart block in patients who are later diagnosed with both cardiac and extracardiac sarcoidosis[11,12] underscores the need for prompt investigation for CS in these cases.

4. Conclusions

This review highlights that sarcoidosis is frequently overlooked or diagnosed late, which impacts patient prognosis. Early treatment initiation is beneficial for maintaining LVEF, likely due to reduced scarring and better LVEF at diagnosis. There is a high incidence of CS in cases of "idiopathic" AVB or VAs; therefore, these cases should be investigated. Initially, non-invasive methods such as CMR and 18F-FDG PET should be used, followed by endomyocardial biopsy if needed. However, endomyocardial biopsy has low sensitivity and specificity for diagnosing CS.[10,25] CMR may also help predict disease progression, particularly with regard to right ventricular LGE. A stepwise management approach – starting with immunosuppression, followed by using an ICD, and finally considering catheter ablation – has proven effective in the

management of CS. Improvements in implantable devices are evident from the significant reduction in inappropriate shock deliveries reported in studies conducted 9 years apart.

CS is a challenging diagnosis due to its varied presentation, genetic diversity, gradual onset, and the highly invasive and low-sensitivity procedure required for a histological confirmation. Early detection and treatment are crucial for improving long-term prognosis and reducing morbidity. This review has discussed current imaging and management strategies for VAs and AVB along with their outcomes. Due to the rarity of CS, most studies included in this review are retrospective and single-center, which introduces inherent biases. Although there is substantial evidence supporting the use of cardiac devices, there is limited research on medical therapy for CS. More studies are needed to evaluate the long-term effects of corticosteroids and steroid-sparing agents on mortality and outcomes. In addition, biologic agents such as infliximab, which are currently used as third- or fourth-line treatments for resistant cases, could serve as a significant advancement in medical therapy. However, their use warrants further investigation, especially in early disease stages, to assess their efficacy.

At present, immunosuppression is recommended for active disease, whereas pharmacological treatment is recommended for heart failure. ICD implantation and catheter ablation for VT may be necessary for certain patients. A multidisciplinary team approach is essential to achieve optimal outcomes.

Acknowledgments

None.

Funding

None.

Conflict of interest

The authors declare that they have no competing interests.

Author contributions

Conceptualization: Raheel Ahmed
Writing–original draft: Caleb Carver
Writing–review & editing: All authors

Ethics approval and consent to participate

Not applicable.

Consent for publication

Not applicable.

Availability of data

Not applicable.

References

1. Sarcoidosis UK. *Sarcoidosis and the Heart*; 2022. Available from: https://www.sarcoidosisuk.org/information-hub/sarcoidosis-heart [Last accessed on 2022 Sep 11].
2. *Cardiac Sarcoidosis-American College of Cardiology*; 2022. Available from: https://www.acc.org/latest-in-cardiology/articles/2021/05/20/13/01/cardiac-sarcoidosis [Last accessed on 2022 Sep 11].
3. Markatis E, Afthinos A, Antonakis E, Papanikolaou IC. Cardiac sarcoidosis: Diagnosis and management. *Rev Cardiovasc Med*. 2020;21:321-338.

   doi: 10.31083/j.rcm.2020.03.102
4. Ahmed, R, Shahbaz, H, Ramphul, K, *et al*. Racial disparities among patients with cardiac sarcoidosis and arrhythmias in the United States: A propensity matched-analysis from the National Inpatient Sample Database 2016-2020. *Curr Probl Cardiol*. 2024;49(4):102450.

   doi: 10.1016/j.cpcardiol.2024.102450
5. Perry A, Vuitch F. Causes of death in patients with sarcoidosis. A morphologic study of 38 autopsies with clinicopathologic correlations. *Arch Pathol Lab Med*. 1995;119:167-172.
6. Ekström K, Lehtonen J, Nordenswan HK, *et al*. Sudden death in cardiac sarcoidosis: An analysis of nationwide clinical and cause-of-death registries. *Eur Heart J*. 2019;40:3121-3128.

   doi: 10.1093/eurheartj/ehz428
7. Patel MR, Cawley PJ, Heitner JF, *et al*. Detection of myocardial damage in patients with sarcoidosis. *Circulation*. 2009;120:1969-1977.

   doi: 10.1161/CIRCULATIONAHA.109.851352
8. Ahmed, R, Sawatari, H, Amanullah, K, *et al*. Characteristics and outcomes of hospitalized patients with heart failure and sarcoidosis: A propensity-matched analysis of the Nationwide Readmissions Database 2010-2019. *Am J Med*. 2024;137:751-760.e8.

   doi: 10.1016/j.amjmed.2024.03.039
9. Rosenthal DG, Fang CD, Groh CA, *et al*. Heart failure, atrioventricular block, and ventricular tachycardia in sarcoidosis. *J Am Heart Assoc*. 2021;10:e017692.

   doi: 10.1161/JAHA.120.017692
10. Hoogendoorn JC, Ninaber MK, Piers SRD, *et al*. The harm of delayed diagnosis of arrhythmogenic cardiac sarcoidosis: A case series. *Eurospace*. 2020;22:1376-1383.

    doi: 10.1093/europace/euaa115
11. Nery PB, Beanlands RS, Nair GM, *et al*. Atrioventricular block as the initial manifestation of cardiac sarcoidosis in middle-

aged adults. *J Cardiovasc Electrophysiol*. 2014;25:875-881.

doi: 10.1111/jce.12401

12. Kandolin R, Lehtonen J, Kupari M. Cardiac sarcoidosis and giant cell myocarditis as causes of atrioventricular block in young and middle-aged adults. *Circ Arrhythm Electrophysiol*. 2011;4:303-309.

doi: 10.1161/CIRCEP.110.959254

13. Terasaki F, Azuma A, Anzai T, *et al*. JCS 2016 guideline on diagnosis and treatment of cardiac sarcoidosis-digest version. *Circ J*. 2019;83(11):2329-2388.

doi: 10.1253/circj.cj-19-0508

14. Judson MA, Costabel U, Drent M, *et al*. The WASOG sarcoidosis organ assessment instrument: An update of a previous clinical tool. *Sarcoidosis Vasc Diffuse Lung Dis*. 2014;18:19-27.

15. Birnie DH, Sauer WH, Bogun F, *et al*. HRS expert consensus statement on the diagnosis and management of arrhythmias associated with cardiac sarcoidosis. *Heart Rhythm*. 2014;7:1304-1323.

doi: 10.1016/j.hrthm.2014.03.043

16. Lee S, Birnie D, Dwivedi G. Current perspectives on the immunopathogenesis of sarcoidosis. *Respir Med*. 2020;173:106161.

doi: 10.1016/j.rmed.2020.106161

17. Williams O, Fatima S. *Granuloma*. Treasure Island, FL: StatPearls Publishing; 2022. Available from: https://www.ncbi.nlm.nih.gov/books/NBK554586 [Last accessed on 2024 Jan 27].

18. Okada DR, Smith J, Derakhshan A, *et al*. Ventricular arrhythmias in cardiac sarcoidosis. *Circulation*. 2018;138:1253-1264.

doi: 10.1161/CIRCULATIONAHA.118.034687

19. Lehtonen J, Uusitalo V, Pöyhönen P, Mäyränpää MI, Kupari M. Cardiac sarcoidosis: Phenotypes, diagnosis, treatment, and prognosis. *Eur Heart J*. 2023;44:1495-1510.

doi: 10.1093/eurheartj/ehad067

20. Birnie DH, Nery PB, Ha AC, Beanlands RSB. Cardiac sarcoidosis. *J Am Coll Cardiol*. 2016;68:411-421.

doi: 10.1016/j.jacc.2016.03.605

21. Kakizaki R, Koitabashi T, Minami Y, *et al*. Untreated cardiac sarcoidosis with active inflammation: Severe left ventricular dysfunction and ventricular wall thinning in three years. *J Cardiol Cases*. 2017;16:141-143.

doi: 10.1016/j.jccase.2017.06.006

22. Di Stefano C, Bruno G, Arciniegas Calle MC, *et al*. Diagnostic and predictive value of speckle tracking echocardiography in cardiac sarcoidosis. *BMC Cardiovascr Disord*. 2020;20:21.

doi: 10.1186/s12872-019-01323-0

23. Cacoub P, Chapelon-Abric C, Resche-Rigon M, Saadoun D, Desbois AC, Biard L. Cardiac sarcoidosis: A long term follow up study. *PLoS One*. 2020;15:e0238391.

doi: 10.1371/journal.pone.0238391

24. Kaida T, Inomata T, Minami Y, *et al*. Importance of early diagnosis of cardiac sarcoidosis in patients with complete atrioventricular block. *Int Heart J*. 2018;59:772-778.

doi: 10.1536/ihj.17-492

25. Ekström K, Räisänen-Sokolowski A, Lehtonen J, Nordenswan HK, Mäyränpää MI, Kupari M. Idiopathic giant cell myocarditis or cardiac sarcoidosis? A retrospective audit of a nationwide case series. *ESC Heart Fail*. 2020;3:1362-1370.

doi: 10.1002/ehf2.12725

26. Divakaran S, Stewart GC, Lakdawala NK, *et al*. Diagnostic accuracy of advanced imaging in cardiac sarcoidosis. *Circ Cardiovasc Imaging*. 2020;12(6):e008975.

doi: 10.1161/circimaging.118.008975

27. Okafor J, Khattar R, Kouranos V, *et al*. Role of serial ^{18}F-fludeoxyglucose positron emission tomography in determining the therapeutic efficacy of immunosuppression and clinical outcome in patients with cardiac sarcoidosis. *J Nucl Cardiol*. 2024;35:101842.

doi: 10.1016/j.nuclcard.2024.101842

28. Zhou Y, Lower EE, Li HP, Costea A, Attari M, Baughman RP. Cardiac sarcoidosis: The impact of age and implanted devices on survival. *Chest*. 2017;151:139-148.

doi: 10.1016/j.chest.2016.08.1457

29. Yodogawa K, Fukushima Y, Tachi M, *et al*. Localization of late gadolinium enhancement and its association with ventricular tachycardia in patients with cardiac sarcoidosis. *Int Heart J*. 2022;63:235-240.

doi: 10.1536/ihj.21-635

30. Crouser ED, Ono C, Tran T, He X, Raman SV. Improved detection of cardiac sarcoidosis using magnetic resonance with myocardial T2 mapping. *Am J Respir Crit Care Med*. 2014;189(1):109-112.

doi: 10.1164/rccm.201309-1668LE

31. Cheng RK, Kittleson MM, Beavers CJ, *et al*. Diagnosis and management of cardiac sarcoidosis: A scientific statement from the American Heart Association. *Circulation*. 2024;149(21):e1197-e1216.

doi: 10.1161/cir.0000000000001240

32. Kato Y, Morimoto S, Uemura A, Hiramitsu S, Ito T, Hishida H. Efficacy of corticosteroids in sarcoidosis presenting with atrioventricular block. *Sarcoidosis Vasc Diffuse Lung Dis*. 2003;20:133-137.

33. Sadek MM, Yung D, Birnie DH, Beanlands RS, Nery PB. Corticosteroid therapy for cardiac sarcoidosis: A systematic review. *Can J Cardiol*. 2013;29:1034-1041.

    doi: 10.1016/j.cjca.2013.02.004

34. Yazaki Y, Isobe M, Hiroe M, *et al.* Prognostic determinants of long-term survival in Japanese patients with cardiac sarcoidosis treated with prednisone. *Am J Cardiol*. 2001;88:1006-1010.

    doi: 10.1016/s0002-9149(01)01978-6

35. Gallegos C, Oikonomou EK, Grimshaw A, Gulati M, Young BD, Miller EJ. Non-steroidal treatment of cardiac sarcoidosis: A systematic review. *Int J Cardiol Heart Vasc*. 2021;34:100782.

    doi: 10.16/j.ijcha.2021.100782

36. Ahmed R, Okafor J, Azzu A, *et al*. The role of infliximab in treating refractory cardiac sarcoidosis. *Eur Heart J*. 2023;44(Supplement_2):ehad655.978.

    doi: 10.1093/eurheartj/ehad655.978

37. Al-Khatib SM, Stevenson WG, Ackerman MJ, *et al*. 2017 AHA/ACC/HRS guideline for management of patients with ventricular arrhythmias and the prevention of sudden cardiac death: Executive summary: A Report of the American College of Cardiology/American Heart Association Task Force on Clinical Practice Guidelines and the Heart Rhythm Society. *Circulation*. 2018;138(13):e210-e271.

    doi: 10.1016/j.jacc.2017.10.054

38. Zeppenfeld K, Tfelt-Hansen J, de Riva M, *et al*. 2022 ESC guidelines for the management of patients with ventricular arrhythmias and the prevention of sudden cardiac death. *Eur Heart J*. 2022;43:3997-4126.

    doi: 10.1093/eurheartj/ehac262

39. Glikson M, Nielsen JC, Kronborg MB, *et al*. 2021 ESC Guidelines on cardiac pacing and cardiac resynchronization therapy. *Eur Heart J*. 2021;42(35):3427-3520.

    doi: 10.1093/eurheartj/ehab364

40. Mohsen A, Jimenez A, Hood RE, *et al*. Cardiac sarcoidosis: Electrophysiological outcomes on long-term follow-up and the role of the implantable cardioverter-defibrillator. *J Cardiovasc Electrophysiol*. 2013;25:171-176.

    doi: 10.1111/jce.12302

41. Nordenswan HK, Pöyhönen P, Lehtonen J, *et al.* Incidence of sudden cardiac death and life-threatening arrhythmias in clinically manifest cardiac sarcoidosis with and without current indications for an implantable cardioverter defibrillator. *Circulation*. 2022;13:964-975.

    doi: 10.1161/CIRCULATIONAHA.121.058120

42. Kron J, Sauer W, Mueller G, *et al*. Outcomes of patients with definite and suspected isolated cardiac sarcoidosis treated with an implantable cardiac defibrillator. *J Interv Card Electrophysiol*. 2015;43:55-64.

    doi: 10.1007/s10840-015-9978-3

43. Mactaggart S, Ahmed R. The role of ICDs in patients with sarcoidosis-A comprehensive review. *Curr Probl Cardiol*. 2024;49(5):102483.

    doi: 10.1016/j.cpcardiol.2024.102483

44. Mathijssen H, Bakker ALM, Balt JC, *et al*. Predictors of appropriate implantable cardiac defibrillator therapy in cardiac sarcoidosis. *J Cardiovasc Electrophysiol*. 2022;33:1272-1280.

    doi: 10.1111/jce.15484

45. Azoulay LD, Waintraub X, Haroche J, Amoura Z, Cohen Aubart F. Factors associated with implantable cardioverter defibrillators appropriate therapy in cardiac sarcoidosis: A meta-analysis. *Sarcoidosis Vasc Diffuse Lung Dis*. 2020;37:17-23.

    doi: 10.36141/svdld.v37i1.8271

46. Franke KB, Marshall H, Kennewell P, *et al*. Risk and predictors of sudden death in cardiac sarcoidosis: A systematic review and meta-analysis. *Int J Cardiol*. 2021;328:130-140.

    doi: 10.1016/j.ijcard.2020.11.044

47. Jefic D, Joel B, Good E, *et al*. Role of radiofrequency catheter ablation of ventricular tachycardia in cardiac sarcoidosis: Report from a multicenter registry. *Heart Rhythm*. 2009;6:189-195.

    doi: 10.1016/j.hrthm.2008.10.039

48. Siontis KC, Santangeli P, Muser D, *et al.* Outcomes associated with catheter ablation of ventricular tachycardia in patients with cardiac sarcoidosis. *JAMA Cardiol*. 2022;7:175-183.

    doi: 10.1001/jamacardio.2021.4738

49. Berte B, Sacher F, Venlet J, *et al*. VT recurrence after ablation: Incomplete ablation or disease progression? A multicentric European study. *J Cardiovasc Electrophysiol*. 2015;27:80-87.

    doi: 10.1111/jce.12858

50. Stevenson WG, Soejima K. Catheter ablation for ventricular tachycardia. *Circulation*. 2007;115:2750-2760.

    doi: 10.1161/circulationaha.106.655720

51. Muser D, Santangeli P, Pathak RK, *et al*. Long-term outcomes of catheter ablation of ventricular tachycardia in patients with cardiac sarcoidosis. *Circ Arrhythm Electrophysiol*. 2016;9:e004333.

    doi: 10.1161/CIRCEP.116.004333

52. Ahmed R, Dulay MS, Liu A, *et al*. Comparing outcomes of an "early" versus "late" diagnosis of cardiac sarcoidosis following a baseline presentation of high-grade atrioventricular block. *Curr Probl Cardiol*. 2024;49(7):102577.

doi: 10.1016/j.cpcardiol.2024.102577

53. Nordenswan HK, Lehtonen J, Ekström K, *et al*. Outcome of cardiac sarcoidosis presenting with high-grade atrioventricular block. *Circ Arrhythm Electrophysiol*. 2018;11(8):e006145.

doi: 10.1161/CIRCEP.117.006145

54. Takaya Y, Kusano KF, Nakamura K, Ito H. Outcomes in patients with high-degree atrioventricular block as the initial manifestation of cardiac sarcoidosis. *Am J Cardiol*. 2015;115:505-509.

doi: 10.1016/j.amjcard.2014.11.028

ACCSCIENCE PUBLISHING

Brain & Heart

REVIEW ARTICLE

Minimalist approach to left atrial appendage occlusion through three-dimensional intracardiac echocardiography: Procedural steps and single-center experience

Ashok Chaudhary[1]*, John Trovato[2], and Ragitha Subodh[1]

[1]Division of Cardiology, Rutgers Robert Wood Johnson Medical School, New Jersey, United States of America

[2]Rutgers Robert Wood Johnson Medical School, New Jersey, United States of America

(This article belongs to the *Special Issue: Structural Heart Disease: Recent Updates*)

Abstract

Atrial fibrillation (AF), the most prevalent arrhythmia worldwide, is associated with an annual risk of ischemic stroke of up to 5%, with approximately 98% of thrombi originating from the left atrial appendage (LAA). Direct oral anticoagulants or vitamin K antagonists remain the gold standard for preventing systemic thromboembolism in patients with AF. LAA occlusion (LAAO) is an alternative stroke prevention technique for patients with AF who cannot tolerate long-term anticoagulation. Percutaneous LAAO typically employs a multimodal imaging approach with contrast fluoroscopy and transesophageal echocardiography (TEE) for visualization, device selection and deployment, and complication monitoring. TEE is also used for follow-up imaging. However, it necessitates general anesthesia or deep sedation and is associated with a high risk of adverse events. Three-dimensional intracardiac echocardiography (3D ICE) has been proposed as a viable alternative to TEE for LAAO procedures. In this review, we summarized the current evidence regarding ICE guidance in LAAO procedures. We also presented a case series of consecutive patients presenting at our center who underwent LAAO, which was performed by a single operator using a minimalist approach of moderate sedation, 3D ICE, and same-day discharge. We also presented a summary of the minimalist approach to LAAO using 3D ICE and detailed procedural steps of 3D ICE catheter manipulation for successful LAAO intervention.

Keywords: Left atrial appendage occlusion; Intracardiac echocardiography; Transesophageal echocardiography; Watchman; Atrial fibrillation; Stroke; Oral anticoagulation

***Corresponding author:**
Ashok Chaudhary
(ashok.chaudhary@rutgers.edu)

Citation: Chaudhary A, Trovato J, Subodh R. Minimalist approach to left atrial appendage occlusion through three-dimensional intracardiac echocardiography: Procedural steps and single-center experience. *Brain & Heart*. 2024;2(4):4018. doi: 10.36922/bh.4018

Received: June 22, 2024

Accepted: August 30, 2024

Published Online: October 18, 2024

1. Introduction

1.1. Advantages and limitations of intracardiac echocardiography (ICE) guidance in left atrial appendage occlusion (LAAO) procedures

The ICE-guided LAAO procedure can be performed with moderate sedation, eliminating the risks associated with general anesthesia and endotracheal intubation, which are

required for the transesophageal echocardiography (TEE)-guided LAAO procedure. However, TEE is associated with major risks. The insertion and manipulation of a TEE probe during examination can result in various complications, ranging from lip pressure injuries, oral mucosal damage, dental injuries, and temporomandibular joint dislocation to visceral perforations.[1] Although most of these injuries affect the upper gastrointestinal tract, respiratory and other abdominal complications have been reported occasionally.[1] Although several TEE-related complications are minor and frequently remain unreported, a few complications can be more severe, resulting in significant morbidity and even mortality. For instance, esophageal perforation during TEE examination is a rare but serious complication, with a incidence of 0.01 – 0.38%. During TEE probe manipulation, mechanical, compressive, and thermal injuries may cause gastrointestinal bleeding.[1]

Most patients undergoing structural heart interventions sustain some form of TEE-associated injury, with prolonged procedural duration and poor or suboptimal image quality contributing to a higher risk. The mechanism underlying esophageal and gastric injuries is likely multifactorial, which includes direct mechanical injury due to blind probe insertion and manipulation, contact pressure from the probe, and thermal injury. Prolonged image acquisition times and patients' underlying comorbidities further exacerbate such injuries.[2] Esophagogastroduodenoscopy can detect TEE-related lesions in up to 86% of patients undergoing structural cardiac interventions. Of these patients, 40% experience complex lesions such as hematomas or lacerations. Most of these lesions are not detected during routine clinical evaluations and may only manifest as discomfort.[3,4] The incidence of clinically detected major TEE-related complications in patients undergoing high-risk structural procedures, including LAAO, has been reported to be 6.1%.[3] In structural heart procedures, TEEs are performed by highly skilled echocardiographers with a minimum of 1 year of experience; however, despite such expertise, >80% of patients experience complications following TEE.[1,5] In addition, TEE has certain limitations, as it cannot be performed in up to 2% of patients due to anatomical constraints, high-risk conditions, or a lack of cooperation.[6] In addition to enhancing patient comfort and satisfaction, ICE improves the efficiency and safety of structural heart procedures.[4,7] The three-dimensional (3D) ICE-guided procedure enables a single operator to complete the procedure, eliminating the need for multiple personnel in the laboratory.[6,8,9] Furthermore, ICE guidance reduces the time required by experienced operators to perform fluoroscopy and improves procedural scheduling by using fewer medical specialties.[10-12]

The introduction of 3D ICE enhances the capabilities of ICE guidance in LAAO procedures.[13] Although 3D images are visually striking, the main advantage of 3D ICE is its ability to digitally rotate the imaging plane, a feature similar to TEE that enables a complete 360° view of the left atrial appendage (LAA). By utilizing this digital rotation, multiple LAA measurements can be recorded and the implanted device can be thoroughly inspected before release, thereby minimizing the need for extensive probe maneuvering in the left atrium (LA).[9,13] However, ICE-guided LAAO may add extra workload on the operator, who must handle both the procedure and the task of obtaining images.[9,14] This can be particularly challenging for less experienced operators. However, with structured training, even the least experienced operator can become more proficient in a relatively short time. Most LAAO procedures under ICE guidance can be performed through a single transseptal puncture, although a second transeptal puncture (TSP) may occasionally be necessary to facilitate the passage of the ICE catheter into the LA. It remains controversial whether this method can increase the incidence of iatrogenic atrial septal defect (iASD). A study by Ma *et al.* indicated that 21.4% of patients developed iASD after 2 months of ICE-guided LAAO, with a 70.6% closure rate achieved at 12 months. Although the iASD size was larger than that reported in other guidance methods, ICE-guided LAAO did not increase the risk of persistent iASD, pulmonary hypertension, or other complications, and there were no cases of right-to-left shunt.[15]

2. Baseline characteristics

We conducted a retrospective analysis of 20 consecutive patients who underwent LAAO at a single center (in New Jersey) between October 19, 2023, and June 14, 2024. All patients exhibited elevated CHA2DS2-VASc and HAS-BLED scores, making them unsuitable for long-term anticoagulation. The LAAO procedure for the first seven patients (Group 1) was performed under both TEE guidance and 3D ICE guidance (the primary operator was blinded to the measurements obtained on TEE). The LAAO procedure for the subsequent 13 patients (Group 2) relied solely upon 3D ICE guidance. The mean age of patients was 74.6 ± 11.1 years, and most of them (65%) were male. The mean CHA2DS2-VASc score was 4.6 ± 1.0, and the mean HAS-BLED score was 4.5 ± 0.9 (additional demographic data are provided in Table 1). Although pre-procedural imaging was not required, some patients who underwent LAAO procedures under 3D ICE guidance alone were subjected to pre-procedural imaging using cardiac computed tomography angiography (CTA) to evaluate appendage anatomy and rule out the presence of LAA thrombus. We also employed FEops software to evaluate appendage anatomy and perform predictive simulations of the LAAO device in eight of these patients.

Table 1. Baseline characteristics

Demographics	TEE and 3D ICE (*n*=7)	3D ICE (*n*=13)
Age (years)	77.4±9.0	73.0±12.1
Sex, *n* (%)		
Male	3 (42.9)	10 (76.9)
Female	4 (57.1)	3 (23.1)
Race, *n* (%)		
White	3 (42.9)	7 (53.8)
Black or African American	0 (0.0)	5 (38.5)
Asian	2 (28.6)	1 (7.7)
Other	2 (28.6)	0 (0.0)
Smoking status, *n* (%)		
Current	0 (0.0)	0 (0.0)
Former	4 (57.1)	4 (30.8)
Never	3 (42.9)	8 (61.5)
Unknown	0 (0.0)	1 (7.7)
Other risk factors		
CHA_2DS_2-VASc score	5.1±1.1	4.3±0.9
HAS-BLED score	4.7±1.1	4.4±0.9
CHF (%)	2 (28.6)	6 (46.2)
Hypertension (%)	6 (85.7)	13 (100)
Diabetes mellitus (%)	3 (42.9)	7 (53.8)
History of stroke/TIA/SE (%)	4 (57.1)	5 (38.5)
Vascular disease (%)	3 (42.9)	1 (7.7)
Abnormal renal function (%)	1 (14.3)	5 (38.5)
Medication usage predisposing to bleeding (%)	6 (85.7)	9 (69.2)
Alcohol (%)	0 (0.0)	1 (7.7)

Notes: CHA2DS2-VASc is the tool to estimate the annual risk of stroke in atrial fibrillation patients and includes CHF, hypertension, age, diabetes mellitus, history of stroke or TIA, vascular disease and sex; HAS-BLED is a tool to estimate annual risk of bleeding in atrial fibrillation patients taking oral anticoagulants and includes hypertension, abnormal renal/liver function, stroke, bleeding history or predisposition, labile INR, older age (>65 years) and drugs/alcohol use concomitantly.
Abbreviations: TEE: Transesophageal echocardiography; 3D ICE: Three-dimensional intracardiac echocardiography; TIA: Transient ischemic attack; SE: Systemic thromboembolism.

Watchman FLX was used for LAA occlusion in all cases. Notably, four patients in the 3D ICE Group 2 had no pre-procedural imaging data available. Table 2 provides a summary of the minimalistic approach to LAAO, which is conducted at our center using a 4D Nuvision ICE catheter (Biosense Webster).

All patients underwent post-procedural echocardiography either the same day or the following day before discharge. The patients were scheduled for a follow-up cardiology appointment at 6 weeks, which included either cardiac CTA or TEE. For Group 1, the preferred imaging strategy at the 6-week follow-up was TEE; however, two patients underwent cardiac CTA. Meanwhile, for Group 2, cardiac CTA was recommended at follow-up instead of TEE; however, two patients underwent TEE. Follow-up imaging was either pending or unavailable for two patients (one from each group).

2.1. Procedural steps for LAAO under the guidance of Nuvision 4D ICE probe

2.1.1. Insertion into the RA

a. Obtain USG-guided common femoral vein access using a micropuncture needle
b. Insert a 12F 30-cm Cook sheath into the inferior vena cava (IVC), ensuring that the 0.035″ wire remains in place for facilitating "fluro-map" easy navigation into the RA (Figure 1A)
c. Advance the ICE probe to the RA by rotating the entire probe clockwise or counterclockwise, ensuring that the IVC remains visible on top of the image throughout the procedure
d. It may be necessary to apply a slight anterior inclination to the deflection knob to remain in the IVC, especially if entering from the left side and before entering the RA. This is performed to prevent entering the hepatic veins and avoid the Eustachian ridge at the IVC/RA junction
e. Upon reaching the mid-RA (facing the tricuspid valve [TV]), return to the home view.

2.1.2. ICE views in mid-RA

a. The following structures can be visualized by performing a gradual clockwise rotation of the probe. Alternatively, this can be accomplished by gradually rotating the tip rotation knob
b. Home view with the right atrium (RA), TV, and right ventricle (RV) in view (Figure 2A)
c. TV, coronary sinus, pulmonic valve, aortic valve
d. Mitral valve (MV), LAA (Figure 2B)
e. Interatrial septum (IAS)
f. Left upper and lower pulmonary veins (PVs) (Figure 2C)
g. Once past the esophagus and descending aorta, the right upper and lower PVs can be visualized. It may be necessary to slightly advance the probe to visualize the upper right PV (Figure 2D)
h. Return to the neutral home view

2.1.3. ICE views in RV

a. Lower the probe into the RA
b. While maintaining the TV in view, apply an anterior tilt (clockwise rotation of the deflection knob) until

Table 2. Minimalist approach to the left atrial appendage occlusion procedure using Nuvision 4D ICE catheter

- Perform preoperative cardiac computed tomography angiography (CTA) for anatomical evaluation of the left atrial appendage (LAA) and procedural planning (using predictive simulation tools such as FEops, if available)
- Perform moderate sedation under local anesthesia
- Perform bilateral common femoral vein access (double puncture performed on the same side, if required)
- Insert a 16F 12-cm Cook sheath from one side (to accommodate a 14F Watchman sheath from Boston Scientific)
- Insert a 12F 30-cm Cook sheath from another side (to accommodate 10F 90-cm Nuvision 4D intracardiac echocardiography [ICE] catheter from Biosense Webster)
- Advance the ICE catheter to the right atrium (RA) under fluoroscopic and echocardiographic guidance (0.035″ wire in the sheath facilitates easy navigation)

Assess the interatrial septum (IAS), pulmonary veins, and LAA for the presence of thrombus (RA and right ventricular outflow tract [RVOT] views)

- Perform transseptal puncture (TSP) under ICE guidance (select the view in which the tenting is directed toward the left-sided pulmonary veins and LAA ostium (usually mid-to-inferior or mid-to-posterior for most anatomical variants). Biplane imaging is useful for precisely localizing TSP. Radiofrequency systems such as VersaCross Connect with RF pigtail wire (Baylis Medical) are useful for performing precise punctures
- Floss the septal puncture site using the 14F Watchman FLX sheath, and pull it back into the inferior vena cava
- Advance the ICE probe into the left atrium (LA) and further advance the Watchman FLX sheath next to it (this may be accomplished using balloon septostomy in few cases; 8-mm Mustang is sufficient)
- Evaluate the LAA using ICE from mid-LA, near LSUPV, and just above the mitral valve. Supra mitral view is helpful in most cases
- Engage the LAA with the pigtail catheter and perform LAA angiography
- Position the ICE probe directed at the LAA in one view, preferably in a supramitral view (analogous to a 135° TEE view)
- Deploy the Watchman FLX under ICE/fluoroscopic imaging guidance. Performing 3D MPR during device deployment is useful
- Assess for compression and leak using 3D MPR views on ICE
- Release the device once the Position, Anchoring, Sizing, Sealing criteria are met
- Remove the Watchman FLX sheath
- Pull back the ICE probe into the RA, evaluate the IAS, exclude pericardial effusion, and remove the probe. Employ the right ventricle view, if required, to check for pericardial effusion
- Administer protamine for reversal, if needed. Achieve hemostasis on both sides using previously placed Perclose or figure-of-8 sutures
- Perform limited echocardiography before same-day discharge
- Conduct follow-up between 6 weeks and 3 months using cardiac CTA (or TEE if GFR <30)

only the lower part of the TV is visible. Subsequently, advance the probe gradually into the RV (Figure 3A). After passing the TV in the RV, gradually release the anterior tilt to the neutral position. This will introduce the probe into the right ventricular outflow tract

c. Using the tip rotation knob, perform a gradual clockwise rotation
d. Left ventricle (LV) long axis (used to check for pericardial effusion), short axis of papillary muscle/LV, and MV (Figure 3B)
e. Rotate the tip rotation knob until the LAA appears in view. This is also known as a Q-tip view, which demonstrates the separation of LAA and Left superior pulmonary vein (LSPV) (Figure 3C)
f. PVs can also be visualized through this view
g. Withdraw the probe into the RA once LAA is cleared of any existing thrombus.

2.1.4. Use of ICE for TSP

a. Rotate the entire probe clockwise until the IAS is visualized and then apply posterior tilt (counterclockwise rotation of the deflection knob). The IAS should be visible in the long axis (analogous to the bicaval TEE view). The X-plane will provide the corresponding short-axis view (Figure 4A)
b. If the IAS is not visible, reset the probe and then rotate the entire probe until the neutral index is facing the operator. Apply a clockwise rotation of the tip rotation knob until the LSPV is visible and then apply an anterior tilt (clockwise rotation of the deflection knob) to bring the IAS in view
c. Perform TSP in the desired location. Choose the view where the tenting is directed toward the left-sided PV and LAA ostium. Typically, this is situated mid-to-inferior and mid-to-posterior for most anatomical variants (Figure 4B). Biplane imaging facilitates precise localization of TSP. This will enable the LAAO device to engage the LAA more co-axially (Figure 4C).

2.1.5. Crossing into the LA

a. Once the pre-shaped rigid wire is placed in the LA or LSPV, it is recommended to first floss the septal puncture site with a 14F Watchman sheath and withdraw the sheath into the IVC
b. Gradually retract the ICE probe lower, remove any tilt, and rotate the entire probe in either direction as necessary to locate the transeptal wire. Apply anterior tilt (clockwise rotation of the deflection knob) and advance while maintaining the wire in view below the puncture site. Utilize both ICE and fluoroscopy (align ICE catheter and transeptal wire on fluoroscopy) to facilitate the passage into the LA (Figure 1C). In the event of resistance, discontinue the procedure, withdraw the ICE catheter, and start again

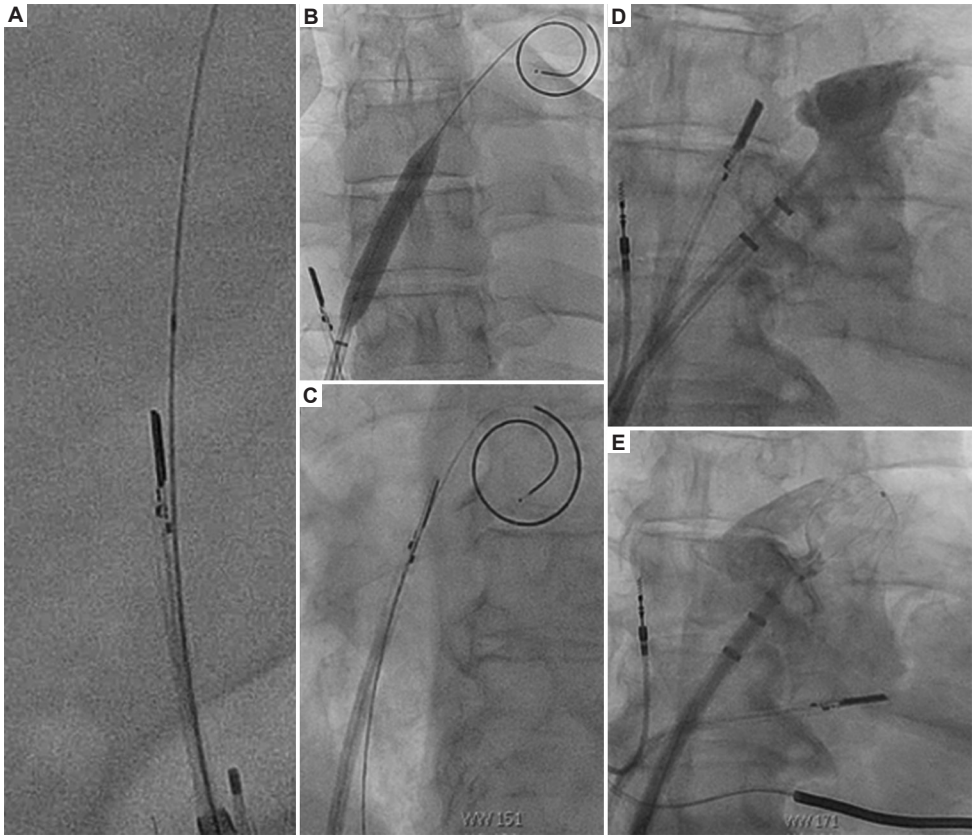

Figure 1. Fluoroscopy views. (A) J Wire in the RA provides a "road map" for facilitating ICE advancement through the iliac veins and inferior vena cava under ICE guidance. (B) Interatrial septostomy may be needed for difficult ICE catheter crossing across the IAS. (C) Flossing the puncture site with the Watchman FLX sheath first and proper alignment of the ICE catheter with the transeptal wire are important steps to facilitate easier passage of the ICE catheter across the IAS. (D) Position of ICE catheter on fluoroscopy for left superior pulmonary vein view of the LAA. (E) Position of ICE catheter on fluoroscopy for supramitral view of the LAA.
Abbreviations: RA: Right atrium; ICE: Intracardiac echocardiography; IAS: Interatrial septum; LAA: Left atrial appendage.

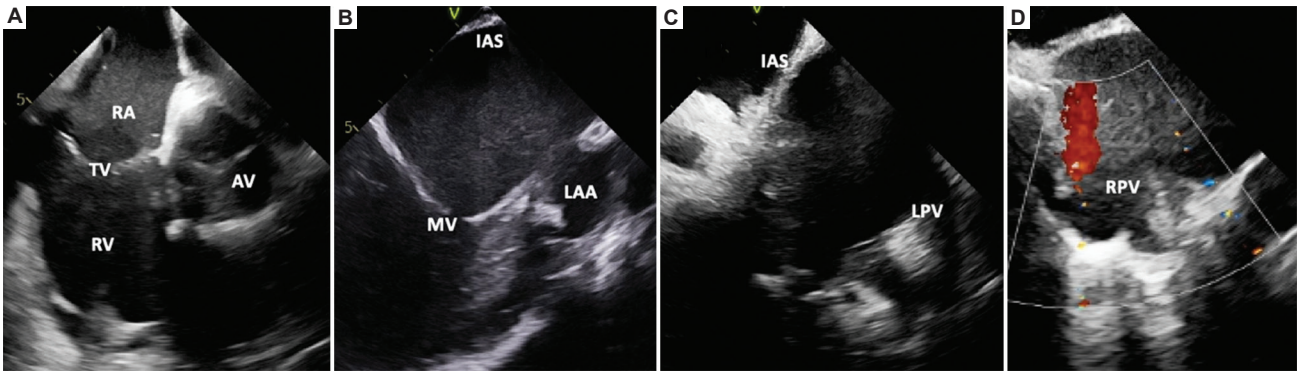

Figure 2. ICE views from RA. (A) Home view, (B) Left atrial appendage, (C) Left-sided pulmonary veins, (D) Right-sided pulmonary veins.
Abbreviations: RA: Right atrium; TV: Tricuspid valve; RV: Right ventricle; MV: Mitral valve; LAA: Left atrial appendage; IAS: Interatrial septum; LPV: Left-sided pulmonary veins; RPV: Right-sided pulmonary veins; ICE: Intracardiac echocardiography.

c. If necessary, balloon septostomy with an 8–10-mm Mustang balloon may be employed to slightly expand the puncture site during the septal crossing (Figure 1B).

2.1.6. ICE views in LA

a. Once the probe reaches the LA, three views can be used. However, due to 3D MPR capability, the entire procedure can also be performed in a single view.

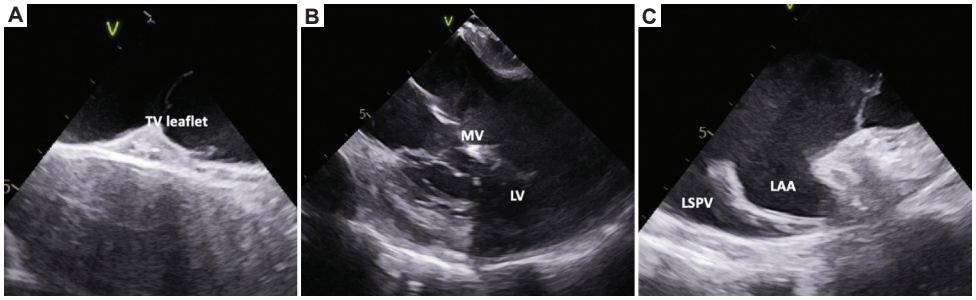

Figure 3. ICE views from RV. (A) Anterior tilt until only the lower portion of the tricuspid valve is visible and slow advancement to enter RV. Upon reaching RV, all tilt is released to rest the probe in the RVOT. (B) LV long axis views to check for pericardial effusion. (C) Q-tip view of the left atrial appendage to rule out thrombi.
Abbreviations: MV: Mitral valve; LV: Left ventricle; LSPV: Left superior pulmonary vein; LAA: Left atrial appendage; RV: Right ventricle, RVOT: Right ventricular outflow tract; ICE: Intracardiac echocardiography.

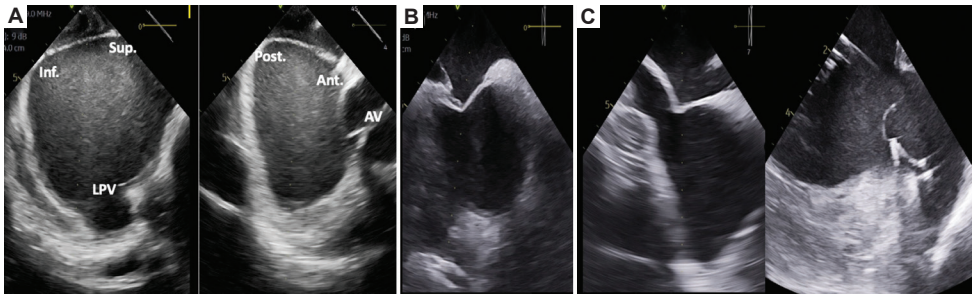

Figure 4. Clockwise rotation of the probe in the right atrium with posterior tilt demonstrates the use of IAS for transeptal puncture. (A) The X-plane across the IAS depicts the superior, inferior, anterior, and posterior aspects of the IAS for precise transeptal puncture. (B) Tenting in the IAS is directed toward the left atrial appendage, which enables more co-axial alignment for easier device placement. (C) The pigtail catheter is easily advanced toward the left atrial appendage due to the co-axial transeptal puncture aided through ICE.
Abbreviations: AV: Aortic valve; IAS: Interatrial septum; LPV: Left-sided pulmonary veins; ICE: Intracardiac echocardiography.

A slight adjustment to the probe's rotation, tilt, and tip rotation will aid in the visualization of the different lobes of LAA

b. LA home view and AV view: Advance the probe to mid-LA and apply a slight posterior tilt (counterclockwise on the deflection knob), if needed, to bring the LAA into the home view (Figure 5A). From this view, rotate the entire probe counterclockwise until the short axis of AV is visible and then advance until LAA comes into view. This is analogous to the 45° TEE view (Figure 5D)
c. Left superior pulmonary view: Advance the probe through the LSPV ostium, if needed, to obtain a comprehensive view of the LAA (Figure 5B). This is comparable to the 0° TEE view. Once the LAA is engaged using the pigtail catheter, fluoroscopy can also be used to visualize the ICE probe position relative to the LAA (Figure 1D)
d. Supramitral or PA view: This offers the best view of the LAA in most cases and is similar to the 135° TEE view. To attain this view, withdraw the ICE probe from mid-LA while facing the LAA, ensuring that the MV is visible. Then, apply a gradual but sharp anterior tilt (clockwise rotation of the deflection knob) along with gradual advancement of the probe until it is positioned above the MV. Subsequently, the LAA will be clearly visible by slowly rotating the tip rotation knob in a clockwise direction (Figure 5C). The ICE probe will be visible in a horizontal position below the LAA in AP view on fluoroscopy, with the probe pointing upward (Figure 1E). Gentle clockwise and counterclockwise rotation of the probe may help identify different lobes. To retrieve the probe in the mid-LA region, withdraw it gradually while simultaneously releasing all the anterior tilt and tip rotation.

2.1.7. Data collection specific for LAAO procedure

a. Using 3D MPR, the en-face 3D view of the LAA ostium can be visualized. The ostium can be measured in 3D for device sizing. All landing zone measurements can be acquired in MPR views (Figure 6A)
b. The LAAO device can be deployed while remaining in the same view, which is typically the supramitral view. Utilize MPR to evaluate device position, compression, stability, and leakage (Figures 6B, 7A and B). Repeat these steps after the release of device to assess for

position, compression, and leakage. It is crucial to conduct a careful 360° evaluation to assess for the peri-device leak (PDL), which can be readily achieved using the 4D ICE probe.

2.1.8. ICE views from RA

a. Once the LAAO device is released and the final assessment is completed, withdraw the probe into the RA to evaluate the IAS at the TSP site for iatrogenic ASD evaluation (size and shunt)

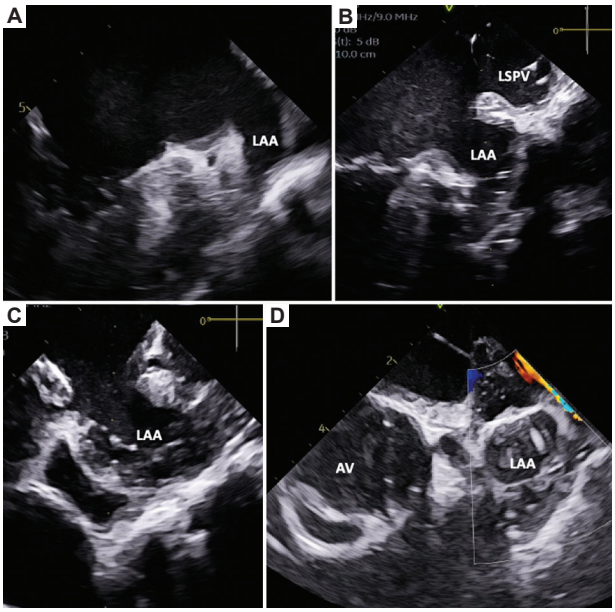

Figure 5. ICE views in LA. (A) Left atrial "home view." (B) Left superior pulmonary vein view, which is analogous to the 0° TEE view. (C) Supramitral view, which is similar to the 135° TEE view. (D) Aortic valve view, which is comparable to the 45° TEE view.
Abbreviations: LAA: Left atrial appendage; AV: Aortic valve; ICE: Intracardiac echocardiography; LA: Left atrium, TEE: Transesophageal echocardiography.

b. To check for pericardial effusion, use the RA home view at a lower magnification. Multiplane imaging is preferred. If there is any concern, RV ICE views can be used to evaluate the pericardial space beyond the LV and RV.

2.1.9. Access site care

a. The ICE probe is then removed along with the sheath
b. Hemostasis is achieved with vascular closure device like Perclose, figure of 8 stitch or manual compression.

2.2. Procedural outcomes

Both groups achieved a technical success rate of 100%, which is defined as successful device deployment without embolization and a PDL of <3 mm. No devices were recaptured in Group 2 (all procedures were accomplished using one device and in one attempt), whereas device recapture was necessary for one case in Group 1; however, it did not alter the final size of the Watchman FLX deployed. In Group 1, the average duration of the entire procedure was 102.0 ± 37.7 min, whereas in Group 2, it was 89.0 ± 11.4 min (Table 3). The average duration from ICE insertion to septal crossing was 16 min, and the average duration from septal crossing to LAAO device deployment was 30 min in Group 2. The fluoroscopy duration improved in Group 2 (24.9 min) compared with that in Group 1 (28.4 min). One patient in each group underwent pre-planned patent foramen ovale (PFO) closure during the LAAO procedure to diminish the overall risk of embolic stroke. The total procedure time reflects the additional time it took to perform PFO closure as well. None of the patients in either group required iASD closure.

The most frequent device size implemented under 3D ICE guidance was 27 mm; no resizing was required.

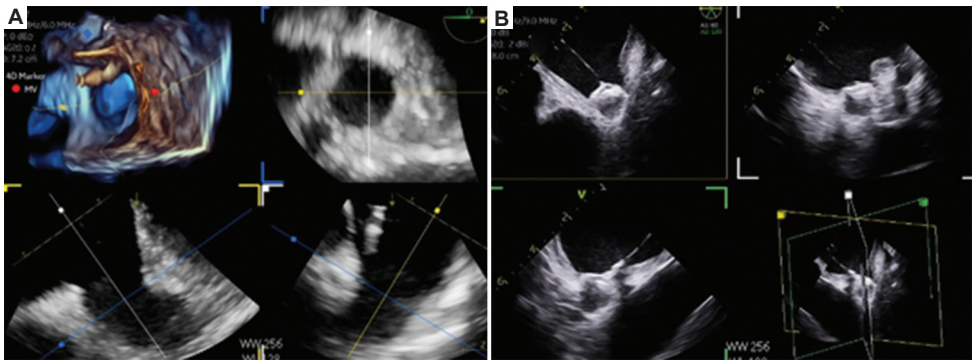

Figure 6. Nuvision 4D ICE used for LAAO with Watchman FLX device. (A) Three-dimensional multiplanar reconstruction of the left atrial appendage using an ICE catheter enables detailed evaluation of its anatomy for device sizing (watchman FLX in this case). (B) Device deployment and assessment for compression and leak. This can be achieved using an ICE catheter positioned in any one view (preferably the supramitral view) and can eliminate the need for multiple manipulations of the catheter in the left atrium.
Abbreviations: ICE: Intracardiac echocardiography, LAAO: Left atrial appendage occlusion.

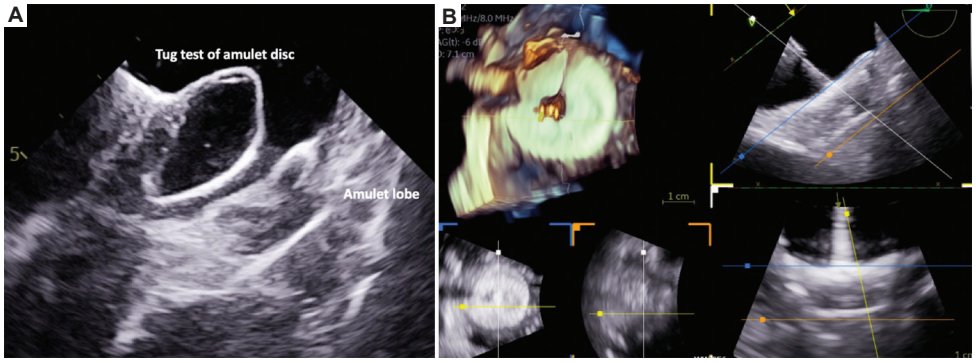

Figure 7. Nuvision 4D ICE was employed for Amulet LAAO. (A) Gentle tug test of the Amulet disc to assess its stability. (B) 3D MPR views to check for position, compression, and leak.
Abbreviations: ICE: Intracardiac echocardiography, LAAO: Left atrial appendage occlusion.

Table 3. Procedural duration

Duration (min)	TEE and ICE (*n*=7)	ICE (*n*=13)
Patient in room to patient out	144	125
Skin to skin	102	89
ICE in to ICE out	65	63
TEE in to TEE out	82	N/A
ICE insertion to septal crossing	20	16
Septal crossing to device deployment	34	30
Fluoroscopy duration	28.4	24.9

Abbreviations: TEE, transesophageal echocardiography; ICE: Intracardiac echocardiography.

Table 4. Procedural outcome

Procedural outcomes	TEE and ICE (*n*=7) (%)	ICE (*n*=13) (%)
Technical success	100	100
Periprocedural complications	0	0
Procedures with device resizing	0	0
Average number of devices used	1	1
General anesthesia	100	15
Moderate sedation	0	70
Monitored anesthetic care w/o intubation	0	15
Average length of stay	1 (days)	0.5 (days)
Follow-up (6 weeks)		
Peri-device leak	0	0
Device-related thrombus	0	0
MACCE events	0	0

Abbreviations: TEE: Transesophageal echocardiography; ICE: Intracardiac echocardiography.

In Group 1, all patients received general anesthesia with mechanical ventilation. In Group 2, 70% of the patients received moderate sedation, 15% received monitored anesthetic care without intubation, and 15% received general anesthesia and mechanical ventilation based on patient preference/body habitus. Following the procedure, all patients received dual antiplatelet therapy for 3 months, and they were subsequently prescribed low-dose aspirin alone. In Group 1, the average post-procedural length of stay (excluding LOS due to other medical issues) was 1.0 day, whereas that in Group 2 was 0.5 day. In either group, no PDL or device-related thrombus was detected at the 6-week follow-up. Both groups experienced no major adverse cardiac or cerebrovascular events after the procedure. In addition, there were no local or systemic bleeding complications (Table 4).

3. Discussion

The LAAO procedure is a feasible alternative to anticoagulant therapy for stroke prevention in patients with atrial fibrillation who cannot tolerate anticoagulation.[16,17] Most centers employ general anesthesia with mechanical ventilation and TEE for LAAO. ICE guidance, primarily 2D and occasionally 3D is employed in a limited number of cases.[11,17] This single-center observational study demonstrated that the minimalist approach of 3D ICE guidance for LAAO procedure with moderate sedation and same-day discharge was both feasible and comparable to TEE in all patients. However, our sample size was insufficient to derive any definitive conclusions. A more extensive study with longer longitudinal follow-up is warranted to verify these findings. High success rates can be achieved using 3D ICE-guided LAAO with no significant adverse events.[7,14,18] In addition, pre-procedural cardiac CTA and routine use of predictive AI-based simulation tools such as FEops can aid in simplifying the planning of the procedure.[19] If feasible, patients may prefer to undergo follow-up using CTA rather than TEE, which can prevent the need for additional invasive procedures.

The elevated radiation exposure and potential impact on kidney function must be considered and discussed with the patients.

The technical aspects of 3D ICE can be mastered through structured learning. Due to its distinctive characteristics compared with other echocardiographic techniques, specialized education is necessary for training in ICE catheter manipulation, image acquisition, and interpretation. Key elements of training include understanding ultrasound physics, individualized instruction for structural heart interventions, and hands-on practice using advanced equipment in a controlled animal model.[20] Operators should gain procedural experience under expert supervision at high-volume centers and be equipped to diagnose and manage complications.[20] The absence of precise data regarding the number of procedures required for ICE competency presents a challenge, especially with continuous development of imaging technology. To ensure proficiency and minimize complications, a consensus on the minimum number of ICE-guided procedures feasible at low-volume sites must be reached. The 2019 guidelines from the American College of Cardiology, American Heart Association, and American Society of Echocardiography recommend a minimum of 10 cases to achieve level III structural heart echocardiography competency.[20] New users may wish to perform their initial cases of 3D ICE with TEE as a backup imaging technique. This will help enhance operator experience and the confidence of the cardiac team in this technology. Eventually, 3D ICE may become the preferred imaging modality for all users and will become key to a minimalist approach to LAAO interventions.

4. Conclusion

TEE has been the primary method for guiding LAAO procedures and is the most widely used imaging modality. However, it has significant disadvantages, such as the need for sedation or general anesthesia for esophageal intubation, an elevated risk of esophageal injury, and reliance on a specialized echocardiography operator.[1,21] A single-center observational study demonstrated that using a minimalist approach with 3D ICE guidance for LAAO procedures under moderate sedation was both feasible and comparable to TEE in all patients. Utilizing 3D ICE can enhance the safety and efficacy of procedures, reduce costs, and increase patient satisfaction.[3,22]

Acknowledgments

None.

Funding

None.

Conflict of interest

The authors declare they have no competing interests.

Author contributions

Conceptualization: Ashok Chaudhary
Writing – original draft: All authors
Writing – review & editing: All authors

Ethics and consent to participate

Not applicable.

Consent for publication

Not applicable.

Availability of data

Not applicable.

References

1. Zhang L, Xie Y, Ren Z, Xie M. Transesophageal echocardiography related complications. Front Cardiovasc Med. 2024;11:1410594.

   doi: 10.3389/fcvm.2024.1410594

2. Patel KM, Desai RG, Trivedi K, Neuburger PJ, Krishnan S, Potestio CP. Complications of transesophageal echocardiography: A review of injuries, risk factors, and management. J Cardiothorac Vasc Anesth. 2022; 36(8):3292-3302.

   doi: 10.1053/j.jvca.2022.02.015

3. Diaz JC, Duque M, Marin J, *et al*. Intracardiac echocardiography-guided left atrial appendage occlusion. *Arrhythm Electrophysiol Rev*. 2024;13:e03.

   doi: 10.15420/aer.2023.29

4. Ramesh T, Budhiraja M, Mehta V, Rajsheker S, Arif I, Sukhija R. Tct-698 intracardiac echocardiography versus transesophageal echocardiography for procedural guidance in patients undergoing left atrial appendage occlusion: A single-center retrospective review. *J Am Coll Cardiol*. 2023;82(17):B280-B281.

   doi: 10.1016/j.jacc.2023.09.709

5. Reddy VY, Doshi SK, Kar S, *et al*. 5-year outcomes after left atrial appendage closure. J Am Coll Cardiol. 2017;70(24):2964-2975.

   doi: 10.1016/j.jacc.2017.10.021

6. Jhand A, Goldsweig AM. The emerging role of intracardiac echocardiography (ICE) in left atrial appendage closure (LAAC). *Curr Cardiol Rep*. 2023;25(10):1223-1232.

   doi: 10.1007/s11886-023-01940-4

7. Nielsen-Kudsk J, Berti S, Caprioglio F, *et al*. Intracardiac

echocardiography to guide watchman FLX implantation: The ICE LAA study. *JACC Cardiovasc Interv*. 2023; 16(6):643-651.

doi: 10.1016/j.jcin.2022.10.024

8. Diaz J, Bastidas O, Duque M, *et al*. Impact of intracardiac echocardiography versus transesophageal echocardiography guidance on left atrial appendage occlusion procedures: A meta-analysis. *J Cardiovasc Electrophysiol*. 2023;35(1):44-57.

   doi: 10.1111/jce.16118

9. Goldsweig AM, Alkhouli M. Let it go: Intracardiac echocardiography is the future of imaging for left atrial appendage occlusion. *J Soc Cardiovasc Angiogr Interv*. 2022;1(6):100518.

   doi: 10.1016/j.jscai.2022.100518

10. Gianni C, Horton RP, Della Rocca DG, *et al*. Intracardiac echocardiography- versus transesophageal echocardiography-guided left atrial appendage occlusion with watchman FLX. J Cardiovasc Electrophysiol. 2021;32(10):2781-2784.

    doi: 10.1111/jce.15220

11. Hemam ME, Kuroki K, Schurmann PA, *et al*. Left atrial appendage closure with the watchman device using intracardiac vs transesophageal echocardiography: Procedural and cost considerations. *Heart Rhythm*. 2019b;16(3):334-342.

    doi: 10.1016/j.hrthm.2018.12.013

12. Stout K, Craig C, Rivington J, Lyden E, Payne JJ, Goldsweig AM. Clinical protocol for selecting intracardiac or transesophageal echocardiography-guided left atrial appendage occlusion. Am J Cardiol. 2024;222:87-94.

    doi: 10.1016/j.amjcard.2024.04.023

13. Della Rocca DG, Magnocavallo M, Gianni C, *et al*. Three-dimensional intracardiac echocardiography for left atrial appendage sizing and percutaneous occlusion guidance. *Europace*. 2023;26(1):euae010.

    doi: 10.1093/europace/euae010

14. Ferro EG, Alkhouli M, Nair DG, *et al*. Intracardiac vs transesophageal echocardiography for left atrial appendage occlusion with watchman FLX in the U.S. *JACC Clin Electrophysiol*. 2023;9(12):2587-2599.

    doi: 10.1016/j.jacep.2023.08.004

15. Ma Y, Guo L, Li J, *et al*. Iatrogenic atrial septal defect after intracardiac echocardiography-guided left atrial appendage closure: Incidence, size, and clinical outcomes. J Clin Med. 2022;12(1):160.

    doi: 10.3390/jcm12010160

16. Betts T, Grygier M, Erik Nielsen-Kudsk J, *et al*. B-po01-078 real-world clinical outcomes with a next-generation left atrial appendage closure device: First report from the flexibility post-approval study. Heart Rhythm. 2021;18(8):S82.

    doi: 10.1016/j.hrthm.2021.06.255

17. Messele L, Khan M, Darden D, *et al*. Outcomes of percutaneous left atrial appendage occlusion device implantation in atrial fibrillation patients based on underlying stroke risk. Europace. 2023;25(4):1415-1422.

    doi: 10.1093/europace/euad049

18. Pastormerlo LE, Tondo C, Fassini G, *et al*. Intra-cardiac versus transesophageal echocardiographic guidance for left atrial appendage occlusion with a watchman FLX device. J Clin Med. 2023;12(20):6658.

    doi: 10.3390/jcm12206658

19. De Backer O, Iriart X, Kefer J, *et al*. Impact of computational modeling on transcatheter left atrial appendage closure efficiency and outcomes. JACC Cardiovasc Interv. 2023;16(6):655-666.

    doi: 10.1016/j.jcin.2023.01.008

20. Tang GHL, Zaid S, Hahn RT, *et al*. Structural heart imaging using 3-dimensional intracardiac echocardiography. JACC Cardiovasc Imaging. 2024.

    doi: 10.1016/j.jcmg.2024.05.012

21. Zhang ZY, Li F, Zhang J, *et al*. A comparable efficacy and safety between intracardiac echocardiography and transesophageal echocardiography for percutaneous left atrial appendage occlusion. Front Cardiovasc Med. 2023;10:119771.

22. Grazina A, Fiarresga A, Ramos R, *et al*. Intracardiac echocardiography-guided left atrial appendage occlusion: The path to independence. Rev Port Cardiol. 2023;42(10):847-855.

    doi: 10.1016/j.repc.2023.01.028

ACCSCIENCE PUBLISHING

Brain & Heart

REVIEW ARTICLE

Beyond the gut: Exploring neurological manifestations in inflammatory bowel disease

Manjeet Kumar Goyal[1]*, Shivam Kalra[2], Abhinav Rao[2], Manisha Khubber[3], Abhinav Gupta[3], and Ashita Rukmini Vuthaluru[4]

[1]Department of Gastroenterology, All India Institute of Medical Sciences, New Delhi, India

[2]Department of Internal Medicine, Trident Medical Center, North Charleston, South Carolina, United States of America

[3]Department of Gastroenterology, Dayanand Medical College and Hospital, Ludhiana, Punjab, India

[4]Department of Anesthesia and Critical Care, All India Institute of Medical Sciences, New Delhi, India

Abstract

Neurological manifestations in inflammatory bowel diseases (IBD), such as Crohn's disease and ulcerative colitis, are increasingly recognized as significant contributors to both disease burden and patient morbidity. This comprehensive review delves into the spectrum of neurological complications linked with IBD, highlighting the involvement of both the central and peripheral nervous systems. The neurological impairments range from more common conditions such as peripheral neuropathy, characterized by nerve damage leading to pain and numbness, and cerebrovascular diseases, which include strokes and transient ischemic attacks, to less frequent but intensely severe conditions such as multiple sclerosis and myasthenia gravis, which involve the immune system attacking components of the nervous system. The complex pathophysiology underlying these manifestations integrates various factors including immune-mediated responses, vascular abnormalities such as thromboembolism, nutritional deficiencies often exacerbated by malabsorption and chronic inflammation, and the adverse effects elicited by IBD medications such as corticosteroids and immunomodulators. This review underscores the importance of adopting a multidisciplinary management approach. By integrating the expertise of gastroenterologists with that of neurologists, rheumatologists, and other specialists, patient outcomes can be significantly optimized. Further emphasis is placed on the necessity for heightened clinical awareness and the implementation of early diagnostic interventions to effectively identify and mitigate the neurological complications associated with IBD. In conclusion, ongoing research aimed at elucidating the underlying mechanisms that connect IBD with neurological disorders is imperative to facilitate the development of more effective preventative and therapeutic strategies for these challenging complications.

Keywords: Inflammatory bowel disease; Crohn's disease; Ulcerative colitis; Neurological complications; Immune-mediated mechanisms; Vascular abnormalities; Nutritional deficiencies; Medication adverse effects

***Corresponding author:**
Manjeet Kumar Goyal
(manjeetgoyal@gmail.com)

Citation: Goyal MK, Kalra S, Rao A, Khubber M, Gupta A, Vuthaluru AR. Beyond the gut: Exploring neurological manifestations in inflammatory bowel disease. *Brain & Heart.* 2024;2(4):3486. doi: 10.36922/bh.3486

Received: April 24, 2024

Accepted: September 27, 2024

Published Online: October 30, 2024

1. Introduction

Inflammatory bowel diseases (IBD), such as primarily comprising Crohn's disease (CD) and ulcerative colitis (UC), are chronic inflammatory conditions of the gastrointestinal (GI) tract characterized by an inappropriate immune response to intestinal flora.[1] IBD is known to affect about 1.6 million Americans, with approximately 70,000 new cases diagnosed each year. While the intestinal symptoms of IBD are well-documented, the neurological manifestations are less commonly discussed but are increasingly recognized as significant factors contributing to the overall disease burden. These neurological complications involve both the central nervous system (CNS) and the peripheral nervous system (PNS), presenting a wide range of clinical challenges that may be directly or indirectly related to the underlying inflammatory processes of IBD.[2]

The prevalence of neurological manifestations in IBD is reported to be higher than previously estimated, with recent studies suggesting a range from 0.25% to 47.5% of patients experiencing some form of neurological complications.[3] This wide range likely reflects variations in study populations, methodologies, and definitions of neurological involvement. The manifestations can be broadly categorized into cerebrovascular diseases, peripheral neuropathies, muscle diseases, and other less common conditions such as multiple sclerosis (MS) and myasthenia gravis (MG).

Cerebrovascular complications are among the most serious neurological manifestations associated with IBD. Patients with IBD are at an increased risk of thromboembolic events, including stroke, particularly during periods of active disease. Peripheral neuropathies represent another common neurological issue in IBD, with a variety of presentations ranging from sensorimotor polyneuropathy to mononeuritis multiplex and autonomic neuropathy. The pathophysiology behind these conditions is complex, involving a combination of immune-mediated damage, nutritional deficiencies, and possibly neurotoxic effects triggered by medications commonly used in IBD treatment, such as metronidazole.[2]

The management of neurological manifestations in IBD requires a multidisciplinary approach, involving gastroenterologists, neurologists, and other specialists. The goals of management include controlling the underlying IBD activity, treating specific neurological symptoms, and adjusting IBD therapies to minimize adverse effects on the nervous system. This comprehensive approach is essential for improving patient outcomes and quality of life.

Therefore, neurological manifestations in IBD represent a critical aspect of the disease that requires further attention and research. Understanding the full spectrum of these manifestations, their pathophysiology, and effective management strategies is essential for improving patient outcomes and quality of life. This review will explore the spectrum of neurological manifestations associated with IBD, delving into their epidemiology, pathophysiology, clinical presentations, and management challenges.

1.1. Epidemiology

The epidemiology of neurological manifestations in IBD is varied, with reported incidences ranging from 0.25% to 47.5%.[2] This wide range likely reflects differences in study designs, populations, and diagnostic criteria. Lossos *et al.*[4] reported neurological involvement in 3% of 638 IBD patients, whereas in 26% of cases, this complication arose up to 10 years before the onset of intestinal symptoms, and in all other patients, it emerged up to 12 years after the onset of IBD. This complication was associated with IBD exacerbation in only 10% of cases, and 53% of these patients also presented with other extraintestinal manifestations and complications.[4] In another study, 67% of patients with CD and 53% of patients with UC had neurologic disorders.[5] Elsehety and Bertorini[6] reported a 33.2% incidence of neurological and neuropsychiatric manifestations in 253 patients with pathologically confirmed CD. Two prospective studies found the prevalence of peripheral neuropathy to be 13.4% and 8.8%.[7,8] Asymptomatic focal brain white matter lesions were also found in the neuroimaging studies using magnetic resonance imaging (MRI) in IBD patients compared to healthy people (43.1% vs. 16.0%; relative risk 2.6, 95% confidence interval 1.3 – 5.3).[9] A recent small study utilizing diffusion tensor imaging and voxel-based morphometry found that IBD patients also present with gray matter atrophy.[10] There has been a surge in the interest for neurological complications after the introduction of anti-tumor necrosis factor alpha (TNFα) and anti-α4 integrin therapy to clinical practice. Although relatively rare, these complications could be severe and include cerebrovascular, peripheral, and central demyelinating events, and progressive multifocal leukoencephalopathy (PML).[11] Neurological complications are considered relatively rare but are significant due to their potential impact on morbidity and quality of life. For instance, peripheral neuropathy is one of the more common neurological complications, while more severe conditions such as cerebrovascular diseases and CNS infections are less frequent but can be life-threatening. Moreover, the presence of neurological signs may exacerbate during the flare or evolve independently from intestinal manifestation without responding to the treatment for the underlying disease.

2. Pathophysiology

The pathogenesis of neurologic disorders associated with IBD has not been fully delineated, but several mechanisms are known to potentially influence their pathogenesis. The most common mechanisms include immunologic abnormalities prothrombotic states, malabsorption and nutritional deficiencies, metabolic agents, iatrogenic complications of medical and surgical treatment of IBD, as well as the brain-gut axis interactions (Figure 1).[12]

2.1. Immune-mediated mechanisms

Many neurological complications in IBD are believed to be immune-mediated. This includes the production of autoantibodies, cytokine-mediated inflammation, and immune complex deposition. These mechanisms can lead to conditions such as peripheral neuropathy, MG, and MS. The inflammatory milieu in IBD, characterized by elevated levels of TNFα, interleukin (IL)-6, and other pro-inflammatory cytokines, can disrupt normal immune function and promote autoimmunity that targets neural tissues.[13]

2.2. Vascular abnormalities

Patients with IBD are at an increased risk of thromboembolic events, including stroke, particularly during disease flares. This risk is compounded by the hypercoagulable state associated with chronic inflammation, which can lead to abnormalities in coagulation pathways and endothelial dysfunction. In addition, vasculitis, although extremely rare in IBD, can contribute to neurological symptoms by affecting blood vessels in the CNS and PNS.[2]

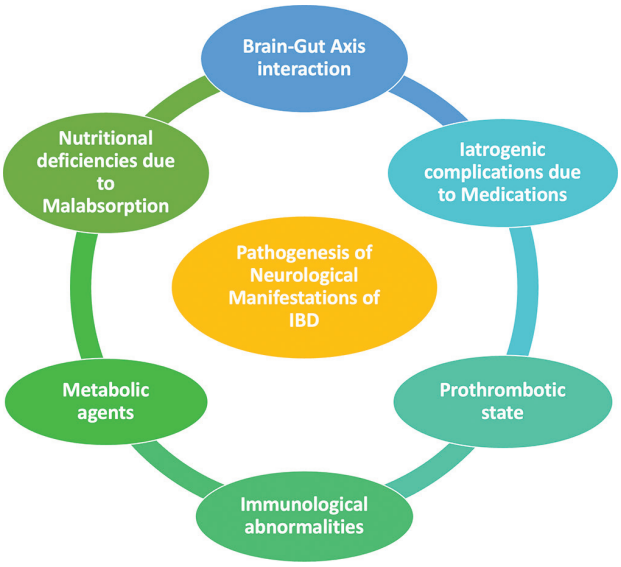

Figure 1. Pathophysiology of neurological manifestations of inflammatory bowel disease. (Image credit: Ashita Rukmini Vuthaluru)

2.3. Nutritional deficiencies

Malabsorption, common in IBD, can lead to deficiencies of essential vitamins such as B12, Vitamin E, and folate, which are crucial for nerve function and integrity. Deficiencies in these nutrients can cause or exacerbate conditions such as peripheral neuropathy and cognitive impairments.[14]

2.4. Side effects of medications

The treatment of IBD often involves the use of medications that can have neurological side effects. For example, metronidazole, commonly used to treat IBD, can cause peripheral neuropathy. Similarly, corticosteroids and immunosuppressants can increase susceptibility to infections, including those affecting the CNS. Anti-TNFα therapy, while effective for managing IBD, is contraindicated in patients with demyelinating diseases such as MS due to the risk of exacerbating neurological symptoms.[11]

3. Neurological manifestations

3.1. Peripheral neuropathy

Peripheral neuropathy is one of the most common neurological involvements in both CD and UC and occurs at a higher incidence in individuals with IBD compared to the general population.[3] Several types of polyneuropathy have been identified in IBD patients, involving demyelination or axonal damage, including autonomic neuropathy, sensory polyneuropathy, acute and chronic inflammatory demyelinating polyneuropathy (CIDP), mononeuropathy, multifocal neuropathy, cranial neuropathy, and plexopathy.[14] The frequency of these conditions remains undetermined, ranging between 0.25% and 35.7% across various studies.[15] A study conducted in Greece observed neurological abnormalities in two out of 45 IBD patients; one with a history of acute motor sensory polyneuropathy complicated by UC and another with mild incidental carpal tunnel syndrome.[15]

The underlying pathophysiology of neuropathy in IBD patients remains unclear, potentially due to immunological anomalies, drug exposure, or nutritional deficiencies. Nemati *et al.*[16] reported a clinical response in a CD patient treated with intravenous immunoglobulin at a dose of 2 g/kg administered twice daily, which aligns with the immune-based theory. Notably, two pathogenic hallmarks of IBD – intestinal dysbiosis and loss of mucosal integrity – in the GI tract have also been implicated in the neuropathy.[17]

Studies on microbial-induced neurological disorders in IBD remain relatively limited. Didesch *et al.*[18] reported that a 71-year-old with *Clostridioides difficile* infection developed acute demyelinating sensorimotor

polyneuropathy after undergoing fecal transplantation. This finding supports the theory of a cross-reaction of pathogenic anti-gut antibodies with neural surface antigens and provides evidence regarding the process of molecular mimicry. The gut-brain axis concept integrates a diverse range of signals, including neural, endocrine, nutrient, and immunological signals between the CNS and the GI system, emphasizing a bidirectional interaction with multiple mechanisms guiding each direction.[19] Other studies have shown clinical responses to immunotherapy in IBD patients with both axonal and demyelinating polyneuropathy, highlighting the involvement of T cells in the pathogenesis of demyelinating neuropathies, although the role of the immune system in axonal damage remains less clear despite being supported by clinical improvements observed with immunomodulatory therapies.

In Brazil, 33 patients with IBD-related peripheral neuropathy, including 18 with CD and 15 with UC, were treated with immunomodulatory therapy. Various agents such as intravenous immunoglobulin, prednisone, fludarabine, cyclophosphamide, azathioprine, etanercept, and plasmapheresis have been used in the management of peripheral neuropathy.[20] It has been observed that among UC patients with peripheral neuropathy, 11% showed major improvement, 56% moderate improvement, and 33% mild improvement. Discrepancies in clinical response across studies may stem from the different immune processes involved in neuropathy, which could be primarily related to IBD, secondary to gut microbiota, or coincidental with autoimmune polyneuropathy.[20] CIDP cases have also been reported, but symptom development during CD treatment complicates determinations of whether the neuropathy is primarily due to CD or a secondary iatrogenic complication.[21]

Furthermore, improvement in the neurological symptoms and abnormal electrophysiologic findings after surgical removal of the peri-appendiceal abscess has been reported, which is possibly attributed to the immunomodulatory properties of the appendix.[22]

3.2. Cerebrovascular diseases

Extensive research has illuminated a discernible link between IBD and prothrombotic state, with studies citing a prevalence of thrombosis ranging from 1% to 39% in this patient population.[23,24] Specifically, the incidence of arterial and venous thrombosis is notably elevated in IBD cases, as evidenced by both clinical studies and autopsy findings.[25] Schneiderman *et al.*[26] have contributed to this understanding by identifying thrombus formations in cerebral small vessels during post-mortem examinations of IBD patients who experienced cerebrovascular incidents.

Further, a constellation of clinical, hematological, and pathological evidence supports the notion that a hypercoagulable state in IBD patients markedly increases their risk of cerebrovascular complications such as strokes. Notably, deep vein thrombosis and pulmonary embolism remain prevalent, yet the incidence of cerebral venous thrombosis (CVT) and ischemic arterial strokes suggests these complications are likely underreported. CVT, in particular, poses a severe threat, manifesting as fatal extraintestinal complications of IBD with high morbidity and mortality rates. Symptoms such as persistent headaches, which appear in approximately 90% of CVT cases, along with increased intracranial pressure leading to neurological deficits, highlight the acute dangers of this condition.[26,27]

In terms of diagnostic practices, MRI and venography are considered definitive for identifying CVT, by virtue of their direct visualization of thrombi predominantly in the sagittal and transverse sinuses.[28] The pro-coagulative activity associated with IBD is further complicated by an array of factors including impaired fibrinolysis, thrombocytosis, and endothelial dysfunction. Interestingly, while IBD is associated with higher thromboembolism rates compared to other autoimmune disorders, genetic factors such as factor V Leiden and prothrombin mutations have not been conclusively linked to these thrombotic manifestations.[29,30]

Moreover, the role of intestinal barrier dysfunction in promoting a prothrombotic state has garnered attention. This is illustrated by elevated levels of lipopolysaccharides (LPS) and the activation of Toll-like receptors in IBD, which correlate poorly with clinical disease activity but strongly with intestinal permeability. Such findings offer insights into the complex interplay between IBD pathophysiology and thrombotic risk, emphasizing the need for heightened vigilance and tailored therapeutic strategies in managing these patients.[30,31]

Both TLR2 and TLR4 are crucially expressed by platelets and endothelial cells, with their ligands initiating procoagulant activities within these cells. The interaction between TLR2 and its ligands triggers thrombo-inflammatory responses in platelets through mechanisms involving phosphoinositide 3-kinase, cyclooxygenase, and the activation of purinergic receptors P2Y1 and P2Y12, alongside the release of alpha-granules. Conversely, the binding of LPS to TLR4 enhances traditional agonist-induced aggregation of platelets.[32,33]

Furthermore, the activation of nuclear factor-κB in endothelial cells by TLR2 and TLR4 signaling plays a pivotal role in the production of proinflammatory mediators, which are instrumental in initiating the coagulation cascade. This process is particularly significant in the context of atherosclerosis, where activated macrophages within plaques respond robustly to TLR stimulation,

releasing inflammatory cytokines that contribute to the disease's pathogenesis.[34,35]

In terms of clinical management, the treatment of CVT in patients with IBD is generally administered in adherence to the standard protocols. Preferred treatments include low molecular weight heparin, intravenous heparin, and Vitamin K antagonists. The ongoing debate about the use of corticosteroids in these patients revolves around their ability to reduce procoagulant activity by mitigating inflammation. However, the administration of intravenous steroids has been associated with an increased risk of thromboembolism, necessitating careful monitoring of IBD patients with a significant risk of thrombotic events. Such patients may require short-term anticoagulant prophylaxis, especially when treated with high doses of systemic steroids.[36]

3.3. MG

MG has been observed in association with both UC and CD, with this relationship seemingly rooted in the aberrant function of T-lymphocytes and the production of acetylcholine receptor antibodies due to autoimmune dysregulation. Furthermore, MG coexists with other autoimmune conditions such as alopecia, lichen planus, vitiligo, and systemic lupus erythematosus. Notably, thymus abnormalities, which are characteristic of MG, have also been linked with IBD, particularly through the persistence of thymus function into later age in MG patients, which correlates with similar phenomena in UC. Comparative studies of T-cells from MG and UC patients show a decreased ratio of suppressor (CD8+) to helper (CD4+) T-cells relative to healthy individuals.[37]

The immunological connections between MG and IBD are highlighted through clinical observations, such as the case reported by Finnie *et al.*,[37] where a female patient developed both MG and CD, further complicated by perineal abscesses and fistulas post-total colectomy. The patient's MG, unresponsive to drug therapy, improved after a thymectomy, which also positively influenced her CD. Conversely, Gower-Rousseau *et al.*[38] documented a case where UC and MG coexisted, and the MG symptoms regressed following proctocolectomy.

MG can manifest in either ocular or generalized forms, displaying symptoms such as paresis, dysphagia, dysarthria, and fatigue. For instance, Foroozan and Sambursky[39] described a 21-year-old male with UC and other complications, who exhibited MG symptoms such as binocular diplopia and ptosis, which resolved after treatments including plasmapheresis and medications such as azathioprine and prednisone. Similarly, Gondim *et al.*[40] reported on two patients in a Brazilian IBD cohort who developed severe MG symptoms rapidly post-colectomy, both of whom responded well to treatment with pyridostigmine and prednisone.

Although the simultaneous presence of these autoimmune diseases in patients is rare, it is crucial to recognize that symptoms such as ocular, bulbar, or limb impairments might be early indicators of MG in IBD patients, especially following alterations in their immunosuppressive regimen.

3.4. Myositis

The occurrence of polymyositis, dermatomyositis, and localized forms of myositis in patients with IBD underscores its systemic nature. These myopathic conditions, though rare, are significant due to their potential impact on morbidity and quality of life.

4. Polymyositis and dermatomyositis

Polymyositis and dermatomyositis are autoimmune diseases characterized by inflammation of the muscles, with dermatomyositis also involving skin manifestations. The association between these conditions and IBD, particularly CD and UC, suggests a shared autoimmune or inflammatory pathway. Despite that, the exact prevalence is unknown, probably due to the rarity of these conditions. However, isolated occurrences of these disorders have been highlighted in case reports.[2] The pathophysiological link between IBD and these myopathies may involve shared immunological mechanisms. Inflammatory cytokines, which are elevated in IBD, could potentially trigger or exacerbate the autoimmune responses seen in polymyositis and dermatomyositis. This is supported by the observation that these conditions can flare with intestinal disease and may improve with treatment of bowel inflammation. Using a large population-based electronic health database from Israel, a recent retrospective cohort study analyzed the association between IBD and polymyositis/dermatomyositis and determined the prevalence of IBD in those with polymyositis/dermatomyositis by assessing data from 2085 polymyositis/dermatomyositis patients and 10,193 matched controls.[40] The findings suggest a statistically significant association between polymyositis/dermatomyositis and IBD, with an increased prevalence of IBD in patients with polymyositis/dermatomyositis, even after adjusting for variables such as age, gender, socioeconomic status, and BMI. Patients with polymyositis/dermatomyositis had 1.73-time higher odds of having IBD compared to controls. Moreover, the presence of antinuclear antibodies in polymyositis/dermatomyositis patients was identified as a significant predictor for the development of IBD.

5. Localized forms of myositis in IBD

Localized myositis in IBD presents as inflammation confined to specific muscle groups, leading to symptoms

such as focal muscle pain, tenderness, and swelling. Similar to polymyositis and dermatomyositis, localized forms of myositis are uncommon in IBD, and specific prevalence data are lacking. Case reports in the literature provide some insights but are too few to establish a clear epidemiological pattern. These reports often describe patients presenting with muscle pain and swelling that were initially attributed to more common IBD-related arthralgia but were later identified as localized myositis upon further investigation. Hayashi *et al.*[41] reported a case of a young male presenting with myalgias and weakness, who was found to have elevated creatinine kinase levels and localized myositis. A meticulous test and observation must be conducted to identify these pathological aberrations. The mechanism likely involves localized immune responses, possibly mediated by cytokines or immune complexes that specifically target muscle tissues. This localized inflammation could be a direct extension of the systemic immune dysregulation observed in IBD.

The management of myositis in the context of IBD involves both treating the muscle inflammation and managing the underlying intestinal disease. Corticosteroids and immunosuppressants are commonly used to reduce muscle inflammation, whereas comprehensive IBD management is crucial to control systemic inflammation. Early diagnosis and timely intervention, which are critical to prevent irreversible muscle damage and disability in IBD patients, can be achieved with regular monitoring for musculoskeletal symptoms, with the aim of improving clinical outcomes.

In summary, while polymyositis, dermatomyositis, and localized myositis are rare in IBD, their impact on patients can be profound. Understanding their associations, recognizing the clinical presentations, and implementing a coordinated management strategy are key to improving the quality of life for these patients. Further research and more detailed case reporting are needed to better understand the epidemiology and pathophysiology of these disorders.

5.1. Epilepsy

Epilepsy, a complex neurological disorder marked by spontaneous recurrent seizures, is influenced by multiple factors including genetic predisposition, developmental issues, and neurological trauma.[42] These factors facilitate synaptic alterations and heightened neuronal excitability, contributing to epileptogenesis – the process of developing epilepsy. While the exact cellular and molecular mechanisms remain somewhat elusive, it is hypothesized that uncontrolled inflammatory responses, both focal and systemic, may drive the formation of a hyper-excitable neuronal network, thus precipitating the onset of epilepsy.[43] Systemic inflammatory conditions such as systemic lupus erythematosus, rheumatoid arthritis, or IBD are believed to be responsible for the impairment of the blood–brain barrier, which potentially exacerbates epileptogenesis. Studies in animal models suggest that intestinal inflammation can lower seizure thresholds by elevating levels of inflammatory mediators such as cytokines.[44,45] Furthermore, a link between intestinal dysbiosis and seizure activity has been established; fecal microbiota transplantation (FMT) from stressed rats to naïve rats was found to induce pro-epileptic effects, whereas FMT from naïve rats to stressed rats appeared to decrease seizure incidence.[46]

Despite these findings, seizures associated with IBD are generally attributed to metabolic disturbances and structural issues rather than to IBD itself. Factors such as dyselectrolytemia, infections, CVT, and medication toxicity are recognized triggers of epilepsy in IBD patients. Prevalence studies reveal varying epilepsy rates among IBD patients, with 1.1 – 5.9% in CD patients and 0.9% in UC patients.[30] Studies indicate that EEG abnormalities are more prevalent among CD patients compared to healthy controls, with a significant portion exhibiting epileptiform disturbances, albeit in the absence of infections, organic anomalies, or medications known to lower seizure thresholds.[47]

The treatment of epilepsy in IBD patients adheres to standard protocols; however, the role of gut microbiota in neurological disorders is garnering interest, particularly in refractory epilepsy. Interventions such as the ketogenic diet, probiotics, prebiotics, antibiotics, and even FMT are being explored as potential strategies for managing drug-resistant epilepsy.[48] Concurrently, vagus nerve stimulation, already a therapeutic option for epilepsy, shows promise in IBD treatment, as shown in animal studies and preliminary human trials. Yet, the application of these treatments in IBD remains contentious due to limited and inconclusive study results.[49]

5.2. Demyelinating disorders

Demyelinating diseases are infrequently observed in IBD patients and can be categorized into those caused by a primary autoimmune mechanism, with MS being the most prevalent, and those associated with the administration of biological therapy.[50] MS symptoms can vary widely among individuals and may impact any part of the nervous system. Common symptoms include fatigue, mobility difficulties, visual impairments, numbness or tingling, muscular stiffness and spasms, and challenges with balance and coordination. MS may manifest before or during the course of IBD. Diagnosing MS in patients with IBD is often complex due

to the commonality of non-specific white matter changes on MRIs and other demyelinating disorders linked to biological treatments.[51] The correlation between MS and IBD has been long suspected and supported by genetic studies, which have identified multiple genetic links between MS and CD through common single nucleotide polymorphisms.[52] These diseases share similar demographics, clinical manifestations, and geographical distributions, yet the exact pathophysiological links remain elusive. There is also evidence suggesting a shared immunologic origin based on the clustering of chronic inflammatory diseases.[53] Moreover, the recent hypothesis posits a role of the microbiome in MS pathogenesis, indicated by elevated antibody responses to GI antigens in MS patients, suggesting a potential overlap in pathogenic mechanisms or co-occurrence.[54]

Furthermore, there may be a reciprocal relationship between IBD and MS. Recent research suggests that the microbiome may play a significant role in the development of MS. Studies indicate that MS patients exhibit a higher frequency of antibody responses to GI antigens than healthy individuals. However, whether this heightened immune reaction, targeting substances such as gliadin, tissue transglutaminase, intrinsic factor, parietal cells, and *Saccharomyces cerevisiae*, stems from a common pathogenic origin or merely coincidental coexistence remains to be clarified.[55] Further research is necessary to determine if these increased antibody levels correlate with changes in the gut microbiota and related T-cell responses. The prevalence of GI among patients with these antibodies may also signal dysfunction within the digestive system. Research by Banati *et al.*[55] has demonstrated the presence of GI antibodies in MS patients, suggesting that the immune system, while typically benign, becomes aggressively auto-reactive under pathological conditions. This shift is often linked to environmental factors, particularly microbial infections. Berer *et al.*[54] have shown that even in the absence of pathogens, the normal gut flora can activate myelin-specific CD4+ T cells, potentially triggering relapses in experimental autoimmune encephalomyelitis.

Managing MS in patients with IBD is complex, requiring meticulous drug selection. Both conditions respond to steroids, but the rising number of patients developing steroid dependence necessitates careful escalation of treatment. TNFα inhibitors are typically ineffective in MS and may exacerbate IBD, whereas interferons can worsen IBD symptoms. Conversely, natalizumab has proven effective for both conditions, though its use is limited in IBD patients due to the risk of developing leukoencephalopathy. Thus, treatment must be customized for each individual, with careful monitoring of adverse effects to prevent complications.[56]

5.3. Related medications

IBD can be treated with various medications. Most of them have been reported to result in various neurological manifestations as summarized in Table 1.

Corticosteroids such as prednisone are frequently employed in the acute management of IBD due to their potent anti-inflammatory effects. However, their side effects are numerous and can be severe, particularly with long-term use. These include osteoporosis, adrenal suppression, hyperglycemia, increased susceptibility to infection, and psychiatric disturbances such as mood swings and psychosis. Corticosteroids can also increase the risk of cataracts, skin thinning, and easy bruising. The risk of infection is particularly concerning, as corticosteroids can mask the symptoms of severe infections, potentially leading to delayed diagnosis and management.[35]

Immunosuppressants, including azathioprine and methotrexate, play a crucial role in maintaining remission in IBD. Azathioprine can lead to leukopenia, hepatotoxicity, and an increased risk of lymphoma. It may also cause nausea, vomiting, and pancreatitis in some patients. Methotrexate, known for its efficacy in reducing the need for steroids, carries risks of hepatotoxicity, pulmonary toxicity, and myelosuppression. Since it is teratogenic, both

Table 1. Complications of therapeutic agents for IBD

Medication	Side effects
Mesalamine	Peripheral neuropathy, Guillain–Barré syndrome, headache, dizziness, confusion, and seizures
Steroids	Myopathy, tremor, insomnia, psychosis, and posterior reversible encephalopathy syndrome
Metronidazole	Headache, dizziness and vertigo, ataxia, irritability, insomnia, confusion, seizures, posterior reversible encephalopathy syndrome, tremors, and peripheral neuropathy (sensory and ataxic or autonomic)
Sulfasalazine	Encephalopathy and peripheral neuropathy
Anti-TNFα agents (infliximab, adalimumab, and certolizumab)	Ischemic stroke, posterior reversible encephalopathy syndrome, vasculitis, TNFα-induced lupus with vasculitis, demyelinating diseases, optic neuritis, acute disseminated encephalomyelitis, multiple sclerosis-like polyneuropathy, Guillan–Barre syndrome, and progressive multifocal leukoencephalopathy
Anti-α4 integrin (natalizumab)	Progressive multifocal leukoencephalopathy
Cyclosporine A	Peripheral and central neuropathy
Tofacitinib	Reversible multifocal CNS demyelination

Abbreviations: CNS: Central nervous system; IBD: Inflammatory bowel disease.

men and women of childbearing potential should stop taking the drug for a period before conceiving.[55]

Biologic therapies targeting specific immune pathways have transformed the treatment for IBD. TNFα inhibitors such as infliximab and adalimumab are associated with serious infections, including tuberculosis, and opportunistic infections such as histoplasmosis. There is also a potential for inducing or exacerbating demyelinating diseases and a slight increase in the risk of malignancy, particularly lymphoma. Natalizumab, used primarily in CD, carries a risk of PML, a rare but often fatal brain infection caused by the John Cunningham virus. Mitigating such risk necessitates strict monitoring and limited usage in patients who do not respond to other treatments.[11]

Vedolizumab, an anti-integrin agent, targets gut-specific lymphocyte trafficking and is associated with fewer systemic infections. However, its side effects include nasopharyngitis, headache, and arthralgia. Its gut-selective action reduces the risk of systemic immunosuppression, but data on the long-term safety of vedolizumab are still lacking.[57]

Ustekinumab, which targets the p40 subunit of IL-12 and IL-23, is another biologic used in CD treatment. It has a relatively mild side effect profile, with the most common adverse effects being injection site reactions and respiratory infections. However, the long-term impact on immune function and the potential for serious infections remains a concern.

The administration of anti-TNFα agents such as infliximab and adalimumab has been implicated in the induction or exacerbation of these conditions. Although TNFα antagonists are effective in controlling the inflammatory processes of IBD, they may disrupt immune homeostasis in the CNS, potentially unmasking or aggravating demyelinating processes. The pathogenic mechanisms are not entirely understood, but it is hypothesized that altering TNFα signaling could interfere with neuroprotective pathways or enhance autoimmune responses against myelin or other CNS components.[57]

Guillain–Barré syndrome and Miller–Fisher syndrome represent acute inflammatory demyelinating polyneuropathies that have also been associated with the use of TNFα inhibitors in IBD patients. These conditions typically manifest with rapid onset of muscle weakness and are thought to result from a maladaptive immune response following infection or immunotherapy. The link between TNFα blockade and these peripheral neuropathies suggests a complex interaction between the drug-induced modulation of immune function and the PNS's susceptibility to immune-mediated injury.[30]

PML is a particularly severe neurological complication associated with immunosuppressive therapy in IBD, notably with the use of natalizumab. This disorder is caused by the reactivation of the John Cunningham virus within the CNS, leading to progressive and often fatal demyelination. Patients with compromised immune surveillance face an increased risk of PML, which can be a consequence of both the underlying IBD and the immunomodulatory effects of biological therapies. The management of PML requires vigilant monitoring for early signs of neurological impairment and may necessitate discontinuation of the offending agent if PML is suspected.[58]

Taken together, the management of IBD with these medications requires a careful consideration of their potential side effects. Clinicians must balance the benefits of these medications against their risks, tailoring therapy to individual patient needs and closely monitoring for adverse effects. This approach is crucial for minimizing complications and achieving optimal outcomes in the treatment of IBD.

6. Conclusion

The neurological manifestations associated with IBD are diverse and complex, with significant implications for patient management and quality of life. This review article highlights the neurological manifestations of IBD, which affect both the CNS and PNS, ranging from common conditions such as peripheral neuropathy to less frequent but severe complications such as cerebrovascular diseases and myopathies.

The pathophysiology underlying these neurological manifestations is multifaceted, involving immune-mediated mechanisms, vascular abnormalities, nutritional deficiencies, and neurotoxic effects of certain medications used in the treatment of IBD. This complexity underscores the importance of a multidisciplinary approach in treating IBD patients, involving gastroenterologists, neurologists, and other specialists to address a wide range of potential neurological complications.

Furthermore, the management of neurological manifestations in IBD presents unique challenges. It requires not only treating the neurological symptoms themselves but also carefully managing the underlying IBD to minimize inflammation and potential triggers of neurological complications. Adjusting therapeutic strategies to avoid exacerbating existing conditions or precipitating new ones is crucial, particularly in the use of medications such as anti-TNFα agents, which may worsen or trigger demyelinating disorders.

This review highlights the need for increased awareness and a better understanding of the neurological aspects

of IBD. Early recognition and appropriate management of neurological symptoms can significantly improve patient outcomes. Moreover, ongoing research into the mechanisms linking IBD with neurological complications will be vital for developing more effective strategies for prevention and treatment.

Ultimately, enhancing our understanding of the neurological manifestations of IBD will lead to more comprehensive care strategies, which reduce the burden of these complications on patients and improve their overall quality of life. As such, continued interdisciplinary research collaboration is essential to advance our knowledge and improve the techniques used in managing patients with these complications.

Acknowledgments

None.

Funding

None.

Conflict of interest

The authors declare they have no competing interests.

Author contributions

Conceptualization: Manjeet Kumar Goyal, Ashita Rukmini Vuthaluru

Writing–original draft: Manjeet Kumar Goyal, Ashita Rukmini Vuthaluru

Writing–review & editing: Shivam Kalra, Abhinav Rao, Abhinav Gupta, Manisha Khubber

Ethics approval and consent to participate

Not applicable.

Consent for publication

Not applicable.

Availability of data

Not applicable.

References

1. Ott C, Schölmerich J. Extraintestinal manifestations and complications in IBD. *Nat Rev Gastroenterol Hepatol*. 2013;10(10):585-595.

   doi: 10.1038/nrgastro.2013.117

2. Ferro JM, Oliveira Santos M. Neurology of inflammatory bowel disease. *J Neurol Sci*. 2021;424:117426.

   doi: 10.1016/j.jns.2021.117426

3. Benavente L, Morís G. Neurologic disorders associated with inflammatory bowel disease. *Eur J Neurol*. 2011;18(1):138-143.

   doi: 10.1111/j.1468-1331.2010.03095.x

4. Lossos A, River Y, Eliakim A, Steiner I. Neurologic aspects of inflammatory bowel disease. *Neurology*. 1995;45(3 Pt 1):416-421.

   doi: 10.1212/wnl.45.3.416

5. Morís G. Inflammatory bowel disease: An increased risk factor for neurologic complications. *World J Gastroenterol*. 2014;20(5):1228-1237.

   doi: 10.3748/wjg.v20.i5.1228

6. Elsehety A, Bertorini TE. Neurologic and neuropsychiatric complications of Crohn's disease. *South Med J*. 1997;90(6):606-610.

   doi: 10.1097/00007611-199706000-00005

7. Sassi SB, Kallel L, Ben Romdhane S, Boubaker J, Filali A, Hentati F. Peripheral neuropathy in inflammatory bowel disease patients: A prospective cohort study. *Scand J Gastroenterol*. 2009;44(10):1268-1269.

   doi: 10.1080/00365520903199871

8. Oliveira GR, Teles BCV, Brasil EF, *et al*. Peripheral neuropathy and neurological disorders in an unselected Brazilian population-based cohort of IBD patients. *Inflamm Bowel Dis*. 2008;14(3):389-395.

   doi: 10.1002/ibd.20304

9. Geissler A, Andus T, Roth M, *et al*. Focal white-matter lesions in brain of patients with inflammatory bowel disease. *Lancet*. 1995;345(8954):897-898.

   doi: 10.1016/s0140-6736(95)90013-6

10. Zikou AK, Kosmidou M, Astrakas LG, Tzarouchi LC, Tsianos E, Argyropoulou MI. Brain involvement in patients with inflammatory bowel disease: A voxel-based morphometry and diffusion tensor imaging study. *Eur Radiol*. 2014;24(10):2499-2506.

    doi: 10.1007/s00330-014-3242-6

11. Singh A, Goyal MK, Midha V, *et al*. Tofacitinib in acute severe ulcerative colitis (TACOS): A randomized controlled trial. *Am Coll Gastroenterol*. 2024;119:1365-1372.

    doi: 10.14309/ajg.0000000000002635

12. Bonaz BL, Bernstein CN. Brain-Gut interactions in inflammatory bowel disease. *Gastroenterology*. 2013;144(1):36-49.

    doi: 10.1053/j.gastro.2012.10.003

13. Ferro JM, Oliveira SN, Correia L. Neurologic manifestations of inflammatory bowel diseases. *Handb Clin Neurol*. 2014;120:595-605.

    doi: 10.1016/B978-0-7020-4087-0.00040-1

14. Zois CD, Katsanos KH, Kosmidou M, Tsianos EV. Neurologic manifestations in inflammatory bowel diseases: Current knowledge and novel insights. *J Crohns Colitis*. 2010;4(2):115-124.

doi: 10.1016/j.crohns.2009.10.005

15. Babali A, Terzoudi A, Vadikolias K, *et al*. Peripheral neuropathy electrophysiological screening in inflammatory bowel disease. *Eur J Gastroenterol Hepatol*. 2013;25(5):539-542.

doi: 10.1097/MEG.0b013e32835ceca6

16. Nemati R, Mehdizadeh S, Salimipour H, *et al*. Neurological manifestations related to Crohn's disease: A boon for the workforce. *Gastroenterol Rep* (*Oxf*). 2019;7(4):291-297.

doi: 10.1093/gastro/gox034

17. Wang Y, Kasper LH. The role of microbiome in central nervous system disorders. *Brain Behav Immun*. 2014;38:1-12.

doi: 10.1016/j.bbi.2013.12.015

18. Didesch MM, Averill A, Oh-Park M. Peripheral neuropathy after fecal microbiota transplantation for *Clostridium difficile* infection: A case report. *PM R*. 2016;8(8):813-816.

doi: 10.1016/j.pmrj.2016.01.009

19. Romijn JA, Corssmit EP, Havekes LM, Pijl H. Gut-brain axis. *Curr Opin Clin Nutr Metab Care*. 2008;11(4):518-521.

doi: 10.1097/MCO.0b013e328302c9b0

20. Spagnoli C, Pisani F, Di Mario F, *et al*. Peripheral neuropathy and gastroenterologic disorders: An overview on an underrecognized association. *Acta Biomed*. 2018;89(Suppl 9):22-32.

doi: 10.23750/abm.v89i9-S.7956

21. Gondim FAA, Brannagan TH 3rd, Sander HW, Chin RL, Latov N. Peripheral neuropathy in patients with inflammatory bowel disease. *Brain*. 2005;128(Pt 4):867-879.

doi: 10.1093/brain/awh429

22. Kim S, Kang SJ, Oh KW, *et al*. Chronic inflammatory demyelinating polyneuropathy-like neuropathy as an initial presentation of Crohn's disease. *BMC Neurol*. 2015;15(1):48.

doi: 10.1186/s12883-015-0302-8

23. Fumery M, Singh S, Dulai PS, Gower-Rousseau C, Peyrin-Biroulet L, Sandborn WJ. Natural history of adult ulcerative colitis in population-based cohorts: A systematic review. *Clin Gastroenterol Hepatol*. 2018;16(3):343-356.e3.

doi: 10.1016/j.cgh.2017.06.016

24. Grainge MJ, West J, Card TR. Venous thromboembolism during active disease and remission in inflammatory bowel disease: A cohort study. *Lancet*. 2010;375(9715):657-663.

doi: 10.1016/S0140-6736(09)61963-2

25. Schneiderman JH, Sharpe JA, Sutton DM. Cerebral and retinal vascular complications of inflammatory bowel disease. *Ann Neurol*. 1979;5(4):331-337.

doi: 10.1002/ana.410050405

26. Jackson LM, O'Gorman PJ, O'Connell J, Cronin CC, Cotter KP, Shanahan F. Thrombosis in inflammatory bowel disease: Clinical setting, procoagulant profile and factor V Leiden. *QJM*. 1997;90(3):183-188.

doi: 10.1093/qjmed/90.3.183

27. Goyal MK, Porwal YC, Gogna A, Gulati S. Splenic infarct with scrub typhus: A rare presentation. *Trop Doct*. 2019;50:234-236.

doi: 10.1177/0049475519892092

28. Cognat E, Crassard I, Denier C, Vahedi K, Bousser MG. Cerebral venous thrombosis in inflammatory bowel diseases: Eight cases and literature review. *Int J Stroke*. 2011;6(6):487-492.

doi: 10.1111/j.1747-4949.2011.00620.x

29. Cho JM, Yang HR. Hair mineral and trace element contents as reliable markers of nutritional status compared to serum levels of these elements in children newly diagnosed with inflammatory bowel disease. *Biol Trace Elem Res*. 2018;185(1):20-29.

doi: 10.1007/s12011-017-1225-6

30. Casella G, Tontini GE, Bassotti G, *et al*. Neurological disorders and inflammatory bowel diseases. *World J Gastroenterol*. 2014;20(27):8764-8782

doi: 10.3748/wjg.v20.i27.8764

31. Lee J, Hwang SW, Lee J, *et al*. A case of ulcerative colitis presenting with cerebral venous thrombosis. *Intest Res*. 2018;16(2):306-311.

doi: 10.5217/ir.2018.16.2.306

32. Karmiris K, Bossuyt P, Sorrentino D, *et al*. Cerebrovascular events in inflammatory bowel disease patients treated with anti-tumour necrosis factor alpha agents. *J Crohns Colitis*. 2015;9(5):382-389.

doi: 10.1093/ecco-jcc/jjv042

33. Oldenburg B, Fijnheer R, van der Griend R, vanBerge-Henegouwen GP, Koningsberger JC. Homocysteine in inflammatory bowel disease: A risk factor for thromboembolic complications? *Am J Gastroenterol*. 2000;95(10):2825-2830.

doi: 10.1111/j.1572-0241.2000.03193.x

34. Miehsler W, Reinisch W, Valic E, *et al*. Is inflammatory bowel disease an independent and disease specific risk factor for thromboembolism? *Gut*. 2004;53(4):542-548.

doi: 10.1136/gut.2003.025411

35. Stolz E, Klötzsch C, Schlachetzki F, Rahimi A. High-dose corticosteroid treatment is associated with an increased risk of developing cerebral venous thrombosis. *Eur Neurol*. 2003;49(4):247-248.

doi: 10.1159/000070197

36. Pastorelli L, Dozio E, Pisani LF, *et al*. Procoagulatory state in inflammatory bowel diseases is promoted by impaired intestinal barrier function. *Gastroenterol Res Pract*. 2015;2015:189341.

doi: 10.1155/2015/189341

37. Finnie IA, Shields R, Sutton R, Donnelly R, Morris AI. Crohn's disease and myasthenia gravis: A possible role for thymectomy. *Gut*. 1994;35(2):278-279.

doi: 10.1136/gut.35.2.278

38. Gower-Rousseau C, Reumaux D, Bellard M, Delecourt L, Ribet M, Colombel JF. Remission of myasthenia gravis after proctocolectomy in a patient with ulcerative colitis. *Am J Gastroenterol*. 1993;88(7):1136-1138.

39. Foroozan R, Sambursky R. Ocular myasthenia gravis and inflammatory bowel disease: A case report and literature review. *Br J Ophthalmol*. 2003;87:1186-1187.

doi: 10.1136/bjo.87.9.1186

40. Gondim FAA, de Oliveira GR, Araújo DF, Souza MHL, Braga LLB, Thomas FP. Two patients with co-morbid myasthenia gravis in a Brazilian cohort of inflammatory bowel disease. *Neuromuscul Disord*. 2014;24(11):999-1002.

doi: 10.1016/j.nmd.2014.06.434

41. Hayashi K, Kurisu Y, Ohshiba S, *et al*. Report of a case of Crohn's disease associated with hyper-creatine phosphokinase-emia. *Jpn J Med*. 1991;30(5):441-445.

doi: 10.2169/internalmedicine1962.30.441

42. Rakhade SN, Jensen FE. Epileptogenesis in the immature brain: Emerging mechanisms. *Nat Rev Neurol*. 2009;5(7):380-391.

doi: 10.1038/nrneurol.2009.80

43. Musto AE, Walker CP, Petasis NA, Bazan NG. Hippocampal neuro-networks and dendritic spine perturbations in epileptogenesis are attenuated by neuroprotectin D1. *PLoS One*. 2015;10(1):e0116543.

doi: 10.1371/journal.pone.0116543

44. Rana A, Musto AE. The role of inflammation in the development of epilepsy. *J Neuroinflammation*. 2018;15(1):144.

doi: 10.1186/s12974-018-1192-7

45. Goyal MK, Singh A, Kumar Gupta Y, Kaur Dhaliwal K, Sood A. Lenvatinib-induced tumor lysis syndrome in advanced hepatocellular carcinoma. *ACG Case Rep J*. 2023;10(9):e01139.

doi: 10.14309/crj.0000000000001139

46. Musto AE, Rosencrans RF, Walker CP, *et al*. Dysfunctional epileptic neuronal circuits and dysmorphic dendritic spines are mitigated by platelet-activating factor receptor antagonism. *Sci Rep*. 2016;6(1):30298.

doi: 10.1038/srep30298

47. De Caro C, Leo A, Nesci V, *et al*. Intestinal inflammation increases convulsant activity and reduces antiepileptic drug efficacy in a mouse model of epilepsy. *Sci Rep*. 2019;9(1):13983.

doi: 10.1038/s41598-019-50542-0

48. Nunes NS, Chandran P, Sundby M, *et al*. Therapeutic ultrasound attenuates DSS-induced colitis through the cholinergic anti-inflammatory pathway. *EBioMedicine*. 2019;45:495-510.

doi: 10.1016/j.ebiom.2019.06.033

49. Elliott RE, Rodgers SD, Bassani L, *et al*. Vagus nerve stimulation for children with treatment-resistant epilepsy: A consecutive series of 141 cases. *J Neurosurg Pediatr*. 2011;7(5):491-500.

doi: 10.3171/2011.2.PEDS10505

50. Kimura K, Hunter SF, Thollander MS, *et al*. Concurrence of inflammatory bowel disease and multiple sclerosis. *Mayo Clin Proc*. 2000;75(8):802-806.

doi: 10.4065/75.8.802

51. Chen X, Wang S, Mao X, *et al*. Adverse health effects of emerging contaminants on inflammatory bowel disease. *Front Public Health*. 2023;11:1140786.

doi: 10.3389/fpubh.2023.1140786

52. Cotsapas C, Voight BF, Rossin E, *et al*. Pervasive sharing of genetic effects in autoimmune disease. *PLoS Genet*. 2011;7(8):e1002254.

doi: 10.1371/journal.pgen.1002254

53. Gupta G, Gelfand JM, Lewis JD. Increased risk for demyelinating diseases in patients with inflammatory bowel disease. *Gastroenterology*. 2005;129(3):819-826.

doi: 10.1053/j.gastro.2005.06.022

54. Berer K, Mues M, Koutrolos M, *et al*. Commensal microbiota and myelin autoantigen cooperate to trigger autoimmune demyelination. *Nature*. 20116;479(7374):538-541.

doi: 10.1038/nature10554

55. Banati M, Csecsei P, Koszegi E, *et al*. Antibody response against gastrointestinal antigens in demyelinating diseases of the central nervous system. *Eur J Neurol*. 2013;20(11):1492-1495.

doi: 10.1111/ene.12072

56. Nelson SM, Nguyen TM, McDonald JW, MacDonald JK. Natalizumab for induction of remission in Crohn's disease. *Cochrane Database Syst Rev*. 2018;8(8):CD006097.

doi: 10.1002/14651858.CD006097.pub3

57. Riazi K, Galic MA, Kuzmiski JB, Ho W, Sharkey KA, Pittman QJ. Microglial activation and TNFalpha production mediate altered CNS excitability following peripheral inflammation. *Proc Natl Acad Sci U S A*. 2008;105(44):17151-17156.

doi: 10.1073/pnas.0806682105

58. Sandborn WJ, Su C, Sands BE, *et al*. Tofacitinib as induction and maintenance therapy for ulcerative colitis. *N Engl J Med*. 2017;376(18):1723-1736.

doi: 10.1056/NEJMoa1606910

ACCSCIENCE PUBLISHING

Brain & Heart

REVIEW ARTICLE

Unlocking the potential of tafamidis in treating transthyretin cardiac amyloidosis: A systematic review

Heet N. Desai[1]*, Riti Sanghvi[2], and Sarthak H. Dhruv[3]

[1]Department of Internal Medicine, California Institute of Behavioral Neurosciences and Psychology, United States of America

[2]Department of Medicine, Grant Government Medical College, Mumbai, Maharashtra, India

[3]Department of Medicine, Dhruv Hospital, Rajkot, Gujarat, India

Abstract

Cardiac amyloidosis has gained increasing attention in recent years due to substantial advancements in diagnostic techniques and treatment options. Among the most notable developments in this field is the approval of tafamidis by the U.S. Food and Drug Administration in May 2019 for treating transthyretin amyloid cardiomyopathy (ATTR-CM). This marked a pivotal step forward in managing this complex condition. This systematic review aimed to comprehensively analyze the efficacy of tafamidis in treating ATTR-CM and determine its broader applications, with a focus on its impact on patient outcomes, optimal dosing strategies, and side effect profiles. We strictly adhered to the Preferred Reporting Items for Systematic Reviews and Meta-Analyses 2020 guidelines, ensuring that the methodology was transparent and rigorous. This review involved an extensive search of multiple databases, including PubMed and Google Scholar, for relevant articles published between January 1, 2014 and January 9, 2024. After a comprehensive screening and quality assessment process, 16 high-quality articles were identified and included in the final analysis. These articles provided abundant data on the clinical outcomes associated with tafamidis use in ATTR-CM. The findings of our review highlight the transformative role of tafamidis in the treatment of ATTR-CM. The drug not only improves the quality of life of patients by significantly alleviating symptoms but also markedly reduces hospitalization rates and all-cause mortality. Tafamidis showed an impressive safety profile across different dosage levels, representing a key therapeutic option. As the use of tafamidis continues to expand in clinical practice, its potential to improve short- and long-term outcomes in patients with ATTR-CM becomes increasingly evident.

Keywords: Tafamidis; Benzoxazole; Cardiac amyloidosis; Transthyretin amyloid cardiomyopathy

***Corresponding author:**
Heet N. Desai
(hdesai879@gmail.com)

Citation: Desai HN, Sanghvi R, Dhruv SH. Unlocking the potential of tafamidis in treating transthyretin cardiac amyloidosis: A systematic review. *Brain & Heart*. 2024;2(4):4250. doi: 10.36922/bh.4250

Received: July 15, 2024

Accepted: September 24, 2024

Published Online: November 5, 2024

1. Introduction

Cardiac amyloidosis (CA) is a type of heart disease characterized by abnormal deposition of amyloid fibrils within the myocardial tissue, leading to heart failure (HF). In the early stages, this condition often presents as HF with a preserved ejection fraction. However, as the disease progresses, patients may experience HF with a reduced ejection fraction

and left ventricular hypertrophy.[1] In postmortem studies, amyloid deposits have been detected in approximately 25% of unselected older patients. However, owing to the non-specific nature of the symptoms, CA is often underdiagnosed. In addition, 13 – 19% of individuals suffering from HF with a preserved ejection fraction present with amyloid involvement.[1] Fatigue and dyspnea are common symptoms of HF in older adults. These manifestations should prompt physicians to consider CA in their differential diagnosis, as these signs are frequently observed in patients with this condition. Amyloid fibrils can also accumulate in the atrium and conduction system, causing arrhythmias, heart block, and atrial tachycardias, including atrial fibrillation, thus further complicating the clinical picture. CA, particularly in older patients with HF, has been increasingly recognized among the medical community.[2]

The pathophysiology of CA involves the accumulation of misfolded proteins within the myocardium, resulting in restrictive cardiomyopathy. One of the key proteins involved in this process is transthyretin (TTR), a protein produced primarily in the liver. TTR plays a crucial role in the transport of thyroxine and retinol-binding proteins. However, under pathological conditions, TTR can misfold, leading to the formation of amyloid fibrils that are deposited in the heart and other organs.[3]

Structurally, TTR is a homotetramer composed of four identical monomers, each comprising 127 amino acids arranged in a barrel-like structure. As the dissociation of the TTR tetramer into monomers is the rate-limiting step in amyloid formation, the stability of the TTR tetramer is critical.[3] Once dissociated, the misfolded TTR monomers aggregate into amyloid fibrils, which are then deposited in the myocardium, leading to TTR amyloid cardiomyopathy (ATTR-CM).[4] The amyloidogenic potential of TTR is exacerbated by aging, which may explain the increased prevalence of CA in older populations. Amyloid deposits formed from TTR are classified into two main types: wild-type ATTR (ATTRwt) and variant ATTR (ATTRv). ATTRwt, also referred to as senile CA, occurs sporadically in older individuals, whereas ATTRv is an inherited type of disease caused by mutations in the TTR gene.[4,5]

In recent years, ATTR-CM has gained significant attention due to its increasing prevalence as well as advancements in diagnostic methods and the introduction of targeted therapies. Traditional methods for diagnosing CA involved invasive procedures such as endomyocardial biopsy. However, recent innovations, such as non-invasive nuclear scintigraphy, allow the diagnosis of ATTR-CM without the need for biopsy.[6,7] These advancements have led to a paradigm shift in the way clinicians approach ATTR-CM. Once considered a rare and untreatable condition, ATTR-CM is now increasingly recognized as a disease that can be diagnosed and treated, thereby significantly improving patient outcomes.[8,9] Considering the median survival rate of 2 – 6 years after diagnosis, early identification and intervention are crucial to improving the quality of life and survival of patients with ATTR-CM.[10,11]

The primary goals of treating ATTR-CM are to improve organ function, manage symptoms, and slow or halt disease progression. Traditional HF therapies, such as beta-blockers and angiotensin-converting enzyme inhibitors or angiotensin II receptor blockers, which address the symptoms of HF, do not target the underlying cause of amyloid deposition.[10] Consequently, a significant focus has been placed on developing disease-modifying therapies that directly address the pathology of ATTR-CM. Current treatments for ATTR-CM aim to either reduce the production of TTR or stabilize the TTR tetramer, thereby preventing its dissociation and subsequent amyloid fibril formation.[2]

Tafamidis, a TTR stabilizer that has been shown to significantly improve outcomes in patients with ATTR-CM, is one of the most promising treatment options. The drug mediates its action by binding to the thyroxine-binding site on the TTR tetramer, which stabilizes the protein and prevents it from dissociating into amyloidogenic monomers.[7] The landmark ATTR-ACT trial demonstrated the efficacy of tafamidis in treating ATTR-CM. In particular, the results showed that tafamidis significantly reduces the mortality and functional decline rates in patients with ATTR-CM.[12] The trial included patients with the wild-type and variant forms of ATTR-CM and found that tafamidis improved survival rates and reduced the number of cardiovascular event-related hospitalizations. Importantly, tafamidis was also shown to improve the quality of life of patients by slowing the progression of functional limitations, thereby allowing patients to maintain their independence for longer periods.[12]

In light of these findings, tafamidis has emerged as the first Food and Drug Administration-approved treatment for ATTR-CM, representing a major milestone in the management of this condition. Considering its ability to stabilize TTR and prevent amyloid deposition, tafamidis is considered a cornerstone of therapy for patients with ATTR-CM.[7] However, despite its efficacy, tafamidis is not a curative option. Although the drug can slow disease progression, it does not reverse existing amyloid deposits, highlighting the importance of early diagnosis and intervention.[8]

CA is a complex condition that is frequently undiagnosed, particularly in older patients with HF. The development of

tafamidis as a targeted therapy for ATTR-CM represents a significant advancement in this field. This drug may offer improved outcomes in affected patients. This systematic review underscores the importance of early detection and timely intervention as well as the need for continued research into additional therapies that can further improve the prognosis of patients with this debilitating disease.[13] The use of tafamidis, coupled with advancements in non-invasive diagnostic techniques, has transformed ATTR-CM from a rare, incurable condition into a treatable and increasingly recognized condition, leading to better patient outcomes and prolonged survival.

2. Methods

2.1. Objective

This systematic review aimed to present comprehensive evidence regarding tafamidis as a novel therapeutic agent for ATTR-CM. This review was conducted in accordance with the Preferred Reporting Items for Systematic Reviews and Meta-Analyses (PRISMA) 2020 guidelines.[14]

2.2. Search strategy

A comprehensive search was conducted across PubMed and Google Scholar to identify relevant articles. The search strategy utilized the terms "Tafamidis," "Cardiac amyloidosis," and "Transthyretin amyloid cardiomyopathy" using BOOLEAN operators "AND" and "OR" to refine the results. A mesh-based approach was employed to further narrow the search, reducing the volume of irrelevant literature. Table 1 shows the total number of articles retrieved from each database after applying appropriate filters.

To facilitate a deeper exploration of the impact of tafamidis on ATTR-CM, this systematic review was extended into a narrative review, as shown in the Discussion section. This approach allowed for a more detailed and nuanced analysis of the clinical efficacy, safety, and broader implications of tafamidis in the management of this condition.

2.3. Eligibility requirements

In accordance with the PRISMA 2020 guidelines, the following participant, intervention, and outcome criteria were established for study inclusion:

- Participants: Studies involving populations diagnosed with ATTR-CM, regardless of race, sex, or ethnicity, were included in the analysis. The selection was not limited by demographic variables to ensure a broad representation of the disease impact across diverse groups
- Intervention: Studies that specifically administered tafamidis as the primary intervention for treating the above-mentioned population were included in the analysis. Trials evaluating tafamidis alone or in combination with other therapies were considered if tafamidis was the main therapeutic focus
- Outcomes: The primary outcome of interest was the efficacy of tafamidis in improving clinical symptoms, quality of life, and/or disease progression in patients with ATTR-CM. The secondary outcomes, such as reduction in all-cause mortality, hospitalization rates, and adverse effects associated with tafamidis, were also considered to ensure a comprehensive evaluation of treatment impact.

2.4. Inclusion and exclusion criteria

The following additional inclusion criteria were used: articles written in English; free full-text articles published within the past 10 years; article types such as cohort studies, case–control studies, randomized control trials (RCTs), non-RCTs, case series, case reports, systematic reviews, literature reviews, and meta-analyses. Animal studies were not considered in this systematic review.

3. Results

Using the appropriate criteria and search methods, 786 articles from the above-mentioned databases published within the past 10 years were retrieved

Table 1. Databases and search strategies

Database	Search strategy	Filters	No. of articles
PUBMED	Tafamidis OR ("Benzoxazoles/administration and dosage" [Mesh] OR "Benzoxazoles/pharmacokinetics" [Mesh] OR "Benzoxazoles/pharmacology" [Mesh] OR "Benzoxazoles/therapeutic use" [Mesh]) AND Cardiac amyloidosis OR Transthyretin amyloid cardiomyopathy OR ("Amyloid Neuropathies, Familial/drug therapy" [Mesh] OR "Amyloid Neuropathies, Familial/etiology" [Mesh] OR "Amyloid Neuropathies, Familial/genetics" [Mesh] OR "Amyloid Neuropathies, Familial/pathology" [Mesh] OR "Amyloid Neuropathies, Familial/physiopathology" [Mesh] OR "Amyloid Neuropathies, Familial/prevention and control" [Mesh] OR "Amyloid Neuropathies, Familial/therapy" [Mesh])	Free full-text, studies published in the past 10 years, studies on humans, and studies written in English	755
GOOGLE SCHOLAR	Allintitle: Tafamidis AND Transthyretin amyloid cardiomyopathy	Studies published in the past 10 years	31

(from January 1, 2014, to January 9, 2024). The SANRA scale[15] was used to assess the quality of narrative review articles, and the Jadad scale[16] was utilized for RCTs and non-RCTs. The Joanna Briggs Institute quality appraisal checklist[17] was used for case series and case reports, and the Newcastle–Ottawa checklist[18] was used for case–control and cohort studies. Duplicates and irrelevant records were removed before the quality assessment. Finally, 16 studies were included in this systematic review. Figure 1 shows the PRISMA chart summarizing the screening process.

Table 2 shows the studies included in this systematic review.

4. Discussion

4.1. Tafamidis in ATTR-CM: Redefining standards of care

Tafamidis has revolutionized the management of ATTR-CM, a rare but increasingly recognized cause of HF. Tafamidis, the first Food and Drug Administration-approved treatment for ATTR-CM, has redefined the standard of care by not only extending survival rates but also remarkably improving the quality of life and functional capacity of patients. The drug's ability to stabilize TTR, which prevents misfolding and amyloid deposition, has opened new avenues for tackling this previously intractable disease. This section provides an in-depth examination of the clinical trial data of functional outcomes, subgroup analyses, and dosage effects of tafamidis and its impact on mortality and hospitalization, thereby illustrating its profound role in inhibiting disease progression.

4.2. Clinical trial data: ATTR-ACT and long-term extension (LTE) studies

The ATTR-ACT trial is a cornerstone for the approval and widespread use of tafamidis in the treatment of ATTR-CM. The trial involved 441 patients diagnosed with ATTRwt or ATTRv who had New York Heart Association (NYHA) class I–III HF. This trial has set the benchmark for the efficacy of tafamidis. This was a randomized, double-blind, placebo-controlled study that evaluated tafamidis at doses of 20 and 80 mg over 30 months. The trial's primary endpoints included all-cause mortality and cardiovascular event-related hospitalizations, both of which are critical markers of disease progression in HF.

The results were groundbreaking, with tafamidis showing a 13.4% absolute reduction in all-cause mortality compared with placebo. This statistical value is particularly notable considering the traditionally poor prognosis associated with ATTR-CM. Furthermore, tafamidis reduced cardiovascular hospitalization rates by 32%. Therefore, it is effective in mitigating acute decompensations that frequently require hospitalization. ATTR-CM is often diagnosed at advanced stages. Therefore, the ability to substantially lower hospitalization rates represents a significant improvement in disease management and the quality of life of patients. These findings are supported by the results of functional measures, such as the 6-min walk test (6MWT) and Kansas City Cardiomyopathy Questionnaire (KCCQ), which showed remarkable improvements in functional capacity and patient-reported quality of life. Patients on tafamidis exhibited an 80-m increase in the 6MWT distance and a 13 – 18-point improvement in KCCQ scores, surpassing the thresholds for clinical relevance.[5,6,8,9,11,22]

After the completion of ATTR-ACT, the participants were invited to enroll in an LTE study, which provided further insights into the long-term effects of tafamidis. The results of the LTE study underscored the importance of early intervention and showed that the median survival of patients who started treatment with tafamidis at the onset of the ATTR-ACT trial and those initially assigned to placebo treatment were 53 and 35 months, respectively. This reinforces the idea that early tafamidis therapy has substantial survival benefits. Importantly, the LTE study revealed that a dose of 80 mg led to better survival rates than a dose of 20 mg, without increasing the incidence of adverse effects, thereby highlighting the potential benefits of higher doses.[5,12] This finding has prompted further discussion on optimizing dosing strategies to maximize patient outcomes.

4.3. Reductions in mortality and hospitalization rates

The profound impact of tafamidis on mortality and hospitalization rates has been consistent across multiple analyses, which underscores its critical role in treating the wild-type and variant forms of ATTR-CM. Patients with ATTRwt exhibited earlier survival benefits than those with ATTRv, likely due to differences in disease progression between the two subtypes. The earlier onset of mortality reduction in ATTRwt indicates that patients with this type of disease have greater benefits from timely initiation of therapy. However, in both subgroups, tafamidis was associated with a 30% decrease in all-cause mortality and a 32% reduction in cardiovascular hospitalization rates compared with placebo, demonstrating its broad efficacy across patient populations.[19]

Subgroup analyses in the ATTR-ACT trial also emphasized the variation in outcomes based on the severity of HF at baseline. Patients with NYHA class I and II HF exhibited the greatest survival benefit, underscoring the importance of treating the disease before it advances to later stages. Patients with NYHA class III HF also showed

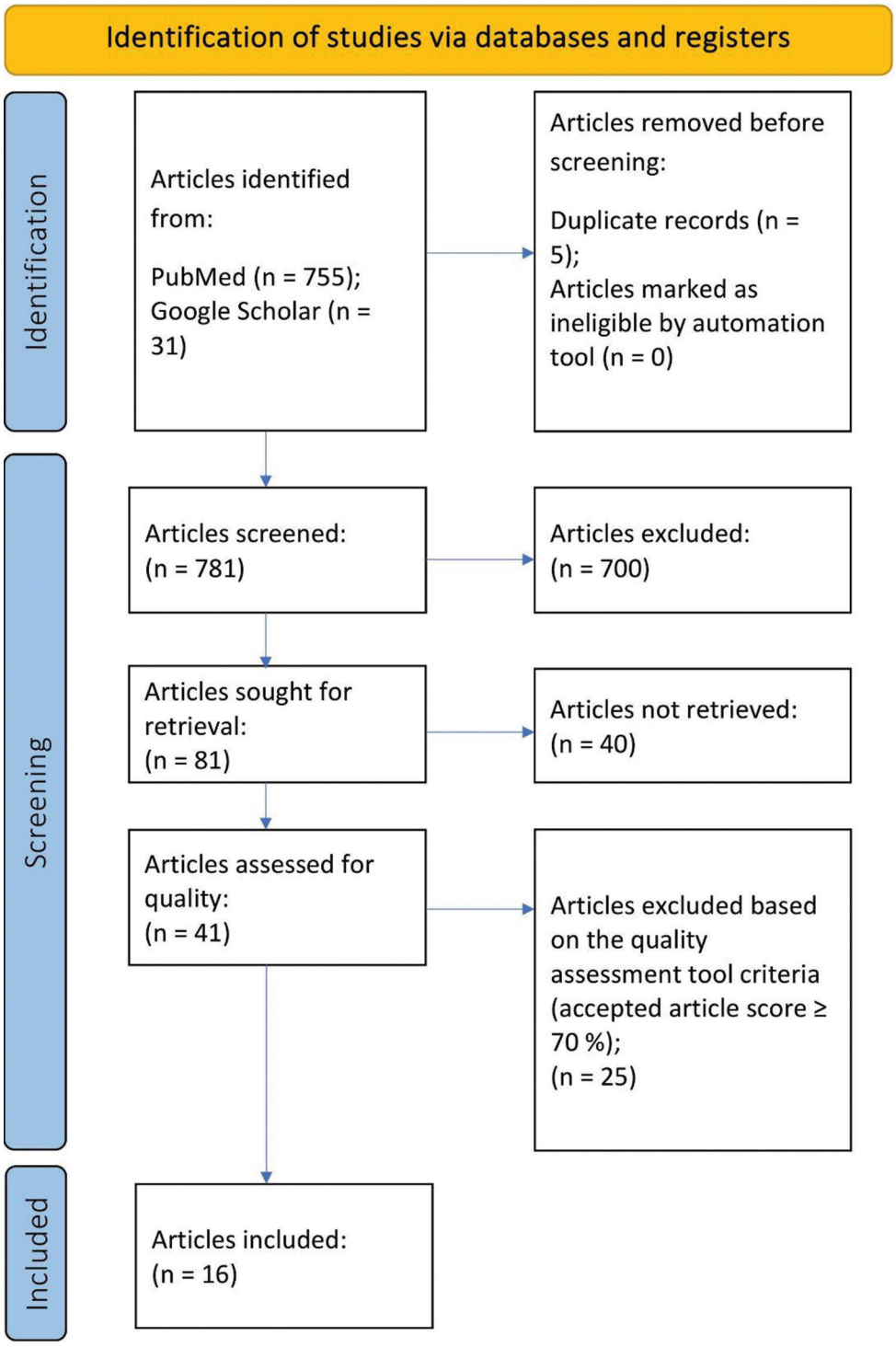

Figure 1. Preferred reporting items for systematic reviews and meta-analyses chart

improvements in mortality, with a smaller magnitude, likely reflecting the more advanced nature of their disease. This finding emphasizes an important point. If tafamidis is initiated earlier, the outcomes may be better, particularly in patients with less severe HF. The mortality benefits across different subtypes and severities of ATTR-CM validate that tafamidis is a versatile and essential therapy for this heterogeneous condition.

Table 2. Studies included in the systematic review

Author(s)	Year of publication	Type of study	Population (sample size and median age)	Major findings
Ruberg *et al.*[9]	2019	Review article	N/A	Better results are anticipated with the development of ATTR-CM treatments. However, early identification of afflicted individuals is essential for these therapies to be successful.
Rapezzi *et al.*[19]	2021	Cohort study	437 patients (median age: 75 years); 274 males, 163 females; ATTRv and ATTRwt	Administration of tafamidis significantly reduced all-cause mortality in patients with ATTR-CM regardless of the genotype. Median follow-up duration: 30 months.
Wang *et al.*[10]	2023	Systematic review and meta-analysis	Pooled data from 16 studies (>2,000 patients, both males and females)	Treatment with tafamidis was related to a reduced risk of adverse cardiovascular events and all-cause mortality without a significant decline in left ventricular ejection fraction in patients with ATTRwt. Median follow-up duration: 24 – 30 months.
Porcari *et al.*[8]	2022	Review article	N/A	Non-invasive imaging techniques are crucial for assessing myocardial involvement in ATTR amyloidosis and can play a significant role in evaluating disease-modifying therapies and guiding treatment adjustments.
Yamamoto *et al.*[20]	2019	Review article	N/A	The introduction of medications such as tafamidis requires individualized treatment strategies based on the disease stage and clinical profile.
Damy *et al.*[4]	2021	RCT	441 patients (median age: 76 years); 307 on tafamidis (212 males and 95 females), 134 on placebo (90 males and 44 females)	Tafamidis at doses of 80 and 20 mg significantly reduced cardiovascular-related mortality and hospitalization rates, with a dose of 80 mg associated with better survival and no dose-related safety issues. Median follow-up duration: 30 months.
Takashio *et al.*[7]	2023	Retrospective cohort study	103 patients with ATTRwt-CM (median age: 78 years); 68 males and 35 females	Patients treated with tafamidis had better outcomes and prognoses compared with those who were untreated. Median follow-up duration: 12 months.
Elliott *et al.*[13]	2023	Cohort study	517 patients (median age: 79 years); 331 males and 186 females	Over a median follow-up of 5 years, patients with NYHA class III symptoms who received continuous tafamidis treatment had a lower all-cause mortality than those who received delayed treatment (placebo first and then tafamidis).
Raval *et al.*[2]	2023	Review article	N/A	Early non-invasive diagnosis using bone scintigraphy, combined with disease-modifying therapies such as tafamidis and bortezomib, has transformed the approach to CA management.
Elliott *et al.*[11]	2022	RCT	441 patients (median age: 76 years); 307 on tafamidis and 134 on placebo; 68% males	In the long-term extension of ATTR-ACT, tafamidis-treated patients had significantly higher survival rates than placebo-treated patients, emphasizing the importance of early detection and treatment. Follow-up duration: up to 5 years.
Nuvolone *et al.*[5]	2022	Review article	N/A	Access to effective ATTR-CM treatment can be expanded by repurposing older, low-cost drugs, and making competitive new medications available.
Kittleson *et al.*[3]	2020	Review article	N/A	Appropriate CA diagnosis allows physicians to manage heart failure and arrhythmias effectively while incorporating disease-modifying treatments such as tafamidis.
Maurer *et al.*[21]	2015	RCT	35 patients (median age: 68 years); 24 males and 11 females	Tafamidis therapy was well-tolerated and could stabilize TTR. However, further research is warranted as most biochemical and echocardiographic parameters showed no significant changes. Follow-up duration: 12 months.
Stern and Patel[22]	2022	Review article	N/A	Tafamidis is the only FDA-approved TTR tetramer stabilizer for treating ATTR-CM.

(Cont'd...)

Table 2. ***(Continued)***

Author(s)	Year of publication	Type of study	Population (sample size and median age)	Major findings
Maurer *et al.*[12]	2018	RCT	441 patients (median age: 76 years); 307 on tafamidis (212 males and 95 females), 134 on placebo (90 males and 44 females)	Compared with patients receiving placebo, tafamidis was associated with lower all-cause mortality, reduced cardiovascular hospitalization rates, slower functional decline, and improved quality of life in patients with ATTR-CM. Follow-up duration: 30 months.
Griffin *et al.*[6]	2021	Review article	N/A	Over the past few decades, research has revealed the mechanisms underlying amyloidogenesis. This led to the development of successful treatments for various classes of amyloidosis.

Abbreviations: FDA: Food and drug administration; RCT: Randomized controlled trial; N/A: Not applicable; ATTR-CM: Transthyretin amyloid cardiomyopathy; TTR: Transthyretin; ATTRv: variant ATTR; ATTRwt: wild-type ATTR; NYHA: New York Heart Association; CA: Cardiac amyloidosis.

Beyond mortality, the impact of tafamidis on cardiovascular hospitalizations cannot be overstated. HF decompensations, often requiring hospitalization, not only cause patient distress but also have significant prognostic implications. The 32% reduction in hospitalization rates observed in tafamidis-treated patients translates to a lower burden on health-care systems and improved patient experiences. Cardiovascular hospitalizations are often accompanied with significant morbidity, and reducing their frequency with tafamidis can remarkably improve the survival and quality of life in this patient population.

4.4. Functional and quality-of-life improvements

Although extending survival is a paramount goal, improving functional capacity and quality of life are equally essential in managing a chronic, debilitating disease such as ATTR-CM. Tafamidis has consistently shown the ability to not only inhibit disease progression but also enhance the day-to-day experiences of patients. In the ATTR-ACT trial, the functional capacity – as measured using the 6MWT – and quality of life – assessed using the KCCQ – of tafamidis-treated patients improved significantly compared with those of placebo-treated patients. These benefits are far from trivial, as the 80-m increase in the 6MWT distance and the 13 – 18-point rise in KCCQ scores underscore the tangible benefits of therapy, enabling patients to perform activities of daily living with greater ease and comfort.[9]

The importance of these findings lies in not only numerical improvements but also the thresholds for clinical relevance. Both the 6MWT and KCCQ have established cutoffs that indicate a meaningful improvement, and tafamidis consistently exceeded these thresholds. These results imply that patients not only lived longer but also lived better, with improved physical functions and emotional well-being. The emotional toll of HF, particularly a progressive and often fatal disease such as ATTR-CM, is substantial, and therapies that can enhance the quality of life of patients should be prioritized alongside those that extend survival.

Further studies have supported these findings. In a study by Ruberg *et al*., tafamidis was associated with a 32% reduction in cardiovascular hospitalizations and a 13.4% reduction in all-cause mortality, thereby further supporting the improvements in survival and functional outcomes. Moreover, the study revealed reductions in the levels of N-terminal pro-B-type natriuretic peptide, a biomarker of HF severity. Based on this finding, tafamidis may stabilize, if not reverse, the clinical decline often observed in ATTR-CM.[9] Similarly, Wang *et al*. conducted a systematic review and meta-analysis and confirmed that tafamidis not only improved survival but also reduced hospitalization rates and enhanced other clinical endpoints, indicating its therapeutic role in ATTR-CM.[10]

4.5. Subgroup analyses of ATTRwt versus ATTRv and differences in NYHA classifications

Subgroup analyses from the ATTR-ACT trial[12] have provided valuable insights into the differential effects of tafamidis across various patient populations. Tafamidis demonstrated similar reductions in all-cause mortality in patients with ATTRwt and ATTRv. However, those with ATTRwt showed earlier survival benefits. This finding suggests that early intervention may be particularly important for this patient group, considering the rapid progression often observed in ATTRwt.

In terms of NYHA class, patients with NYHA class I and II HF showed the most significant survival benefits from tafamidis therapy. Patients with NYHA class III HF also experienced reductions in mortality rates. However, the magnitude of the benefit was somewhat limited. These subgroup analyses indicate that if the disease is treated with

tafamidis earlier, the outcomes will be better, particularly in patients with ATTRwt and those with less advanced HF.[10,20]

4.6. Dosage efficacy: 80 versus 20 mg

Several studies[4,12] have explored the question of optimal dosing, with tafamidis at a dose of 80 mg emerging as a more potent option. Damy *et al*. investigated the efficacy of different tafamidis dosages and found that a dose of 80 mg provided faster and potentially more robust therapeutic effects than a dose of 20 mg, particularly in improving functional outcomes such as 6MWT distance and KCCQ scores.[4] Patients receiving a dose of 80 mg exhibited improvements as early as 6 months of treatment, whereas those on the 20 mg dose exhibited similar improvements after 12 months.

Despite these differences in the speed of effect, both doses of tafamidis resulted in significant reductions in mortality and hospitalization rates, underscoring the drug's overall efficacy across dosage levels. Importantly, there were no significant safety differences between the two doses, making both options viable based on patient-specific factors and health-care provider recommendations.[4]

4.7. Long-term outcomes and biomarkers

Beyond immediate clinical outcomes, long-term studies have begun exploring the broader impact of tafamidis on disease progression, particularly in terms of biomarkers. Tafamidis has been shown to reduce the levels of N-terminal pro-B-type natriuretic peptide, a biomarker associated with HF severity and prognosis. In addition, reductions in the levels of troponin, another biomarker of cardiac injury, have been observed. Therefore, tafamidis may exert cardioprotective effects beyond its role in TTR stabilization.[7] Nevertheless, further research should be performed to fully elucidate the mechanisms by which tafamidis affects these biomarkers. However, early data are promising.

LTE studies have also provided insights into the durability of the effects of tafamidis. Patients who remained on tafamidis after the completion of the ATTR-ACT trial continued to experience survival and functional benefits, with a minimal decline in their quality of life. This long-term efficacy underscores the potential of tafamidis as a chronic therapy for chronic disease, with the possibility of transforming the natural history of ATTR-CM from rapid decline to stabilization as well as improvement in specific cases.[6,11,12]

4.8. Tafamidis as a foundation for future therapies

Tafamidis has undoubtedly revolutionized the treatment of ATTR-CM. However, it also lays the groundwork for future therapies. The success of tafamidis has spurred interest in developing additional treatments that target the underlying pathology of ATTR-CM, including gene-silencing therapies and other small molecules. As the field continues to evolve, tafamidis will likely remain a cornerstone of therapy, particularly for patients who cannot tolerate or do not respond to newer treatments.

Furthermore, the experience gained from tafamidis therapy has provided valuable insights into the importance of early diagnosis and intervention in ATTR-CM. The notion that tafamidis is most effective when started early in the disease course emphasizes the need for increased awareness and screening, particularly in at-risk populations such as older adults and those with a family history of amyloidosis. With earlier diagnosis, tafamidis and future therapies will have an even greater impact on patient outcomes.[11,12]

5. Limitations

This systematic review had certain limitations. First, only studies published within the past decade were included. In addition, only full-text articles that were freely accessible across various databases were utilized. Articles in languages other than English were excluded during the screening process. Previous studies involving participants aged <18 years were also excluded. Finally, the review focuses solely on the efficacy of tafamidis in ATTR-CM, excluding data on its use in other subtypes of CA.

6. Conclusion

Tafamidis has fundamentally transformed the treatment landscape for ATTR-CM, thereby offering patients several benefits such as reduced mortality, fewer hospitalizations, and enhanced functional capacity. Clinical trials such as ATTR-ACT and LTE studies have demonstrated the efficacy of tafamidis, especially when initiated early in the disease course. Although economic challenges remain, the therapeutic benefits of tafamidis are undeniable, making it a cornerstone treatment for ATTR-CM. The use of tafamidis, the interaction of tafamidis with different drug classes, and the prognosis of patients with ATTR-CM coupled with various comorbidities, such as diabetes mellitus, hypertension, and chronic renal failure, are some potential topics of future research.

Acknowledgments

None.

Funding

None.

Conflict of interest

The authors declare that they have no known competing interests.

Author contributions

Conceptualization: Heet N. Desai
Data curation: Sarthak H. Dhruv
Methodology: Heet N. Desai, Riti Sanghvi, Sarthak H. Dhruv
Writing–original draft: Heet N. Desai
Writing–review & editing: Heet N. Desai, Riti Sanghvi

Ethics approval and consent to participate

Not applicable.

Consent for publication

Not applicable.

Availability of data

Data are available from the corresponding author upon reasonable request.

References

1. Gościniak P, Baron T, Milczarek S, Kostkiewicz M, Machaliński B. Updates for the diagnosis and management of cardiac amyloidosis. *Adv Clin Exp Med*. 2022;31(2):175-185.

   doi: 10.17219/acem/142252

2. Raval M, Siddiq S, Sharma K, *et al.* A review of recent advances in the diagnosis of cardiac amyloidosis, treatment of its cardiac complications, and disease-modifying therapies. *F1000Research*. 2023;12:192.

   doi: 10.12688/f1000research.130285.1

3. Kittleson MM, Maurer MS, Ambardekar AV, *et al*. Cardiac amyloidosis: Evolving diagnosis and management: A scientific statement from the American heart association. *Circulation*. 2020;142(1):E7-E22.

   doi: 10.1161/CIR.0000000000000792

4. Damy T, Garcia-Pavia P, Hanna M, *et al.* Efficacy and safety of tafamidis doses in the tafamidis in transthyretin cardiomyopathy clinical trial (ATTR-ACT) and long-term extension study. *Eur J Heart Fail*. 2021l;23(2):277-285.

   doi: 10.1002/ejhf.2027

5. Nuvolone M, Girelli M, Merlini G. Oral Therapy for the treatment of transthyretin-related amyloid cardiomyopathy. *Int J Mol Sci*. 2022;23(24):16145.

   doi: 10.3390/ijms232416145

6. Griffin JM, Rosenblum H, Maurer MS. Pathophysiology and therapeutic approaches to cardiac amyloidosis. *Circ Res*. 2021;128(10):1554-1575.

   doi: 10.1161/CIRCRESAHA.121.318187

7. Takashio S, Morioka M, Ishii M, *et al*. Clinical characteristics, outcome, and therapeutic effect of tafamidis in wild-type transthyretin amyloid cardiomyopathy. *ESC Heart Fail*. 2023;10(4):2319-2329.

   doi: 10.1002/ehf2.14380

8. Porcari A, Fontana M, Gillmore JD. Transthyretin cardiac amyloidosis. *Cardiovasc Res*. 2022;118(18):3517-3535.

   doi: 10.1093/cvr/cvac119

9. Ruberg FL, Grogan M, Hanna M, Kelly JW, Maurer MS. Transthyretin amyloid cardiomyopathy: JACC state-of-the-art review. *J Am Coll Cardiol*. 2019;73(22):2872-2891.

   doi: 10.1016/j.jacc.2019.04.003

10. Wang J, Chen H, Tang Z, *et al.* Tafamidis treatment in patients with transthyretin amyloid cardiomyopathy: A systematic review and meta-analysis. *EClinicalMedicine*. 2023;63:102172.

    doi: 10.1016/j.eclinm.2023.102172

11. Elliott P, Drachman BM, Gottlieb SS, *et al.* Long-term survival with tafamidis in patients with transthyretin amyloid cardiomyopathy. *Circ Heart Fail*. 2022;15(1):e008193.

    doi: 10.1161/CIRCHEARTFAILURE.120.008193

12. Maurer MS, Schwartz JH, Gundapaneni B, *et al.* Tafamidis Treatment for patients with transthyretin amyloid cardiomyopathy. *N Engl J Med*. 2018;379(11):1007-1016.

    doi: 10.1056/NEJMoa1805689

13. Elliott P, Gundapaneni B, Sultan MB, Ines M, Garcia-Pavia P. Improved long-term survival with tafamidis treatment in patients with transthyretin amyloid cardiomyopathy and severe heart failure symptoms. *Eur J Heart Fail*. 2023;25:2060-2064.

    doi: 10.1002/ejhf.2974

14. Page MJ, McKenzie JE, Bossuyt PM, *et al.* The PRISMA 2020 statement: An updated guideline for reporting systematic reviews. *BMJ*. 2021;372:n71.

    doi: 10.1136/bmj.n71

15. Baethge C, Goldbeck-Wood S, Mertens S. SANRA-a scale for the quality assessment of narrative review articles. *Res Integr Peer Rev*. 2019;4(1):5.

    doi: 10.1186/s41073-019-0064-8

16. Halpern SH. Appendix: Jadad scale for reporting randomized controlled trials. In: *Evidence-based Obstetric Anesthesia*. United States: Wiley; 2005. p. 237-238.

    doi: 10.1002/9780470988343.app1.

17. *Checklist for Case Reports Critical Appraisal tools for use in JBI Systematic Reviews*. Available from: https://www.coursehero.com/file/215346388/checklist-for-case [Last accessed on 2024 Jul 15].

18. Hartling L, Hamm M, Milne A, *et al. Validity and Inter-rater Reliability Testing of Quality Assessment Instruments*; 2012. Available: https://www.ahrq.gov [Last accessed on 2024 Jul 15].

19. Rapezzi C, Elliott P, Damy T, *et al.* Efficacy of tafamidis in patients with hereditary and wild-type transthyretin amyloid cardiomyopathy: Further analyses from ATTR-ACT. *JACC Heart Fail*. 2021;9(2):115-123.

doi: 10.1016/j.jchf.2020.09.011

20. Yamamoto H, Yokochi T. Transthyretin cardiac amyloidosis: An update on diagnosis and treatment. *ESC Heart Failure*. 2019;6(6):1128-1139.

doi: 10.1002/ehf2.12518

21. Maurer MS, Grogan DR, Judge DP, *et al.* Tafamidis in transthyretin amyloid cardiomyopathy: Effects on transthyretin stabilization and clinical outcomes. *Circ Heart Fail*. 2015;8(3):519-526.

doi: 10.1161/CIRCHEARTFAILURE.113.000890

22. Stern LK, Patel J. Cardiac amyloidosis treatment. *Methodist Debakey Cardiovasc J.* 2022;18(2):59-72.

doi: 10.14797/mdcvj.1050

ACCSCIENCE PUBLISHING

Brain & Heart

PERSPECTIVE ARTICLE

The future of cardiac care: How stem cells are revolutionizing cardiovascular disease treatment

Aliki Iliadou[1]*, Panteleimon Pantelidis[2], Athina Goliopoulou[2], Ioannis Gialamas[2], Georgios E. Zakynthinos[2], Georgios Paparoidamis[3], Evangelos Oikonomou[2], and Georgios Koliakos[1]

[1]Laboratory of Biological Chemistry, Medical School, Faculty of Health Sciences, Aristotle University of Thessaloniki, Thessaloniki, Greece

[2]3rd University Department of Cardiology, Chest Disease Hospital "Sotiria", Medical School, National and Kapodistrian University of Athens, Athens, Greece

[3]3rd University Department of Orthopaedics, Medical School, Aristotle University of Thessaloniki, Thessaloniki, Greece

Abstract

Cardiovascular diseases (CVDs) are a major global health issue, with current treatments often insufficient for addressing long-term cardiac damage. Stem cell therapy provides a promising alternative by potentially repairing damaged heart tissue and improving cardiac function. This review highlights recent advancements in stem cell applications for CVDs, focusing on heart tissue regeneration using various cell types, including mesenchymal stem cells and the newly discovered very small embryonic-like stem cells. Each cell type has unique characteristics that contribute to heart regeneration. Combining these cells with appropriate natural, synthetic, or decellularized scaffolds creates environments that better mimic the heart, resulting in improved outcomes. The clustered regularly interspaced short palindromic repeat/Cas9 gene editing technology advances these efforts by enabling precise genetic modifications. Despite these advancements, challenges such as cell culture variability, biomaterial selection, and clinical protocol standardization remain. Continued research and clinical trials are crucial to overcome these challenges and integrate stem cell therapies into standard cardiac care.

Keywords: Cardiac tissue engineering; Heart tissue regeneration; Stem cells; Very small embryonic-like stem cells; Stem cell therapy; Cardiac function

***Corresponding author:**
Aliki Iliadou
(ailiadou@auth.gr)

Citation: Iliadou A, Pantelidis P, Goliopoulou A, *et al*. The future of cardiac care: How stem cells are revolutionizing cardiovascular disease treatment. *Brain & Heart*. 2024;2(4):4521.
doi: 10.36922/bh.4521

Received: August 14, 2024

Accepted: October 29, 2024

Published Online: November 20, 2024

1. Introduction

Cardiovascular diseases (CVDs) remain the leading cause of death worldwide, with the World Health Organization reporting 17.9 million deaths in 2019, which accounted for 32% of global deaths.[1] Although lifestyle changes and medications aid in the prevention of CVDs, secondary treatments for coronary artery disease (CAD) still face limitations. Techniques such as percutaneous coronary intervention, thrombolysis, and coronary artery bypass grafting can restore blood flow but cannot reverse the permanent damage caused by heart attacks, often resulting in heart failure with reduced ejection fraction. Surgical options such as ventriculoplasty and heart transplants are limited in either scope or availability. Alternatives such as xenotransplantation and artificial hearts

are still under development.[2] Among the 157 recipients of ventricular assist devices in the UK, 50% achieved a 5-year survival rate.[3] Stem cell therapy, with its potential to regenerate heart tissue, provides a promising solution, opening new avenues in cardiac care. This article explores recent advancements in stem call applications for treating CVDs, underscoring their potential to repair the damaged myocardium and improve heart function. Figure 1 illustrates a summary of the applications of stem cells in cardiac regeneration, including heart tissue regeneration, tissue engineering, and stem cell-derived exosomes.

2. Exploring stem cell types for cardiac tissue regeneration

Due to the limited regenerative capacity of the heart, scientists are exploring alternative sources of cardiomyocytes (CM), particularly embryonic stem cells (ESCs), which are derived from the inner cell mass of blastocysts and can differentiate into various cell types, including ESC-CMs.[4] In 2006, Yamanaka's team demonstrated that adult somatic cells can be reprogrammed into induced pluripotent stem cells (iPSCs), providing a rapid and cost-effective source for heart cell therapies.[5] iPSCs have been instrumental in creating cardiac organoids – 3D structures that mimic the human heart – and modeling diseases such as long QT syndrome and hypertrophic cardiomyopathy (HCM).[6] Furthermore, cardiac progenitor cells, specialized stem cells in the heart, hold promise for improving self-healing and angiogenesis as well as for disease modeling and drug testing in HCM.[7]

Another cell type demonstrating significant potential in improving cardiac function is mesenchymal stem cells (MSCs), which improve heart tissue regeneration after myocardial infarction through paracrine signaling. MSCs are adult stem cells derived from the bone marrow (BM), adipose tissue, deciduous teeth, and umbilical cord blood (UCB).[2] Their efficacy and safety have been investigated in different clinical trials. For instance, TAC-HFT investigated how MSCs combined with BM cells can reduce arrhythmias and improve repair in ischemic cardiomyopathy.[8] Moreover, BM stem cells, primarily related to osteoblast differentiation, are being investigated in trials such as BOOST and BAMI for their potential to improve left ventricular ejection fraction after myocardial infarction.[9] In addition, the CHART-1, SCIENCE, and DREAM-HF trials are among the largest and most significant studies exploring the clinical application of stem cells in heart diseases. These trials have advanced our understanding of stem cell therapy, demonstrating promising benefits, such as improved heart function, reduced heart enlargement, and better quality of life, for patients with heart failure. Nevertheless, numerous ongoing studies today continue to highlight the importance and need of integrating stem cell therapies into clinical practice, showing the evolving role of regenerative medicine in cardiovascular care.[10] Table 1

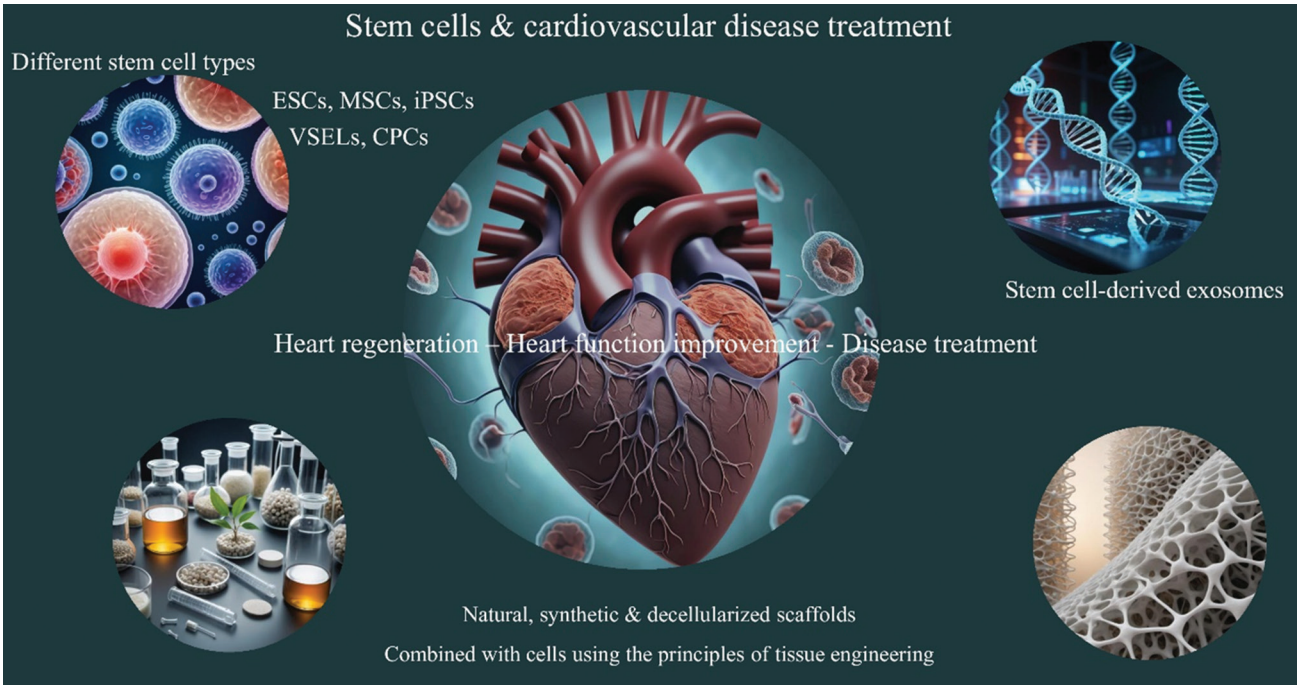

Figure 1. Applications of stem cells in cardiac regeneration. Image created by the authors.
Abbreviations: CPCs: Cardiac progenitor cells; ESCs: Embryonic stem cells; iPSCs: Induced pluripotent stem cells; MSCs: Mesenchymal stem cells; VSELs: Very small embryonic-like stem cells.

Table 1. Overview of clinical trials evaluating stem cell therapies for ischemic heart disease

NCT number	Trial name	Stem cell type	Administration method	Target disease	Status	Enrollments	Result	Years active
NCT06087848	StromaForte	Allogeneic MSCs	IV	CVD	Active (Phase 1/2)	100	Evaluating the potential of MSCs to reduce CV events	2023–Present
NCT06154044	CELL-VAD	CD34 + SCs	IC	HF with LVAD	Active (Phase 1)	10	Evaluating whether CD34 + cells can improve heart function in patients with LVADs	2022–Present
NCT05068674	HECTOR	hESC-CMs	IM	Chronic ischemic LV dysfunction	Active	18	Evaluating the safety and efficacy of SC-CMs for improving heart function in ischemic LV dysfunction	2022–Present
NCT05147766		Allogeneic UC-MSCs	IV	HD	Active	20	Evaluating the safety and efficacy of IV infusion of cultured allogeneic adult UC-MSCs for the treatment of congestive HF and angina	2022–Present
NCT04396899	BioVAT-HF	iPSCs-Engineered Human Myocardium	IMP	HF	Active	53	Evaluating the safety and efficacy of iPSC-derived myocardium as a biological ventricular assist tissue in HF	2021–Present
NCT04476901	DCMII	Allogeneic MSCs	IV	Non-ischemic dilated cardiomyopathy	Active	136	Evaluating the safety and efficacy of MSCs in improving cardiac function and quality of life over 1 year	2021–Present
NCT04776239	ACESO-IHD	Allogeneic MSCs	IV	Endothelial dysfunction, ischemic HD	Active	30	Investigating improvements in endothelial function and CV outcomes in diabetic patients	2021–Present
NCT04907526		Autologous UCB-MNCs	IM	Single ventricle CHD	Active	30	Evaluating the safety and efficacy of UCB-MNC injected during Fontan surgery to improve outcomes in single ventricle-dependent CHD	2021–Present
NCT04996966		hUC-MSCs	IV	Non-cardiac surgery, lung injury, IHD	Active	16	Evaluating the safety and effectiveness of human UC-MSCs on non-cardiac surgery-induced lung injury in patients with IHD	2021–Present
NCT04052191	MCRcI® Stem Cell Treatment	MCRcI® SCs	IC INJ	Diffuse CAD	Active	40	Evaluating the safety and efficacy of MCRcI® SCs	2020–Present

(Cont'd...)

Table 1. *(Continued)*

NCT number	Trial name	Stem cell type	Administration method	Target disease	Status	Enrollments	Result	Years active
NCT04011059	SCOREM-CELLS	AllogeneicMSCs	IV	CVD	Active	40	Study of coronary revascularization surgery with injection of WJ-MSCs, placement of an epicardial extracellular matrix	2019–Present
NCT01517425		iPSCs	N/A	CAD	Active	200	Investigating genetic variations related to CAD using iPSCs generated from blood/skin samples	2012–Present
NCT03042572	SAIL	Allogeneic MSCs	IM	Critical limb ischemia	Completed (Phase 2/3)	60	Evaluating the safety and efficacy of MSCs in improving limb outcomes in patients ineligible for revascularization	2018–2021
NCT03172507	ATHERO STEM	Hematopoietic SCs	IV	CAD	Phase 1	28	Investigating the phenotypical characteristics of HSPCs and cytokine responses in patients with CAD	2017 – 2018
NCT02462330	MESAMI 2	Autologous MSCs	IM	IHD	Completed (Phase 2)	39	MSC therapy demonstrated improvement in peak VO_2 and overall cardiac function, particularly in NYHA functional class	2016 – 2022
NCT02673164	SCIENCE	Allogeneic Adipose-Derived Stromal Cells	IC	IHD, HF	Completed (Phase 2)	133	Demonstrated the safety of IM allogeneic CSCC_ASC therapy in patients with HFrEF	2015 – 2020
NCT02032004	DREAM-HF	MPC	END	HFrEF	Completed (Phase 3)	566	Reduced MI, stroke, cardiac death	2014 – 2021
NCT01753440		MPC (iMP)	IMP	IHD at the time of coronary artery bypass grafting	Completed	11	Scar reduction at 4 months, improvement in LVEF at 12 months	2013 – 2016
NCT01768702	CHART-1	Autologous MSCs, reprogrammed into cardiopoietic cells	IM	Symptomatic IHD, HF, severe heart enlargement	Completed (Phase 3)	315	Patients with LV end-diastolic volumes 200–370 mL benefited from the treatment in terms of improved heart function and quality of life. No major safety concerns	2012 – 2017

(Cont'd...)

doi: 10.36922/bh.4521

Table 1. ***(Continued)***

NCT number	Trial name	Stem cell type	Administration method	Target disease	Status	Enrollments	Result	Years active
NCT01739777	RIMECARD	UC-MSCs	IV	HF, Cardiomyopathy in dilated stage	Completed	30	Safety and potential efficacy for treating HD	2012 – 2015
NCT01569178	BAMI	BM-SCs	IC	AMI, LVEF≤45%	Completed	375	No significant improvement in mortality	2011 – 2017
NCT01392625	POSEIDON	Autologous & Allogeneic MSCs	END	Non-ischemic dilated cardiomyopathy	Completed (Phase 1/2)	37	Improved cardiac function, reduced adverse events after treatment	2011 – 2017
NCT00474461	SCIPIO	Autologous CSCs	IC	IHD	Completed	33	Significant increase in LVEF (from 30.3% to 38.5% at 4 months, further improvement at 1 year), reduction in infarct size	2009 – 2013
NCT00765453	REGEN-AMI	BM-adult SCs	IC	AMI	Completed	100	Improvement in LV function, reduction in scar tissue size	2008 – 2018
NCT00426868	PRECISE	ADSCs	IC	Non-revascularizable ischemic myocardium	Completed	27	Improvement in global LVEF, reduction of LV infarct size, and scar formation	2007 – 2012
NCT00587990	PROMETHEUS	MSCs	IM	Chronic ischemic LV dysfunction secondary MI undergoing CABG	Terminated	60	Improved LV function, reduction in HF symptoms post-surgery	2007 – 2011
NCT00279175	REPAIR-AMI	BM-Progenitor Cells	IC	AMI	Completed (Phase 3)	204	Showed significant improvement in LVEF, reduced adverse CV events	2004 – 2009

Abbreviations: LVEF: Left ventricular ejection fraction; ADSCs: Adipose-derived stem cells; AMI: Acute myocardial infarction; CABG: Coronary artery bypass grafting; CAD: Coronary artery disease; CHD: Cardiac heart disease; CMs: Cardiomyocytes; CSCs: Cardiac stem cells; CSCC_ASCs: Adipose tissue-derived mesenchymal stromal cells; CV: Cardiovascular; CVD: Cardiovascular disease; EF: Ejection fraction; END: Transendocardial delivery; hESC: Human embryonic stem cells; HF: Heart failure; IC: Intracoronary infusion; IC INJ: Intracoronary injection; IHD: Ischemic heart disease; IM: Intramyocardial injection; IMP: Implantation; IV: Intravenous infusion; iPSCs: induced pluripotent stem cells; LV: Left ventricle; LVAD: Left ventricular assist device; MNCs: Mononuclear cells; MPC: Mesenchymal precursor cell; MSCs: Mesenchymal stem cells; N/A: Not applicable; SCs: Stem cells; UC (B): Umbilical cord (blood); WJ: Wharton's jelly, HFrEF: Heart failure with reduced ejection fraction; UCB: Umbilical cord blood.

doi: 10.36922/bh.4521

presents an overview of clinical trials evaluating stem cell therapies for ischemic heart disease.[9-12]

Finally, but importantly, there is a recently discovered population of stem cells that have garnered increasing attention due to their unique properties. Very small embryonic-like stem cells (VSELs) are small (3–5 μm smaller than red blood cells) and exhibit pluripotency similar to that of ESCs.[13] These cells are believed to be remnants of ESCs that persist into adulthood, typically remaining in a quiescent state, which may protect them from environmental damage and teratoma formation. Various preclinical models have demonstrated their regenerative potential, including the regeneration of myocardial post-infarction tissue. Ratajczak, the pioneer in VSEL' research, and his group,[13] have successfully differentiated VSELs *in vitro* from murine BM into CMs, indicating their potential for cardiac regeneration. Gounari *et al.*[14] successfully differentiated human UCB(hUCB)-VSELs into hematopoietic cells *in vitro*, thereby demonstrating their potential for cardiac differentiation through similar signaling pathways.

3. Engineering simulates the 3D cardiac environment

Cardiac tissue engineering addresses previous challenges using scaffolds – synthetic, natural, or decellularized – to support cell growth. These scaffolds can be improved with cytokines, growth factors, or peptides to mimic the physiological conditions of cardiac tissue. This method promotes cell attachment and differentiation while protecting cells from the hostile environment of the infarcted myocardium.

When comparing natural and synthetic materials, each has distinct advantages and disadvantages. Natural materials (e.g., fibrin and collagen) are valued for their biological origin, biocompatibility, and adhesive sequences that promote cell adhesion and differentiation; however, they often suffer from inadequate mechanical properties, rapid degradation, and a risk of contamination, which increase production costs.[15] In contrast, synthetic materials (e.g., poly(lactic-co-glycolic) acid) are cost-effective and provide consistent mechanical properties; however, they have limited scale-up potential, lack biocompatibility, and pose the risk of biodegradation-related side effects.[15] Therefore, ideally, the scaffold architecture (surface topography and pore size) should balance these factors, supporting cell attachment, nutrient exchange, cell–extracellular matrix (ECM) interactions, and differentiation, along with providing biocompatibility, mechanical integrity, and controlled biodegradability.[15]

Decellularized scaffolds, mimicking the healthy cardiac tissue, help preserve the native structure ECM and show promise in reducing LV remodeling and improving heart function when engineered into biocompatible materials such as injectable hydrogels.[16] When combined with cardiac patches – laboratory-grown pieces of heart tissue designed to replace damaged cardiac areas, these scaffolds support heart tissue regeneration and prevent further damage.[16]

Prat-Vidal *et al.*[17] reported the first human application of an allogeneic decellularized pericardial matrix bioimplant with Wharton's jelly-derived MSCs in patients with myocardial infarction, reducing the scar size by 9% without causing adverse effects such as myocarditis. Moreover, Sun *et al.*[18] improved heart function, cell survival, and engraftment by co-transplanting human iPSC (hiPSC)-CMs with preformed microvessels from adipose tissue.

Gene editing is another innovative tool for cardiac care. The clustered regularly interspaced short palindromic repeat system, originally discovered as a bacterial immune mechanism, has become a crucial method for disease modeling and therapy.[19] It has been used to correct *in vitro* mutations in conditions such as Duchenne muscular dystrophy[19] and has improved MSC reparative function for heart repair both *in vitro* and *in vivo* by targeting genes such as *TLR4*.[20] Furthermore, editing *PCSK9* in mice was found to significantly reduce cholesterol levels,[21] whereas patient-specific iPSC-derived organoids have been used to replicate the heart muscle thickening observed in HCM.[6] These approaches provide novel strategies to prevent heart failure by improving the function of stem cells used for heart repair.

4. Challenges in stem cell applications for cardiac care

Stem cells can be transplanted into injured myocardium either directly or after *in vitro* differentiation. Furthermore, methods such as chemical and drug-based treatments can improve cell survival and retention in the myocardium. Tissue engineering may further optimize conditions by better mimicking the natural cardiac environment. Finally, stem cell-derived exosomes exhibit potential for cardiac repair. Figure 2 summarizes the pathways for improving stem cell efficacy in cardiac regeneration.[2,7,22-24] Nonetheless, challenges exist at every step of the process.

Regarding the appropriate stem cell type, ESC-CM transplants face significant hurdles, including ventricular arrhythmias, ethical concerns, teratoma formation, and immune rejection.[25,26] Before iPSCs can replace traditional PSCs sources, it is essential to investigate the impact of residual epigenetic and transcriptional anomalies on their

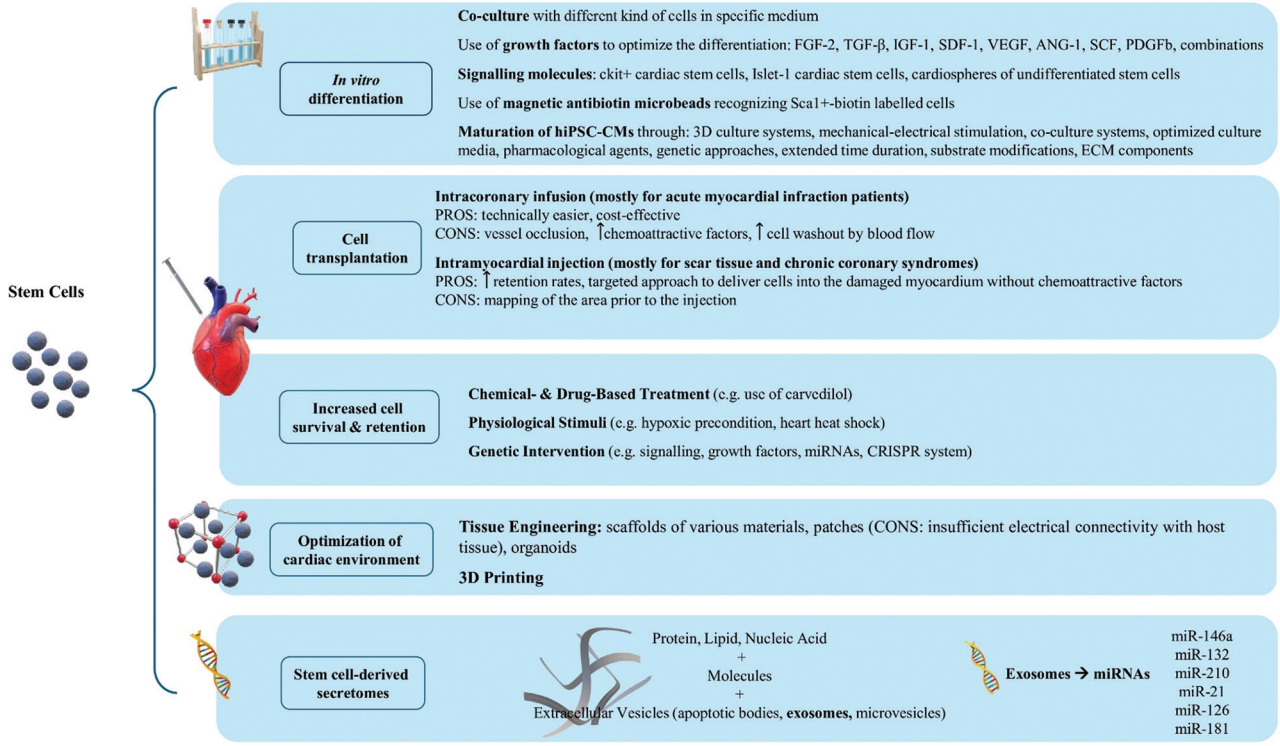

Figure 2. Improving the targeted transplantation of stem cells through *in vitro* differentiation: improving survival rates and adaptation within 3D cardiac environments in tissue engineering and the significant role of exosome utilization. Image created by the authors.

clinical safety. Genomic instability during reprogramming raises concerns, making ESCs the preferred choice for now until more stable reprogramming methods are developed.[5] MSCs are widely used in cardiac research due to their potential. Optimizing the isolation and expansion of VSELs is also important, because banking hUCB-VSELs could create a valuable cell reservoir for treating congenital or acquired heart diseases.

Major challenges for transplanted stem cells include minimizing apoptosis, oxidative stress, and inflammation that can result in cell death and cardiac complications. Efforts must focus on improving cell survival, angiogenesis, and cardiac function to support the damaged myocardium. It is also important for transplanted cells to survive, integrate properly, and receive appropriate electrical and mechanical signals to develop into functional heart cells. There are also challenges related to exosomes, such as specificity, dosing, and target binding.

A major challenge with undifferentiated stem cells is their tendency to differentiate into various cell types *in vivo*, resulting in poor cardiomyogenic outcomes. Predifferentiating them toward a cardiomyogenic lineage *in vitro* significantly improves their efficacy. Unlike *in vivo* conditions, where oxidative stress and unpredictable factors can affect cell development, the laboratory provides controlled environments to guide differentiation. All pluripotent cells, including VSELs, can be predifferentiated to align with specific therapeutic goals, thereby improving their engraftment and therapeutic potential.[23,24,27] For instance, Szaraz *et al.*[27] found that human umbilical cord perivascular cells formed contracting clusters within a week when cocultured on cardiac feeder layers, thus addressing low survival rates post-transplantation due to leakage, ischemic conditions, or oxidative stress.[24] Furthermore, exosomes from failing hearts exhibit diminished cardioprotective properties compared with those from healthy hearts, emphasizing the need for *ex vivo* improvements to stem cell function.[22]

The stem cell secretome is pivotal in therapies, comprising proteins, nucleic acids, lipids, and extracellular vesicles (EVs). EVs, categorized by size and origin, include exosomes, mRNAs, microRNAs, and non-coding RNAs, all of which are essential for intercellular communication.[24,28] Exosomes, involved in processes such as immune modulation and differentiation, demonstrate potential for cardiac regeneration. For instance, Farahzadi *et al.*[28] demonstrated that injecting MSC-derived exosomes into mice shortly before cardiac reperfusion significantly

reduced infarct size within 24 h and improved cardiac function over 28 days compared with that in untreated controls.

hiPSCs are used to generate cardiomyocytes (hiPSC-CMs) for investigating cardiac diseases. Nevertheless, these cells often resemble immature, fetal-like cardiomyocytes, limiting their use in disease modeling and drug testing.[29] Recent advancements, such as culturing hiPSC-CMs in 3D microtissue environments or cardiac maturation media for 15 – 18 days, have resulted in cells that are approximately 50% closer to adult heart cells in gene expression.[29] Matured hiPSC-CMs exhibit improved structure, mechanics, and electrophysiology, including better contractile strength and calcium cycling. For diseases linked to SCN5A mutations, such as Brugada syndrome, matured hiPSC-CMs provide better disease modeling. Ongoing research aims to further improve maturation using electrical stimulation and 3D cultures.[30]

The combination of stem cell therapy with tissue engineering demonstrates significant promise for heart regeneration, disease modeling, drug testing, and valvular disease treatment. Nevertheless, unlike chemical drugs, cellular therapies are complex, and variability in cell culture conditions poses difficulties. Selecting the precise biocompatible material, having porosity and elasticity that match cardiac mechanics and support neovascularization, is crucial. These materials must ensure effective cell adhesion and controlled degradation as well as avoid toxic byproducts. As there is no single ideal material for cardiac regeneration, researchers select biocompatible materials based on desired properties for optimal outcomes.

The implementation of stem cell therapies on a large scale requires developing standardized clinical protocols, quality control measures, and strong regulatory oversight to ensure patient safety and ethical compliance, as outlined by the ISSCR guidelines.[31] Despite their potential, PSCs face significant ethical and regulatory challenges. Although MSCs have gained prominence in biomedical research, variability in their isolation, expansion, and cell characterization methods complicates the comparison of results. To address this issue, the International Society for Cellular Therapy proposed minimal criteria to define human MSCs in 2006.[31] Since then, researchers such as Rojewski *et al.*[32] and Codinach *et al.*[33] have developed reproducible bioprocesses for manufacturing MSC-based products for clinical applications using closed systems that require minimal manipulation and allow continuous monitoring; however, certain challenges remain, including scaling up production, managing the inherent heterogeneity of MSCs, and implementing robust quality control measures. Further consensus on MSC definitions and reporting standards is essential to improve rigor, reproducibility, and transparency in MSC research.

5. Conclusion

Stem cell research has the potential to revolutionize cardiac care by providing innovative treatment strategies for heart disease. Continued advancements and collaborative efforts are essential for overcoming existing challenges and unlocking the complete potential of stem cell therapies.

Acknowledgments

None.

Funding

None.

Conflict of interest

The authors declare that they have no competing interests.

Author contributions

Conceptualization: Aliki Iliadou, Panteleimon Pantelidis
Visualization: Aliki Iliadou, Panteleimon Pantelidis, Georgios Paparoidamis
Writing–original draft: All authors
Writing–review & editing: All authors

Ethics approval and consent to participate

Not applicable.

Consent for publication

Not applicable.

Availability of data

Not applicable.

References

1. Muharram FR, Multazam CE, Mustofa A, *et al.* The 30 years of shifting in the Indonesian cardiovascular burden-analysis of the global burden of disease study. *J Epidemiol Glob Health*. 2024;14(1):193-212.

   doi: 10.1007/s44197-024-00187-8

2. Heng BC, Haider HK, Sim EK, Cao T, Ng SC. Strategies for directing the differentiation of stem cells into the cardiomyogenic lineage *in vitro*. *Cardiovasc Res.* 2004;62(1):34-42.

   doi: 10.1016/j.cardiores.2003.12.022

3. Bottle A, Faitna P, Aylin PP, Cowie MR. Five-year outcomes following left ventricular assist device implantation in England. *Open Heart*. 2021;8(1):e001658.

doi: 10.1136/openhrt-2021-001658

4. Zhang Y, Mignone J, MacLellan WR. Cardiac regeneration and stem cells. *Physiol Rev*. 2015;95(4):1189-1204.

   doi: 10.1152/physrev.00021.2014

5. Yoshida Y, Yamanaka S. Induced pluripotent stem cells 10 years later: For cardiac applications. *Circ Res.* 2017;120(12):1958-1968.

   doi: 10.1016/j.ijsu.2013.05.037

6. Escribá R, Larrañaga-Moreira JM, Richaud-Patin Y, *et al.* iPSC-based modeling of variable clinical presentation in hypertrophic cardiomyopathy. *Circ Res*. 2023;133(2):108-119.

   doi: 10.1161/CIRCRESAHA.122.321951

7. Bryl R, Kulus M, Bryja A, *et al.* Cardiac progenitor cell therapy: Mechanisms of action. *Cell Biosci*. 2024;14:30.

   doi: 10.1186/s13578-024-01211-x

8. Natsumeda M, Suncion V, Balkan W, Hare J. The impact of intramyocardial mesenchymal stem cell injection according to scar size for the treatment of ischemic cardiomyopathy. *J Am Coll Cardiol*. 2016;67(13 Supplement):158-158.

   doi: 10.1016/S0735-1097(16)30159-0

9. Bartunek J, Wojakowski W. Intracoronary autologous bone marrow cell transfer after acute myocardial infarction: Abort and refocus. *Eur Heart J*. 2017;38(39):2944-2947.

   doi: 10.1093/eurheartj/ehx300

10. Povsic TJ. Emerging therapies for congestive heart failure. *Clin Pharmacol Ther*. 2018;103(1):77-87.

    doi: 10.1002/cpt.913

11. Correia CD, Ferreira A, Fernandes MT, *et al.* Human stem cells for cardiac disease modeling and preclinical and clinical applications-are we on the road to success? *Cells*. 2023;12(13):1727.

    doi: 10.3390/cells12131727

12. Clinical Trials, National Library of Medicine (National Center for Biotechnology Information. Available from: https://clinicaltrials.gov [Last accessed on 2024 Oct 17].

13. Ratajczak MZ, Ratajczak J, Kucia M. Very small embryonic-like stem cells (VSELs) – an update and future directions. *Circ Res*. 2019;124(2):208-210.

    doi: 10.1161/CIRCRESAHA.118.314287

14. Gounari E, Daniilidis A, Tsagias N, *et al.* Isolation of a novel embryonic stem cell cord blood–derived population with *in vitro* hematopoietic capacity in the presence of Wharton's jelly-derived mesenchymal stromal cells. *Cytotherapy*. 2019;21(2):246-259.

    doi: 10.1016/j.jcyt.2018.11.006

15. Sedláková V, Mourcos S, Pupkaitė J, *et al.* Biomaterials for direct cardiac repair-A rapid scoping review 2012-2022. *Acta Biomater*. 2024;180:61-81.

    doi: 10.1016/j.actbio.2024.04.008

16. Liu W, Zhang X, Jiang X, *et al.* Decellularized extracellular matrix materials for treatment of ischemic cardiomyopathy. *Bioact Mater*. 2024;33:460-482.

    doi: 10.1016/j.bioactmat.2023.10.015

17. Prat-Vidal C, Rodríguez-Gómez L, Aylagas M, *et al*. First-in-human PeriCord cardiac bioimplant: Scalability and GMP manufacturing of an allogeneic engineered tissue graft. *EBioMedicine*. 2020;54:102729.

    doi: 10.1016/j.ebiom.2020.102729

18. Sun X, Wu J, Qiang B, *et al.* Transplanted microvessels improve pluripotent stem cell-derived cardiomyocyte engraftment and cardiac function after infarction in rats. *Sci Transl Med*. 2020;12(562):eaax2992.

    doi: 10.1126/scitranslmed.aax2992

19. Saeed S, Khan SU, Khan WU, *et al.* Genome editing technology: A new frontier for the treatment and prevention of cardiovascular diseases. *Curr Probl Cardiol*. 2023;48(7):101692.

    doi: 10.1016/j.cpcardiol.2023.101692

20. Schary Y, Rotem I, Caller T, *et al*. CRISPR-Cas9 editing of TLR4 to improve the outcome of cardiac cell therapy. *Sci Rep.* 2023;13(1):4481.

    doi: 10.1038/s41598-023-31286-4

21. Bao X, Liang Y, Chang H, *et al.* Targeting proprotein convertase subtilisin/kexin type 9 (PCSK9): From bench to bedside. *Signal Transduct Target Ther*. 2024;9(1):13.

    doi: 10.1038/s41392-023-01690-3

22. Bakinowska E, Kiełbowski K, Boboryko D, *et al.* The role of stem cells in the treatment of cardiovascular diseases. *Int J Mol Sci.* 2024;25(7):3901.

    doi: 10.3390/ijms25073901

23. Chamuleau SA, van Belle E, Doevendans PA. Enhancing cardiac stem cell differentiation into cardiomyocytes. *Cardiovasc Res*. 2009;82(3):385-387.

    doi: 10.1093/cvr/cvp114

24. Wu R, Hu X, Wang J. Concise review: Optimized strategies for stem cell-based therapy in myocardial repair: Clinical translatability and potential limitation. *Stem Cells*. 2018;36(4):482-500.

    doi: 10.1002/stem.2778

25. Olatunji G, Kokori E, Yusuf I, *et al.* Stem cell-based therapies for heart failure management: A narrative review of current evidence and future perspectives. *Heart Fail Rev*. 2024;29(3):573-598.

    doi: 10.1007/s10741-023-10351-0

26. Liu C, Han D, Liang P, *et al.* The current dilemma and breakthrough of stem cell therapy in ischemic heart disease. *Front Cell Dev Biol*. 2021;9:636136.

doi: 10.3389/fcell.2021.636136

27. Szaraz P, Gratch YS, Iqbal F, Librach CL. *In vitro* differentiation of human mesenchymal stem cells into functional cardiomyocyte-like cells. *J Vis Exp.* 2017;126:55757.

doi: 10.3791/55757

28. Farahzadi R, Fathi E, Valipour B, Ghaffary S. Stem cells-derived exosomes as cardiac regenerative agents. *Int J Cardiol Heart Vasc*. 2024;52:101399.

doi: 10.1016/j.ijcha.2024.101399

29. Afzal J, Liu Y, Du W, *et al.* Cardiac ultrastructure inspired matrix induces advanced metabolic and functional maturation of differentiated human cardiomyocytes. *Cell Rep.* 2022;40(4):111146.

doi: 10.1016/j.celrep.2022.111146

30. Ottaviani D, ter Huurne M, Elliott DA, Bellin M, Mummery CL. Maturing differentiated human pluripotent stem cells *in vitro*: Methods and challenges. *Development*. 2023;150(11):dev201103.

doi: 10.1242/dev.201103

31. Lovell-Badge R, Anthony E, Barker RA, *et al.* ISSCR Guidelines for stem cell research and clinical translation: The 2021 update. *Stem Cell Reports*. 2021;16(6):1398-1408.

doi: 10.1016/j.stemcr.2021.05.012

32. Rojewski MT, Fekete N, Baila S, *et al.* GMP-Compliant isolation and expansion of bone marrow-derived MSCs in the closed, automated device quantum cell expansion system. *Cell Transplant*. 2013;22(11):1981-2000.

doi: 10.3727/096368912X657990

33. Codinach M, Blanco M, Ortega I, *et al.* Design and validation of a consistent and reproducible manufacture process for the production of clinical-grade bone marrow–derived multipotent mesenchymal stromal cells. *Cytotherapy*. 2016;18(9):1197-1208.

doi: 10.1016/j.jcyt.2016.05.012

ACCSCIENCE PUBLISHING

Brain & Heart

ORIGINAL RESEARCH ARTICLE

Deciphering molecular atlas of Alzheimer's disease: A comprehensive bioinformatic analysis of gene expression and protein interaction networks

Shan Luo[1†], Yifei Wang[1†], and Kohji Fukunaga[2*]

[1]Department of Integrated Biosciences, Graduate School of Frontier Sciences, The University of Tokyo, Kashiwa, Chiba, Japan

[2]Department of CNS Drug Innovation, Graduate School of Pharmaceutical Sciences, Tohoku University, Sendai, Miyagi, Japan

Abstract

Alzheimer's disease (AD) represents a formidable challenge in the realm of neurodegenerative research due to its complex pathology. Despite tremendous scientific endeavors, the intricate molecular underpinnings of AD remain incompletely understood, necessitating a multidimensional approach to decipher its complexity. In this study, we analyzed differential gene expression, gene ontology (GO) enrichment, and protein–protein interaction (PPI) networks using advanced bioinformatics tools to dissect the molecular landscape of AD. Initially, our research identified 732 differentially expressed genes (DEGs), which provided a comprehensive view of the genetic disruptions associated with AD. The results of subsequent GO enrichment analyses revealed that DEGs were enriched in several critical biological processes, predominantly including translation, neuroinflammation, and synaptic functionality, underscoring the multifaceted nature of AD pathology. The PPI network analysis further unveiled the central role of ribosomal proteins, such as RPL12, RPL15, RPL18, RPL19, RPL27, RPL35, RPL36, RPS16, RPS19, and RPS9, establishing a novel link between protein synthesis disruptions and the molecular mechanisms of AD. These results not only deepen the understanding of molecular mechanisms underlying AD but also illuminate potential therapeutic pathways and biomarkers for AD. Overall, our comprehensive bioinformatics exploration unraveled the complex molecular mechanisms that govern AD pathogenesis and highlighted promising new targets for the diagnosis and treatment of AD, creating a foundational framework for future research on AD.

Keywords: Alzheimer's disease; Differential gene expression; Bioinformatics; Protein–protein interaction; Molecular mechanisms

1. Introduction

Alzheimer's disease (AD) is a progressive neurodegenerative disorder that not only impairs the cognition and memory of patients but also severely compromises the emotional and physical well-being of patients and family caregivers. As the global

[†]These authors contributed equally to this work.

***Corresponding author:**
Kohji Fukunaga
(kfukunaga@tohoku.ac.jp)

Citation: Luo S, Wang Y, Fukunaga K. Deciphering molecular atlas of Alzheimer's disease: A comprehensive bioinformatic analysis of gene expression and protein interaction networks. *Brain & Heart.* 2024;2(4):2906. doi: 10.36922/bh.2906

Received: February 8, 2024

Accepted: May 23, 2024

Published Online: August 29, 2024

population ages, understanding and addressing this condition has become increasingly urgent. The etiology of AD is notoriously complex, ranging from molecular dysfunction to cellular dysfunction. Central to AD pathogenesis is the pathological accumulation of amyloid-beta (Aβ) peptides and neurofibrillary tangles (NFTs) composed of hyperphosphorylated tau, which collectively contribute to synaptic degradation and neuronal death.[1-3] The trafficking of amyloid precursor proteins (APP) and secretases within neurons, modulated by numerous proteins, further exacerbates Aβ production and accumulation, thereby influencing the disease process.[4] Although Aβ-targeted therapeutic strategies have been extensively investigated, most have failed to demonstrate significant clinical efficacy. Therefore, the search for new protein targets or biomarkers for AD is both important and urgent,[5] potentially offering new approaches for the prevention and treatment of AD.

Recent studies have unraveled that dysregulated APP processing, fueled by alterations in the Aβ40/42 ratio, is a pivotal contributor to AD's molecular pathology. In addition, APP processing dysregulation is often propelled by mutations in genes, including *PSEN1*, which are common in familial AD. These genetic mutations primarily affect the cleavage of APP by γ-secretase, skewing the production of Aβ peptides.[6] Consequently, a convoluted interplay among gene mutations, protein processing, and intracellular transport orchestrates AD's molecular landscape. Understanding these multifaceted molecular interactions is crucial for the development of targeted therapeutic strategies. In addition, the molecular intricacies of AD can be further unraveled by analyzing nuances in mechanisms, such as the trafficking of APP and the activity of secretases.[7] As research progresses, it is increasingly necessary to develop a multi-targeted approach addressing various aspects of the molecular basis for effectively combating AD.[8,9]

In several studies, AD animal models have been utilized to examine disease-related changes in the brain.[10] Nevertheless, these animal studies have limitations, one of which is the inability to fully replicate the pathology of human AD. In addition, key metabolic pathways and regulators in AD have been analyzed using epigenomic, transcriptomic, proteomic, metabolomic, and genomic profiles from human-derived samples, facilitating the search for diverse targets for preventive or therapeutic interventions.[11]

It is well-reported that the entorhinal cortex is the first cortical region influenced by the neurodegenerative process of AD, followed by the hippocampus and limbic system, and, ultimately, the neocortex.[9] In our study, we utilized a gene expression dataset from the entorhinal cortex of 10 patients with mid-stage AD (GSE4757) for a multifaceted investigation integrating advanced bioinformatics techniques and computational tools. This investigation encompassed three crucial dimensions: differential gene expression analysis, gene ontology (GO) enrichment analysis, and protein–protein interaction (PPI) network analysis. Each dimension provided a unique perspective on the molecular landscape of AD, thereby increasing the knowledge of this disease.

In our study, numerous differentially expressed genes (DEGs) were identified[12,13] by comparing AD samples with control samples within GSE4757, illuminating the extensive genetic alterations underlying AD.[14] These DEGs may serve as potential biomarkers for early diagnosis and promising targets for treatment in AD. Accordingly, GO enrichment analysis was performed on these DEGs[15] to reveal the biological functions and pathways significantly associated with AD. The GO results underscored the multifaceted nature of AD pathology and offered a robust foundation for further exploration of specific molecular pathways contributing to AD pathogenesis. Finally, the PPI network was analyzed using the STRING database (https://string-db.org/)[16,17] and Cytoscape software to unveil densely connected regions and hub genes within the AD-related network. The results highlighted ribosomal proteins as key players in AD, hinting at potential connections between protein synthesis processes and AD pathogenesis. These results challenge traditional paradigms and open a novel avenue for research on the molecular basis of AD. Furthermore, several genes, including *RPL15* and *RPS19*, were identified as hub genes by the CytoHubba plugin in Cytoscape, which may serve as key factors in the intricate interaction network of AD. The identification of these hub genes sheds light on the critical nodes orchestrating AD-related pathways.

This study probed the molecular mechanisms of AD using bioinformatics and computational biology, providing critical insights into genetic alterations, disrupted pathways, and central players in AD. Through data and computational analyses, this multidimensional exploration enriched the understanding of AD pathology and advanced the search for effective treatments and diagnostic tools for AD.

2. Materials and methods

2.1. Data preprocessing

GSE4757 is a public gene expression dataset in the Gene Expression Omnibus (GEO) database (https://www.ncbi.nlm.nih.gov/geo/) maintained by the National Center for Biotechnology Information. This dataset pertains to a

study on AD and focuses on the molecular mechanisms underlying NFT formation, a hallmark of AD pathology. In this dataset, laser capture microdissection was utilized to select 1,000 neurons with NFTs and 1,000 normal neurons from the entorhinal cortex of 10 patients with mid-stage AD (https://www.ncbi.nlm.nih.gov/geo/query/acc.cgi?acc=GSE4757).[18-20] Each patient's contribution to the neuron pool was carefully balanced to ensure representativeness. Pooling was performed by combining the extracted RNA from the respective neuron types across all patients before conducting the microarray analysis. Here, the term "normal" refers to neurons without visible neurofibrillary tangles when examined under a microscope. Although these neurons are from a diseased environment, they do not exhibit the specific pathological hallmark (NFTs) and thus serve as a comparative baseline within the scope of our study. Mid-stage AD aligns with the moderate stage of the disease, characterized by more pronounced deterioration in cognitive functions, significantly impairing patients' ability to perform daily activities independently but not yet encompassing the severe end-stage symptoms. GSE4757 was downloaded from the GEO database with the GEOquery package or analogous tools.

2.2. DEG analysis

To screen AD-related DEGs, bioinformatics analyses were conducted using the R package "limma," which is integral to the Bioconductor project. The microarray dataset GSE4757 acquired from the GEO database[18,20] was subjected to data preprocessing, normalization, and quality control. Subsequent to preprocessing, the 'limma' package was used to construct a linear model for each gene, and gene expression was compared between AD and control samples to identify genes with significantly altered expression. The empirical Bayes method in 'limma' was then applied to minimize the standard errors of the estimated log-fold changes, thereby enhancing the reliability of the inferences drawn from the dataset. DEGs[21-23] were selected with stringent criteria: absolute log-fold change (|log FC|) ≥1 and $p < 0.05$, thus ensuring that only the most statistically significant genes were included.

2.3. GO enrichment analysis

To determine AD-related gene expression profiles, the GO enrichment analysis was performed with the R clusterProfiler package, a powerful tool within the Bioconductor project designed for comparing and visualizing biological themes among gene clusters, to decipher the biological functions and pathways significantly associated with the disease.[24,25] The enrichment analysis was carried out after the identification of DEGs from the dataset. The DEGs were mapped to GO terms with the clusterProfiler package, and the overrepresentation of these terms was tested with a hypergeometric distribution model. The analysis was conducted using the human genome as a reference to clarify the specificity of the functions and pathways enriched in AD. Following the enrichment process, the results were visualized with enrichplot and ggplot2 packages. Specifically, enrichplot was used to generate bubble plots that comprehensively displayed the enriched GO terms, incorporating factors such as gene ratio and significance levels, while ggplot2 was utilized to create bar plots that concisely display the most significant GO terms based on their *p*-values. Supplementary File lists the genes that were found to be significantly upregulated in the AD samples compared to control samples. Each entry includes the gene's identifier, common name, log fold change quantifying the level of upregulation, and the *p*-value indicating the statistical significance of this change. The genes listed here meet the criteria of absolute log fold change (|log FC|) ≥1 and $p < 0.05$, highlighting their potential relevance in AD pathology.

2.4. PPI network construction

To explore the molecular interplay underlying AD, the PPI network was constructed and analyzed with an approach that integrated the STRING database and Cytoscape software. This integration provided a platform for the visualization of molecular interaction networks. The use of the STRING database ensured that only interactions with substantial evidence were included in our analysis,[17] as it is instrumental in obtaining high-confidence interactions based on a predefined threshold. After obtaining the PPI network using STRING, the data were imported into Cytoscape, a versatile tool for analyzing and visualizing complex networks. The Molecular Complex Detection (MCODE) plugin in Cytoscape, which operates by scoring network nodes based on local neighborhood density and recursively expands clusters based on pre-set parameters, was applied to identify densely connected regions. These regions are indicative of molecular complexes or significant biological modules in the large network.

2.5. Hub gene identification

The CytoHubba plugin in Cytoscape[26] is a versatile tool for identifying hub genes and significant molecular interactions, offering a variety of ranking algorithms to assess the centrality of nodes within the network. CytoHubba was utilized to analyze the intricate interactions among enriched genes. Considering factors such as degree, betweenness, or closeness centrality, an appropriate algorithm was selected to determine hub genes in AD. Subsequently, the interconnectivity among these hub genes was analyzed and visualized with Cytoscape.

2.6. MicroRNA-hub gene regulatory network analysis

The microRNA (miRNA)-hub gene regulatory network was constructed using the miRNet database (https://www.mirnet.ca/),[27,28] a comprehensive database containing both predicted and experimentally confirmed miRNA-target interactions with a range of innovative features. Briefly, hub genes were identified from the DEGs using the miRNet database, followed by the visualization and refinement of the miRNA-hub gene regulatory network with Cytoscape software (version 3.8.2).

2.7. Hub gene validation through receiver-operating characteristic curve analysis

Receiver-operating characteristic (ROC) curve analyses were performed using the R package pROC to evaluate the diagnostic potential of the hub genes for AD.[28] This analysis enabled the examination of the sensitivity and specificity of the hub genes as biomarkers for AD. The prediction accuracy was quantified by calculating the area under the ROC curve (AUC), which is an indicator for comparing the diagnostic efficacy of the identified genes.

3. Results

3.1. DEG identification

Initially, differential gene expression was conducted by comparing AD samples with control samples within GSE4757.[29,30] A substantial number of DEGs were screened with the R package limma (Figure 1). This data were further refined with the criteria of $|\log FC| \geq 1$ and $p < 0.05$, identifying 732 DEGs, including 465 upregulated genes and 267 downregulated genes (Supplementary Files). This important finding unraveled the extensive genetic alterations associated with AD, providing crucial insights for further investigation. The identified DEGs could potentially serve as biomarkers for early diagnosis or targets for therapeutic interventions in AD.

3.2. Functional enrichment analysis

A comprehensive GO enrichment analysis was performed to delineate the functional involvement of the retrieved genes in AD-related pathways, which was critical in uncovering the biological implications of the identified DEGs.

GO enrichment analysis results exhibited significant pathways and functions in AD (Figure 2). Specifically, the cytosolic ribosome (GO:0022626) was identified as a key component since 26 of 498 genes of interest were enriched in this pathway, suggesting the substantial involvement of these genes in ribosomal function, which is vital for protein synthesis and cellular homeostasis. Moreover, 29 out of 485 genes were enriched in the cytoplasmic translation (GO:0002181) pathway, underscoring potential alterations in protein translation processes in AD. In addition, 28 and 29 genes were respectively enriched in ribosomal subunit (GO:0044391) and ribosome (GO:0005840), indicating possible disruptions or modifications in ribosomal structure and function in AD. Moreover, 26 out of 507 genes were significantly enriched in the structural constituent of the ribosome (GO:0003735) pathway, further affirming the

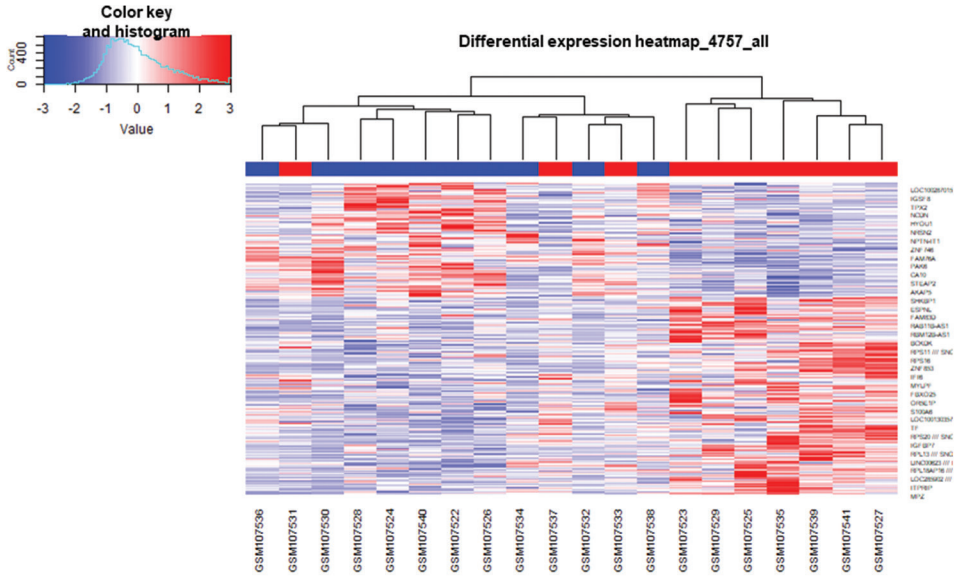

Figure 1. Overview of the GSE4757 heatmap illustrating the comparative analysis of the top 30 significant differentially expressed genes in Alzheimer's disease (AD) vs. normal controls. The color gradient, ranging from blue to red, represents gene expression levels, with blue indicating low expression and red denoting high expression. In the heatmap, the AD group is positioned on the right and marked in red, while the normal control group is on the left.

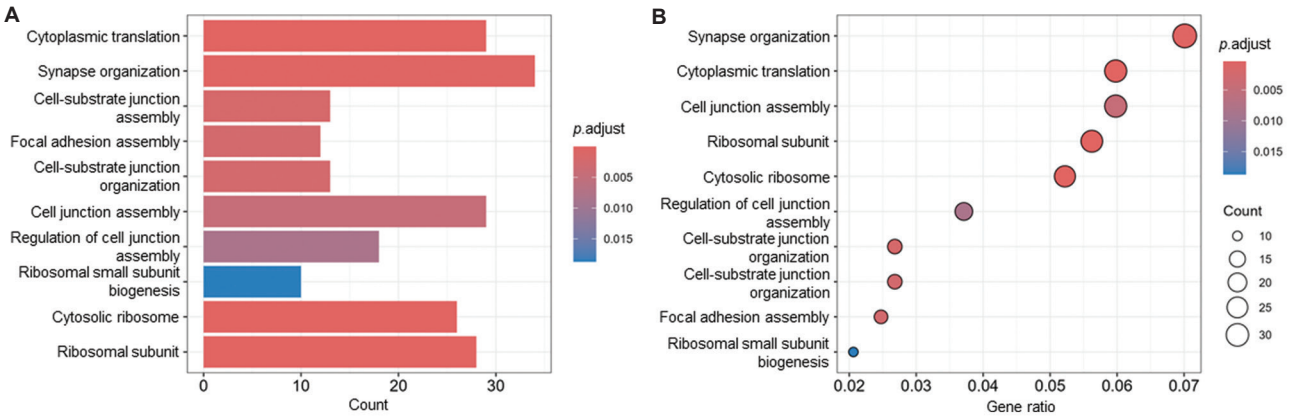

Figure 2. Gene ontology (GO) enrichment analysis of differentially expressed genes in Alzheimer's disease (AD). The bar chart represents the number of genes (A), while the bubble plot represents the proportion of genes (B) associated with the top 10 enriched GO terms. The color gradient indicates the *p*-value, with a significance threshold of $p < 0.05$, highlighting the most statistically significant terms related to AD pathology.

importance of ribosomal components in the pathogenesis of AD.

These GO results collectively underscore the profound impact of ribosomal functions and protein synthesis processes on AD, providing valuable insights into molecular mechanisms underpinning the disease. In addition, these results are beneficial for boosting the understanding of AD progression and offer new avenues for the development of therapeutic interventions for AD.

3.3. Module screening from the PPI network

The PPI network was constructed using the STRING database, based on intersected genes derived from three datasets and text mining, to elucidate the complex interaction networks vital for the pathogenesis of AD. Several significant clusters of interacting proteins were identified (Figure 3). One notable cluster (cluster 1) achieved a high confidence score of 0.432, illustrating a robust set of interactions among the involved proteins. This cluster consisted of proteins predominantly associated with key biological processes and molecular functions associated with AD. Subsequently, individual protein interactions within these clusters were examined and categorized based on various confidence measures, including co-expression, experimental evidence, and text mining scores. For example, the interaction between proteins represented by ENSP00000009530 and ENSP00000498019 had a high STRING confidence score of 0.978, supported by co-expression data (score: 0.829) and experimental evidence (score: 0.842). These interactions collectively formed a network, offering a deeper understanding of molecular mechanisms underlying AD.

3.4. Hub genes

Our analysis identified a subset of genes as central nodes in the PPI network, commonly referred to as hub genes. These genes are crucial due to their high connectivity degree and potential regulatory significance in disease-related molecular networks. Among the identified hub genes, the top 10 were *RPL12*, *RPL15*, *RPL18*, *RPL19*, *RPL27*, *RPL35*, *RPL36*, *RPS16*, *RPS19*, and *RPS9* (Figure 4). Importantly, all these genes encoded ribosomal proteins, which are integral components of the ribosome responsible for protein synthesis. The prominence of ribosomal proteins among the hub genes underscores the possible link between protein synthesis processes and the etiology of AD.

RPL12 and *RPL15*, the top two hub genes, are implicated in the translational control of key proteins and play roles in cellular stress responses. *RPL18* and *RPL19* are associated with apoptosis, which is often dysregulated in neurodegenerative diseases. The identification of *RPL27*, *RPL35*, and *RPL36*, which also encode proteins belonging to the ribosomal protein family, further supports the hypothesis that ribosome function might be impaired in AD. The small ribosomal subunits, encoded by the hub genes *RPS16*, *RPS19*, and *RPS9*, are essential for translation initiation and are linked to neurodevelopmental and neurodegenerative processes. The identification of these hub genes offers a novel insight into the potential molecular mechanisms of AD and suggests alterations in ribosomal function as a hallmark of the disease.

3.5. MicroRNA-hub gene regulatory network construction

The constructed network comprised 212 nodes, encompassing five hub genes (*RPL12*, *RPL15*, *RPL18*, *RPL19*, and *RPL27*) and 207 miRNAs (Figure 5). The large pink nodes were central to the network and denoted ribosomal proteins, indicating their potential regulatory significance. Each ribosomal protein node was connected by lines (edges) to multiple small blue nodes, each

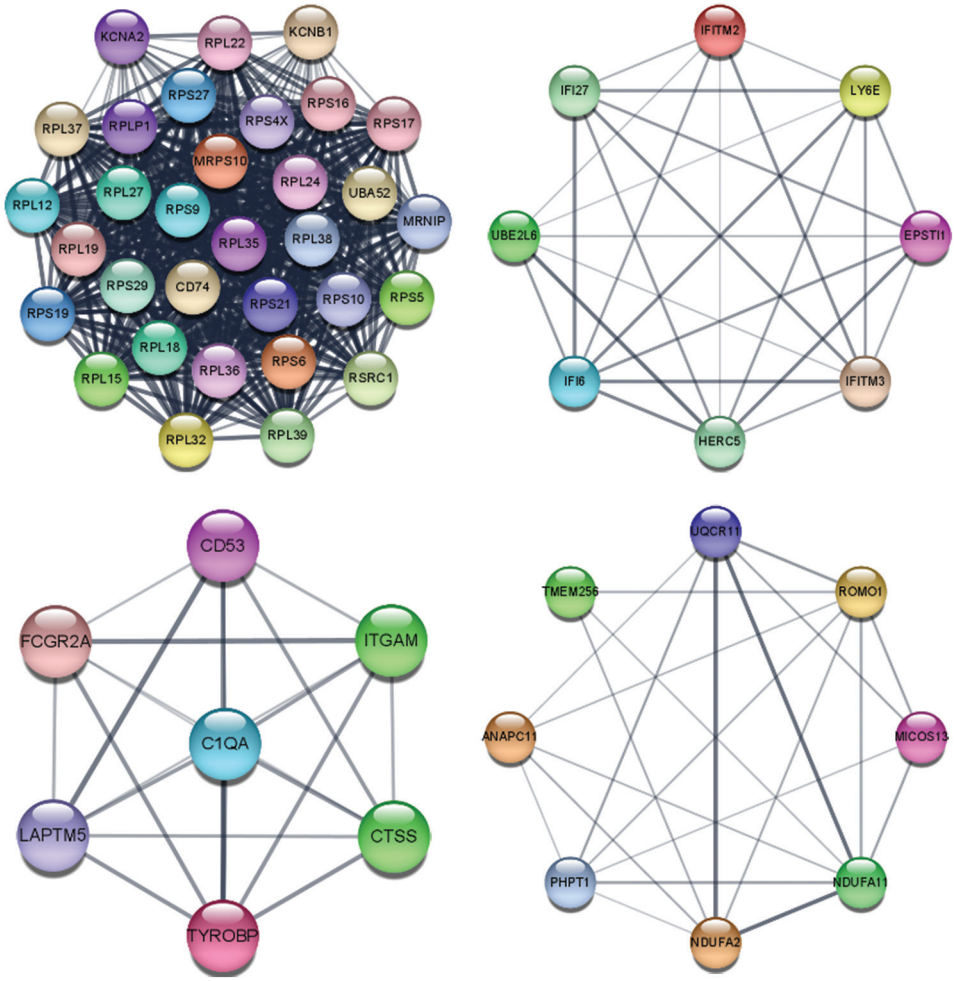

Figure 3. Construction of protein–protein interaction networks showing the top four significant gene modules

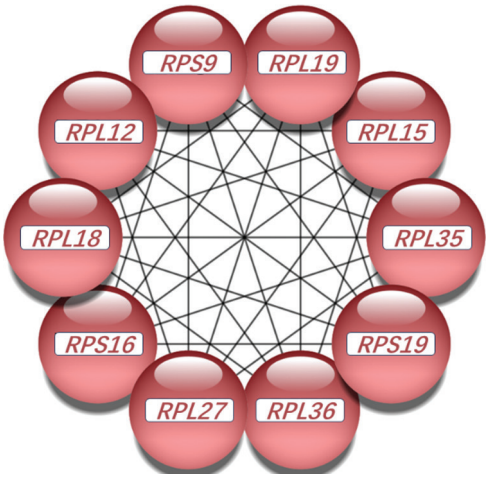

Figure 4. Top 10 hub genes

representing a specific miRNA, such as hsa-miR-103-3p and hsa-miR-484-3p. The thickness of the edges in this network corresponded to the strength or confidence of the interaction data. The extensive web of connections visualized the complexity of the post-transcriptional regulation of these ribosomal components by miRNAs. In terms of connectivity, the network comprised 248 edges, highlighting the relationships between miRNAs and their target genes. Some of the hub genes were targeted by a high number of miRNAs; for instance, *RPL15* was targeted by 81 miRNAs, *RPL12* by 60 miRNAs, and *RPL18* by 43 miRNAs. In addition, *RPL27* and *RPL19* were targeted by a relatively lower number of miRNAs (32 and 31, respectively).

These results illustrated the complex interplay between miRNAs and hub genes in the regulatory network and underscored the potential for miRNAs to highly regulate these proteins, suggesting that sophisticated gene expression control is relevant to both normal cellular function and disease states. The identification of these hub genes and their associated miRNAs provided valuable

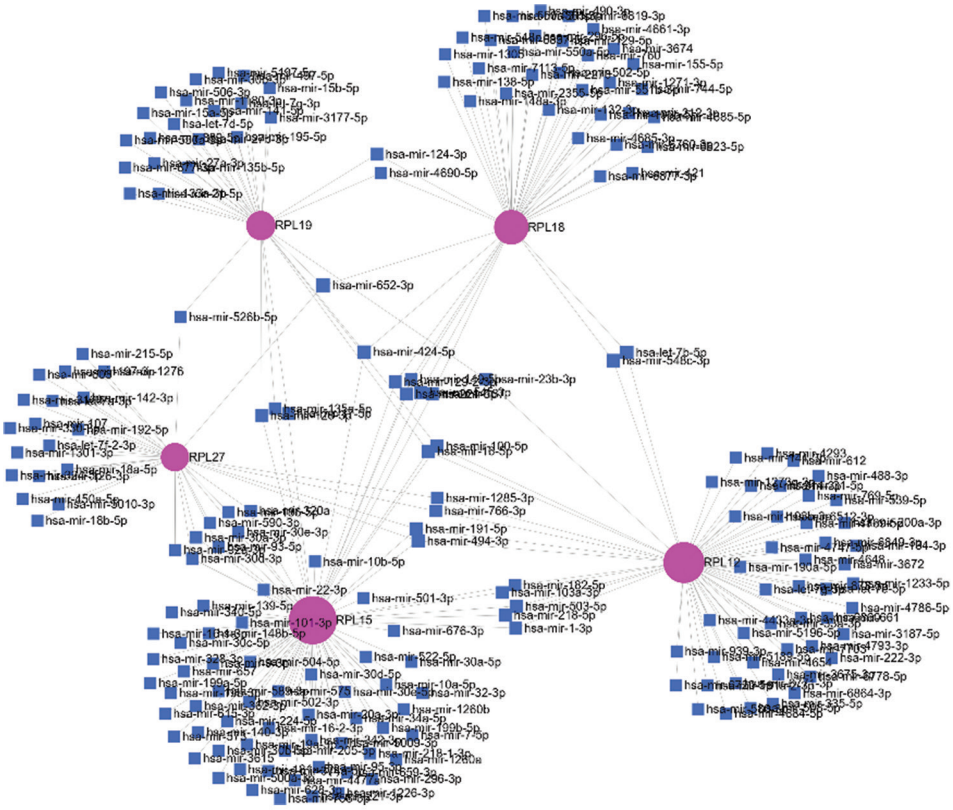

Figure 5. Network diagram of top five hub genes and microRNA interactions

insights into the molecular mechanisms underlying various biological processes and diseases.

3.6. Validation of hub genes through receiver-operating characteristic curve analysis

Receiver-operating characteristic curves were plotted for five genes (*RPL12*, *RPL15*, *RPL18*, *RPL19*, and *RPL27*), and corresponding AUC values were calculated to quantify the ability of gene expression to discriminate between AD patients (case) and normal individuals (control) (Figure 6). The results showed that the AUC values of these genes varied from 0.73 to 0.86, indicating their moderate to high discriminatory performance. A higher AUC value was associated with better performance of gene expression in discriminating between the two groups. The highest AUC value (0.86) was observed for *RPL18*, indicating that *RPL18* may be the most effective and reliable single predictor among the tested ribosomal proteins for differentiating AD from normal status. The ROC curves were located markedly above the diagonal line of no discrimination, reflecting a clear distinction between the control and case groups. These results underscore the potential of these ribosomal proteins as biomarkers for AD, with varying degrees of sensitivity and specificity.

4. Discussion

In this study, comprehensive analyses incorporating differential gene expression analysis, GO enrichment analysis, and PPI network analysis were conducted, providing essential insights into the cytosolic ribosome mechanism underlying AD and offering a panoramic view of the molecular landscape of AD. In addition, ribosomal proteins were revealed as key players in AD, hinting at potential connections between protein synthesis processes and AD pathogenesis. These findings challenge traditional paradigms and open new avenues for research on the molecular basis of AD.

The differential gene expression analysis identified 732 DEGs in AD, highlighting that extensive genetic alterations are associated with the disease. These DEGs may serve as potential biomarkers for early diagnosis and novel targets for therapeutic interventions. The GO enrichment analysis of these DEGs shed light on the biological functions and pathways impacted in AD, revealing that the prominently enriched biological functions and pathways were related to neuroinflammation, synaptic transmission, and neuronal development, emphasizing the multifaceted nature of AD pathology. These findings form a robust foundation for

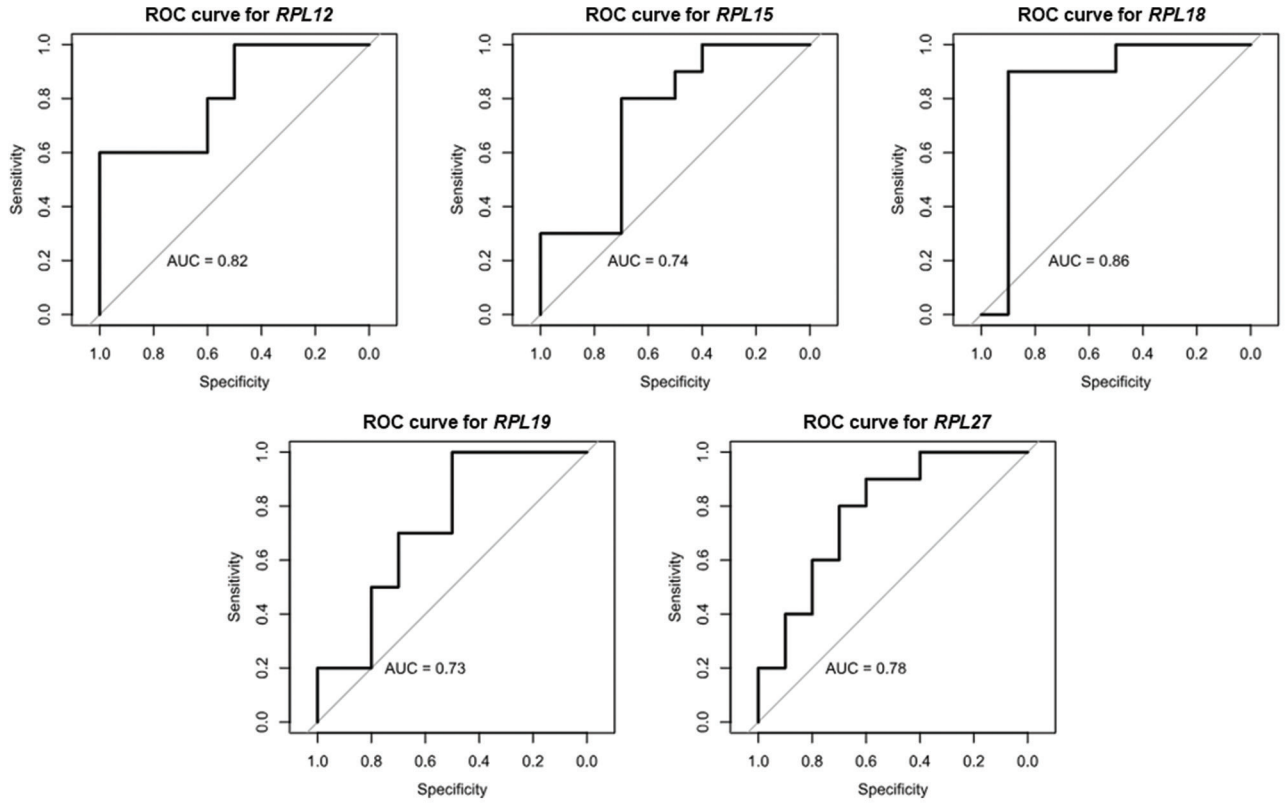

Figure 6. Receiver operating characteristic curves for the top five human ribosomal protein-encoding genes
Abbreviations: AUC: Area under the curve; ROC: Receiver operating characteristic.

the further exploration of specific molecular pathways contributing to AD pathogenesis. Subsequently, the PPI network analysis revealed densely connected regions and hub genes in the AD-related network. The construction of the PPI network, particularly the discovery of the prominent clusters and their high-confidence interactions, offers new targets for therapeutic interventions or potential biomarkers for early diagnosis in AD. The identification of hub genes, including *RPL12*, *RPL15*, *RPL18*, *RPL19*, *RPL27*, *RPL35*, *RPL36*, *RPS16*, *RPS19*, and *RPS9*, underlines the potential significance of ribosomal proteins and translational control in AD. Accordingly, the roles of these genes in neurodegeneration warrant further research,[31,32] and further functional studies on these hub genes may uncover new therapeutic targets and contribute to the development of preventive and therapeutic strategies for AD.

Moreover, the CytoHubba plugin in Cytoscape was used to identify hub genes in the PPI network. These hub genes, including *RPL15* and *RPS19*,[33,34] may be key mediators of AD-related pathways and warrant further research attention. In the realm of AD research, *RPL18* has emerged as a potential biomarker, evidenced by its high AUC value in the ROC curve analysis. A prior study exhibited that *Rpl18* was markedly upregulated in the hippocampus of APP/PS1 mice, illustrating that this gene may be related to the pathogenesis of AD.[35] Consistently, our results displayed a substantial association between *RPL18* expression and AD pathophysiology, providing a compelling argument for its role in the early detection of AD. In addition to protein synthesis, ribosomal proteins possess a wide range of extra-ribosomal functions, such as modulating gene transcription, mRNA translation, cell proliferation, cell differentiation, and cell apoptosis independently of the ribosome.[36] Therefore, the tight regulation of ribosomal protein expression is essential to maintain the normal physiological function of cells.

The ribosome is an intracellular organelle composed of multiple rRNAs and small (40S) and large (60S) subunits responsible for protein translation in eukaryotic cells.[37] The implication of ribosomal proteins, including RPL12, RPL15, RPL19, RPL27, RPL35, RPL36, RPS16, RPS19, and RPS9 in AD, emphasizes a potentially complex relationship between protein synthesis processes and neurodegeneration, which calls for further molecular interrogation.[38,39] The combination of these analyses offers

a comprehensive picture of the molecular landscape of AD, underlining the complexity of the disease. The identified genes, pathways, and hub proteins collectively place the spotlight on the ribosomal protein pathway associated with AD pathogenesis. Prior proteomic analyses of AD donors revealed that 28 ribosomal proteins were significantly upregulated in AD samples, among which RPL12, RPL15, RPL18, RPL27, RPL35, and RPS16 overlapped with the hub genes identified in our study. This prior study also exhibited that ribosomal proteins were upregulated only in the brain capillaries but not in the brain parenchyma, signifying the functional impairment of the blood-brain barrier (BBB).[40] The relationship between the functional impairment of the BBB and neuroinflammation in AD was also demonstrated in our previous study.[41] In addition to their canonical roles in protein synthesis, ribosomal proteins, including hub genes in our study (such as *RPL12*, *RPL15*, *RPL18*, *RPL19*, and *RPL27*), have been implicated in a variety of extra-ribosomal functions responsible for cellular homeostasis and stress responses. Of note, several ribosomal proteins have been demonstrated to interact with MDM2 protein, a key regulator of the tumor suppressor p53. Under conditions of cellular stress, such interactions can stabilize and activate p53, thereby initiating a cascade of events that can cause cell cycle arrest, DNA repair, or apoptosis. Our bioinformatic analysis also demonstrated the presence of ribosomal pathway abnormalities in the entorhinal cortex.

Our findings are concordant with previous studies that have underscored the importance of neuroinflammation, synaptic dysfunction, and protein synthesis dysregulation in AD.[42,43] Innovatively, our study offered a novel perspective by spotlighting specific genes and pathways among these factors. Importantly, our results unravel that ribosomal proteins, traditionally associated with protein synthesis, may exert multifaceted effects on AD by potentially mediating neuroinflammation and maintaining synaptic integrity. This finding opens a new avenue for probing the crosstalk between these two processes and their contribution to disease progression. Nevertheless, the detailed mechanisms by which ribosomal proteins influence AD remain unclear. Accordingly, further molecular biological studies are warranted to analyze the involvement and sequence of events of ribosomal proteins in AD and to examine potential differences in the expression patterns of specific proteins among the identified hub genes and their implications in AD pathology.

As the samples and sequencing data utilized in this study were not originally prepared by the authors, there is a potential for biases that could influence the results. These gaps, due to the reliance on pre-existing data sets, may introduce variables that are not accounted for in our study design, potentially leading to biased or misleading results. In addition, our study has not independently validated the findings through experimental or additional computational methods, which is an evident limitation in affirming the reliability of our conclusions.

5. Conclusion

Our multifaceted analyses provide precious insights into the molecular complexity of AD. The identified genes, pathways, and hub proteins related to ribosomal function form the basis for future mechanistic studies and the search for therapeutic targets.

Acknowledgments

None.

Funding

None.

Conflict of interest

The authors declare that they have no competing interests.

Author contributions

Conceptualization: Shan Luo
Investigation: Shan Luo
Methodology: Shan Luo, Yifei Wang
Project administration: Kohji Fukunaga
Supervision: Kohji Fukunaga
Writing – original draft: Shan Luo
Writing – review & editing: Yifei Wang

Ethics approval and consent to participate

Not applicable.

Consent for publication

Not applicable.

Availability of data

Data used in the study can be obtained from the GSE4757 dataset in the GEO database (https://www.ncbi.nlm.nih.gov/geo/query/acc.cgi?acc=GSE4757).

References

1. Hutton M, Hardy J. The presenilins and Alzheimer's disease. *Hum Mol Genet*. 1997;6(10):1639-1646.

   doi: 10.1093/hmg/6.10.1639

2. Bush AI. The metallobiology of Alzheimer's disease. *Trends Neurosci*. 2003;26(4):207-214.

   doi: 10.1016/S0166-2236(03)00067-5

3. DeTure MA, Dickson DW. The neuropathological diagnosis of Alzheimer's disease. *Mol Neurodegener*. 2019;14(1):32.

doi: 10.1186/s13024-019-0333-5

4. Goedert M, Spillantini MG. A century of Alzheimer's disease. *Science*. 2006;314(5800):777-781.

doi: 10.1126/science.1132814

5. Jucker M, Walker LC. Alzheimer's disease: From immunotherapy to immunoprevention. *Cell*. 2023;186(20):4260-4270.

doi: 10.1016/j.cell.2023.08.021

6. Ballard C, Gauthier S, Corbett A, Brayne C, Aarsland D, Jones E. Alzheimer's disease. *Lancet*. 2011;377(9770): 1019-1031.

doi: 10.1016/S0140-6736(10)61349-9

7. Asher S, Priefer R. Alzheimer's disease failed clinical trials. *Life Sci*. 2022;306:120861.

doi: 10.1016/j.lfs.2022.120861

8. Scheltens P, De Strooper B, Kivipelto M, *et al*. Alzheimer's disease. *Lancet*. 2021;397(10284):1577-1590.

doi: 10.1016/S0140-6736(20)32205-4

9. Trejo-Lopez JA, Yachnis AT, Prokop S. Neuropathology of Alzheimer's Disease. *Neurotherapeutics*. 2022;19(1):173-185.

doi: 10.1007/s13311-021-01146-y

10. Zhang H, Zhang, Y, Li, Y, *et al*. Bioinformatics and network pharmacology identify the therapeutic role and potential mechanism of melatonin in AD and Rosacea. *Front Immunol*. 2021;12:756550.

doi: 10.3389/fimmu.2021.756550

11. Horgusluoglu E, Neff R, Song WM, *et al*. Integrative metabolomics-genomics approach reveals key metabolic pathways and regulators of Alzheimer's disease. *Alzheimers Dement*. 2022;18(6):1260-1278.

doi: 10.1002/alz.12468

12. Clark NR, Hu KS, Feldmann AS, *et al*. The characteristic direction: A geometrical approach to identify differentially expressed genes. *BMC Bioinformatics*. 2014;15:79.

doi: 10.1186/1471-2105-15-79

13. Broberg P. Statistical methods for ranking differentially expressed genes. *Genome Biol*. 2003;4(6):R41.

doi: 10.1186/gb-2003-4-6-r41

14. Chen S, Chai X, Wu X. Bioinformatical analysis of the key differentially expressed genes and associations with immune cell infiltration in development of endometriosis. *BMC Genom Data*. 2022;23(1):20.

doi: 10.1186/s12863-022-01036-y

15. Boyle EI, Weng S, Gollub J, *et al*. GO: TermFinder--open source software for accessing Gene Ontology information and finding significantly enriched Gene Ontology terms associated with a list of genes. *Bioinformatics*. 2004;20(18):3710-3715.

doi: 10.1093/bioinformatics/bth456

16. Von Mering C, Huynen M, Jaeggi D, Schmidt S, Bork P, Snel, B. STRING: A database of predicted functional associations between proteins. *Nucleic Acids Res*. 2003;31(1):258-261.

doi: 10.1093/nar/gkg034

17. Szklarczyk D, Kirsch R, Koutrouli M, *et al*. The STRING database in 2023: Protein-protein association networks and functional enrichment analyses for any sequenced genome of interest. *Nucleic Acids Res*. 2023;51(D1):D638-D646.

doi: 10.1093/nar/gkac1000

18. Yan T, Ding F, Zhao Y. Integrated identification of key genes and pathways in Alzheimer's disease via comprehensive bioinformatical analyses. *Hereditas*. 2019;156:25.

doi: 10.1186/s41065-019-0101-0

19. Fiscon G, Sibilio P, Funari A, Conte F, Paci P. Identification of potential repurposable drugs in Alzheimer's disease exploiting a bioinformatics analysis. *J Pers Med*. 2022;12(10):1731.

doi: 10.3390/jpm12101731

20. Liu W, Chen S, Rao X, Yang Y, Chen X, Yu L. The inflammatory gene *PYCARD* of the entorhinal cortex as an early diagnostic target for Alzheimer's disease. *Biomedicines*. 2023;11(1):194.

doi: 10.3390/biomedicines11010194

21. Shi L, Jones WD, Jensen RV, *et al*. The balance of reproducibility, sensitivity, and specificity of lists of differentially expressed genes in microarray studies. *BMC Bioinformatics*. 2008;9 Suppl 9:S10.

doi: 10.1186/1471-2105-9-S9-S10

22. Wei B, Wang L, Du C, Hu G, *et al*. Identification of differentially expressed genes regulated by transcription factors in glioblastomas by bioinformatics analysis. *Mol Med Rep*. 2015;11(4):2548-2554.

doi: 10.3892/mmr.2014.3094

23. Yang X, Zhu S, Li L, *et al*. Identification of differentially expressed genes and signaling pathways in ovarian cancer by integrated bioinformatics analysis. *Onco Targets Ther*. 2018;11:1457-1474.

doi: 10.2147/OTT.S152238

24. Fowler DM, Araya CL, Gerard W, Fields S. Enrich: Software for analysis of protein function by enrichment and depletion of variants. *Bioinformatics*. 2011;27(24):3430-3431.

doi: 10.1093/bioinformatics/btr577

25. Ding Z, Wei Q, Kihara D. Computing and visualizing gene function similarity and coherence with NaviGO. *Methods Mol Biol*. 2018;1807:113-130.

doi: 10.1007/978-1-4939-8561-6_9

26. Chin CH, Chen SH, Wu HH, Ho CW, Ko MT, Lin CY. cytoHubba: Identifying hub objects and sub-networks from complex interactome. *BMC Syst Biol*. 2014;8 Suppl 4:S11.

doi: 10.1186/1752-0509-8-S4-S11

27. Chang L, Zhou G, Soufan O, Xia J. miRNet 2.0: Network-based visual analytics for miRNA functional analysis and systems biology. *Nucleic Acids Res*. 2020;48(W1):W244-W251.

doi: 10.1093/nar/gkaa467

28. Zhang J, Lou W. A Key mRNA-miRNA-lncRNA competing endogenous RNA triple sub-network linked to diagnosis and prognosis of hepatocellular carcinoma. *Front Oncol*. 2020;10:340.

doi: 10.3389/fonc.2020.00340

29. Feng X, Bai Z, Wang J, *et al*. Robust gene dysregulation in Alzheimer's disease brains. *J Alzheimers Dis*., 2014;41(2):587-597.

doi: 10.3233/JAD-140147

30. Kakati T, Bhattacharyya DK, Barah P, Kalita JK. Comparison of methods for differential co-expression analysis for disease biomarker prediction. *Comput Biol Med*. 2019;113:103380.

doi: 10.1016/j.compbiomed.2019.103380

31. Asgari N, Akbari MT, Zare S, Babamohammadi G. Positive association of apolipoprotein E4 polymorphism with recurrent pregnancy loss in Iranian patients. *J Assist Reprod Genet*. 2013;30(2):265-268.

doi: 10.1007/s10815-012-9897-5

32. Cha DJ, Mengel D, Mustapic M, *et al*. miR-212 and miR-132 are downregulated in neurally derived plasma exosomes of Alzheimer's patients. *Front Neurosci*. 2019;13:1208.

doi: 10.3389/fnins.2019.01208

33. Hernández-Ortega K, Garcia-Esparcia P, Gil L, Lucas JJ, Ferrer I. Altered machinery of protein synthesis in Alzheimer's: From the nucleolus to the ribosome. *Brain Pathol*. 2016;26(5):593-605.

doi: 10.1111/bpa.12335

34. Gui H, Gong Q, Jiang J, Liu M, Li H. Identification of the Hub genes in Alzheimer's disease. *Comput Math Methods Med*. 2021;2021:6329041.

doi: 10.1155/2021/6329041

35. Feng L, Wang G, Song Q, *et al*. Proteomics revealed an association between ribosome-associated proteins and amyloid beta deposition in Alzheimer's disease. *Metab Brain Dis*. 2024;39(2):263-282.

doi: 10.1007/s11011-023-01330-3

36. Wang W, Nag S, Zhang X, *et al*. Ribosomal proteins and human diseases: Pathogenesis, molecular mechanisms, and therapeutic implications. *Med Res Rev*. 2015;35(2):225-285.

doi: 10.1002/med.21327

37. Wilson DN, Cate JH. The structure and function of the eukaryotic ribosome. *Cold Spring Harb Perspect Biol*. 2012;4(5):a011536.

doi: 10.1101/cshperspect.a011536

38. Pelekoudas-Oikonomou F, Zachos G, Papaioannou M, *et al*. Blockchain-based security mechanisms for IoMT edge networks in IoMT-based healthcare monitoring systems. *Sensors* (*Basel*). 2022;22(7):2449.

doi: 10.3390/s22072449

39. Ito S, Yagi R, Ogata S, *et al*. Proteomic alterations in the brain and blood-brain barrier during brain Aβ accumulation in an APP knock-in mouse model of Alzheimer's disease. *Fluids Barriers CNS*. 2023;20(1):66.

doi: 10.1186/s12987-023-00466-9

40. Suzuki M, Tezuka K, Handa T, *et al*. Upregulation of ribosome complexes at the blood-brain barrier in Alzheimer's disease patients. *J Cereb Blood Flow Metab*. 2022;42(11):2134-2150.

doi: 10.1177/0271678X221111602

41. Luo S, Tamada A, Saikawa Y, Wang Y, Yu Q, Hisatsune T. P2Y1R silencing in astrocytes protected neuroinflammation and cognitive decline in a mouse model of Alzheimer's disease. *Aging Dis*. 2024;15(4):1969-1988.

doi: 10.14336/AD.2023.1006

42. Sowell RA, Owen JB, Butterfield DA. Proteomics in animal models of Alzheimer's and Parkinson's diseases. *Ageing Res Rev*. 2009;8(1):1-17.

doi: 10.1016/j.arr.2008.07.003

43. Zhou X, Huang K, Wang Y, *et al*. Evaluation of therapeutic effects of tetramethylpyrazine nitrone in Alzheimer's disease mouse model and proteomics analysis. *Front Pharmacol*. 2023;14:1082602.

doi: 10.3389/fphar.2023.1082602

ACCSCIENCE PUBLISHING

Brain & Heart

ORIGINAL RESEARCH ARTICLE

Rapid assessment of cardiac autonomic modulation and adaptive stress responses: Automatic calculation of time-varying parasympathetic, sympathetic, and Baevsky stress indexes

Donatella Brisinda[1,2,3†*], Marco Picerni[3], Peter Fenici[1,3], and Riccardo Fenici[3†*]

[1]Catholic University of Sacred Heart, Faculty of School of Medicine and Surgery, Rome, Italy

[2]Department of Ageing, Neurosciences, Head-Neck, and Orthopaedics Sciences. Fondazione Policlinico Universitario A. Gemelli IRCCS, Rome, Italy

[3]Biomagnetism and Clinical Physiology International Center, Associazione Biomagnetismo Sport Serenità e Salute, Rome, Italy

†These authors contributed equally to this work.

***Corresponding authors:**
Riccardo Fenici
(riccardo.fenici@unicatt.it)
Donatella Brisinda
(donatella.brisinda@unicatt.it)

Citation: Brisinda D, Picerni M, Fenici P, Fenici R. Rapid assessment of cardiac autonomic modulation and adaptive stress responses: Automatic calculation of time-varying parasympathetic, sympathetic, and Baevsky stress indexes. *Brain & Heart.* 2024;2(4):3503.
doi: 10.36922/bh.3503

Received: April 25, 2024

Accepted: August 26, 2024

Published Online: October 9, 2024

Abstract

Cardiac autonomic modulation (CAM), which is regulated by the balance between the sympathetic and parasympathetic nervous systems, is involved in various physiological and pathological conditions. Heart rate variability (HRV) analysis has been used to explore the complex relationship between the brain and heart, as described by Porges' polyvagal theory and Thayer's neurovisceral integration model. Recently, an automated calculation of new parasympathetic, sympathetic, and Baevsky stress indexes based on HRV parameters has been introduced for faster and more comprehensive CAM assessment, though their normal ranges remain undefined. This study aimed to determine the average values of these indexes in a healthy population of different ages during rest, daily activities, non-rapid eye movement sleep, graded physical effort, and acute psychophysiological stress. At rest, the parasympathetic and sympathetic indexes were consistently within the proposed normal range and inversely related. However, Baevsky stress index values from Kubios were higher than expected, conflicting with the assumption that they are simply the square root of those calculated using the original formula. Despite this, time-varying assessment of all indexes can provide valuable insights into CAM adaptation during physical effort and acute psychophysiological stress in real-world critical situations. Notably, our novel finding shows that the inverse correlation between parasympathetic and sympathetic/stress indexes under stress is better explained by non-linear functions, offering a potential new measure of brain–heart interaction during real-life critical events.

Keywords: Heart rate variability; Autonomic nervous system; Sympathetic nervous system; Parasympathetic nervous system; Baevsky stress index; Psychophysiological stress

1. Introduction

Cardiac autonomic modulation (CAM), regulated by the balance between the sympathetic (SNS) and parasympathetic nervous systems (PNS), is vital in both health and disease, making its evaluation crucial.[1,2] The study of heart rate variability (HRV), which reflects autonomic nervous system (ANS) function, began in the 1960s, initially for monitoring astronauts in space.[3] Since the 1980s, HRV analysis has been widely used as a non-invasive method to evaluate CAM in clinical settings, with autonomic imbalance recognized as a strong predictor of all-cause cardiac mortality.[4]

Early HRV assessments followed a "reductionist" approach,[5] relying on linear methods such as time-domain (TD) and frequency-domain (FD) analysis.[4,6,7] Many studies were based on the premise that increased sympathetic activity corresponds with decreased parasympathetic activity, with the spectral low frequency/high frequency (LF/HF) ratio suggested as a marker for stress responses, though this remains debated.[7,8]

HRV tends to decline with age due to structural and functional changes,[9-12] and significant reductions in HRV are associated with lower life expectancy and various diseases.[5,9-18] It is important to note that the LF component is not exclusively a marker of sympathetic activity, as both SNS and PNS influence LF.[5] In addition, the very-low-frequency (VLF) band may reflect broader systemic stress, not just cardiac stress.[19-21]

A more systematic perspective suggests that HRV is not only a marker of ANS dysfunction but also a means for understanding interactions between bodily systems, especially between the brain and cardiovascular system.[5] In health, "organized variability" is present, whereas disease leads to a "decomplexification" of this variability, resulting in more periodic and cyclic behaviors, as seen in conditions such as Cheyne–Stokes breathing, Parkinson's disease tremors, or cyclic neutrophil oscillations in chronic myelogenous leukemia.[22]

The vagal system plays a key role in brain–heart interaction, particularly in stress regulation, as explained by Porges' "polyvagal theory"[23,24] and Thayer's "neurovisceral integration model," which links HRV to emotional and stress responses.[25-30]

To better study these complex interactions, non-linear (NL) mathematical methods have been introduced. For instance, NL entropy is associated with vagal activity, whereas recurrence plot analysis reflects sympathetic activation.[31,32] In stress-related studies, such as those examination-induced stress, combining linear and NL methods has improved stress detection.[33] Mathematical models for the time-varying analysis of both linear and NL HRV parameters have enhanced the ability to assess CAM responses to clinical or real-world stressors, even in real time.[34-39]

Recently, the software has been developed to automatically compute time-varying parasympathetic (PNSi), sympathetic (SNSi), and Baevsky stress (BSTRi) indexes, enabling faster assessments of CAM, particularly in acute stress situations.[40] Although HRV parameters are well-established, the normal ranges for these new indexes, especially BSTRi, remain unclear, particularly in stressful conditions.[41-46]

This pilot study aims to determine the average values of PNSi, SNSi, and BSTRi in a healthy population during various activities (rest, daily activities, non-rapid eye movement (NREM) sleep, graded physical effort, and acute psychophysiological stress) to create a preliminary reference for CAM assessment in real-world high-stress or pathological conditions, such as dysautonomic syndromes.

2. Methods

2.1. Study population, ethics, and inclusion criteria

We retrospectively analyzed 24-h Holter electrocardiogram (ECG) recordings from 104 healthy individuals, categorized into three age groups: Age1 (16–34 years), Age2 (35–52 years), and Age3 (53–84 years), all consecutively evaluated in our clinic for fitness or clinical evaluations. Among these participants, 16 were police officers monitored during fitness assessments and highly stressful, realistic tactical training. In addition, ECG data from a 75-year-old healthy male who volunteered to be monitored 3 times/week from April to November 2022 during training on a professional bicycle ergometer (Technogym, Italy) were included (Table 1).

All participants were free of cardiovascular and neurological conditions based on clinical history, physical examinations, and laboratory results. They were required to refrain from smoking, consuming coffee, or using any substances or medications that could affect their natural sympathovagal balance for at least 24 h before ECG recording.

All participants provided informed consent for ECG recording and monitoring, primarily related to preventive checkups for non-competitive sports or fitness-for-duty evaluations. They also agreed to the anonymous use of their ECG data for scientific and publication purposes. All recording procedures were conducted in accordance with good clinical practice (GPC) guidelines and ethical standards outlined in the Helsinki Declaration of 1975, revised in 2013.[47]

2.2. HRV recordings and analysis

We conducted 24-h 12-lead Holter ECG recordings using the H12 (Mortara Instruments). Real-time ECG monitoring during tactical and physical training was carried out with a 3-lead wearable ECG (Nuubo, Spain).

For longitudinal monitoring during physical training, each session included 10 min of baseline rest, 5 min of warm-up, 30 min of exercise, and 10 min of recovery. The training workload was categorized by age into low (65–75 watts/min), moderate (75–85 watts/min), semi-intense (85–95 watts/min), and intense (95–110 watts/min). For this study, ECG data from 40 training sessions (10 sessions for each workload) were analyzed.

HRV parameters were calculated using Kubios Premium software (version 3.5.0) in TD, FD, and NL methods, along with time-varying algorithms,[40] following "detrending" with the "smooth priors" function (lambda = 500).

Short-term HRV was calculated over 5 min[4] during regular daily activities and NREM sleep for all participants, as well as during highly stressful police tactical training (16 cases). In addition, HRV parameters were assessed from 2-min intervals, as illustrated in Figure 1, to evaluate the reliability of PNSi, SNSi, and BSTRi measurements from these shorter intervals.

For the training sessions, HRV parameters were calculated using 2-min intervals taken at baseline rest, every 4 min during exertion, and at the first, fifth, and tenth min of recovery. ECG data from 40 training sessions (10 sessions for each workload) were analyzed. The PNSi, SNSi, and BSTRi values resulting from each workload were averaged and compared to evaluate reproducibility across sessions with the same workload.

Kubios calculates the PNSi by integrating three parameters: the mean RR interval, the RMSSD (the mean square root of successive RR interval differences, closely related to parasympathetic cardiac activation), and the SD1 index from Poincaré plot (in normalized units), which correlates with the RMSSD. The PNS index is considered normal during rest if it falls within ±2 standard deviations (SD) of the normal population distribution.[40]

The SNSi is computed using three parameters: the mean HR interval, the BSTRi, and the SD2 index from the Poincaré plot (in normalized units), which correlates with SDNN.[42] Similar to the PNSi, the SNS index is deemed normal if it is within ±2 SD of the normal population distribution. During psychophysiological stress or high-intensity exercise, significantly lower PNSi and higher SNSi values are expected.

The BSTRi is a geometric measure of HRV that indicates stress on the cardiovascular system, calculated using the following formula:

$$SI = \frac{AMo}{Mo} MxDMn \quad (I)$$

Table 1. Demographics of the studied participants

Subgroups	No. of cases	Sex		Age range (years)
		Male	Female	
Age1	36	10	26	16–34
Age2	29	15	14	35–52
Age3	23	10	13	53–84
Police officers	16	15	1	31–50
Senior training	1	1		75

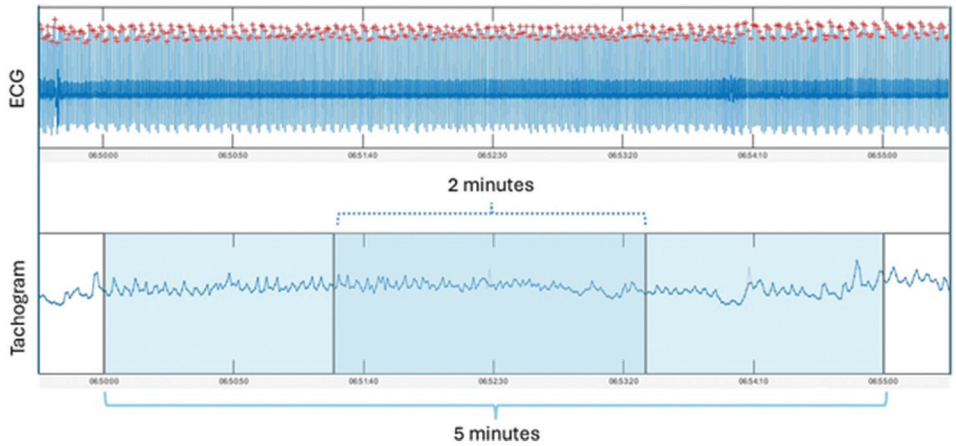

Figure 1. Time segment selection method. The upper row shows 6 min of ECG recording, whereas the lower row displays examples of 5-min (light sky blue) and 2-min (darker sky blue) tachogram segments selected
Abbreviation: ECG: Electrocardiogram.

where AMo is the mode amplitude (the percentage of intervals corresponding to the mode value relative to the sample size), Mo is the mode, and MxDMn represents the degree of interval variability, calculated from the difference between the maximum (Mx) and minimum (Mn) intervals. According to Baevsky, BSTRi values are considered normal at rest when they range from 80 to 150 conventional units and are 1.5–2 times higher during physical or emotional stress. High BSTRi values suggest reduced variability and increased sympathetic cardiac activation.[43,44] In Kubios, BSTRi values are expressed as the square root of the original Baevsky values.[40]

To calculate both PNSi and SNSi, each parameter is first compared to the normal population values reported by Nunan.[41] These values are then scaled using the SD of the normal population and refined with undisclosed proprietary weighting factors to ensure robust and reliable index values. This process considers the relationships between exercise intensity, heart rate, and HRV.[40]

2.3. Statistical analysis

Data were input into SPSS (21.0 version, Chicago, Illinois) for quantitative analysis. All data were examined for expected ranges, outliers, and abnormal values. Continuous variables are presented as mean and SD. Differences between groups were assessed using either parametric or non-parametric tests, as appropriate. A $P < 0.05$ was considered statistically significant. The Pearson correlation was used to evaluate the relationships between selected quantitative variables, with a correlation considered strong if $R > 0.7$.

3. Results

3.1. Population

The demographics of the 105 healthy participants are summarized in Table 1.

3.2. Linear and NL HRV parameters

3.2.1. Variations in HRV parameters based on short-term interval duration

Compared to those calculated from 5-min intervals, the average values of most HRV parameters were not significantly different when calculated from 2-min intervals across all examined situations (daily activity, NREM sleep, and acute psychophysiological stress). Significant differences ($P < 0.05$) for 5-min intervals were found only for certain recurrence plot parameters (in all conditions), approximated entropy (not under stress), the triangular index, TINN (during NREM sleep), and minimum heart rate under stress (Table 2).

For clarity, only a selection of Kubios-calculated parameters will be presented in the following tables.

Table 2. Difference in each HRV parameter calculated from short-term time segments of 2 and 5 min, during regular daily activity (104 cases), NREM sleep (104 cases), and high-stress tactical training (16 police officers)

	Daily activity						NREM sleep						High stress					
	2 min interval		5 min		*n*	*P*	2 min interval		5 min interval		*n*	*P*	2 min interval		5 min interval		*n*	*P*
	Mean	SD	Mean	SD			Mean	SD	Mean	SD			Mean	SD	Mean	SD		
MeanRR *ms*	734.3	120.1	731.9	116.8	104		977.8	148.7	975.0	154.0	104		438.0	75.0	445.3	70.2	16	
SDNN *ms*	31.7	15.1	31.2	13.7	104		27.2	12.5	27.5	12.2	104		13.7	13.1	15.0	12.6	16	
MeanHR *bpm*	83.8	13.2	84.0	13.0	104		62.7	9.1	63.0	9.9	104		140.2	20.2	137.3	17.7	16	
MinHR *bpm*	74.7	11.5	72.7	10.9	104		59.6	8.6	59.1	9.2	104		122.9	20.9	106.6	16.8	16	#
MaxHR *bpm*	93.7	14.5	97.0	14.9	104		65.7	9.7	67.4	11.6	104		155.6	18.6	160.1	17.7	16	
RMSSD *ms*	22.3	12.1	21.8	11.0	104		32.7	16.0	32.7	16.1	104		6.4	6.1	7.0	6.5	16	
pNN50	5.1	8.5	4.6	7.7	104		14.1	16.5	14.2	16.5	104		0.4	1.2	0.6	1.8	16	
HRVtriang index	7.6	2.6	8.3	3.0	104		7.1	2.4	7.8	2.8	104	#	3.6	2.3	3.5	2.5	16	
TINN *ms*	140.9	65.0	155.9	67.7	104		117.3	52.2	135.4	62.2	104	#	63.9	57.2	84.3	59.7	16	
DC *ms*	18.3	12.4	17.6	11.5	104		28.0	18.6	27.9	17.9	104		5.4	9.6	5.2	8.6	16	
DCmod *ms*	23.1	12.3	22.5	11.4	104		36.8	18.6	36.7	18.6	104		6.5	7.4	6.8	8.0	16	
AC *ms*	−18.1	12.7	−17.5	11.9	104		−28.9	18.3	−28.9	18.1	104		−4.2	6.0	−4.3	5.8	16	
ACmod *ms*	−23.7	14.0	−23.0	12.8	104		−38.7	19.9	−38.6	20.0	104		−5.8	5.6	−6.3	6.6	16	
VLFpow FFT ms^2	98.6	130.7	99.4	102.8	104		39.0	60.4	45.5	58.3	104		25.0	29.3	25.7	27.0	16	
LFpow FFT ms^2	880.4	1,051.9	844.5	921.3	104		250.1	364.3	286.3	397.6	104		276.6	504.1	317.2	596.6	16	

(Contd...)

Table 2. ***(Continued)***

	Daily activity						NREM sleep						High stress					
	2 min interval		5 min		*n*	*P*	2 min interval		5 min interval		*n*	*P*	2 min interval		5 min interval		*n*	*P*
	Mean	SD	Mean	SD			Mean	SD	Mean	SD			Mean	SD	Mean	SD		
HFpow FFT *ms*^{2}	218.0	336.6	203.2	235.3	104		508.7	647.1	512.6	662.8	104		47.8	81.6	37.6	62.2	16	
VLFpow FFT log	3.9	1.3	4.1	1.1	104		3.1	1.0	3.3	0.9	104		2.5	1.3	2.7	1.2	16	
LFpow FFT log	6.2	1.1	6.3	1.0	104		5.1	0.9	5.3	0.8	104		4.1	1.9	4.3	1.8	16	
HFpow FFT log	4.8	1.1	4.8	1.1	104		5.8	0.9	5.8	0.9	104		2.3	1.9	2.4	1.7	16	
VLFpow FFT	9.4	6.5	10.2	6.5	104		6.0	4.7	6.4	4.9	104		18.0	11.7	18.0	13.6	16	
LFpow FFT	72.7	10.5	71.9	10.0	104		32.5	12.1	35.1	12.0	104		70.3	8.8	71.3	11.8	16	
HFpow FFT	17.9	8.5	17.8	7.8	104		61.5	14.1	58.5	14.2	104		11.7	6.8	10.7	5.3	16	
LFpow FFT nu	80.1	9.4	80.0	8.9	104		34.8	13.6	37.8	14.0	104		86.3	7.3	87.2	5.8	16	
HFpow FFT nu	19.9	9.4	19.9	8.9	104		65.1	13.6	62.2	14.0	104		13.7	7.3	12.8	5.8	16	
TOTpow FFT *ms*^{2}	1,197.2	1,342.9	1,147.4	1,168.6	104		798.1	955.8	844.7	1,014.2	104		349.4	605.0	380.5	681.8	16	
LF/HF*ratio* FFT	5.2	3.3	5.1	3.0	104		0.6	0.7	0.8	1.2	104		9.9	9.2	8.7	4.9	16	
VLFpow AR *ms*^{2}	121.9	127.8	121.7	106.8	104		51.0	56.6	55.8	50.0	104		41.4	66.2	48.9	69.5	16	
LFpow AR *ms*^{2}	820.0	907.9	783.4	767.1	104		265.4	395.7	279.2	340.9	104		270.6	506.6	317.6	588.5	16	
HFpow AR *ms*^{2}	210.3	293.9	201.0	248.7	104		488.9	636.9	497.5	635.5	104		30.9	54.1	33.6	56.4	16	
VLFpow AR log	4.4	1.0	4.5	0.9	104		3.6	0.8	3.7	0.7	104		2.8	1.5	3.2	1.3	16	
LFpow AR log	6.2	1.1	6.2	1.0	104		5.1	0.9	5.2	0.9	104		4.1	1.9	4.6	1.5	16	
HFpow AR log	4.7	1.1	4.8	1.1	104		5.7	0.9	5.7	0.9	104		2.2	1.6	2.5	1.5	16	
VLFpow AR	12.1	5.1	12.8	5.0	104		7.9	4.8	8.3	4.7	104		21.1	11.0	18.3	8.7	16	
LFpow AR	70.5	10.0	69.9	9.3	104		33.3	11.4	35.0	12.4	104		68.4	9.6	72.5	8.1	16	
HFpow AR	17.4	8.5	17.3	7.6	104		58.8	13.8	56.7	14.8	104		10.5	4.9	9.2	4.4	16	
LFpow AR nu	80.1	9.7	80.0	9.0	104		36.4	13.4	38.5	14.7	104		86.9	5.7	88.9	5.0	16	
HFpow AR nu	19.8	9.7	19.9	8.9	104		63.5	13.4	61.5	14.7	104		13.1	5.7	11.1	5.0	16	
TOTpow AR *ms*^{2}	1,152.5	1,204.8	1,106.4	1,065.9	104		805.6	1,003.0	832.7	944.4	104		342.9	614.0	400.0	703.9	16	
LF/HF *ratio* AR	5.1	2.8	5.1	2.8	104		0.7	0.7	0.8	1.1	104		8.0	3.7	9.3	3.4	16	
RESP Hz	0.2	0.1	0.2	0.1	104		0.3	0.0	0.3	0.1	104		0.4	0.1	0.5	0.1	16	
SD1 *ms*	15.8	8.6	15.4	7.8	104		23.2	11.4	23.1	11.4	104		4.5	4.3	5.0	4.6	16	
SD2 *ms*	41.9	19.9	41.1	18.1	104		30.4	14.1	31.1	13.7	104		18.8	18.0	20.6	17.2	16	
SD2/SD1 *ratio*	2.7	0.7	2.8	0.7	104		1.4	0.3	1.4	0.4	104		4.1	1.3	4.3	1.1	16	
ApEn	0.8	0.1	1.2	0.1	104	#	0.6	0.1	1.1	0.1	104	#	1.0	0.2	1.0	0.2	16	
SampEn	1.5	0.3	1.5	0.2	104		1.9	0.4	1.9	0.2	104		1.2	0.4	1.0	0.3	16	
D2	1.3	1.2	1.2	1.3	104		1.2	1.3	1.2	1.4	104		0.3	0.7	0.3	0.7	16	
DFA1	1.4	0.2	1.4	0.2	104		0.7	0.2	0.8	0.2	104		1.5	0.2	1.6	0.1	16	
DFA2	0.5	0.1	0.5	0.1	104		0.3	0.1	0.3	0.1	104		0.9	0.3	0.8	0.3	16	
RP_Lmean *beats*	9.5	2.7	10.3	2.6	104	#	7.7	2.2	8.5	2.2	104	#	14.0	2.2	20.7	5.6	16	#
RP_Lmax *beats*	107.3	45.6	204.5	108.9	104	#	38.1	16.2	63.5	31.2	104	#	205.0	59.3	516.4	185.6	16	#
RP_REC	29.1	7.6	30.6	6.9	104		17.5	4.9	18.9	5.0	104	#	40.4	4.8	48.8	8.1	16	#
RP_DET	97.6	1.8	98.0	1.3	104		94.8	2.4	95.6	1.8	104	#	99.1	0.9	99.5	0.3	16	
RP_ShanEn	2.9	0.3	3.1	0.3	104	#	2.6	0.3	2.8	0.3	104	#	3.4	0.2	3.8	0.3	16	#

Note: All parameters calculated by Kubios are included, with statistically significant differences (P<0.05) among groups indicated by # in the P columns.
Abbreviations: min: Minute; *bpm*: *Beats* per minute; *ms*: Milliseconds.

3.2.2. Variations in selected HRV parameters related to daily activity and NREM sleep

As expected, the average values of most HRV parameters were significantly different between daily activity and NREM sleep, with no significant effect from the duration of the selected short-term intervals (Table 3).

3.2.3. Age-related differences in HRV parameters

Consistent with previous studies, a significant decline in HRV was observed in most TD and FD parameters associated with aging, during both daily activity and NREM sleep. Statistically significant differences were noted between the Age3 values (C in Table 4, which shows

Table 3. Variations of selected HRV parameters during daily activity and NREM sleep conditions (values calculated from 2-min and 5-min time segments are provided)

	2-min interval					*P*	5-min interval					*P*
	Daily activity		NREM sleep				Daily activity		NREM sleep			
	Mean	SD	Mean	SD	*n*		Mean	SD	Mean	SD	*n*	
MeanRR *ms*	734.26	120.12	977.81	148.69	104	#	731.95	116.82	975.00	153.99	104	#
SDNN *ms*	31.74	15.06	27.21	12.53	104		31.15	13.69	27.53	12.23	104	
MeanHR *bpm*	83.78	13.20	62.71	9.07	104	#	83.97	13.00	63.05	9.93	104	#
MinHR *bpm*	74.73	11.50	59.63	8.58	104	#	72.70	10.95	59.15	9.18	104	#
MaxHR *bpm*	93.66	14.48	65.65	9.70	104		97.02	14.85	67.36	11.63	104	#
R*MS*SD *ms*	22.30	12.11	32.71	15.99	104	#	21.77	11.01	32.65	16.10	104	#
pNN50	5.07	8.49	14.08	16.49	104	#	4.63	7.65	14.21	16.50	104	#
HRVtriang index	7.56	2.61	7.09	2.43	104		8.27	3.04	7.83	2.77	104	
TINN *ms*	140.87	64.96	117.31	52.15	104		155.89	67.74	135.38	62.20	104	
VLFpow FFT ms^2	98.64	130.69	39.03	60.39	104		99.42	102.79	45.55	58.30	104	#
LFpow FFT ms^2	880.39	1,051.88	250.05	364.28	104	#	844.50	921.31	286.27	397.62	104	#
HFpow FFT ms^2	217.98	336.56	508.72	647.12	104		203.24	235.34	512.60	662.76	104	#
LFpow FFT nu	80.09	9.42	34.84	13.61	104	#	80.04	8.93	37.78	13.98	104	#
HFpow FFT nu	19.88	9.41	65.09	13.61	104	#	19.93	8.92	62.17	13.98	104	#
TOTpow FFT ms^2	1,197.25	1,342.90	798.11	955.76	104		1,147.42	1,168.60	844.74	1,014.20	104	
LF/HF *ratio* FFT	5.21	3.31	0.65	0.66	104	#	5.11	3.01	0.81	1.22	104	#
SD1 *ms*	15.82	8.60	23.23	11.36	104	#	15.41	7.80	23.13	11.40	104	#
SD2 *ms*	41.85	19.89	30.42	14.12	104	#	41.12	18.08	31.06	13.66	104	#
SD2/SD1 *ratio*	2.75	0.67	1.36	0.30	104	#	2.77	0.67	1.42	0.43	104	#
ApEn	0.83	0.09	0.65	0.09	104	#	1.16	0.09	1.08	0.09	104	#
SampEn	1.54	0.30	1.95	0.39	104	#	1.53	0.25	1.89	0.22	104	#
DFA1	1.37	0.21	0.74	0.19	104	#	1.38	0.21	0.77	0.20	104	#
DFA^2	0.46	0.15	0.29	0.13	104	#	0.48	0.13	0.30	0.11	104	#
RP_Lmean *beats*	9.51	2.71	7.70	2.16	104	#	10.28	2.62	8.48	2.21	104	#
RP_Lmax *beats*	107.28	45.60	38.12	16.23	104	#	204.55	108.91	63.53	31.21	104	#
RP_REC	29.06	7.63	17.48	4.94	104	#	30.59	6.92	18.91	5.05	104	#
RP_DET	97.62	1.77	94.79	2.38	104	#	97.96	1.32	95.55	1.81	104	#
RP_ShanEn	2.91	0.29	2.60	0.29	104	#	3.09	0.28	2.84	0.29	104	#
RESP Hz	0.24	0.09	0.26	0.04	104		0.25	0.09	0.27	0.05	104	

Note: Statistically significant differences ($P<0.05$) among groups are marked with # in the *P*-value columns.
Abbreviations: NREM: Non-rapid eye movement; RR: Interval between 2 subsequent R peaks; SDNN: Standard deviation Normal to Normal; R*MS*SD: Root Mean Square of Successive Differences; pNN50: The percentage of successive normal cardiac interbeat intervals >50 *m*sec HR heart rate; HF: High frequency. LF: Low frequency; TOT: total. pwr: power; SD1 and SD2: Poincare Plot parameters; DFA1 and DFA2: Detrended Fluctuation Analysis alfa parameters; ApEn: Approximated Entropy; SamEn: Sample entropy; RP: Recurrence Plot parameters.

Table 4. TD, FD, and NL parameters calculated during daily activity and NREM sleep across the three age groups.

	Daily activity						(A)	(B)	(C)	NREM sleep						(A)	(B)	(C)
	(A) Age1 (*n.* 37)		(B) Age2 (*n.* 44)		(C) Age3 (*n.* 23)					(A) Age1 (*n.* 37)		(B) Age2 (*n.* 44)		(C) Age3 (*n.* 23)				
	Mean	SD	Mean	SD	Mean	SD	*P*<0.05			Mean	SD	Mean	SD	Mean	SD	*P*<0.05		
MeanRR *ms*	690.1	96.1	737.8	113.8	788.0	131.0			A	917.9	151.2	992.3	149.7	1033.8	141.9			A
SDNN *ms*	34.5	14.6	33.0	12.9	22.2	9.7	C	C		28.5	9.7	31.5	14.3	18.3	5.2	C	C	
MeanHR *bpm*	88.7	13.1	83.1	12.2	78.0	11.8	C			66.8	9.0	62.0	10.5	59.1	8.6	C		
MinHR *bpm*	75.3	10.7	71.6	10.7	70.7	11.5				62.0	8.8	58.1	9.6	56.7	8.2			
MaxHR *bpm*	104.0	13.4	96.0	14.4	87.7	12.5	B C			71.9	10.3	66.3	12.5	62.0	9.4	C		
R*MS*SD *ms*	23.5	12.9	22.6	10.7	17.4	6.8				33.6	13.1	37.4	19.3	22.0	5.9	C	C	
pNN50	6.0	9.8	5.1	7.1	1.5	2.3				15.1	15.4	19.4	18.8	2.9	3.1	C	C	
HRVtriang index	9.2	3.6	8.5	2.5	6.3	2.2	C	C		8.3	2.3	8.7	3.0	5.5	1.4	C	C	
TINN *ms*	172.3	72.4	164.9	62.4	112.2	52.0	C	C		141.8	52.2	153.9	70.1	89.7	33.4	C	C	
VLFpow FFT ms^2	101.3	77.9	107.9	129.0	80.2	80.3				42.8	62.3	60.1	65.5	22.1	13.0		C	
LFpow FFT ms^2	919.5	820.9	1,017.3	1,118.3	393.2	380.2		C		272.9	200.8	393.2	559.0	103.2	72.5		C	
HFpow FFT ms^2	281.6	323.0	196.7	164.6	89.6	108.2	C			496.1	432.2	699.7	891.6	181.2	109.0		C	
LFpow FFT nu	78.2	8.2	81.5	9.8	80.3	8.1				37.7	12.6	38.5	16.9	36.4	9.8			
HFpow FFT nu	21.8	8.2	18.5	9.8	19.6	8.1				62.2	12.6	61.4	16.9	63.5	9.8			
TOTpow FFT ms^2	1,302.8	1,146.4	1,322.2	1,341.0	563.1	519.5	C	C		812.1	593.8	1,153.4	1,378.5	306.7	172.5		C	
LF/HF *ratio* FFT	4.5	3.3	5.7	3.0	4.9	2.3				0.7	0.7	1.0	1.7	0.6	0.3			
SD1 *ms*	16.7	9.2	16.0	7.5	12.3	4.8				23.8	9.3	26.5	13.7	15.6	4.2	C	C	
SD2 *ms*	45.8	18.8	43.7	16.9	28.8	13.4	C	C		32.3	10.7	35.5	15.8	20.6	6.4	C	C	
SD2/SD1 *ratio*	2.9	0.6	2.9	0.6	2.3	0.7	C	C		1.4	0.3	1.5	0.6	1.3	0.3			
ApEn	1.2	0.1	1.1	0.1	1.2	0.1				1.1	0.1	1.1	0.1	1.1	0.1			
SampEn	1.5	0.3	1.5	0.2	1.7	0.2			A B	1.9	0.2	1.8	0.2	2.0	0.2			B
D2	1.4	1.4	1.4	1.2	0.5	0.9	C	C		1.4	1.5	1.7	1.4	0.1	0.2	C	C	
DFA1	1.4	0.2	1.4	0.2	1.3	0.3		C		0.8	0.2	0.8	0.2	0.8	0.2			
DFA2	0.5	0.1	0.4	0.1	0.5	0.1			B	0.3	0.1	0.3	0.1	0.3	0.1			
RP_Lmean *beats*	10.5	3.0	10.5	2.2	9.4	2.6				8.4	2.0	9.0	2.3	7.5	2.0		C	
RP_Lmax *beats*	229.8	114.7	209.1	107.5	155.3	88.0	C			64.0	29.4	67.6	34.4	55.1	26.9			
RP_REC	31.3	7.5	31.4	6.0	27.9	7.2				18.8	3.9	19.8	5.8	17.3	5.0			
RP_DET	98.2	1.1	98.2	1.2	97.2	1.7	C	C		95.7	1.5	96.0	1.8	94.5	2.1	C	C	
RP_ShanEn	3.1	0.3	3.1	0.2	3.0	0.3				2.8	0.3	2.9	0.3	2.7	0.3		C	
RESP *Hz*	0.2	0.1	0.3	0.1	0.3	0.1			A	0.3	0.0	0.3	0.1	0.3	0.0			

Note: Statistically significant differences among groups are indicated by A, B, and C in the *P*<0.05 columns.
Abbreviations: TD: Time domain; FD: Frequency domain; NL: Non-linear; RR: The interval between 2 subsequent R peaks; SDNN: Standard deviation Normal to Normal; R*MS*SD: Root Mean Square of Successive Differences; HR: heart rate; HF: High Frequency; LF: Low Frequency; TOT: total; pwr: Powe; SD1 and SD2: Poincare Plot parameters; DFA1 and DFA2: Detrended Fluctuation Analysis alfa parameters; ApEn: Approximated Entropy; SamEn: Sample entropy; RP: Recurrence Plot parameters.

data analyzed from 5-min intervals) and those of both Age1 and Age2 groups (A and B in Table 4).

During daily activity, sympathetic modulation was indicated by higher LFpower (919.5 $msec^2$ in Age1, 1017.3 $msec^2$ in Age2, and 393.0 $msec^2$ in Age3) and LF/HF ratio (4.5 in Age1, 5.7 in Age2, and 4.9 in Age3), along with lower RMSSD (23.5 ms in Age1, 22.6 in Age2, and 17.4 in Age3), HFpower (281.6 $msec^2$ in Age1, 196.7 $msec^2$ in Age2, and 89.6 $msec^2$ in Age3), and SD1 (16.7 ms in Age1, 16.0 in Age2, and 12.3 in Age3).

In addition, the VLFpower values were higher during activity (101.3 $msec^2$ in Age1, 107.9 $msec^2$ in Age2, and

80.2 msec^2 in Age3) compared to NREM sleep (42.8 msec^2 in Age2, 60.1 msec^2 in Age2, and 22.1 msec^2 in Age3), with a statistically significant difference noted only between Age2 and Age3 during NREM (Table 4).

3.3. Kubios indexes

The PNSi, SNSi, and BSTRi values showed no significant differences when calculated from 2- and 5-min intervals during daily activity and NREM sleep (Table 5).

3.3.1. Age-related variations in Kubios indexes during daily activity and NREM sleep

Average PNSi values fell within the recommended normal range,[40] with no significant age-related variations noted during either daily activity or NREM sleep.

Average SNSi values were slightly above the normal range during daily activity but remained within normal limits during NREM sleep, particularly in the Age2 group (0.36 ± 1.33) compared to Age1 (0.82 ± 1.17) and Age3 (0.92 ± 0.98).

Average BSTRi values were considerably lower than the "normal range" indicated in the original literature,[43,44] as Kubios' BSTRi is calculated as the square root of Baevsky's values.[40] There were no significant differences within each age group between daily activity and NREM sleep. However, a gradual increase was observed from Age1 to Age3, with Age3 values significantly higher ($P < 0.05$) than those of Age1 and Age2 during both daily activity and NREM sleep (Table 6).

3.3.2. Kubios indexes during physical training

Figure 2 illustrates an example of Kubios' synthetic output for PNSi and SNSi during regular daily activity and physical effort.

Average values for PNSi, SNSi, and BSTRi were significantly different ($P < 0.05$) between measurements taken at rest and at peak effort, with PNSi decreasing and SNSi and BSTRi increasing. This trend reversed at 1 and 5 min into recovery (Table 7X) and also varied across different training sessions (Table 7Y).

As expected, the relationship between SNSi and BSTRi was strictly linear ($R^2 = 0.98$), whereas the inverse

Table 5. Average values of PNSi, SNSi, and BSTRi for all 104 participants during daily activity and NREM sleep, calculated from 2- and 5-min time segments

	Daily activity					NREM sleep				
	2-min interval		*P*	5-min interval		2-min interval		*P*	5-min interval	
	Mean	SD		Mean	SD	Mean	SD		Mean	SD
PNSi	−1.46	0.80	*ns*	−1.49	0.76	0.12	0.92	*ns*	0.09	0.95
SNSi	2.47	1.74	*ns*	2.30	1.64	0.77	1.19	*ns*	0.65	1.22
BSTRi	17.21	6.90	*ns*	16.01	6.40	16.34	5.12	*ns*	15.33	4.86

Abbreviations: min: Minute; *ns*: Non-significant.

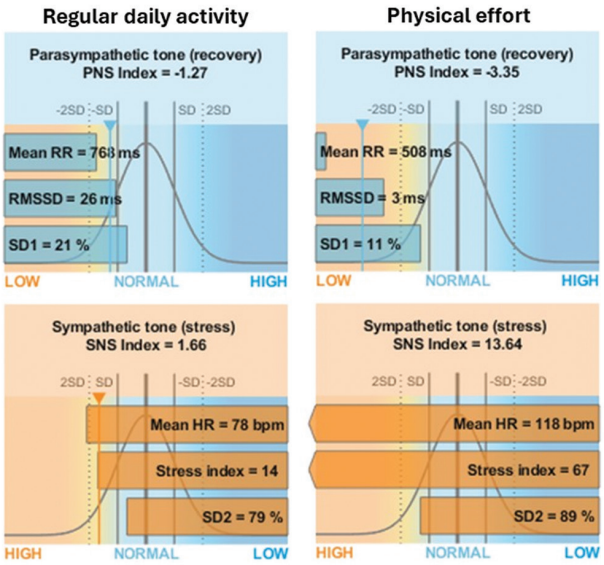

Figure 2. Example of the Kubios[40] graphic display of PNSi and SNSi, calculated from selected short-term time segments during regular daily activity and physical effort
Abbreviations: PNS: Parasympathetic nervous system; SNS: Sympathetic nervous system; RMSSD: Root mean square of successive differences; HR: Heart rate; SD1 and SD2: Poincare plot parameters.

Table 6. Age-dependent behavior of the parasympathetic (PNSi), sympathetic (SNSi), and Baevsky's stress (BSTRi) indexes during daily activity and NREM sleep

	Daily activity								NREM sleep							
	(A) Age1 (*n*. 37)		*P*	(B) Age2 (*n*. 44)		*P*	(C) Age3 (*n*. 23)		(A) Age1 (*n*. 37)		*P*	(B) Age2 (*n*. 44)		*P*	(C) Age3 (*n*. 23)	
	Mean	SD		Mean	SD		Mean	SD	Mean	SD		Mean	SD		Mean	SD
PNSi	−1.66	0.77	ns	−1.44	0.78	ns	−1.30	0.67	−0.14	0.90	ns	0.29	1.07	ns	0.09	0.71
SNSi	2.44	1.54	ns	2.13	1.64	ns	2.38	1.81	0.82	1.17	ns	0.36	1.33	ns	0.92	0.98
BSTRi	14.77	4.85	ns	15.29	6.31	#	19.39	7.73	14.92	4.50	ns	13.88	4.87	#	18.79	3.77

Note: Statistically significant differences ($P<0.05$) among groups are marked with # in the *P*-value columns.

correlations between PNSi and both SNSi and BSTRi were better fitted by quadratic or cubic functions (R^2 = 0.92 for quadratic and R^2 = 0.96 for cubic, compared to R^2 = 0.77 for linear) and (R^2 = 0.79 for quadratic and R^2 = 0.84 for cubic, compared to R^2 = 0.66 for linear), respectively, when evaluated during physical effort (Figure 3A).

Table 7. Average values of PNSi, SNSi, and BSTRi at rest, at peak effort, and at the first and fifth min of recovery (X). Average values of PNSi, SNSi, and BSTRi across training sessions with different workloads (Y)

X	Selected training phases							
	(A) Rest		(B) Peak effort		(C) First min rec		(D) Fifth min rec	
	Mean	SD	Mean	SD	Mean	SD	Mean	SD
PNSi	−1.10	0.46	−3.53	0.40	−2.99	0.55	−2.10	0.27
SNSi	1.92	0.78	17.59	6.10	8.97	4.67	4.47	1.27
BSTRi	18.22	3.54	82.91	26.97	41.30	20.82	26.58	6.43
P<0.05	B C D				B		B C	
			A C D		A D		A	
			A C D		A D			
Y	**Session training workloads (watts/min)**							
	(A) 65–75		**(B) 75–85**		**(C) 85–95**		**(D) 95–110**	
	Mean	**SD**	**Mean**	**SD**	**Mean**	**SD**	**Mean**	**SD**
PNSi	−2.21	0.58	−2.44	0.85	−2.53	0.76	−2.73	0.80
SNSi	5.28	2.73	7.26	5.20	7.56	5.36	9.21	6.37
BSTRi	30.34	12.10	38.32	22.15	38.92	22.72	45.39	27.59
P<0.05	C D							
			D					
			A		A		A B C	

Note: Statistically significant differences (*P*<0.05) among groups are indicated by A, B, C, and D, as applicable.
Abbreviation: rec: recovery.

Figure 4 provides an example of the time-varying behavior of PNSi, SNSi, and BSTRi throughout a training session, highlighting four short intervals at baseline rest, medium and peak effort, and during recovery.

3.3.3. Kubios indexes during police tactical training (psychophysiological stress)

The average baseline values of PNSi and SNSi for the 16 police officers were within the suggested normal range,[40] showing no significant differences when calculated from 2- and 5-min intervals. Average baseline BSTRi values were already above the normal limit before the tactical training began and increased up to 3 times during two subsequent scenarios designed to escalate challenging operational tasks. BSTRi values during stress were higher when calculated from 2-min intervals, though this difference was not statistically significant (Table 8). As expected, the increase in psychophysiological stress from realistic tactical training resulted in a significant increase in SNSi, reaching up to 6 times the upper normal limit, alongside a progressive decrease in PNSi (from −1.4 ± 0.8 to −3.8 ± 0.7) (Table 9).

An example of the time-varying behavior of PNSi and SNSi during a realistic training session is shown in Figure 5A, alongside HRV spectral components (Figure 5B). Individual BSTRi values exceeded 80 conventional units at peak stress (Figure 5C).

Similar to findings during physical training, the relationship between SNSi and BSTRi was strictly linear

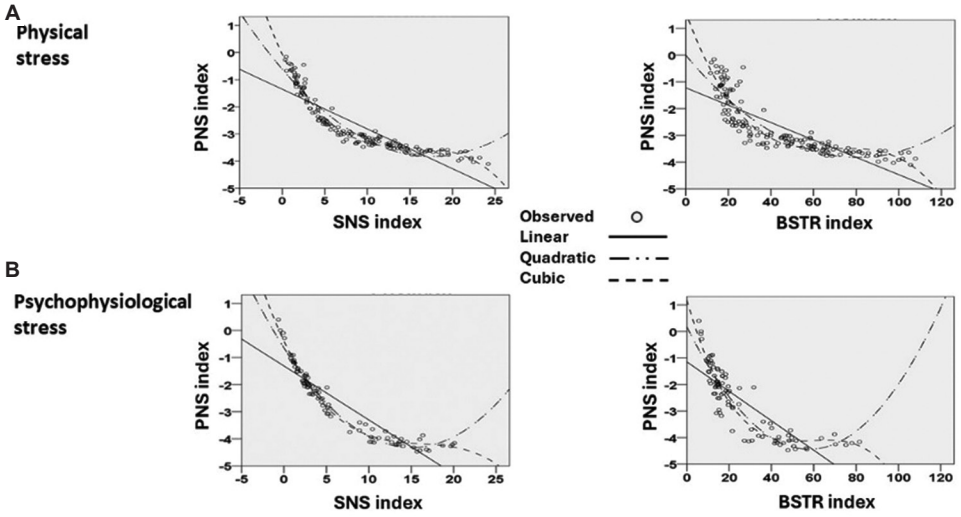

Figure 3. Curves depicting the relationships between PNSi and SNSi (A) and between PNSi and BSTRi (B), illustrating different patterns under physical and psychophysiological stress (see text for details)
Abbreviations: PNS: Parasympathetic nervous system; SNS: Sympathetic nervous system; BSTR: Baevski stress.

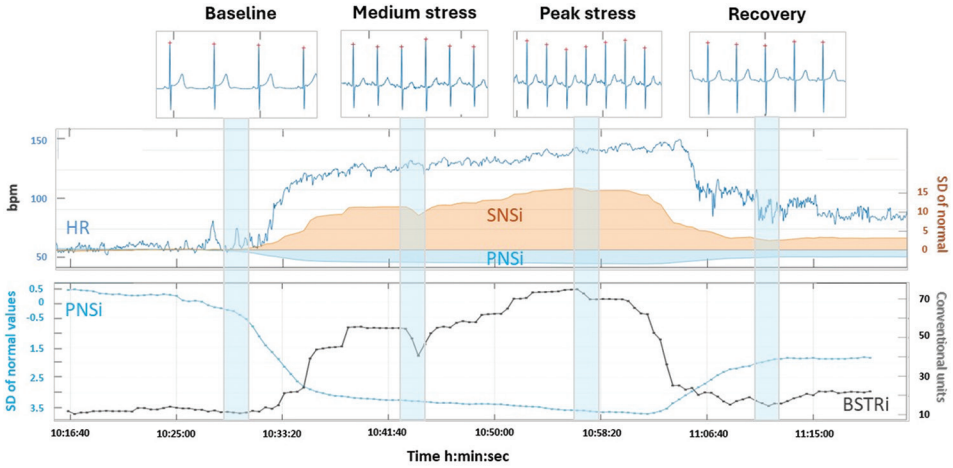

Figure 4. Example of the time-varying behavior of heart rate (HR), PNSi, SNSi, and BSTRi during a training session
Abbreviations: PNSi: Parasympathetic nervous system index; SNSi: Sympathetic Nervous System index; BSTRi: Baevski stress index; HR: heart rate.

Table 8. Average values of PNSi, SNSi, and BSTRi for the 16 police officers, calculated from 2- and 5-min intervals, before and during realistic tactical scenarios involving varying levels of psychophysiological stress

	Baseline					Medium stress					High stress				
	2-min interval		*P*	5-min interval		2-min interval		*P*	5-min interval		2-min interval		*P*	5-min interval	
	Mean	SD		Mean	SD	Mean	SD		Mean	SD	Mean	SD		Mean	SD
PNSi	−1.4	0.8	ns	−1.6	0.7	−2.8	1.1	ns	−2.8	1.0	−3.8	0.7	ns	−3.7	0.7
SNSi	1.9	1.5	ns	2.1	1.4	7.6	6.4	ns	6.5	5.3	12.5	5.6	ns	10.0	3.7
BSTRi	14.0	5.9	ns	13.9	4.7	30.4	21.6	ns	25.0	15.9	45.8	21.5	ns	34.0	13.8

Abbreviations: min: Minute; ns: Non-significant.

Table 9. Stress-induced changes of PNSi, SNSi, and BSTRi

	(A) Baseline		*P*	(B) Medium stress		*P*	(C) High stress		*P*
	Mean	SD		Mean	SD		Mean	SD	
PNSi	−1.4	0.8	#	−2.8	1.1	*	−3.8	0.7	
SNSi	1.9	1.5		7.6	6.4	°	12.5	5.6	§
BSTRi	14.0	5.9		30.4	21.6	°	45.8	21.5	&

Note: Average values of 16 police officers calculated from 2-min time segments are shown. # $P<0.05$ A vs. B and vs. C; '&' denotes $P<0.05$ C vs. A; '§' denotes $P<0.05$ C vs. A and B; *$P<0.05$ B vs. C; $P<0.05$ B vs. A.

(R^2 = 0.98), whereas the inverse relationship between PNSi and either SNSi or BSTRi was better modeled by NL functions (Figure 3B). The type of non-linearity between PNSi and SNSi appears to depend on whether the participant is experiencing physical or psychophysiological stress. The NL regression fitting PNSi and SNSi with a quadratic polynomial yielded an R^2 value slightly lower than that obtained from a cubic regression (from R^2 = 0.978 to R^2 = 0.965). In contrast, when analyzing physical stress data, the decrease in R^2 was more pronounced (from R^2 = 0.961 to R^2 = 0.920) (Figure 3A). Moreover, for SNSi values between 10 and 20 units, PNSi values during effort and psychophysiological stress differed by nearly one unit on average. A similar trend was noted in the relationship between PNSi and BSTRi.

3.3.4. Relationship between Kubios indexes and HRV spectral parameters

The Pearson correlation between the PNS, SNS, and BSTR indexes calculated by Kubios and the HRV spectral parameters is presented in Table 10. Although significant ($P < 0.01$), the correlations between each index and the VLF, LF, HF, and Totalpower spectral components were moderate during daily activity and physical effort (R values ranging from 0.470 to 0.668) and moderate to strong during psychophysiological stress. Notably, there was no correlation with the LF/HF ratio in any situation.

4. Discussion

The dynamic nature of CAM is essential for maintaining physiological homeostasis, adapting to environmental demands, and ensuring proper responses to acute stress, thereby supporting survival in life-threatening

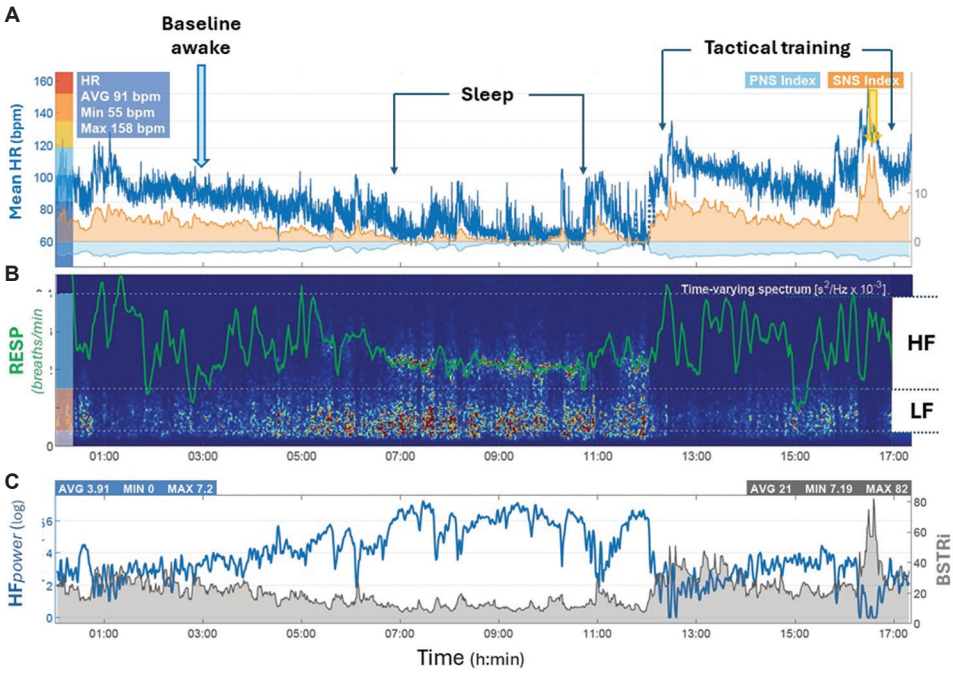

Figure 5. 24-h Holter recording from a police officer, including a realistic tactical training session. (**A**) Time-varying behavior of the mean heart rate, SNSi (orange area), and PNSi (light blue area). (**B**) Time-varying behavior of respiration (green line) and HRV spectral components (HF and LF). (**C**) Time-varying behavior of HFpower (blue line) and BSTRi (gray area), which temporarily reached a value of 82, accompanied by a drop in the HF spectral component

Abbreviations: PNS: Parasympathetic nervous system; SNS: Sympathetic nervous system; BSTRi: Baevski stress index; HR: heart rate; HF: High Frequency; LF: Low Frequency; RESP: Respiration.

situations.[1,2,5,35] HRV analysis serves as a powerful non-invasive tool or assessing ANS function, deepening our understanding of CAM across various psychophysiological contexts. However, identifying which HRV parameters can serve as definitive markers of human stress responses and evaluating the suitability of different analytical methods has been widely debated.[4,6-8,48] Notably, the use of LF/HF ratio as an indicator of "sympathovagal balance"[6,7] has been called into question,[8] with criticisms aimed at the rigid framework based on frequency bands.[49,50]

In this study, a preliminary evaluation showed that short-term HRV analysis from 2-min intervals, which is useful for assessing transient CAM changes (such as those triggered by sudden acute stress), did not significantly alter the quantitative estimates of most HRV parameters (except for the recurrence plot) (Table 2). It also confirmed established differences between regular daily activity and NREM sleep (Table 3), as well as the age-related decline in HRV, regardless of whether linear or NL methods were used (Table 4).

Although there are known correlations between certain HRV parameters – such as TD SDNN with spectral Totalpower and VLF/LF components (sympathetic indexes) and TD RMSSD, pNN50 with spectral HFpower (parasympathetic indexes) – the manual integration of multiple TD, FD, and NL HRV parameters remains challenging and time-consuming.[44] Many years ago, several indexes (e.g., the index of regulatory system activity) were proposed in space medicine to simplify the complex HRV-based evaluation of individual functional states.[43,44] With the recent availability of automatically calculated indexes like PNSi, SNSi, and BSTRi,[40] this retrospective study aimed to evaluate their normality range in a healthy population, considering variability due to aging and situational factors such as normal daily activity, NREM sleep, physical effort, and real-world psychophysiological stress.

Notably, all three Kubios indexes incorporate non-HRV spectral parameters, making them potentially useful for independently assessing the functional significance of HRV spectral components in these contexts. Although a moderate but significant correlation was observed between each index and the VLF, LF, HF, and Totalpower, no correlation was found between the indexes and the LF/HF ratio (Table 10). This supports the ongoing criticism regarding the use of the LF/HF ratio as a definitive measure of sympathovagal balance.[8]

In recent decades, greater attention has been given to the FD VLF band due to its potential correlation with

Table 10. Pearson's correlation coefficients between PNSi, SNSi, and BSTRi and the HRV spectral components during baseline daily activity, physical effort, and psychophysiological stress

	PNSi	SNSi	BSTRi
Baseline			
VLFpow FFT ms^2	0.470**	−0.497**	−0.533**
LFpow FFT ms^2	0.492**	−0.530**	−0.626**
HFpow FFT ms^2	0.549**	−0.484**	−0.545**
TOTpow FFT ms^2	0.557**	−0.575**	−0.668**
LF/HF *ratio* FFT	−0.132	0.018	−0.033
Physical effort			
VLFpow FFT ms^2	0.510**	−0.465**	−0.468**
LFpow FFT ms^2	0.681**	−0.638**	−0.638**
HFpow FFT ms^2	0.579**	−0.659**	−0.660**
TOTpow FFT ms^2	0.599**	−0.591**	−0.602**
LF/HF *ratio* FFT	0.031	0.036	0.051
Psychophysiological			
VLFpow FFT ms^2	0.596**	−0.644**	−0.624**
LFpow FFT ms^2	0.787**	−0.756**	−0.727**
HFpow FFT ms^2	0.636**	−0.627**	−0.611**
TOTpow FFT ms^2	0.805**	−0.779**	−0.750**
LF/HF *ratio* FFT	−0.147	0.190	0.209

Note: $^{**}P < 0.01$.
Abbreviation: FFT: Fast Fourier transform.

stressful stimuli.[19,20] In our study, VLFpower was higher during daily activity than during NREM sleep across all age groups, confirming its association with homeostatic mechanisms such as thermoregulation, baroreflex activity, and the renin–angiotensin system.[20] However, although significant, the correlations found between VLFpower and PNSi (positive correlation) and with SNS and BSTR indexes (negative correlation) were only moderate (Table 10).

Notably, a recent study reported a time-varying increase in VLFpower that followed the same trend as heart rate and the Kubios Baevsky stress index,[51] suggesting that VLFpower may serve as a marker for stress-related increases in intrinsic cardiac sympathetic activity.[21,52] However, the VLF spectral component is generally viewed as indicative of slower physiological mechanisms, sympathovagal balance, and a reduction in vagal tone during mental stress.[20,21,53] The discrepancy between that study and our findings may be attributed to the VLF filtering effect of the detrending with the smoothness priors function used in our study.

Despite the notable changes in linear parameters associated with the well-known decline of HRV due to aging,[12] average PNSi values remained within the suggested normal range during both daily activity and NREM sleep. Average SNSi values were slightly above normal during regular daily activity and, as expected, significantly lower during NREM (Table 5), with no significant age-related variations observed (Table 6). In contrast, the BSTRi was significantly higher in Age3 compared to both Age1 and Age2. This unexpected result may indicate that "healthy elderly" individuals exhibit a more complex adaptation of CAM, potentially influenced by a moderate increase in physiological stress. However, further research involving a larger population is needed to confirm this preliminary observation.

Although the evaluation of PNSi and SNSi was not affected by the duration of the time segments used for calculation, BSTRi values during high stress were higher (though not significantly) when calculated from 2-min intervals (Table 8), which may be more suitable for assessing the complex brain–heart interaction during critical events. However, we believe that the assessment of Kubios' BSTRi "normality range" requires further investigation. Notably, an interesting finding from this study, which has not been reported previously, is that average BSTRi values around 45 and even exceeding 80 conventional units were observed at peak stress during police tactical training. This suggests a variable combination of physical and psychophysiological stress, with individual peaks exceeding 60 in five cases and above 80 in one case (Figure 5). If squared (since Kubios' stress index is the square root of Baevsky's values), the observed values of 45–80 would correspond to 2025–6400 Baevsky conventional units, which are extremely high and theoretically inconsistent with a healthy status and adequate functional capabilities.[43,44] This was not the case for our police officers; however, in a few instances, values exceeding 60 during highly stressful tactical scenarios were linked to poor tactical performance. Moreover, similar values were consistently achieved and tolerated by a 75-year-old volunteer during intensive effort without any subjective clinical symptoms or functional or ECG changes. Furthermore, as suggested by space medicine, individual physiological responses in critical situations may not align with average statistical normality, as adaptive reactions can vary based on individual psychophysiological and functional capabilities.[43] Interestingly, previous reports indicated that a similar BSTRi value in a highly fit police officer, without significant physical effort, was linked to a loss of situational control, resulting in operational failure and the sudden onset of paroxysmal arrhythmia, attributed to a marked acute CAM imbalance.[51] Under such intense and uncontrolled psychophysiological stress, which can lead to immobilization (freezing) and an inability to respond to external threats, HRV decreases significantly. An unexpected increase in the delayed HF component has been noted in ultra-short-term HRV analysis,[35] aligning

with Porges' "polyvagal theory," which suggests that the *unmyelinated vagus* (the most primitive parasympathetic pathway), is activated when other defensive strategies (the *myelinated social vagus* and the *sympathetic* "fight or flight" response) fail to manage behavioral and physiological adaptation in life-threatening situations.[23,54]

According to the "neurovisceral integration model," the interaction with the complex "brain–heart–body system," which allows for flexibility and adaptability to stressors, can be assessed through HRV analysis. Specifically, the HF spectral component serves as a reliable parasympathetic biomarker for measuring self-regulation and health.[27,28,55]

A significant challenge in psychophysiology is quantifying the extent of stress-induced psychophysiological overload with HRV analysis[56] and its correlation with adaptive or maladaptive behaviors. The previously unreported finding that, under stress, the inverse correlation between the PNSi and the SNSi (and BSTRi) is NL (Figure 3), rather than the usual linear relationship at rest, could introduce a new framework for evaluating sympathovagal interaction in complex real-life critical situations. This may help define a critical level of dysfunctional parasympathetic modulation that impairs the "brain–heart–body system's" flexibility, resulting in insufficient rational control of stressful situations. This is supported by two additional findings indicating a significant mechanistic difference in CAM based on the type of stress encountered: (1) Although the relationship between the two indexes is NL in both cases, the nature of the non-linearity differs, with cubic functions providing a better fit for physical stress than quadratic functions. (2) For SNSi values between 10 and 20 units, the level of parasympathetic withdrawal was greater under psychophysiological stress, averaging nearly one SD of PNSi. If confirmed through targeted experimental studies, examining the dynamic relationship between PNSi and SNSi could serve as a valuable tool for identifying individual psychophysiological stress levels, which may influence the success or failure of operational outcomes, particularly in complex real-world situations that also involve physical effort, as seen in sports competitions or tactical operations.

Finally, the time-varying calculation of the PNS, SNS, and BSTR indexes effectively provided a quick overview of how CAM adapts to increasing physical effort (Figure 4) and the temporary rise in sympathetic drive alongside parasympathetic withdrawal during realistic tactical training (Figure 5). Further research is needed to determine if these additional parameters can enhance the ability to differentiate between psychophysiological stress and concurrent physical strain during real-world critical events.[36,37]

5. Conclusion

The automatic calculation of PNSi, SNSi, and BSTRi indexes provides a quicker and more comprehensive assessment of adaptive CAM in both physiological and pathological conditions. Monitoring these indexes over time and in real time could greatly improve our understanding of heart–brain interaction dynamics, especially during acute stress from real-life critical events.[51]

In this study, PNSi and SNSi remained within the suggested normality range[40] at rest, with their variations during physical and psychophysiological stress showing the expected inverse correlation. If further research confirms that the inverse correlation between PNSi and SNSi (and BSTRi) under stress is NL and better fitted by NL functions (Figure 3), it could introduce a new approach for assessing sympathovagal interaction in complex real-world situations.

Given the relatively small sample size in this pilot study, although the results are promising, further research involving a larger population under dynamic physiological conditions is necessary to establish a reliable and potentially unbiased normality database. The BSTRi values calculated using Kubios software did not match those derived from the original Baevsky formula. Squaring the values obtained from this study of healthy individuals under effort or psychophysiological stress resulted in units that exceeded the range suggested by Baevsky, even for critical cardiac conditions.[43,44] Therefore, the evaluation of the normality range for BSTRi calculated with Kubios software requires further investigation.

Acknowledgments

None.

Funding

None.

Conflict of interest

The authors declare they have no competing interests.

Author contributions

Conceptualization: Donatella Brisinda, Riccardo Fenici
Investigation: Donatella Brisinda, Riccardo Fenici
Methodology: Donatella Brisinda, Riccardo Fenici, Marco Picerni
Formal analysis: Donatella Brisinda, Riccardo Fenici, Marco Picerni
Writing–original draft: Donatella Brisinda, Riccardo Fenici
Writing–review & editing: All authors

Ethics approval and consent to participate

Not applicable, being the study a retrospective analysis of ECG database data available from previous investigations carried out on a volunteered basis and/or for sports or duty fitness evaluation. All subjects had given verbal informed consent for the performance of their ECG recordings and analysis.

Consent for publication

All subjects had given verbal informed consent for the eventual use of their anonymized data for scientific and publication purposes.

Availability of data

The original clinical data are not publicly sharable due to ongoing privacy norms.

Further disclosure

A partial analysis of the 75-year-old volunteer training sessions was accepted as a poster presentation at the European Congress of Cardiology 2021.

References

1. Levy MN. Autonomic interactions in cardiac control. *Ann N Y Acad Sci*. 1990;601:209-221.

   doi: 10.1111/j.1749-6632.1990.tb37302.x

2. Kleiger RE, Miller JP, Bigger JT Jr., Moss AJ. Decreased heart rate variability and its association with increased mortality after acute myocardial infarction. *Am J Cardiol*. 1987;59(4):256-262.

   doi: 10.1016/0002-9149(87)90795-8

3. Parin VV, Baevsky RM, Gazenko OG. Heart and circulation under space conditions. *Cor Vasa*. 1965;7:165-184.

4. Malik M. Guidelines heart rate variability. *Eur Heart J*. 1996;17:354-381.

   doi: 10.1161/01.CIR.93.5.1043

5. Ernst G. Heart-rate variability-more than heart beats? *Front Public Heal*. 2017;5:240.

   doi: 10.3389/fpubh.2017.00240

6. Pagani M, Lombardi F, Guzzetti S, *et al*. Power spectral analysis of heart rate and arterial pressure variabilities as a marker of sympatho-vagal interaction in man and conscious dog. *Circ Res*. 1986;59(2):178-193.

7. Malliani A, Pagani M, Lombardi F, Cerutti S. Cardiovascular neural regulation explored in the frequency domain. *Circulation*. 1991;84(2):482-492.

   doi: 10.1161/01.cir.84.2.482

8. Eckberg DL. Sympathovagal balance: A critical appraisal. *Circulation*. 1997;96(9):3224-3232.

   doi: 10.1161/01.cir.96.9.3224

9. Umetani K, Singer DH, McCraty R, Atkinson M. Twenty-four hour time domain heart rate variability and heart rate: Relations to age and gender over nine decades. *J Am Coll Cardiol*. 1998;31(3):593-601.

   doi: 10.1016/s0735-1097(97)00554-8

10. Jäncke L, Mérillat S, Liem F, Hänggi J. Brain size, sex, and the aging brain. *Hum Brain Mapp*. 2015;36(1):150-169.

    doi: 10.1002/hbm.22619

11. Gribbin B, Pickering TG, Sleight P, Peto R. Effect of age and high blood pressure on baroreflex sensitivity in man. *Circ Res*. 1971;29(4):424-431.

    doi: 10.1161/01.res.29.4.424

12. Voss A, Schroeder R, Heitmann A, Peters A, Perz S. Short-term heart rate variability--influence of gender and age in healthy subjects. *PLoS One*. 2015;10(3):e0118308.

    doi: 10.1371/journal.pone.0118308

13. Batchinsky AI, Cooke WH, Kuusela T, Cancio LC. Loss of complexity characterizes the heart rate response to experimental hemorrhagic shock in swine. *Crit Care Med*. 2007;35(2):519-525.

    doi: 10.1097/01.CCM.0000254065.44990.77

14. Werdan K, Schmidt H, Ebelt H, *et al*. Impaired regulation of cardiac function in sepsis, SIRS, and MODS. *Can J Physiol Pharmacol*. 2009;87(4):266-274.

    doi: 10.1139/Y09-012

15. Signorini MG, Ferrario M, Marchetti M, Marseglia A. Nonlinear analysis of heart rate variability signal for the characterization of cardiac heart failure patients. *Conf Proc IEEE Eng Med Biol Soc*. 2006;2006:3431-3434.

    doi: 10.1109/IEMBS.2006.259744

16. Perkiömäki JS, Hämekoski S, Junttila MJ, Jokinen V, Tapanainen J, Huikuri HV. Predictors of long-term risk for heart failure hospitalization after acute myocardial infarction. *Ann Noninvasive Electrocardiol*. 2010;15(3):250-258.

    doi: 10.1111/j.1542-474X.2010.00372.x

17. Morris JA Jr., Norris PR, Waitman LR, Ozdas A, Guillamondegui OD, Jenkins JM. Adrenal insufficiency, heart rate variability, and complex biologic systems: A study of 1,871 critically ill trauma patients. *J Am Coll Surg*. 2007;204(5):883-885.

    doi: 10.1016/j.jamcollsurg.2007.01.019

18. Ryan ML, Ogilvie MP, Pereira BM, *et al*. Heart rate variability is an independent predictor of morbidity and mortality in hemodynamically stable trauma patients. *J Trauma Acute Care Surg*. 2011;70(6):1371-1380.

    doi: 10.1097/TA.0b013e31821858e6

19. Taylor JA, Carr DL, Myers CW, Eckberg DL. Mechanisms underlying very-low-frequency RR-interval oscillations in humans. *Circulation*. 1998;98(6):547-555.

doi: 10.1161/01.CIR.98.6.547

20. Usui H, Nishida Y. The very low-frequency band of heart rate variability represents the slow recovery component after a mental stress task. *PLoS One.* 2017;12:e0182611.

doi: 10.5061/dryad.7

21. Shaffer F, McCraty R, Zerr CL. A healthy heart is not a metronome: An integrative review of the heart's anatomy and heart rate variability. *Front Psychol*. 2014;5:1040.

doi: 10.3389/fpsyg.2014.01040

22. Goldberger AL. Fractal variability versus pathologic periodicity: Complexity loss and stereotypy in disease. *Perspect Biol Med*. 1997;40(4):543-561.

doi: 10.1353/pbm.1997.0063

23. Porges SW. The polyvagal theory: New insights into adaptive reactions of the autonomic nervous system. *Cleve Clin J Med*. 2009;76(Suppl 2):S86-S90.

doi: 10.3949/ccjm.76.s2.17

24. Porges SW. Orienting in a defensive world: Mammalian modifications of our evolutionary heritage. A polyvagal theory. *Psychophysiology*. 1995;32(4):301-318.

doi: 10.1111/j.1469-8986.1995.tb01213.x

25. Wacker J, Heldmann M, Stemmler G. Separating emotion and motivational direction in fear and anger: Effects on frontal asymmetry. *Emotion*. 2003;3(2):167-193.

doi: 10.1037/1528-3542.3.2.167

26. Stemmler G, Aue T, Wacker J. Anger and fear: Separable effects of emotion and motivational direction on somatovisceral responses. *Int J Psychophysiol*. 2007;66(2):141-153.

doi: 10.1016/j.ijpsycho.2007.03.019

27. Thayer JF, Lane RD. A model of neurovisceral integration in emotion regulation and dysregulation. *J Affect Disord*. 2000;61(3):201-216.

doi: 10.1016/S0165-0327(00)00338-4

28. Thayer JF, Åhs F, Fredrikson M, Sollers JJ 3rd, Wager TD. A meta-analysis of heart rate variability and neuroimaging studies: Implications for heart rate variability as a marker of stress and health. *Neurosci Biobehav Rev*. 2012;36(2):747-756.

doi: 10.1016/j.neubiorev.2011.11.009

29. Smith R, Thayer JF, Khalsa SS, Lane RD. The hierarchical basis of neurovisceral integration. *Neurosci Biobehav Rev*. 2017;75:274-296.

doi: 10.1016/j.neubiorev.2017.02.003

30. Kim HG, Cheon EJ, Bai DS, Lee YH, Koo BH. Stress and heart rate variability: A meta-analysis and review of the literature. *Psychiatry Investig*. 2018;15(3):235-245.

doi: 10.30773/pi.2017.08.17

31. Richman JS, Moorman JR. Physiological time-series analysis using approximate and sample entropy. *Am J Physiol Hear Circ Physiol*. 2000;278(6 47-6):2039-2049.

doi: 10.1152/ajpheart.2000.278.6.h2039

32. Eckmann JP, Oliffson Kamphorst S, Ruelle D. Recurrence plots of dynamical systems. *Europhys Lett.* 1987;4:973-977.

doi: 10.1209/0295-5075/4/9/004

33. Melillo P, Bracale M, Pecchia L. Nonlinear heart rate variability features for real-life stress detection. Case study: Students under stress due to university examination. *Biomed Eng Online*. 2011;10(1):96.

doi: 10.1186/1475-925X-10-96

34. Brisinda D, Di Florio E, Savorgnan C, *et al*. Clinical validation of a novel wearable system for real-time telemetric transmission of transient changes of cardiac autonomic modulation induced by psychophysiological and physical stress. *Eur Heart J*. 2020;41(Suppl 2):ehaa946.3476.

doi: 10.1093/ehjci/ehaa946.3476

35. Fenici R, Brisinda D, Sorbo AR. Methods for real-time assessment of operational stress during realistic police tactical training. In: Kitaeff J, editor. *Handbook of Police Psychology*. England: Routledge/Taylor and Francis Group; 2011. p. 295-319.

doi: 10.4324/9780203836170

36. Brisinda D, Venuti A, Cataldi C, Efremov K, Intorno E, Fenici R. Real-time imaging of stress-induced cardiac autonomic adaptation during realistic force-on-force police scenarios. *J Police Crim Psychol*. 2015;30(2):71-86.

doi: 10.1007/s11896-014-9142-5

37. Brisinda D, Fioravanti F, Sorbo AR, Venuti A, Fenici R. Psychophysiological assessment of acute stress induced by high-pressure law-enforcement driving : A pilot study. *Psychol Soc Behav Res*. 2015;2(3):36-50.

doi: 10.12966/psbr.06.03.2015

38. Affani A, Zontone P, Fenici R, *et al*. Assisted/Autonomous vs. Human Driving Assessment on the DiM driving Simulator using Objective/Subjective Characterization. In: Pfeffer PE, editor. *10th International Munich Chassis Symposium 2019*. Wiesbaden: Springer Fachmedien; 2020. p. 307-321.

doi: 10.1007/978-3-658-26435-2_23

39. Bateni P, Sigal L. *Real-Time Monitoring of User Stress, Heart Rate and Heart rATE Variability on Mobile Devices* [Preprint]; 2022.

doi: 10.48550/arXiv.2210.01791

40. Tarvainen MP, Lipponen J, Niskanen JP, Ranta-aho PO. *Kubios HRV Software USER'S GUIDE*; 2021. p. 4-39.

Available from: https://www.kubios.com/downloads/kubios_hrv_users_guide.pdf [Last accessed on 2024 Oct 07].

41. Nunan D, Sandercock GR, Brodie DA. A quantitative systematic review of normal values for short-term heart rate variability in healthy adults. *Pacing Clin Electrophysiol*. 2010;33(11):1407-1417.

doi: 10.1111/j.1540-8159.2010.02841.x

42. Brennan M, Palaniswami M, Kamen P. Do existing measures of Poincaré plot geometry reflect nonlinear features of heart rate variability? *IEEE Trans Biomed Eng*. 2001;48(11):1342-1347.

doi: 10.1109/10.959330

43. Baevsky RM, Berseneva AP. *Methodical Recommendations-Use Kardivar System for Determination of the Stress Level and Estimation of the Body Adaptability-Standards of Measurements and Physiological Interpretation; Moscow*; 2008. Available online: https://www.academia.edu/35296847/methodical_recommendations_use_kardivar_system_for_determination_of_the_stress_level_and_estimation_of_the_body_adaptability_standards_of_measurements_and_physiological_interpretation_moscow_prague_2008?auto=download [Last accessed on 2024 Oct 07].

44. Baevsky RM, Chernikova AG. Heart rate variability analysis: Physiological foundations and main methods. *Cardiometry*. 2017;(10):66-76.

doi: 10.12710/cardiometry.2017.10.6676

45. Sahoo TK, Mahapatra A, Ruban N. Stress Index Calculation and Analysis Based on Heart Rate Variability of ECG Signal with Arrhythmia. *2019 Innovations in Power and Advanced Computing Technologies (i-PACT)*; 2019. p. 1-7.

46. Ali MK, Liu L, Chen JH, Huizinga JD. Optimizing autonomic function analysis via heart rate variability associated with motor activity of the human colon. *Front Physiol*. 2021;12:619722.

doi: 10.3389/fphys.2021.619722

47. World Medical Association. World medical association declaration of Helsinki: Ethical principles for medical research involving human subjects. *JAMA* 1974;353(1):1418-1419.

doi: 10.1001/jama.2013.281053

48. Lee SG, Song Y Do, Lee EC. Experimental verification of the possibility of reducing photoplethysmography measurement time for stress index calculation. *Sensors* (*Basel*). 2023;23(12):5511.

doi: 10.3390/s23125511

49. Grasso R, Schena F, Gulli G, Cevese A. Does low-frequency variability of heart period reflect a specific parasympathetic mechanism? *J Auton Nerv Syst*. 1997;63(1-2):30-38.

doi: 10.1016/s0165-1838(96)00128-2

50. Perlitz V, Lambertz M, Cotuk B, *et al*. Cardiovascular rhythms in the 0.15-Hz band: Common origin of identical phenomena in man and dog in the reticular formation of the brain stem? *Pflugers Arch*. 2004;448(6):579-591.

doi: 10.1007/s00424-004-1291-4

51. Brisinda D, Fenici P, Fenici R. Police Realistic tactical training is not risk-free: Stress-induced wide-QRS paroxysmal tachyarrhythmia in a healthy police officer and professional athlete. *J Police Crim Psychol*. 2024;39(1):93-103.

doi: 10.1007/s11896-023-09616-z

52. Armour JA. Potential clinical relevance of the "little brain" on the mammalian heart. *Exp Physiol*. 2008;93(2):165-176.

doi: 10.1113/expphysiol.2007.041178

53. Shaffer F, Ginsberg JP. An overview of heart rate variability metrics and norms. *Front Public Heal*. 2017;5:258.

doi: 10.3389/fpubh.2017.00258

54. Porges SW. Polyvagal theory: A science of safety. *Front Integr Neurosci*. 2022;16:871227.

doi: 10.3389/fnint.2022.871227

55. Laborde S, Mosley E, Thayer JF. Heart rate variability and cardiac vagal tone in psychophysiological research-recommendations for experiment planning, data analysis, and data reporting. *Front Psychol*. 2017;8:213.

doi: 10.3389/fpsyg.2017.00213

56. Amira T, Dan I, Atta B, Said G, Azeddine B, Katarzyna WW. Stress level classification using heart rate variability. *Adv Sci Technol Eng Syst*. 2019;4(3):38-46.

doi: 10.25046/aj040306

ACCSCIENCE PUBLISHING

Brain & Heart

ORIGINAL RESEARCH ARTICLE

Human dental pulp MSCs attenuated motor neuron dysfunction and prolonged lifespan in ALS murine model

Shihe Jiang[1†], Xiuchen Guan[2†], Meng Shi[3], Ying Zhang[1], Xindi Li[1], Yingying Su[3], Hao Wang[3], Jian Zhou[4], Fu-Dong Shi[1], Songling Wang[5], and Wei-Na Jin[1*]

[1]China National Clinical Research Center for Neurological Diseases, Beijing Tiantan Hospital, Capital Medical University, Beijing, China

[2]Department of Orthodontics, Beijing Stomatological Hospital, School of Stomatology, Capital Medical University, Beijing, China

[3]Department of Stomatology, Beijing Tiantan Hospital, Capital Medical University, Beijing, China

[4]Laboratory of Tissue Regeneration and Immunology and Department of Periodontics, Beijing Key Laboratory of Tooth Regeneration and Function Reconstruction, School of Stomatology, Capital Medical University, Beijing, China

[5]Salivary Gland Disease Center and Beijing Key Laboratory of Tooth Regeneration and Function Reconstruction, Beijing Laboratory of Oral Health and Beijing Stomatological Hospital, Capital Medical University, Beijing, China

[†]*These authors contributed equally to this work.*

***Corresponding author:**
Wei-Na Jin
(weina.jin@ncrcnd.org.cn)

Citation: Jiang S, Guan X, Shi M, *et al*. Human dental pulp MSCs attenuated motor neuron dysfunction and prolonged lifespan in ALS murine model. *Brain & Heart*. 2024;2(4):3996. doi: 10.36922/bh.3996

Received: June 20, 2024

Accepted: September 4, 2024

Published Online: October 10, 2024

Abstract

Amyotrophic lateral sclerosis (ALS) is a devastating neurodegenerative disease that causes skeletal muscle weakness and atrophy, resulting in respiratory failure and a short lifespan. Considering the lack of effective treatment, this study investigated the effects of human dental pulp stem cells (hDPSCs) on the clinical symptoms and potential mechanisms in a mouse model of ALS superoxide dismutase 1 (SOD1-G93A). Neurological assessments, including neurological scoring, rotarod testing, and 7-T magnetic resonance imaging, were conducted to evaluate neurological impairments. Survival rates and body weight of the mice were also recorded. Immunofluorescence staining and flow cytometry analyses were performed to investigate the number of neurons and infiltrated inflammatory cells in the spinal cord as well as the central nervous system. The results indicate that infusion of hDPSCs increased the body weight, mitigated motor neuron dysfunction, and extended the lifespan of SOD1-G93A mice by approximately 15 days. Moreover, hDPSCs infusion reduced the degree of spinal cord atrophy. Results suggested that the number of neurons in the central nervous system of SOD1-G93A mice was significantly decreased, but hDPSCs infusion resulted in an increase in these numbers. However, hDPSCs infusion had no obvious effect on microglia phenotypes in SOD1-G93A mice. This study emphasizes the potential of hDPSCs to mitigate neuronal loss in an ALS mouse model, suggesting a promising therapeutic avenue for ALS.

Keywords: Human dental pulp stem cells; Amyotrophic lateral sclerosis; Neurons; Inflammation; Murine model

1. Introduction

Amyotrophic lateral sclerosis (ALS) is a progressive, debilitating disorder that is characterized by the deterioration of motor neurons that results in muscle weakness and atrophy, bulbar palsy, and pyramidal tract signs.[1,2] The incidence of ALS is between 0.6 and 3.8/100,000 person-years and increases with age.[3,4] This devastating neurodegenerative disease has a poor prognosis, with 50% of patients passing away within 30 months of symptom onset and only 20% surviving for 5 – 10 years.[5] Hence, the primary aim of current treatment was to extend life expectancy in patients with ALS.

The pathophysiology of ALS is the result of complex interactions between genetic and molecular pathways.[6] Mutations in the copper-zinc superoxide dismutase 1 (SOD1) gene may be a major factor, because they cause conformational instability and misfolding of the SOD1 peptide, leading to the formation of intracellular aggregates and disruption of axonal transport systems and cellular functions.[7] At present, no definitive cure exists for ALS. Riluzole and edaravone are the only approved medications with limited beneficial effects.[8,9] Nonetheless, there has been increasing research in recent years on the use of stem cells for treating neurodegenerative diseases.[10-12] This therapy works by replacing cells and secreting neurotrophic factors, which help regenerate neurons and glial cells.[10,11] Mesenchymal stem cells (MSCs) originate from the mesoderm during early development[13] and can differentiate into neurons under certain stimulation conditions. MSCs may be a promising potential therapy for ALS treatment.[14] Human dental pulp stem cells (hDPSCs) are a type of MSCs found in dental pulp tissue and possess strong self-renewal and multidirectional differentiation potential. Compared with other MSCs, hDPSCs are easier to obtain, have higher proliferation rates,[15] and can also differentiate into a variety of somatic cells in an appropriate environment.[16,17] Furthermore, hDPSCs have a lower potential to transform into tumors.[18] Therefore, this study was conducted to investigate the efficacy of hDPSCs treatment based on clinical and pathological changes in an ALS mouse model.

2. Methods

2.1. Administration of hDPSCs

Here, hDPSCs were extracted from the third molars of healthy volunteers at the Dental Clinic of the Beijing Stomatological Hospital, with ethical approval (Approval Number: KJ-2021- 016-C-01-CS, Beijing, China). Written informed consent was provided to all donors who participated in the study. The hDPSCs injection was prepared and appraised by Beijing Chengnuo Medical Technology Co., Ltd. After cleaning and disinfecting the teeth, a bone chisel was used to segment the tooth tissue. The pulp tissue was extracted and rinsed repeatedly, after which it was cut with curved scissors into small pieces of approximately 0.5 mm^3. Subsequently, 0.3% collagenase type I (MP Biomedicals LLC, CA, USA) and 0.4% dispase II (Sigma, SLZ, USA) were added to digest for 1 h at 37°C. Digestion was terminated with Dulbecco's phosphate-buffered saline (PBS), and the cells were inoculated into a six-well cell culture plate and cultured in a cell incubator at 37°C and 5% CO_2. Then, the cells were washed and resuspended with 0.9% sterile saline solution for counting. Two batches of cells were used in the experiment, and cells were identified by flow cytometry. The hDPSCs were positive for the surface antigens CD73/CD90/CD44/CD166/CD105/CD146 and negative for CD11b/CD19/CD34/CD45/HLA-DR[19] (Figure S1). Next, 1×10^6 cells were resuspended in 200 μl of 0.9% sterile physiological saline and injected into SOD1-G93A mice through the tail vein. The SOD1-G93A vehicle group and wild-type (WT) mice group were administered 200 μL of 0.9% sterile physiological saline. The hDPSCs or 0.9% sterile physiological saline were infused once through the tail vein at disease onset.

2.2. Mice

High-copy SOD1-G93A 72 transgenic mice (B6.Cg-Tg[SOD1∗G93A]1Gur/J) were obtained from the Jackson Laboratory (Strain#: 004435). PCR genotype identification was performed on mice according to the genotype identification scheme provided by the Jackson Laboratory. Mice containing transgenic bands (molecular size, 236 bp) were identified as SOD1-G93A mice and those without magnetic bands were WT controls.[20] Hemizygous carriers (males) were bred with C57BL/6J inbred mice. The SOD1-G93A transgenic mice were obtained by genotyping. All mice were housed in a specific pathogen-free environment with a 12 – 12-h dark–light cycle and had free access to food and water. The animals were randomly assigned to individual groups. The endpoint in this study was based on the criteria previously reported by the ALS-Therapy Development Institute (ALS-TDI), that is, the loss of self-righting ability within 10 s (neurological score = 4) or the inability to move to reach food on the cage floor. Mice that reached the humane endpoint were euthanized within 3 h. No animal deaths occurred during the evaluation, and there were no post-infusion deaths. All experimental procedures were conducted according to the guidelines of the Institutional Animal Care and Use Committee of Beijing Tiantan Hospital and the Chinese Small Animal Protection Association Experimental Protocol with approval from the Institutional Animal Care and Use Committee Institutional Animal Care and Use Committee (IACUC) under the protocol number 202203004.

2.3. Rotarod test

Mice were placed on a fixed-speed rotating rod (3 cm in diameter and rotating at 40 rpm). All mice were trained twice daily for 3 days after the injection at day 80. At each experimental time point, the time the mice spent on the rotating rod was calculated up to a maximum of 180 s. Each mouse was tested 3 times at the same time each week, and the results were calculated as the average of the three trials.

2.4. 7-T magnetic resonance imaging (MRI)

MRI was performed using a 7.0-T MRI scanner (BioClinScan, Bruker, Germany) equipped with a 31-cm aperture Ultra Shield Refrigerated Magnet, with a gradient field strength of 290 mT/m and a switching rate of 1160 T/m/s at days 120 and 150. T2-weighted imaging (T2WI) – turbo spin echo images were acquired by a spin-echo echo-planar imaging sequence with 15 slices (repetition time/echo time = 2240/38 ms; matrix size = 192 × 320; field of view = 24 × 30 mm; and slice thickness = 1.0 mm). The T2-weighted images were used to obtain the cross-sectional area of the lumbar spinal cord without any contrast agent. The MRI scans were analyzed by experts blinded to the experimental group using an anatomical atlas for guidance. Freehand region-of-interest measurements were conducted using the ImageJ software (National Institutes of Health, MD, USA). The cross-sectional area of the lumbar spinal cord was measured manually by outlining relevant anatomical structures. Six slices were analyzed per mouse and averaged to obtain a mean value for each animal.[21]

2.5. Immunofluorescence staining

The brain and spinal cord of mice were separated at day 150 and fixed overnight in 4% paraformaldehyde at 4°C. The brain was dehydrated in 15% and 30% sucrose sequentially. After embedding in Optimal cutting temperature compound (OCT), brain tissues were cut into 8-μm-thick slices using a cryostat. The sections were washed 3 times (5 min each) with PBS and blocked using 5% normal donkey serum and 0.3% Triton X-100 in PBS for 1 h. Then, the sections were incubated overnight at 4°C with the following primary antibodies: rabbit anti-Iba1 (1:200; Abcam, ab178846), mouse anti-NeuN (1:400; Abcam, ab104224), rabbit anti-glial fibrillary acidic protein (1:400; Abcam, ab7260), and rabbit brain-derived neurotrophic factor (anti-BDNF) (1:100; Abcam, ab108319). The next day, the sections were rinsed 3 times with PBS for 10 min and then incubated with corresponding secondary antibodies (Alexa Fluor® 488 donkey anti-rabbit Immunoglobulin G [IgG], 1:1000; Thermo Fisher Scientific, USA, R37118; Alexa Fluor® 488 donkey anti-mouse IgG, 1:1000; Thermo Fisher Scientific, USA, R37114) for 1 h at room temperature. Finally, the sections were observed under the PerkinElmer Launches Vectra® Polaris™ Automated Quantitative Pathology Imaging System. Cells were quantified for each spinal cord section using the ImageJ software (National Institutes of Health, MD, USA).

2.6. Flow cytometry analysis

Fresh mice brain and spinal cord were separated on day 150 and analyzed using flow cytometry. First, 500 μL of collagenase I (1 mg/mL, Solarbio, C8140) was added to fresh mouse brain tissues, which were then cut into pieces using pre-cooled ophthalmic scissors on ice. Next, an additional 500 μL of collagenase I was added and gently mixed. The mixture was digested for 30 min in an incubator at 37°C. Then, 2 mL of 1 × PBS (Solarbio, P1020) was added to stop the digestion process, followed by centrifugation (4°C, 10 min, and 1000 rpm). The resulting supernatant was discarded, and 10 mL of 30% percoll per tube was added, followed by centrifugation (4°C, 10 min, and 2,000 rpm) to eliminate myelin. After discarding the supernatant, the pellet was mixed and washed with 1 mL of 1× PBS. After another round of centrifugation to remove the supernatant, a single-cell suspension was obtained by resuspending the cells in 1 mL of 1 × PBS. The cells were then suspended in 100 μL of 2% bovine serum albumin for blocking. Zombie Violet™ (BioLegend, 423114) staining was performed at room temperature for 20 min to distinguish between live and dead cells. Next, the cells were incubated with conjugated antibodies for surface staining at 4°C for 30 min, followed by fixing using a fixation buffer (BioLegend, 420801) at 4°C for 20 min and two washing steps in a 1× permeabilization buffer (BioLegend, 421002) for 30 min for intracellular staining. The following antibodies were used: NeuN (Abcam, ab223994), CD45 (BioLegend, 103116), and CD11b (BioLegend, 101216). Data and images were acquired using a FACSAria™ II flow cytometer (BD, Biosciences) and analyzed using the FlowJo software (version 10.5.3).

2.7. Statistical analysis

All statistical details are provided in figure legends. Animals were randomly assigned to the experimental groups using the random number generator function in the computer. All data analyses were performed independently by investigators who were blinded to the experimental groups. Data are expressed as mean ± standard error of the mean. $p < 0.05$ was considered statistically significant. Statistical significance was determined using the unpaired *t*-test for two groups and two-way analysis of variance for three groups. All statistical analyses were conducted using GraphPad Prism version 10.0 (GraphPad Software, La Jolla, CA).

3. Results

3.1. hDPSCs infusion attenuated motor neuron dysfunction and extended the life expectancy of SOD1-G93A mice

Experiments to investigate the efficacy of hDPSCs infusion in SOD1-G93A mice were conducted by considering the body weight, motor performance in the rotarod test, neurological scores, and survival days of the mice (Figure 1A). All SOD1-G93A mice began losing weight in the 15th week. The infusion of hDPSCs caused no significant change in the body weight of SOD1-G93A mice compared with that of untreated mice (Figure 1B). Nevertheless, mice treated with hDPSCs exhibited improved performance in the rotarod test compared with untreated mice (Figure 1C, 17th week $p < 0.0001$). We evaluated the neurological scores using the ALS-TDI criteria and found that both hDPSCs infusion and vehicle-treated SOD1-G93A mice exhibited continuous motor deficits after the 11th week. The infusion of hDPSCs attenuated motor neuron dysfunction compared

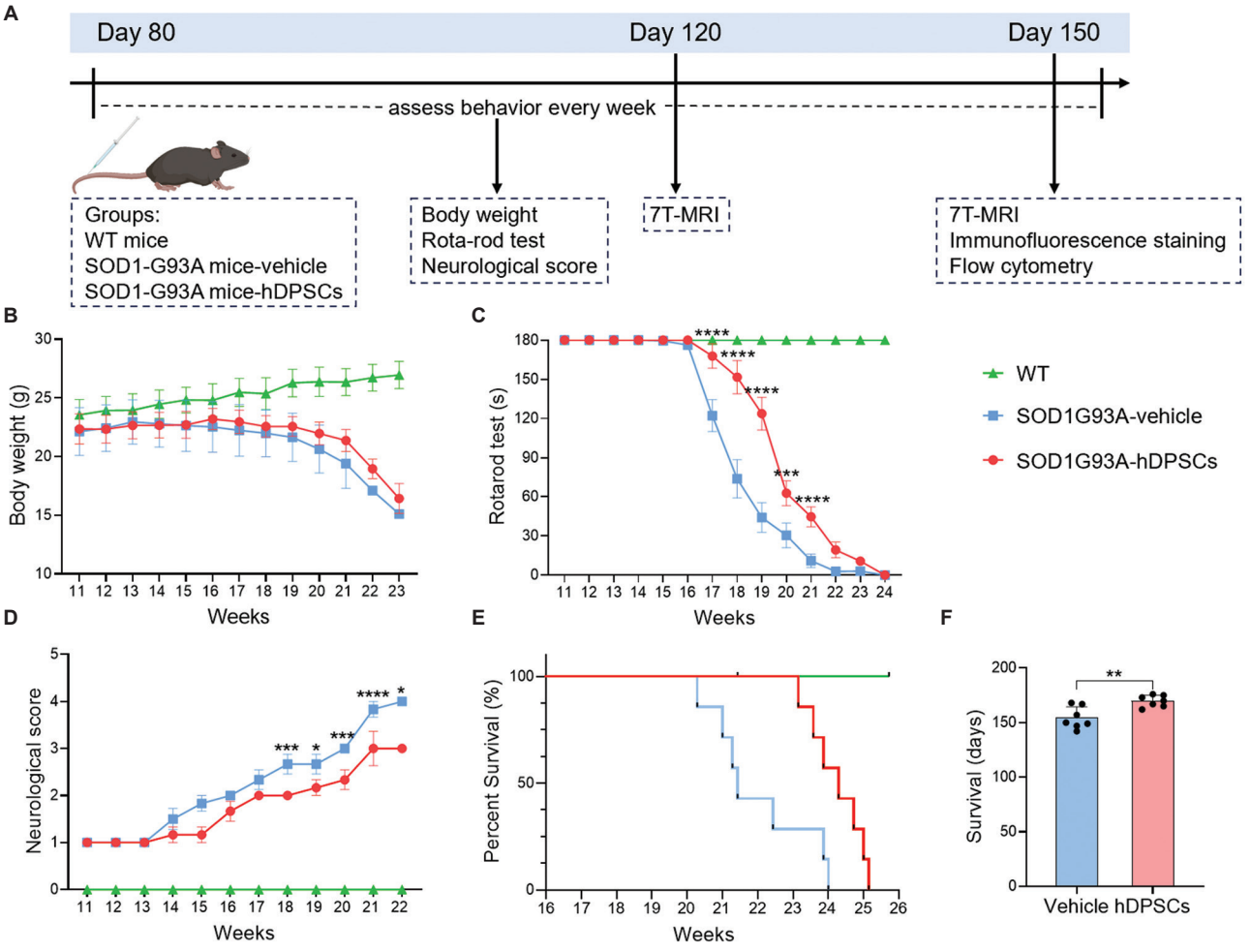

Figure 1. hDPSCs treatment delayed ALS progression and extended lifespan in SOD1-G93A mice. (A) Schematic of the experimental design conducted on SOD1-G93A mice with vehicle (0.9% sterile physiological saline) or with hDPSCs treatment. On day 80, mice were administered injections of hDPSCs or vehicles. Starting from day 80, the body weight, rotarod test results, and neurological scores of each mouse were recorded weekly. Flow cytometry and immunofluorescence staining were conducted on day 150 to evaluate neuronal loss and neuroinflammation. 7-T MRI scans taken on days 120 and 150 were used to measure spinal cord atrophy progression. (B) Body weight was measured in WT and SOD1-G93A mice treated with vehicle or hDPSCs. $n = 6$ per group. Data were statistically analyzed by two-way ANOVA. (C) Persistence running times were recorded in the rotarod test of WT and SOD1-G93A mice treated with vehicle or hDPSCs. $n = 6$ per group. Data were statistically analyzed by two-way ANOVA. (D) Neurological deficits were evaluated using behavioral scores in WT and SOD1-G93A mice treated with vehicle or hDPSCs. $n = 6$ per group. Data were statistically analyzed by two-way ANOVA. (E) Kaplan–Meier cumulative survival curve of WT and SOD1-G93A mice treated with vehicle or hDPSCs. Endpoint was defined as the death point when mice could no longer regain their upright position within 30 s after being placed on their back; $n = 7$ per group. (F) Histogram of survival days of SOD1-G93A mice treated with vehicle or hDPSCs. $n = 7$ per group. Data were statistically analyzed using the unpaired t-test. Data were expressed as mean ± SEM. Notes: *$p<0.05$, ***$p<0.005$, and ****$p<0.001$. Abbreviations: ALS: Amyotrophic lateral sclerosis; hDPSCs: Human dental pulp stem cells; ALS: Amyotrophic lateral sclerosis; WT: Wild type; SEM: Standard error of mean; ANOVA: Analysis of variance.

with that in vehicle-treated SOD1-G93A mice from the 13th week onward (Figure 1D, 18th week $p = 0.0008$). Finally, the infusion of hDPSCs prolonged the survival of SOD1-G93A mice by approximately 15 days (169.7 ± 1.997 vs. 154.3 ± 3.803 days; $p = 0.0037$, Figure 1E and F).

3.2. hDPSCs infusion reduced the degree of spinal cord atrophy in SOD1-G93A mice

Cross-sectional images of lumbar enlargement (LE) were acquired by 7-T MRI. Comparatively, the average area of LE in T2WI scans was reduced in all SOD1-G93A mice on days 120 and 150 (Figure 2A and C). On day 120, the average area of LE was smaller in vehicle-treated SOD1-G93A mice than in WT mice (2.999 ± 0.031 vs. 3.280 ± 0.044 mm^2; Figure 2B; $p = 0.0004$). The average area of LE in hDPSC-treated SOD1-G93A mice was greater than that in untreated mice (3.149 ± 0.033 vs. 2.999 ± 0.031 mm^2; Figure 2B; $p = 0.0053$). On day 150, the average area of LE was smaller in vehicle-treated SOD1-G93A mice than in WT mice (2.733 ± 0.031 vs. 3.451 ± 0.066 mm^2; Figure 2D; $p < 0.0001$). The hDPSCs infusion preserved the average area of LE in SOD1-G93A mice compared with that in vehicle-treated SOD1-G93A mice (2.927 ± 0.027 vs. 2.733 ± 0.031 mm^2; Figure 2D; $p = 0.0008$). Hence, treatment with hDPSCs could delay spinal cord atrophy in SOD1-G93A mice.

3.3. hDPSCs infusion preserved neurons in SOD1-G93A mice

The pathological features of hDPSCs infusion in the ALS mouse model were characterized using flow cytometry and immunofluorescence. The results of immunofluorescence indicated a significant reduction in the number of neurons in the spinal cord of SOD1-G93A mice at 150 days (Figure 3A and B; $p = 0.0001$). Conversely, hDPSCs-treated SOD1-G93A mice exhibited preservation of spinal cord neuron numbers compared with vehicle-treated SOD1-G93A mice (Figure 3A and B; $p = 0.0030$). Consistent with these immunofluorescence findings, a remarkable decrease in the number of neurons was observed in the brains and spinal cord of SOD1-G93A mice (Figure 3D and E; $p = 0.0005$ for brain, $p = 0.0019$ for the spinal cord). After the infusion of hDPSCs, the SOD1-G93A mice presented with an increase in the percentage of neurons in their brains and spinal cords (Figure 3D and E; $p = 0.0076$ for the brain, $p = 0.0063$ for the spinal cord). Moreover, the number of BDNF-positive cells remarkably increased in SOD1-G93A mice after treatment with hDPSCs (Figure S2). These data suggest that hDPSCs have the potential to protect against neuronal loss and improve the secretion of neurotrophic factors in an ALS mouse model.

3.4. hDPSCs infusion exerted no obvious effect on glial cell phenotypes in SOD1-G93A mice

Previous research has shown that microglial activation can exacerbate cellular damage in ALS development.[22] To further investigate the effect of hDPSCs infusion on microglia in ALS mice, we performed immunofluorescence staining and flow cytometry. Immunofluorescence staining revealed an increased number of microglia in the spinal cords of all SOD1-G93A mice on day 150 (Figure 4A and B; $p < 0.0001$). The number of microglia in the spinal cord and brain of SOD1-G93A mice was significantly higher than that of WT mice (Figure 4D and E; $p = 0.0005$ for the brain, $p < 0.0001$ for the spinal cord), suggesting that microglia are involved in the disease progression of ALS mice. However, a significant difference was detected in the number of microglia between the hDPSCs-infused and vehicle groups (Figure 4B, D, E; $p = 0.1433$ for the brain, $p = 0.1581$ for the spinal cord), suggesting a limited effect of hDPSCs on microglia in ALS mice. Furthermore, no significant differences were observed in the number of astrocytes between the hDPSCs-infused and vehicle groups ($p = 0.0937$, Figure S3).

4. Discussion

This study examined the efficacy of hDPSCs infusion in a mouse model of ALS. Our findings indicated that the infusion of hDPSCs not only mitigated motor neuron dysfunction but also extended the lifespan of SOD1-G93A mice. Moreover, immunofluorescence and flow cytometry revealed that hDPSCs infusion could reduce the degree of spinal cord atrophy and relatively preserve neurons in SOD1-G93A mice.

MSCs, as pluripotent stem cells, are used to treat a variety of diseases, including ALS.[23,24] Compared with other MSCs, hDPSCs have the characteristics of simple acquisition and easy expansion[25,26]; however, their therapeutic effects in ALS have not yet been reported. In the present study, the infusion of hDPSCs could significantly ameliorate clinical disability and prolong survival time in ALS mice. This effect was evidenced by 7-T MRI analysis, which showed that the extent of spinal cord atrophy in hDPSCs-treated mice was significantly less than that in untreated mice. To further explore the cellular changes brought about by hDPSCs infusion, we performed flow cytometry and immunofluorescence staining to analyze neurons. The results were consistent with those of previous studies that used MSCs for ALS treatment, indicating that the number of neurons was relatively preserved after the infusion of hDPSCs.[27,28]

Studies have shown that transplanted MSCs can differentiate into motor neuron-like cells, expressing

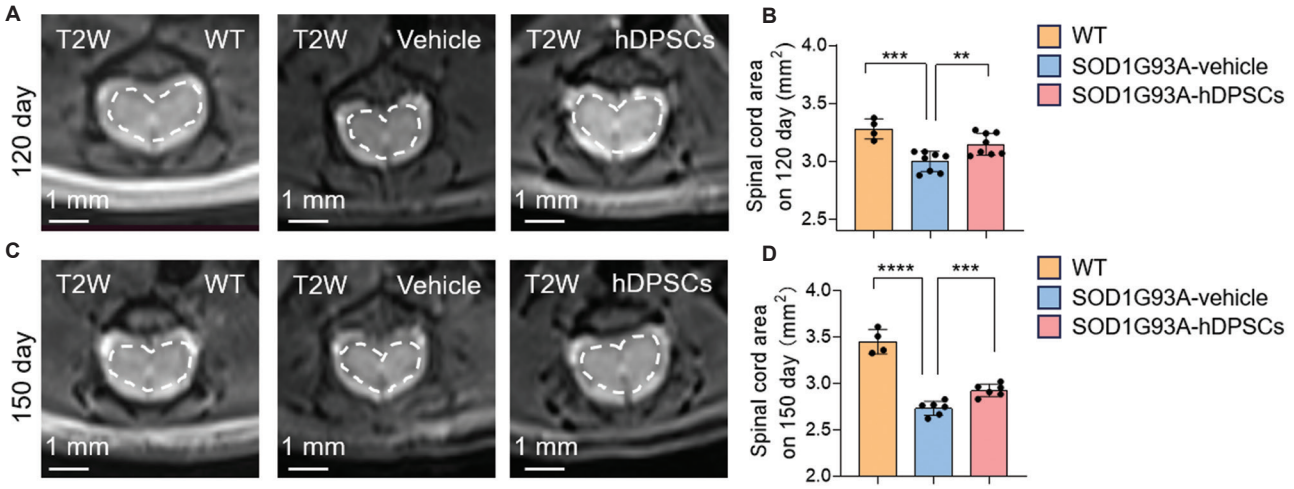

Figure 2. hDPSC treatment reduced spinal cord atrophy in SOD1-G93A mice. (A) 7-T MRI scans showing the cross-sectional area of spinal cord lumbar enlargement (LE) within the axial position of WT and SOD1-G93A mice treated with vehicle or hDPSCs on day 120, scale bar = 1 mm. (B) Histogram showing the cross-sectional area of spinal cord LE in WT and SOD1-G93A mice treated with vehicle or hDPSCs on day 120. n = 4 in the WT mice group, n = 8 in the vehicle- or hDPSCs-treated SOD1-G93A mice group. (C) 7-T MRI scans showing the cross-sectional area of spinal cord LE within the axial position of WT and SOD1-G93A mice treated with vehicle or hDPSCs on day 150, scale bar = 1 mm. (D) Histogram showing the cross-sectional area of spinal cord LE in WT and SOD1-G93A mice treated with vehicle or hDPSCs on day 150. n = 4 in the WT mice group, n = 6 in the vehicle- or hDPSCs-treated SOD1-G93A mice group. Data were statistically analyzed using the unpaired t-test. Data were expressed as mean ± SEM. Notes: $^{**}p<0.01$, $^{***}p<0.001$, and $^{****}p<0.0001$.

Abbreviations: 7T MRI: 7T magnetic resonance imaging; hDPSCs: Human dental pulp stem cells; WT: Wild type; SEM: Standard error of mean.

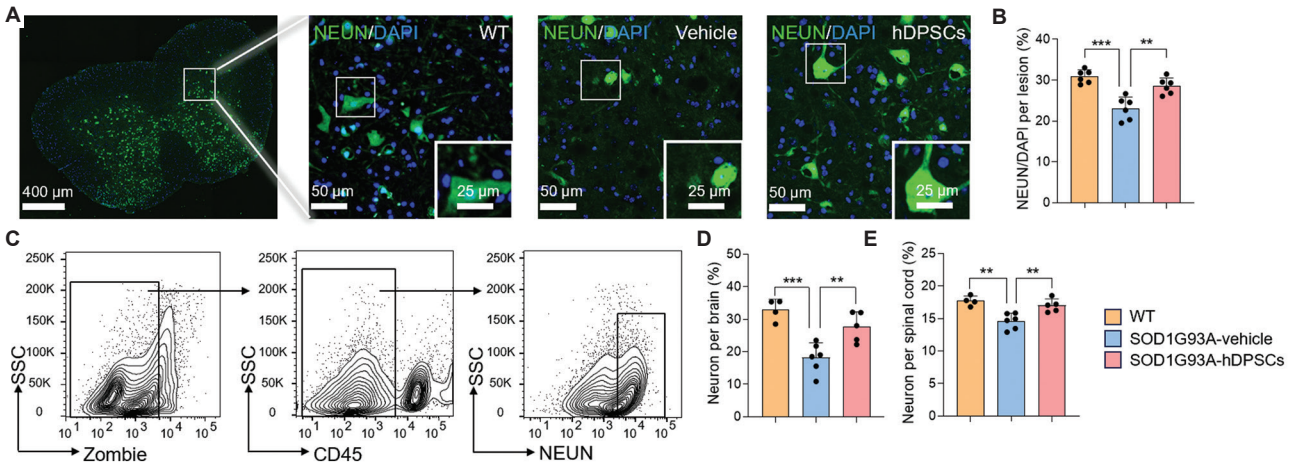

Figure 3. Augmentation of neuronal cells in SOD1-G93A mice after hDPSCs treatment. (A) Immunofluorescence images showing the number of neurons in lumbosacral enlargement of the anterior horn of the spinal cord of WT and SOD1-G93A mice treated with vehicle or hDPSCs on day 150. Scale bar = 50 μm. (B) Histogram illustrating the relative proportions of neurons in WT and SOD1-G93A mice treated with vehicle or hDPSCs. n = 6 per group. (C) Flow cytometry analysis depicting the gating strategies used for neurons on day 150. (D) Histogram showing the population of neurons in the brain of WT and SOD1-G93A mice treated with vehicle or hDPSCs on day 150. n = 4 in the WT mice group, n = 6 in the vehicle-treated SOD1-G93A mice group, and n = 5 in the hDPSCs-treated SOD1-G93A mice group. (E) Histogram depicting the population of neurons in the spinal cord of WT and SOD1-G93A mice treated with vehicle or hDPSCs on day 150. n = 4 in the WT mice group, n = 6 in the vehicle-treated SOD1-G93A mice group, and n = 5 in the hDPSCs-treated SOD1-G93A mice group. Data were statistically analyzed using the unpaired t-test. Data were expressed as mean ± SEM. Notes: $^{**}p<0.01$ and $^{***}p<0.001$.

Abbreviations: hDPSCs: Human dental pulp stem cells; WT: Wild type; SEM: Standard error of mean.

markers typically found on the surface of motor neurons, and can thus rescue neuronal loss and improve clinical disabilities.[29,30] It has also been confirmed that decellularized dental pulp acts as a potential scaffold for pulp regeneration, which can drive the differentiation of MSCs into neuronal cells under certain electrophysiological conditions with the expression of odontoblastic markers. The application of mechanical force cues from exogenous scaffolds at

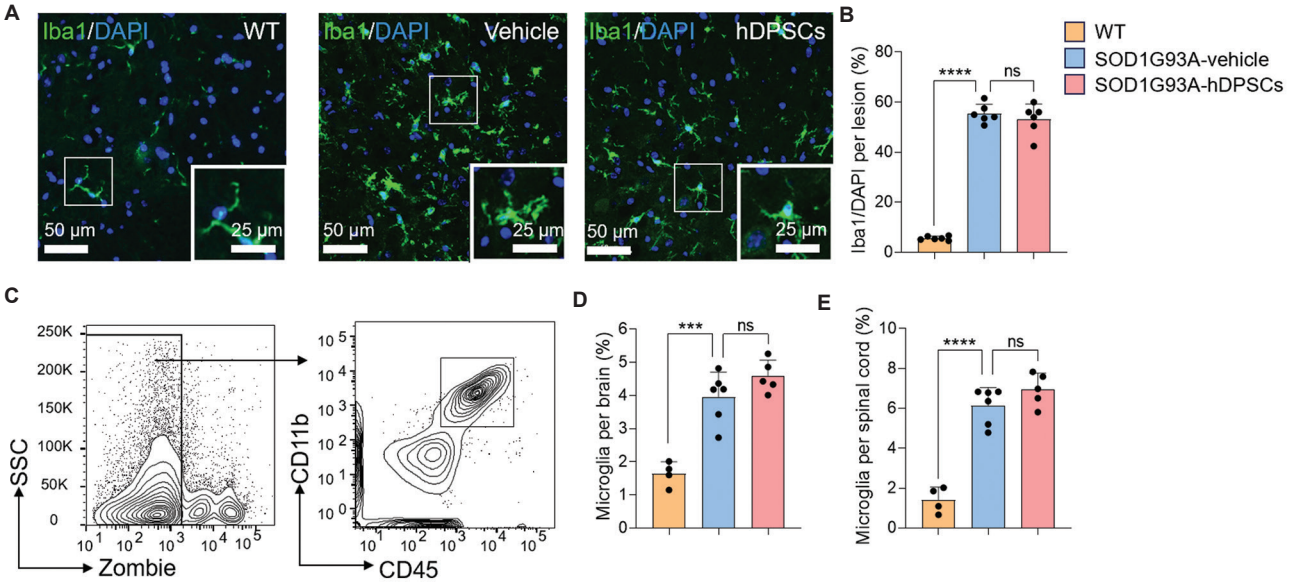

Figure 4. Microglia in SOD1-G93A mice showed no evident significant changes after treatment with hDPSCs. (A) Immunofluorescence images depicting the amount of microglia in lumbosacral enlargement of the anterior horn of the spinal cord of WT and SOD1-G93A mice treated with vehicle or hDPSCs on day 150. Scale bar = 50 μm. (B) Histogram illustrating the relative proportions of microglia in WT and SOD1-G93A mice treated with vehicle or hDPSCs. $n = 6$ per group. (C) Flow cytometry analysis depicting the gating strategies used for microglia at day 150. (D) Histogram showing the percentage of $CD45^{intermediate}CD11b^{+}$ microglia ($CD45^{int}CD^{11b+}$) in the brain of WT and SOD1-G93A mice treated with vehicle or hDPSCs on day 150. $n = 4$ in the WT mice group, $n = 6$ in the vehicle-treated SOD1-G93A mice group, and $n = 5$ in the hDPSCs-treated SOD1-G93A mice group. (E) Histogram depicting the percentage of $CD45^{intermediate}CD11b^{+}$ microglia ($CD45^{int}CD11b^{+}$) in the spinal cord of WT and SOD1-G93A mice treated with vehicle or hDPSCs on day 150. $n = 4$ in the WT mice group, $n = 6$ in vehicle-treated SOD1-G93A mice group, and $n = 5$ in the hDPSCs-treated SOD1-G93A mice group. Data were statistically analyzed using an unpaired t-test. Data were expressed as mean ± SEM. Notes: $^{**}p<0.01$, $^{***}p<0.001$, and $^{****}p<0.0001$.
Abbreviations: hDPSCs: Human dental pulp stem cells; WT: Wild type; SEM: Standard error of mean.

the nanoscale plays a vital role in the differentiation process of MSCs.[31,32] Furthermore, hDPSCs can secrete some essential neurotrophic factors, including nerve growth factor proteins, BDNF, and glial cell line-derived neurotrophic factor, which can nourish damaged neurons and promote neural regeneration.[33-35] Previous findings suggesting that hDPSCs play a potential regulatory role in the inflammatory response during disease progression were contradicted by the findings of the present study, as the population of microglia or astrocytes in SOD1-G93A mice exhibited no significant changes after the infusion of hDPSCs.[36] Studies have reported that extracellular vesicles released by MSCs induce functional modifications in microglia.[37,38] Further investigation is required to clarify the impact of hDPSCs on glial cell features in ALS mice. Moreover, our study is limited by the fact that NeuN is not a specific marker for motor neurons. In addition, the mechanism through which hDPSCs infusion increases the levels of trophic factors that reduce the clinical symptoms of ALS mice remains unknown.

5. Conclusion

The infusion of hDPSCs ameliorated clinical impairment and prolonged the lifespan of ALS mice by retarding spinal cord atrophy and conserving neurons, demonstrating the beneficial effects of hDPSCs infusion in ALS mice. This evidence based on murine models needs further validation by well-executed randomized controlled clinical trials. Moreover, future optimized protocols for engineered hDPSCs and the identification of reliable biomarkers to predict therapeutic outcomes are essential steps toward the innovative use of hDPSCs for ALS treatment. Nevertheless, the use of hDPSCs as a therapeutic approach holds promise for future clinical interventions for patients with ALS.

Acknowledgments

The authors thank Beijing Chengnuo Medical Technology Co., Ltd. for providing the hDPSCs injection.

Funding

This work was supported in part by the National Science Foundation of China (82122021).

Conflict of interest

Wei-Na Jin is an Editorial Board Member of this journal but was not in any way involved in the editorial and peer-review process conducted for this paper, directly or

indirectly. Separately, other authors declared that they have no known competing financial interests or personal relationships that could have influenced the work reported in this paper.

Author contributions

Conceptualization: Wei-Na Jin, Songling Wang, Fu-Dong Shi

Formal analysis: Yingying Su, Hao Wang, Jian Zhou

Methodology: Shihe Jiang, Xiuchen Guan, Meng Shi, Ying Zhang, Xindi Li

Writing–original draft: Wei-Na Jin, Songling Wang, Fu-Dong Shi, Shihe Jiang, Xiuchen Guan

Writing–review & editing: Wei-Na Jin, Songling Wang, Fu-Dong Shi

Ethics approval and consent to participate

The hDPSCs were extracted from healthy volunteers' third molars, which were obtained from the Dental Clinic of the Beijing Stomatological Hospital, with ethical approval (Approval Number: KJ-2021- 016-C-01-CS, Beijing, China). The written informed consent was provided to all donors who participated in the study. All experimental procedures were performed in accordance with the guidelines of the Institutional Animal Care, Use Committee of Beijing Tiantan Hospital, and the Chinese Small Animal Protection Association Experimental Protocol with approval from the IACUC under protocol number 202203004.

Consent for publication

Not applicable.

Availability of data

Not applicable.

References

1. Gitler AD, Dhillon P, Shorter J. Neurodegenerative disease: Models, mechanisms, and a new hope. *Dis Model Mech*. 2017;10(5):499-502.

   doi: 10.1242/dmm.030205

2. Mehta P, Raymond J, Punjani R, *et al*. Prevalence of Amyotrophic Lateral Sclerosis (ALS), United States, 2016. *Amyotroph Lateral Scler Frontotemporal Degener*. 2022;23(3-4):220-225.

   doi: 10.1080/21678421.2021.1949021

3. Longinetti E, Fang F. Epidemiology of amyotrophic lateral sclerosis: An update of recent literature. *Curr Opin Neurol*. 2019;32(5):771-776.

   doi: 10.1097/wco.0000000000000730

4. Brown RH, Al-Chalabi A. Amyotrophic lateral sclerosis. *N Engl J Med*. 2017;377(2):162-172.

   doi: 10.1056/NEJMra1603471

5. Batagov AO, Kurochkin IV. Exosomes secreted by human cells transport largely mRNA fragments that are enriched in the 3'-untranslated regions. *Biology Direct*. 2013;8:12.

   doi: 10.1186/1745-6150-8-12

6. Kiernan MC, Vucic S, Cheah BC, *et al*. Amyotrophic lateral sclerosis. *Lancet*. 2011;377(9769):942-955.

   doi: 10.1016/s0140-6736(10)61156-7

7. Bruijn LI, Houseweart MK, Kato S, *et al*. Aggregation and motor neuron toxicity of an ALS-linked SOD1 mutant independent from wild-type SOD1. *Science*. 1998;281(5384):1851-1854.

   doi: 10.1126/science.281.5384.1851

8. Oskarsson B, Gendron TF, Staff NP. Amyotrophic lateral sclerosis: An update for 2018. *Mayo Clin Proc*. 2018;93(11):1617-1628.

   doi: 10.1016/j.mayocp.2018.04.007

9. Brooks BR, Berry JD, Ciepielewska M, *et al*. Intravenous edaravone treatment in ALS and survival: An exploratory, retrospective, administrative claims analysis. *EClinicalMedicine*. 2022;52:101590.

   doi: 10.1016/j.eclinm.2022.101590

10. Ford E, Pearlman J, Ruan T, *et al*. Human pluripotent stem cells-based therapies for neurodegenerative diseases: Current status and challenges. *Cells*. 2020;9(11):2517.

    doi: 10.3390/cells9112517

11. De Gioia R, Biella F, Citterio G, *et al*. Neural stem cell transplantation for neurodegenerative diseases. *Int J Mol Sci*. 2020;21(9):3103.

    doi: 10.3390/ijms21093103

12. Wang D, Wang Y, Tian W, Pan J. Advances of tooth-derived stem cells in neural diseases treatments and nerve tissue regeneration. *Cell Prolif*. 2019;52(3):e12572.

    doi: 10.1111/cpr.12572

13. Horwitz EM, Le Blanc K, Dominici M, *et al*. Clarification of the nomenclature for MSC: The International Society for Cellular Therapy position statement. *Cytotherapy*. 2005;7(5):393-395.

    doi: 10.1080/14653240500319234

14. Kim C, Lee HC, Sung JJ. Amyotrophic lateral sclerosis - Cell based therapy and novel therapeutic development. *Exp Neurobiol*. 2014;23(3):207-214.

    doi: 10.5607/en.2014.23.3.207

15. Mortada I, Mortada R, Al Bazzal M. Dental pulp stem cells and neurogenesis. *Adv Exp Med Biol*. 2018;1083:63-75.

doi: 10.1007/5584_2017_71

16. Nuti N, Corallo C, Chan BMF, Ferrari M, Gerami-Naini B. Multipotent differentiation of human dental pulp stem cells: A literature review. *Stem Cell Rev Rep.* 2016;12(5):511-523.

doi: 10.1007/s12015-016-9661-9

17. De Almeida FM, Marques SA, Ramalho Bdos S, *et al*. Human dental pulp cells: A new source of cell therapy in a mouse model of compressive spinal cord injury. *J Neurotrauma*. 2011;28(9):1939-1949.

doi: 10.1089/neu.2010.1317

18. Crende O, García-Gallastegui P, Luzuriaga J, *et al*. Is there such a thing as a genuine cancer stem cell marker? Perspectives from the gut, the brain and the dental pulp. *Biology* (*Basel*). 2020;9(12):426.

doi: 10.3390/biology9120426

19. Hollands P, Aboyeji D, Orcharton M. Dental pulp stem cells in regenerative medicine. *Br Dent J*. 2018;224:747-750.

doi: 10.1038/sj.bdj.2018.348

20. Guégan C, Vila M, Rosoklija G, Hays AP, Przedborski S. Recruitment of the mitochondrial-dependent apoptotic pathway in amyotrophic lateral sclerosis. *J Neurosci.* 2001;21(17):6569-6576.

doi: 10.1523/jneurosci.21-17-06569.2001

21. Sartoretti T, Ganley RP, Ni R, Freund P, Zeilhofer HU, Klohs J. Structural MRI reveals cervical spinal cord atrophy in the P301L mouse model of tauopathy: Gender and transgene-dosing effects. *Front Aging Neurosci*. 2022;14:825996.

doi: 10.3389/fnagi.2022.825996

22. Chen H, Kankel MW, Su SC, Han SWS, Ofengeim D. Exploring the genetics and non-cell autonomous mechanisms underlying ALS/FTLD. *Cell Death Differ*. 2018;25(4):648-662.

doi: 10.1038/s41418-018-0060-4

23. Jo CH, Lee YG, Shin WH, *et al*. Intra-articular injection of mesenchymal stem cells for the treatment of osteoarthritis of the knee: A proof-of-concept clinical trial. *Stem Cells*. 2014;32(5):1254-1266.

doi: 10.1002/stem.1634

24. Bartolucci J, Verdugo FJ, Gonzalez PL, *et al*. Safety and efficacy of the intravenous infusion of umbilical cord mesenchymal stem cells in patients with heart failure: A Phase 1/2 randomized controlled trial (RIMECARD trial [Randomized clinical trial of intravenous infusion umbilical cord mesenchymal stem cells on cardiopathy]). *Circ Res*. 2017;121(10):1192-1204.

doi: 10.1161/CIRCRESAHA.117.310712

25. Gronthos S, Mankani M, Brahim J, Robey PG, Shi S. Postnatal human Dental Pulp Stem Cells (DPSCs) *in vitro* and *in vivo*. *Proc Natl Acad Sci U S A*. 2000;97(25):13625-13630.

doi: 10.1073/pnas.240309797

26. Huang GTJ, Gronthos S, Shi S. Mesenchymal stem cells derived from dental tissues vs. Those from other sources: Their biology and role in regenerative medicine. *J Dent Res*. 2009;88(9):792-806.

doi: 10.1177/0022034509340867

27. Magota H, Sasaki M, Kataoka-Sasaki Y, *et al*. Repeated infusion of mesenchymal stem cells maintain the condition to inhibit deteriorated motor function, leading to an extended lifespan in the SOD1G93A rat model of amyotrophic lateral sclerosis. *Mol Brain*. 2021;14(1):76.

doi: 10.1186/s13041-021-00787-6

28. Magota H, Sasaki M, Kataoka-Sasaki Y, *et al*. Intravenous infusion of mesenchymal stem cells delays disease progression in the SOD1G93A transgenic amyotrophic lateral sclerosis rat model. *Brain Res.* 2021;1757:147296.

doi: 10.1016/j.brainres.2021.147296

29. Hosokawa M, Arai T, Yamashita M, *et al*. Differential diagnosis of amyotrophic lateral sclerosis from Guillain-Barré syndrome by quantitative determination of TDP-43 in cerebrospinal fluid. *Int J Neurosci*. 2014;124(5):344-349.

doi: 10.3109/00207454.2013.848440

30. Nosrat IV, Smith CA, Mullally P, Olson L, Nosrat CA. Dental pulp cells provide neurotrophic support for dopaminergic neurons and differentiate into neurons *in vitro*; Implications for tissue engineering and repair in the nervous system. *Eur J Neurosci*. 2004;19(9):2388-2398.

doi: 10.1111/j.0953-816X.2004.03314.x

31. Magazzù A, Marcuello C. Investigation of soft matter nanomechanics by atomic force microscopy and optical tweezers: A comprehensive review. *Nanomaterials* (*Basel*). 2023;13(6):963.

doi: 10.3390/nano13060963

32. Wei X, Yang M, Yue L, *et al*. Expert consensus on regenerative endodontic procedures. *Int J Oral Sci*. 2022;14(1):55.

doi: 10.1038/s41368-022-00206-z

33. Hata M, Omi M, Kobayashi Y, *et al*. Transplantation of human dental pulp stem cells ameliorates diabetic polyneuropathy in streptozotocin-induced diabetic nude mice: The role of angiogenic and neurotrophic factors. *Stem Cell Res Ther*. 2020;11(1):236.

doi: 10.1186/s13287-020-01758-9

34. Luzuriaga J, Polo Y, Pastor-Alonso O, *et al*. Advances and perspectives in dental pulp stem cell based neuroregeneration therapies. *Int J Mol Sci*. 2021;22(7):3546.

doi: 10.3390/ijms22073546

35. Bar JK, Lis-Nawara A, Grelewski PG. Dental pulp stem cell-derived secretome and its regenerative potential. *Int J Mol*

Sci. 2021;22(21):12018.

doi: 10.3390/ijms222112018

36. Leong WK, Henshall TL, Arthur A, *et al*. Human adult dental pulp stem cells enhance poststroke functional recovery through non-neural replacement mechanisms. *Stem Cells Transl Med*. 2012;1(3):177-187.

doi: 10.5966/sctm.2011-0039

37. Zhang Z, Zou X, Zhang R, *et al*. Human umbilical cord mesenchymal stem cell-derived exosomal miR-146a-5p reduces microglial-mediated neuroinflammation via suppression of the IRAK1/TRAF6 signaling pathway after ischemic stroke. *Aging (Albany NY)*. 2021;13(2):3060-3079.

doi: 10.18632/aging.202466

38. Liu YY, Li Y, Wang L, *et al*. Mesenchymal stem cell-derived exosomes regulate phenotypes: A promising treatment for acute central nervous system injury. *Neural Regen Res*. 2023;18(8):1657-1665.

doi: 10.4103/1673-5374.363819

ACCSCIENCE PUBLISHING

Brain & Heart

ORIGINAL RESEARCH ARTICLE

Respiratory sinus arrhythmia in humans: Correlation analysis with breathing-specific heart rate

Jacopo P. Mortola*

Department of Physiology, Faculty of Medicine, McGill University, Montreal, Quebec, Canada

Abstract

In adult humans at rest, pulmonary ventilation and cardiac output share similar values, both approximately 5 L/min. Airflow is intermittent, with tidal volumes exceeding dead space, low breathing frequency (f_{resp}), and zero air velocity at both end-inspiration and end-expiration. In contrast, the cardiac pump is in series with the vasculature, such that the small stroke volume and high heart rate (HR) (f_h) allow for quasi-continuous blood flow. Based on experimental findings in dogs, it has been suggested that an elevated f_h during inspiration (known as respiratory sinus arrhythmia [RSA]) decreases the disparity between air and blood flow patterns. Thus, one might hypothesize a positive correlation between the peak-trough difference of instantaneous f_h ($\Delta HR' = HR'_{peak} - HR'_{trough}$) and the breathing-specific f_h (f_h/f_{resp}). To test this hypothesis, we combined breath-by-breath data for $\Delta HR'$ from several previous studies, resulting in a database of over 600 subjects. This extensive dataset allowed us to construct statistically meaningful correlations between $\Delta HR'$ and variables associated with RSA (f_h, f_{resp}, HR'_{peak}, and HR'_{trough}). A strong statistically significant ($r > 0.9$) correlation between f_h/f_{resp} and $\Delta HR'$ was observed. These findings support the hypothesis that RSA may be a mechanism for improving the match between the quasi-continuous blood flow and the intermittent airflow.

Keywords: Cardiac arrhythmia; Cardiorespiratory design; Parasympathetic control; Pulmonary gas exchange; Ventilation-perfusion matching

***Corresponding author:**
Jacopo P. Mortola
(jacopo.mortola@mcgill.ca)

Citation: Mortola JP. Respiratory sinus arrhythmia in humans: Correlation analysis with breathing-specific heart rate. *Brain & Heart*. 2024;2(4):3956. doi: 10.36922/bh.3956

Received: June 17, 2024

Accepted: October 29, 2024

Published Online: December 2, 2024

1. Introduction

The acceleration of the heart during inspiration, known as respiratory sinus arrhythmia (RSA), is perhaps the most recognized and most benign form of cardiac arrhythmia. Documented nearly two centuries ago,[1] RSA can often be detected through simple auscultation or by palpating pulses at the wrist. The heart rate (HR) (f_h) accelerates synchronously with inspiration due to the temporary inhibition of the nucleus ambiguus (the cardioinhibitory center), which results in the inhibition of the vagal (parasympathetic) output to the sinoatrial node of the heart and a shortening of the inter-beat interval (IBI). The inspiratory inhibition of the nucleus ambiguus arises from peripheral inputs sensing changes in intrathoracic pressure or lung expansion, as well as from central inputs, involving direct interaction between the respiratory pattern generator in the nucleus of the tractus solitarius and the nucleus ambiguus. Since the early work in the 1930s,[2,3] many experiments have investigated the relative contributions

of peripheral and central inputs to the mechanistic basis of RSA. The results have been mixed,[4-9] possibly because the relative importance of each factor may vary depending on the specific experimental or clinical conditions.[10] What is firmly established, however, is that the manifestation of RSA results from the temporary abolition of the vagal output; this means that the f_h values at end-inspiration solely depend on the sympathetic regulation of the heart.

Although the neurological basis of RSA is well documented, its physiological significance remains a subject of debate. Some have argued that the decrease in f_h during expiration lowers cardiac work during the low-oxygen phase of the breathing cycle, or that RSA helps stabilize blood pressure or blood carbon dioxide levels. Others suggest that RSA might be an epiphenomenon with no meaningful physiological role.[11-13] The latter hypothesis seems less likely, given that RSA is widespread among mammals, ranging from small species such as mice and rats[14,15] to larger animals like dogs, sheep, horses, and cows.[9,16,17] In studies involving paralyzed and artificially ventilated dogs, where stimulation of the cardiac nerves was applied at various phases of the breathing cycle, the most favorable blood gas values occurred when f_h was increased during the inflation phase of the breathing cycle. These results prompted the hypothesis that RSA may improve ventilation-perfusion matching by adjusting f_h to the inspiratory airflow.[18-21]

The magnitude of RSA has been shown to have an inverse relationship with the breathing frequency (f_{resp}). This phenomenon, revealed through direct breath-by-breath measures of RSA,[4,6,22,23] complicates the interpretation of RSA as a simple balance between parasympathetic and sympathetic cardiac control. The involvement of f_{resp} in RSA could be seen as another manifestation of RSA's role in optimizing ventilation-perfusion matching. The cardiorespiratory system is designed such that the pulmonary airflow is intermittent, while pulmonary blood flow is quasi-continuous. Thus, a higher f_{resp} relative to f_h should reduce the disparity between the pulmonary air and blood flow regimens. Based on this interpretation, one could hypothesize that the magnitude of RSA is more strongly correlated with the ratio of f_h to f_{resp} (f_h/f_{resp}, or the "breathing-specific HR") than with f_{resp} or f_h alone. The aim of this work, therefore, is to test the correlation between f_h/f_{resp} and RSA. This required direct measurements of RSA amplitude in a large sample size of subjects to minimize the influence of the inter-subject variability.

Most commonly, RSA is derived from the high-frequency band of the power spectrum of a series of IBI. Changes in the high-frequency component (typically between 0.15 and 0.45 Hz) relative to the low-frequency component (0.04 – 0.15 Hz) are often interpreted as indicating changes in "vagal tone".[24,25] This approach is widely used in clinical settings for the rapid identification of RSA and has even been adopted as a predictor of cardiac patient outcomes.[26-34] However, the assumption that the high- and low-frequency components of the IBI power spectrum correspond to parasympathetic and sympathetic control, respectively, has been repeatedly questioned, especially since selective pharmacologic block studies have shown that these components do not always align with autonomic influences on the heart.[8,19,21,35-37] Importantly, changes in the high-low frequency ratio of the IBI power spectrum cannot measure the magnitude of RSA with accuracy.

In contrast to power spectrum analysis, the breath-by-breath calculation of the difference between the peak and trough of instantaneous HR ($\Delta HR' = HR'_{peak} - HR'_{trough}$) provides a direct quantification of RSA magnitude. This approach has been applied to analyze short periods of IBI recordings in humans[4,6,23,38,39] and occasionally in other species.[9,15,16,40] Although more time-consuming than power spectrum analysis, breath-by-breath computation of ΔHR' offers a more accurate measurement of RSA.

The present work combined the data of several previous studies in which ΔHR' was measured directly, breath-by-breath. The resulting database, which included over 600 subjects, allowed us to construct statistically meaningful correlations between ΔHR' and the variables thought to influence RSA magnitude, i.e., f_h, f_{resp}, HR'_{peak}, and HR'_{trough}. The results indicated a highly statistically significant correlation between f_h/f_{resp} and ΔHR', strongly supporting the idea that RSA may play a role in improving the matching between quasi-continuous blood flow and intermittent airflow.

2. Methods

The data for the present work were collected between 2013 and 2020 for research on the effects of chest wall distortion, mental tasks, and muscle exercises on RSA.[23,38,39,41] A re-examination of the original individual data files resulted in a sample of several hundred subjects, all of whom had RSA measured at rest using identical methodology and analysis.

2.1. Subjects

The study population consisted of 635 undergraduate students (272 males and 363 females) aged 19 – 21 years. All participants were non-smokers, free of cardiorespiratory disorders, and not undergoing any medical treatment. The students were enrolled in a 1-year laboratory course in

"Experimental Physiology" (McGill University, Montreal, Canada, course # Physiology Lab 213). Each participant was instructed on the maneuver to be performed, but the specific purpose of the study was not disclosed. All measurements were non-invasive. The study adhered to the ethical standards set by the Declaration of Helsinki, and the procedures were approved by the ethics committee of the university.

2.2. Instrumentation

Measurements were taken in the early afternoon. The subjects were positioned supine on a comfortable mattress, with no visual access to the computer monitor. To minimize external disturbances, participants wore an ear set and were allowed to close their eyes while remaining awake.

Electrocardiogram (ECG) and breathing movements were measured. ECG was recorded from standard peripheral lead placements. An *ad hoc* algorithm detected the peak of the R-waves of the ECG to compute IBI (ms). IBI was converted into instantaneous HR (HR', beats/min) using the formula HR' = 60/(IBI/1000), which represents the number of heartbeats per minute, assuming successive R-R intervals remain constant. Breathing movements were recorded using impedance pneumography, with two Piezo Respiratory Belt Transducers (ADInstruments, United States) positioned around the rib cage (rc, approximately at the level of the fifth intercostal space) and around the abdomen (abd, at the level of the umbilicus). The sum of the rc and abd measurements in supine males reliably reflects changes in lung volume.[42-44]

The rc and abd signals were digitally acquired at 100 Hz, while the ECG was acquired at 400 Hz. These signals, along with the electronically computed beat-to-beat HR', were displayed on a computer monitor and saved for later analysis (Figure 1).

2.3. Data analysis

During the resting condition, once the breathing pattern was stable and reproducible, a 5-min recording period was initiated. At the end of this period, 10 consecutive breathing cycles were analyzed. The mean f_h (beats/min) and mean f_{resp} (breaths/min) were calculated for the analysis period. The highest (HR'_{peak}) and lowest (HR'_{trough}) values of HR' within each breath were identified, and their difference ($\Delta HR' = HR'_{peak} - HR'_{trough}$) was used to represent the magnitude of RSA, expressed in beats/min. Detailed descriptions of the instrumentation and data analysis can be obtained from earlier studies.[23,38,39,41]

When a subject had more than one recording period, the values from each epoch were averaged. Data from all subjects, either separated by gender or combined, were pooled together to obtain the group grand mean. To construct the correlations between parameter X and RSA, the following procedure was used: First, X-values were divided into seven approximately equidistant bins. This binning process minimized the potential skewing effect of uneven distributions. The average value for each bin was calculated, and the resulting seven data points were fitted using linear regression ($Y = a + b \cdot X$), where X is the parameter of interest, and Y is ΔHR'. Group

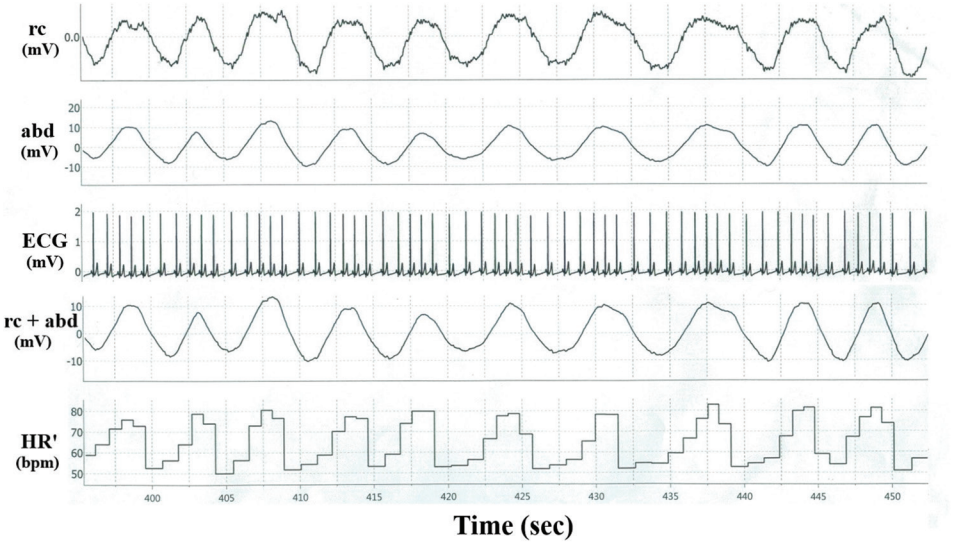

Figure 1. Representative experimental tracing from one subject at rest. From the top, rib cage (rc) and abdomen (abd) motion, with their combined motion (rc + abd; channel 4) proportional to the tidal volume (inspiration is upward). The electrocardiogram (ECG; channel 3) was used to compute the instantaneous heart rate (HR', beats/min) from the inter-beat intervals (channel 5). In this subject, HR' at end-inspiration (HR'*peak*) ranged from 75 – 83 bpm, while HR' at end-expiration (HR'*trough*) ranged from 52 – 56 bpm

data were reported as means ± 1 standard error of the mean and as the coefficient of variation (CV = standard deviation/mean; %). A two-tailed *t*-test was used to compare the two groups. Critical values for correlation coefficients, differences between slopes (b) and intercepts (a) of the linear function, and differences in mean values were considered statistically significant at $p < 0.05$. Since each X-Y relationship contained seven data points (with 7 – 2 = 5° of freedom), the critical value for statistical significance of the correlation coefficient *r* (for a two-tailed test at $\alpha = 0.05$) was 0.754, which corresponds to a coefficient of determination (R^2) of 0.569.

3. Results

3.1. Resting values

Table 1 summarizes the average anthropometric and cardiorespiratory values relevant to RSA.

ΔHR' was observed in all 635 subjects. On average, ΔHR' was 8.6 ± 0.3 bpm, which was similar between males (8.3 ± 0.3 bpm) and females (8.8 ± 0.3 bpm), but with considerable variability among subjects (Figure 2), ranging from 1 bpm (observed in one male and one female) to 46 bpm. Normalizing ΔHR' by the mean f_h (ΔHR' as a percentage of f_h) did not reduce the variability, because ΔHR' showed no correlation with f_h (see below). On average, RSA accounted for 12.6% ± 0.5% of f_h, with a CV of 60%. This was not significantly different between males (12.1% ± 0.4%) and females (12.9% ± 0.5%). The mode and the median RSA values were slightly lower than the average (10.4% and 10.9%, respectively).

Table 1. Respiratory sinus arrhythmia correlations: Anthropometric and cardiorespiratory values

Parameters	Males (*n*=272)	Females (*n*=363)	Combined (*n*=635)
Age, years	19.5±0.1 (5.1)	19.5±0.1 (4.9)	19.5±0.1 (5.0)
Height, cm	177±0.4 (3.8)	*164±0.5 (4.9)	170±0.6 (5.9)
Weight, kg	74±0.7 (14.9)	*59±0.7 (19.0)	65.4±0.8 (20.4)
f_h, bpm	68.6±0.7 (15.6)	69.4±0.7 (15.6)	69.1±0.7 (15.6)
f_{resp}, br/min	13.6±0.3 (30.9)	14±0.2 (27.4)	13.8±0.2 (28.9)
HR'*peak*, bpm	72.8±0.7 (15.7)	73.8±0.7 (15.4)	73.4±0.7 (15.5)
HR'*trough*, bpm	64.5±0.6 (16.4)	65±0.7 (16.9)	64.8±0.7 (16.7)
ΔHR', bpm	8.3±0.3 (61.6)	8.8±0.3 (60.0)	8.6±0.3 (60.6)
RSA, %	12.1±0.4 (61.0)	12.9±0.5 (59.7)	12.6±0.5 (60.2)
f_h/f_{resp}, beats/breath	5.6±0.1 (38.6)	5.4±0.1 (34.3)	5.5±0.1 (36.3)

Notes: Values are means±1 standard error of the mean in brackets or the coefficient of variations (CV=standard deviation/mean, %). f_h: Mean heart rate (bpm=beats/min). f_{resp}: Breathing rate (br/min=breaths/min). HR': Instantaneous heart rate (bpm). ΔHR': Peak-trough difference in instantaneous heart rate (bpm). RSA: Respiratory sinus arrhythmia expressed in percent of fh (ΔHR'/f_h 100). f_h/f_{resp}: Breathing-specific heart rate (beats/breath). *Statistically significant difference between genders (p<0.001).

3.2. Correlations

3.2.1. Body weight and height

Neither f_h nor f_{resp} showed statistically significant correlations with body height or weight, whether males, females, or the combined group were considered. Similarly, no significant correlation was found between ΔHR' and body height or weight.

3.2.2. Breathing frequency and HR

Table 2 presents the intercepts (a) and slopes (b) of the linear regressions between the cardiorespiratory variables pertinent to RSA and ΔHR'. In all three groups

Table 2. Respiratory sinus arrhythmia correlations: Cardiorespiratory variables relevant to respiratory sinus arrhythmia

	X	A	b	*r*	*p*
All subjects	f_{resp}	16.6	−0.57	0.97	<0.001
	f_h	3.1	0.078	0.85	<0.02
	HR'$_{trough}$	13.3	−0.072	0.903	<0.01
	HR'$_{peak}$	−4.4	0.18	0.996	<0.001
	f_h/f_{resp}	2.2	1.16	0.96	<0.001
	HR'$_{trough}/f_{resp}$	3.5	0.98	0.96	<0.001
	HR'$_{peak}/f_{resp}$	0.7	1.34	0.98	<0.001
Males	f_{resp}	15.9	−0.56	0.98	<0.001
	f_h	1.3	0.10	0.86	<0.02
	HR'$_{trough}$				ns
	HR'$_{peak}$	−6.5	0.20	0.98	<0.001
	f_h/f_{resp}	1.8	1.10	0.91	<0.01
	HR'$_{trough}/f_{resp}$	2.7	1.002	0.94	<0.01
	HR'$_{peak}/f_{resp}$	0.8	1.22	0.95	<0.001
Females	*fresp*	17.4	−0.59	0.94	<0.01
	f_h				ns
	HR'$_{trough}$	14. 8	−0.091	0.957	<0.001
	HR'$_{peak}$	−1.3	0.14	0.961	<0.001
	fh/f_{resp}	2.9	1.16	0.96	<0.001
	HR'$_{trough}/f_{resp}$	4.1	0.98	0.94	<0.01
	HR'$_{peak}/f_{resp}$	0.8	1.43	0.98	<0.001

Notes: Linear regression Y=a + b·X, where Y is the HR'$_{peak}$-HR'$_{through}$ difference (ΔHR'), b is the slope of the linear function, and a is the intercept of the linear function. *r*: Correlation coefficient. *p*: Probability of the null hypothesis (i.e., no correlation at the level indicated) to be correct. f_{resp}: Breathing frequency (breaths/min). fh: Heart rate (beats/min). f_h/f_{resp}: Breathing-specific heart rate (beats/breath). ns: Not significant (p>0.05). Critical value *r* for two-tail test=0.754).

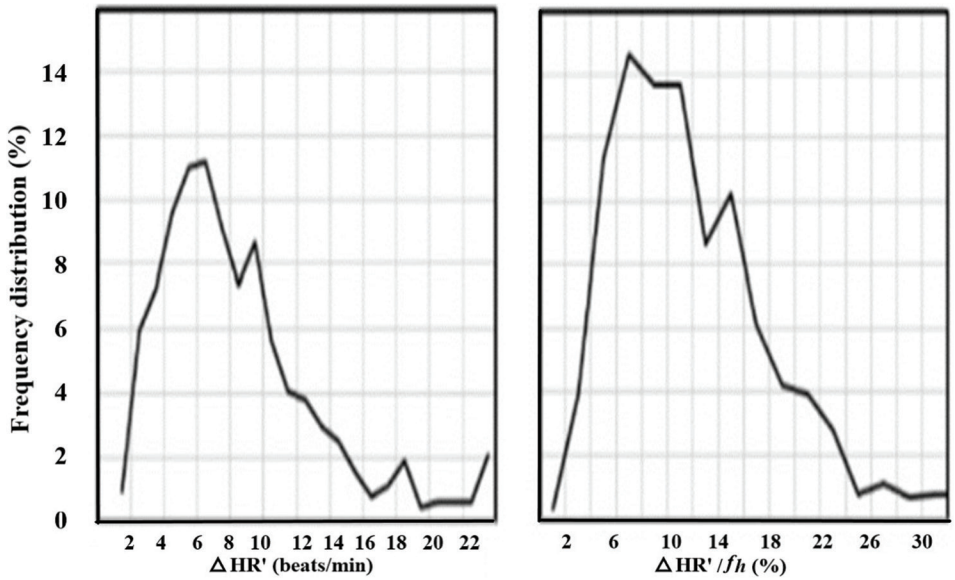

Figure 2. Frequency distribution of respiratory sinus arrhythmia in the entire sample, expressed as ΔHR' (HR'*peak* - HR'*trough*, beats/min; left panel) and as a percentage of the mean heart rate (ΔHR'/f_h, %; right panel)

(males, females, and combined), ΔHR' showed strong negative correlations with f_{resp} (Figure 3), with correlation coefficients ranging from 0.94 to 0.97. On the contrary, the relationships between f_h and ΔHR' exhibited lower correlation coefficients, with the correlation being non-significant in females.

3.2.3. Peak and trough of instantaneous HR

Both HR'_{peak} and HR'_{trough} were significantly correlated with ΔHR' in the combined group, with HR'_{peak} showing an almost perfect linear correlation (r = 0.996, Figure 4). However, HR'_{trough} showed lower correlation coefficients in females and in the combined group, and did not reach statistical significance in males.

3.2.4. Breathing-specific HR

The ratio between f_h and f_{resp} showed a very strong correlation with ΔHR' in all three groups of subjects. The correlations between HR'_{peak}/f_{resp} and ΔHR' were even stronger, with correlation coefficients ranging from 0.95 to 0.98 (Table 2). An almost perfect positive correlation was obtained by fitting a logarithmic function to the data: $\Delta HR' = 7.54 \ln (HR'_{peak}/f_{resp}) - 4.10$, which resulted in a correlation coefficient of 0.9992 (Figure 5).

4. Discussion

The primary goal of the this analysis is to test the hypothesis that RSA is strongly correlated with f_h/f_{resp}. The large dataset used in this study helped minimize the confounding effects of the inter-subject variability,

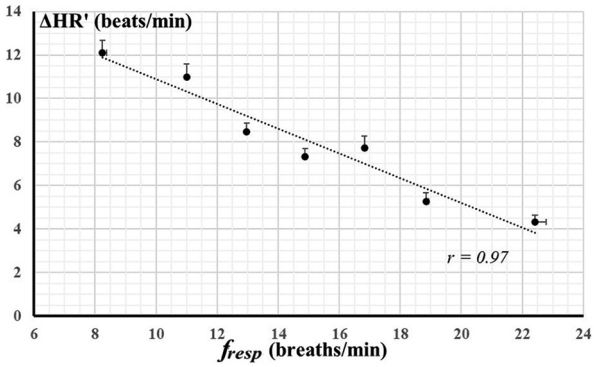

Figure 3. Relationship between breathing frequency (f_{resp}, breaths/min) and ΔHR' (HR'*peak*-HR'*trough*, beats/min). Data were grouped into bins, with symbols representing the average value of each bin. Bars show bidirectional standard errors (where not visible, they fall within the symbol size). The oblique dotted line represents the best-fit linear regression through the data points
Note: *r*: Correlation coefficient

allowing us to construct statistically meaningful functions. The results demonstrated an excellent correlation between f_h/f_{resp} and ΔHR', supporting the concept that RSA may be a mechanism to improve pulmonary gas exchange.

4.1. RSA variability

The average ΔHR' of the group was 8.6 ± 0.3 bpm (approximately 12.5% of the resting f_h), with considerable inter-individual variability that was not correlated with anthropometric traits or gender. A similar ΔHR' (~10 bpm) emerged from an earlier study by Hirsch and Bishop.[4] No

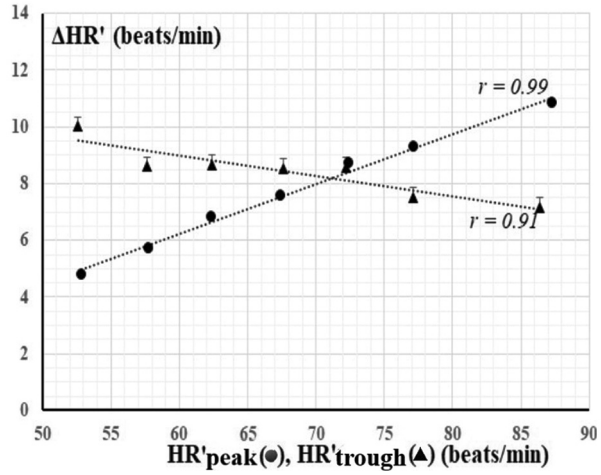

Figure 4. Relationship between the peak (HR'_{peak}, beats/min, circles) and the trough (HR'_{trough}, beats/min, triangles) of instantaneous heart rate and ΔHR' (HR'_{peak} - HR'_{trough}, beats/min). Data were grouped into bins, with symbols representing the average value of each bin. Bars show bidirectional standard errors (where not visible, they fall within the symbol size). The oblique dotted line represents the best-fit linear regression through the data points
Note: *r*: Correlation coefficient

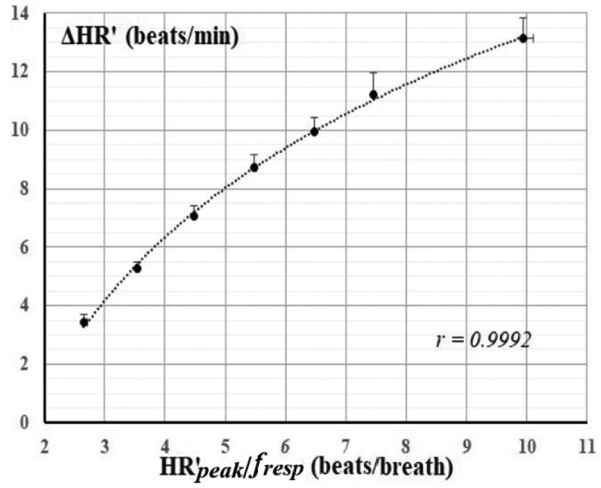

Figure 5. Relationship between the breathing-specific heart rate (HR'_{peak}/f_{resp}, beats/breath) and ΔHR' (HR'_{peak} - HR'_{trough}, beats/min). Data were grouped into bins, with symbols representing the average value of each bin. Bars show bidirectional standard errors (where not visible, they fall within the symbol size). The dotted line represents the best-fit logarithmic function through the data points
Note: *r*: Correlation coefficient

significant difference was observed in f_h or ΔHR' between males and females, likely because the consistently higher f_h observed in women typically becomes more pronounced at ages older than those of the subjects in this study.[45-47] The CV for RSA (whether expressed as ΔHR' or as ΔHR'/f_h) was approximately 60%, which is about four times larger than that for mean f_h, HR'_{peak} or HR'_{trough} because the average values (the denominator in the CV computation) were four times smaller (Table 1).

The variability in ΔHR' could have been lower if the inter-individual differences in HR'_{peak} and HR'_{trough} were of similar magnitude, but this was not the case. In fact, the correlation between ΔHR' and HR'_{peak} (i.e., when parasympathetic control is absent) was stronger than that with HR'_{trough} (Figure 4), where no significant correlation was found in males. Since cardiac vagal output is inhibited at end-inspiration, it seems reasonable to conclude that the inter-subject variability in RSA is largely driven by the inter-subject variability in the sympathetic regulation of f_h. The stronger correlation between ΔHR' with HR'_{peak} compared to HR'_{trough} suggests that sympathetic output plays a more significant role in modulating the magnitude of RSA than the parasympathetic output. This finding indicates that RSA cannot be equated with "vagal tone." Further complicating the relationship between RSA and vagal tone is the fact that RSA also depends on f_{resp}, which is not regulated by the parasympathetic nervous system. Previous studies have raised concerns about the validity of interpreting RSA as an indicator of vagal tone.[8,19,35-37]

Comparing human RSA (approximately 12% of the resting f_h) to RSA in other species to explore potential relationships with species-specific f_h[48] could be informative. However, direct measurements of ΔHR' in other species are rare. Available data from small groups of dogs, horses, cows, and sheep suggest that RSA can range from 1.4% of their resting f_h in cows to 40% in dogs,[16,17] with no evidence of any allometric pattern.

4.2. Correlations

The large dataset allowed for the construction of X-Y functions that were comparable across subjects, due to the consistent number of bins and the considerable number of subjects per bin. By minimizing the noise of the inter-subject variability, we were able to reveal clear X-Y patterns, as evidenced by the very high correlation coefficients. While a strong correlation, though not definitive, can suggest a causal relationship, a lack of correlation raises doubts about the existence of a mechanistic link between the variables.

The clear inverse relationship between f_{resp} and ΔHR' (Figure 3) has been well documented in previous studies;[4,22,23,49] however, no physiological explanations have been proposed. Here, we found that this relationship became stronger when f_{resp} was coupled with HR', and even more so when coupled with HR'_{peak}. In fact, the higher the f_{resp} relative to HR'_{peak}, the smaller the ΔHR' (Figure 5), with an exceptionally strong correlation (r = 0.995). Previous

studies in dogs[9] found a weaker f_{resp}/f_h-ΔHR' relationship, likely due to the small sample size and large data variability.

What could explain the physiological mechanism behind the f_{resp}/f_h-ΔHR' correlation? If RSA is indeed a mechanism to improve pulmonary gas exchange, it is reasonable to expect that f_{resp} and f_h would combine to optimize RSA. In paralyzed dogs ventilated by phrenic nerve stimulation (diaphragm pacing) to maintain constant ventilation, Hayano and Yasuma[18,19] manipulated f_h to either remain constant or synchronize with lung inflation or deflation. These experimental conditions were designed to simulate, respectively, the absence of RSA, physiological RSA, or "reversed" RSA. The authors found that blood gases were optimal when f_h was increased during the inflation phase of the breathing cycle. From these experiments on anesthetized dogs, the authors proposed that the function of RSA was to improve ventilation-perfusion matching by adjusting f_h to the inspiratory airflow. The present finding of a tight f_h/f_{resp}-ΔHR' relationship (Figure 5) extends this concept to healthy humans, supporting Hayano and Yasuma's conclusions about RSA.[18,19] To appreciate the significance of the f_h/f_{resp}-ΔHR' relationship, we must consider the fundamental differences between pulmonary air and blood flow.

At rest, cardiac output and pulmonary ventilation in adult humans are approximately equal, about 5 L/min. However, the cardiovascular and respiratory systems are designed differently, which leads to contrasting flow regimes. The parallel arrangement of the chest wall and lungs, along with the presence of a dead space, implies that pulmonary ventilation must have a tidal volume at least as large as the dead space, resulting in a relatively lower f_{resp}. Furthermore, the back-and-forth movement of air through the tracheobronchial tree causes airflow to be highly intermittent: It is zero at the start of inspiration, peaks mid-inspiration, and returns to zero again at end-inspiration when the air changes direction for the expiration. In contrast, the cardiac pump is positioned in series with the circulatory system, allowing for high f_h with small stroke volumes and unidirectional blood flow with minimal oscillation. Although airflow is inherently intermittent, the higher the f_{resp}, the less intermittent the airflow becomes in relation to blood flow. The f_h/f_{resp} (also known as the ratio between HR'_{peak} to f_{resp}) can be seen as a proxy for the difference between cardiac flow and airflow. A higher ratio implies greater disparity between the two flows, suggesting a higher demand for RSA. Conversely, a lower f_h/f_{resp} value may indicate less disparity between the two flows and a lower need for RSA. The slightly better fit of the logarithmic function compared to the linear function (Figure 5) can be explained by the fact that as f_{resp} increases, the number of heartbeats per breath decreases. Hypothetically, if a subject's f_{resp} matched their f_h, the HR'_{peak}/f_{resp} would be equal to one, and ΔHR' would be zero.

The observed stronger correlation (Figure 5) when f_h was represented by its peak (HR'_{peak}) rather than its trough or mean values supported our hypothesis. HR'_{peak} is not influenced by parasympathetic regulation of f_h, which, when present, introduces variability to both f_h and HR'_{trough}.

The average f_h/f_{resp} was approximately 5 beats/min (Table 1), which is within the range observed in many mammals. In fact, the allometric functions of f_h and f_{resp} in terrestrial mammals, spanning body weights from a few grams to several tons, show similar slopes and a ratio of about 4 beats/breath.[48] This could suggest that 4 beats/breath (which, with an average RSA of 20%, corresponds to a 2.4:1.6 distribution of beats between inspiration and expiration) represents an optimal compromise for coordinating the two convection systems — the ventilatory and the cardiovascular — and for maximizing pulmonary gas exchange efficiency.

The results of this study clearly indicate that the larger the mismatch between f_h and f_{resp} (i.e., the greater f_h/f_{resp}), the greater the RSA. This finding supports the hypothesis that RSA may function to improve gas exchange. A large RSA means that heartbeats predominantly occur during inspiration, keeping the blood flow high when the oxygen content of air is highest. However, many subjects at rest do not exhibit a large RSA, and some have a small RSA. Does this put them at a disadvantage? From the perspective of gas exchange, probably yes, but extra-pulmonary factors may require a more even distribution of heartbeats than a large RSA would allow. For example, excessive arrhythmia and the resultant irregular blood flow may not be desirable during muscle exercise, when a more even delivery of oxygen may take precedence over-optimizing pulmonary gas exchange. It would be valuable to compare RSA between resting and exercise conditions in individuals with very different resting RSA values. One could predict that RSA might decrease during exercise, particularly in subjects with high RSA at rest.

5. Conclusion

The breath-by-breath data on ΔHR' from a large sample revealed that the inspiratory-expiratory difference averaged approximately 8 beats/min or about 12% of the mean f_h. Variability in sympathetic control was a significant contributor to the inter-individual variability in RSA. Consequently, RSA should not be interpreted as an index of parasympathetic control (or "vagal tone"), particularly considering that f_{resp} is a key determinant of RSA. Most importantly, f_h/f_{resp} showed an excellent correlation with

ΔHR', supporting the hypothesis that RSA serves as a mechanism to mitigate the mismatch between the flow regimes of air and blood, thereby improving ventilation-perfusion matching.

Acknowledgments

None.

Funding

None.

Conflict of interest

The author declares no competing interests in this article.

Author contributions

This is a single-authored article.

Ethics approval and consent to participate

Each of the studies contributing data to the present analysis adhered to the standards set by the Declaration of Helsinki, and the procedures were approved by the local ethics committee. In addition, the subjects were informed about the measurements to be taken and the study protocols, and they provided written informed consent.

Consent for publication

Consent was obtained from the participants to publish their data.

Availability of data

Data used for the present analysis are available from the author.

References

1. Ludwig C. The influences of respiratory movements on blood flow in the aorta (Beiträge zur kenntniss des einflusses der respirationbewegungen auf den blutlauf im Aortensysteme). *Arch. Anat. Physiol.* 1847;13:242-302.
2. Anrep GV, Pascual W, Rössler R. Respiratory variations of the heart rate. I. The reflex mechanisms of the respiratory arrhythmia. *Proc R Soc Lond B Biol Sci.* 1936;119:191-217.
3. Anrep GV, Pascual W, Rössler R. Respiratory variations of the heart rate. II. The central mechanism of the respiratory arrhythmia and the inter-relations between the central and the reflex mechanisms. *Proc R Soc Lond B Biol Sci.* 1936;119:218-232.
4. Hirsch JA, Bishop B. Respiratory sinus arrhythmia in humans: How breathing pattern modulates heart rate. *Am J Physiol.* 1981;241:H620-H629.

   doi: 10.1152/ajpheart.1981.241.4.H620
5. Daly MDB. Interactions between respiration and circulation. In: Cherniak NS, Widdicombe JG, editors. *Handbook of Physiology*, *The Respiratory System*. Vol. 2., Ch. 16. Control of Breathing Part 2. Bethesda (MD): Williams & Wilkins; 1986. p. 529-594.
6. Taha BH, Simon PM, Dempsey JA, Skatrud JB, Iber C. Respiratory sinus arrhythmia in humans: An obligatory role for vagal feedback from the lungs. *J Appl Physiol* (1985). 1995;78:638-645.

   doi: 10.1152/jappl.1995.78.2.638
7. Schäfer C, Rosenblum MG, Kurths J, Abel HH. Heartbeat synchronized with ventilation. *Nature*. 1998;392:239-240.

   doi: 10.1038/32567
8. Farmer DGS, Dutschmann M, Paton JFR, Pickering AE, McAllen RM. Brainstem sources of cardiac vagal tone and respiratory sinus arrhythmia. *J Physiol.* 2016;594:7249-7265.

   doi: 10.1113/JP273164
9. Grosso G, Vezzosi T, Briganti A, Di Franco C, Tognetti R, Mortola JP. Breath-by-breath analysis of respiratory sinus arrhythmia in dogs. *Respir Physiol Neurobiol.* 2021;294:103776.

   doi: 10.1016/j.resp.2021.103776
10. Larsen PD, Tzeng YC, Sin PYW, Galletly DC. Respiratory sinus arrhythmia in conscious humans during spontaneous respiration. *Respir Physiol Neurobiol.* 2010;174:111-118.

    doi: 10.1016/j.resp.2010.04.021
11. Tzeng YC, Sin PYW, Galletly DC. Human sinus arrhythmia: Inconsistencies of a teleological hypothesis. *Am J Physiol Heart Circ Physiol.* 2009;296:H65-H70.

    doi: 10.1152/ajpheart.00716.2008
12. Sin PYW, Webber MR, Galletly DC, *et al*. Interaction between heart rate variability and pulmonary gas exchange in humans. *Exp Physiol.* 2010;95:788-797.

    doi: 10.1113/expphysiol.2010.052910
13. Ben-Tal A, Shamailov SS, Paton JFR. Evaluating the physiological significance of respiratory sinus arrhythmia: Looking beyond ventilation-perfusion efficiency. *J Physiol.* 2012;590:1989-2008.

    doi: 10.1113/jphysiol.2011.222422
14. Uechi M, Asai K, Osaka M, *et al*. Depressed heart rate variability and arterial baroreflex in conscious transgenic mice with overexpression of cardiac G_s^{α}. *Circ Res.* 1998;82:416-423.

    doi: 10.1161/01.res.82.4.416
15. Hashizume NS, Kitajima Y, Ide R, Nakamura E, Saiki C. Respiratory sinus arrhythmia in spontaneously breathing, unanesthetized newborn and adult Wistar rats. *Respir Physiol Neurobiol.* 2024;321:104207.

doi: 10.1016/j.resp.2023.104207

16. Piccione G, Giudice E, Giannetto C, Mortola JP. The magnitude of respiratory sinus arrhythmia of a large mammal (the horse) is like that of humans. *Respir Physiol Neurobiol.* 2019;259:170-172.

doi: 10.1016/j.resp.2018.09.006

17. Orsetti C, Vitale V, Mortola JP, Sgorbini M, Bonelli F. Respiratory sinus arrhythmia magnitude quantification as a potential marker of stress and pain in cows and sheep. *Vet Res Commun.* 2023;47:279-284.

doi: 10.1007/s11259-022-09922-7

18. Hayano J, Yasuma F, Okada A, Mukai S, Fujinami T. Respiratory sinus arrhythmia. A phenomenon improving pulmonary gas exchange and circulatory efficiency. *Circulation*. 1996;94:842-847.

doi: 10.1161/01.cir.94.4.842

19. Hayano J, Yasuma F. Hypothesis: Respiratory sinus arrhythmia is an intrinsic resting function of cardiopulmonary system. *Cardiovasc Res*. 2003;58:1-9.

doi: 10.1016/S0008-6363(02)00851-9

20. Giardino ND, Glenny RW, Borson S, Chan L. Respiratory sinus arrhythmia is associated with efficiency of pulmonary gas exchange in healthy humans. *Am J Physiol Heart Circ Physiol.* 2003;284:H1585-H1591.

doi: 10.1152/ajpheart.00893.2002

21. Yasuma F, Hayano JI. Respiratory sinus arrhythmia: Why does the heartbeat synchronize with respiratory rhythm? *Chest*. 2004;125:683-690.

doi: 10.1378/chest.125.2.683

22. Angelone A, Coulter NA Jr. Respiratory sinus arrhythmia: A frequency dependent phenomenon. *J Appl Physiol.* 1964;19:479-482.

doi: 10.1152/jappl.1964.19.3.479

23. Mortola JP, Marghescu D, Siegrist-Johnstone R. Respiratory sinus arrhythmia in young men and women at different chest wall configurations. *Clin Sci.* 2015;128:507-516.

doi: 10.1042éCS20140543

24. Malik M. Heart rate variability: Standards of measurement, physiological interpretation, and clinical use. Task Force of the European Society of Cardiology and the North American Society of Pacing and Electrophysiology. *Circulation*. 1996;93:1043-1065.

25. Barnett SR, Morin RJ, Kiely DK, *et al*. Effects of age and gender on autonomic control of blood pressure dynamics. *Hypertension*. 1999;33:1195-1200.

doi: 10.1161/01.HYP.33.5.1195

26. Grossman P, van Beek J, Wientjes C. A comparison of three quantification methods for estimation of respiratory sinus arrhythmia. *Psychophysiol.* 1990;27:702-714.

doi: 10.1111/j.1469-8986.1990.tb03198.x

27. Zhang J, Yu X, Xie D. Effects of mental tasks on the cardiorespiratory synchronization. *Respir Physiol Neurobiol.* 2010;170:91-95.

doi: 10.1016/j.resp.2009.11.003

28. Gilfriche P, Arsac LM, Daviaux Y, *et al*. Highly sensitive index of cardiac autonomic control based on time-varying respiration derived from ECG. *Am J Physiol Regul Integr Comp Physiol.* 2018;315:R469-R478.

doi: 10.1152/ajpregu.00057.2018

29. Mestanik M, Mestanikova A, Langer P, *et al*. Respiratory sinus arrhythmia - testing the method of choice for evaluation of cardiovagal regulation. *Respir Physiol Neurobiol.* 2019;259:86-92.

doi: 10.1016/j.resp.2018.08.002

30. Schechtman VL, Raetz SL, Harper RK, *et al*. Dynamic analysis of cardiac R-R intervals in normal infants and in infants who subsequently succumbed to the sudden infant death syndrome. *Pediatr Res.* 1992;31:606-612.

doi: 10.1203/00006450-199206000-00014

31. Fei L, Copie X, Malik M, Camm AJ. Short- and long-term assessment of heart rate variability for risk stratification after acute myocardial infarction. *Am J Cardiol.* 1996;77:681-684.

doi: 10.1016/s0002-9149(97)89199-0

32. Fei L, Keeling PJ, Sadoul N, *et al*. Decreased heart rate variability in patients with congestive heart failure and chronotropic incompetence. *Pacing Clin Electrophysiol.* 1996;19:477-483.

doi: 10.1111/j.1540-8159.1996.tb06519.x

33. La Rovere MT, Pinna GD, Maestri R, *et al*. Short-term heart rate variability strongly predicts sudden cardiac death in chronic heart failure patients. *Circulation*. 2003;107:565-570.

doi: 10.1161/01.CIR.0000047275.25795.17

34. Tonhajzerova I, Ondrejka I, Javorka M, *et al*. Respiratory sinus arrhythmia is reduced in adolescent major depressive disorder. *Eur J Med Res.* 2009;14 (Suppl 4):280-283.

doi: 10.1186/2047-783X-14-S4-280

35. Langewitz W, Rüddel H, Schächinger H, *et al*. Changes in sympathetic and parasympathetic cardiac activation during mental load: An assessment by spectral analysis of heart rate variability. *Homeost. Health Dis.* 1991;33:23-33.

36. Taylor JA, Myers CW, Halliwill JR, Seidel H, Eckberg DL. Sympathetic restraint of respiratory sinus arrhythmia: Implications for vagal-cardiac tone assessment in humans. *Am J Physiol Heart Circ Physiol.* 2001;280:H2804-H2814.

doi: 10.1152/ajpheart.2001.280.6.H2804

37. Brown SJ. Dissociation of respiratory sinus arrhythmia

and high frequency heart rate variability following exercise (English translation). *Med Sport*. 2010;14:43-49.

doi: 10.2478/v10036-010-0009-2

38. Mortola JP, Marghescu D, Siegrist-Johnstone R. Thinking about breathing: Effects on respiratory sinus arrhythmia. *Respir Physiol Neurobiol.* 2016;223:28-36.

doi: 10.1016/j.resp.2015.12.004

39. Mortola JP, Marghescu D, Siegrist-Johnstone R, Matthes E. Respiratory sinus arrhythmia during a mental attention task: The role of breathing-specific heart rate. *Respir Physiol Neurobiol.* 2020;272:103331.

doi: 10.1016/j.resp.2019.103331

40. Hanton G, Rabemampianina Y. The electrocardiogram of the Beagle dog: Reference values and effect of sex, genetic strain, body position and heart rate. *Lab Anim.* 2006;40:123-136.

doi: 10.1258/002367706776319088

41. Mortola JP, Marghescu D, Siegrist-Johnstone R. Respiratory sinus arrhythmia in the immediate post-exercise period: Correlation with breathing-specific heart rate. *Eur J Appl Physiol.* 2018;118:1397-1406.

doi: 10.1007/s00421-018-3871-6

42. Konno K, Mead J. Measurement of the separate volume changes of rib cage and abdomen during breathing. *J Appl Physiol.* 1967;22:407-422.

doi: 10.1152/jappl.1967.22.3.407

43. Mead J, Peterson N, Grimby G, Mead J. Pulmonary ventilation measured from body surface movements. *Science*. 1967;156:1383-1384.

doi: 10.1126/science.156.3780.1383

44. Mortola JP, Anch AM. Chest wall configuration in supine man; wakefulness and sleep. *Respir Physiol.* 1978;35:201-213.

doi: 10.1016/0034-5687(78)90022-1

45. Smetana P, Malik M. Sex differences in cardiac autonomic regulation and in repolarization electrocardiography. *Pflugers Arch Eur J Physiol.* 2013;465:699-717.

doi: 10.1007/s00424-013-1228-x

46. Quer G, Gouda P, Galarnyk M, Topol EJ, Steinhubl SR. Inter- and intraindividual variability in daily resting heart rate and its associations with age, sex, sleep, BMI, and time of year: Retrospective, longitudinal cohort study of 92,457 adults. *PLoS One*. 2020;15:0227709.

doi: 10.1371/journal.pone.0227709

47. Goorakani Y, Rahimabadi MS, Dehghan A, *et al*. Correlation of resting heart rate with anthropometric factors and serum biomarkers in a population-based study: Fasa PERSIAN cohort study. *BMC Cardiovasc Dis*. 2020;20:319-328.

doi: 10.1186/s12872-020-01594-y

48. Mortola JP. The heart rate - breathing rate relationship in aquatic mammals: A comparative analysis with terrestrial species. *Curr Zool.* 2015;61:569-577.

doi: 10.1093/czoolo/61.4.569

49. Davis CTM, Neilson JMM. Sinus arrhythmia in man at rest. *J Appl Physiol.* 1967;22:947-955.

doi: 10.1152/jappl.1967.22.5.947

ACCSCIENCE PUBLISHING

Brain & Heart

CASE REPORT

Acute coronary syndrome or cardiac involvement due to leptospirosis: A case report

Ayşe Sağmak Tartar[1]*, Mehmet Ali Aşan[1], Murat Harman[2], and Türkkan Öztürk Kaygusuz[1]

[1]Department of Infectious Diseases and Clinical Microbiology, Faculty of Medicine, Firat University, Elazig, Turkey

[2]Department of Cardiology, Faculty of Medicine, Firat University, Elazig, Turkey

Abstract

Leptospirosis is a globally prevalent zoonotic infection. Cardiac involvement in leptospirosis, including myocarditis, can be easily missed due to non-specific symptoms and concurrent multiorgan dysfunction. A 46-year-old male presented to the emergency department with weakness, fever, palpitations, and widespread joint and muscle pain. His temperature was 40°C, and his blood pressure dropped to 50/30 mm Hg. The patient, with elevated high-sensitivity troponin levels in laboratory findings, was referred to the cardiology department. Anti-ischemic treatment was started for a preliminary diagnosis of acute coronary syndrome. The leptospirosis polymerase chain reaction (PCR) test in serum was positive, whereas the urine *Leptospira* PCR test was negative. The patient presented with septic shock and elevated cardiac biomarkers and was re-evaluated based on electrocardiogram and echocardiogram findings. Considering these clinical and laboratory results, acute coronary syndrome was ruled out, and myocardial involvement due to leptospirosis was considered. This case highlights the importance of recognizing cardiac involvement in leptospirosis.

Keywords: Leptospirosis; Zoonotic infection; Myocarditis

***Corresponding author:**
Ayşe Sağmak Tartar
(dr.ayse01@gmail.com)

Citation: Tartar AS, Aşan MA, Harman M, Kaygusuz TO. Acute coronary syndrome or cardiac involvement due to leptospirosis: A case report. *Brain & Heart.* 2024;2(4):3496. doi: 10.36922/bh.3496

Received: April 24, 2024

Accepted: July 29, 2024

Published Online: October 8, 2024

1. Background

Leptospirosis is a globally prevalent zoonotic infection. Severe leptospirosis is characterized by multiorgan dysfunction involving the liver, kidneys, lungs, and heart.[1,2] Cardiac involvement in leptospirosis, including myocarditis, is sometimes overlooked owing to its non-specific symptoms and the presence of multiorgan dysfunction. Accurate diagnosis of cardiac involvement in leptospirosis requires a high level of clinical suspicion, as fatal outcomes may often be linked to myocarditis.

Mathew *et al.*[3] examined cardiac findings and biomarker levels in 113 severe patients with leptospirosis requiring intensive care and compared them with 31 patients with sepsis. They found similar electrocardiographic (EKG) abnormalities and myocardial dysfunction levels (51% – 55%) in both groups. However, patients with leptospirosis exhibited higher troponin-T levels (61.0% vs. 40.0%, $p = 0.057$). Elevations in the ST-segment and troponin levels were identified as independent predictors of reduced left ventricular (LV) ejection fraction in leptospirosis.

In a series of five patients with cardiac involvement reported by Jayathilaka *et al*.,[4] all experienced hypotensive shock and acute kidney injury. Four out of the five patients received positive inotropic support. One patient exhibited EKG findings suggestive of myocarditis during shock, whereas an echocardiogram (ECHO) confirmed myocarditis in another case. All five patients exhibited a positive cardiac troponin I titer, either low or high, and eventually recovered from the illness.

In another study by Shah *et al*.,[5] autopsies of 24 patients who died from leptospirosis revealed myocarditis in 96% of the patients. Endocardial inflammation was observed in 50% of these patients and was associated with vasculitis.

Cardiac involvement in leptospirosis is thought to be due to a glycoprotein component of the leptospiral cell wall that inhibits Na–K ATPase, causing arrhythmias and vasculitis.[5,6]

Elevated creatine kinase-myocardial band (CK-MB) and troponin levels are found in nearly half of leptospirosis cases, but their importance in predicting cardiac involvement is unclear.[7,8]

Further investigations are needed to confirm cardiac involvement. In cases of leptospirosis with cardiac involvement, non-specific EKG changes such as conduction disorders, ST-T changes, and atrial arrhythmias are often observed.[9] However, very few cases report an absence of EKG changes despite cardiac involvement.[9] Although cardiac involvement has been frequently reported in the literature, our case, which was initially considered to have cardiac involvement, showed elevated creatine kinase (CK), CK-MB, and high-sensitivity troponin I (HSTI) levels but no EKG changes.

This rare condition, often overlooked owing to its broad clinical presentation and lack of distinctive symptoms, is highlighted in our case. We present a case that was initially managed as an acute coronary syndrome but later re-evaluated as cardiac involvement due to leptospirosis based on serum polymerase chain reaction (PCR) results.

2. Case presentation

A 46-year-old male with no known chronic conditions arrived at our hospital's emergency department with symptoms of weakness, fever, palpitations, and widespread muscle and joint pain. He had previously visited the emergency department twice in the past 4 days for similar issues and was diagnosed with an upper respiratory tract infection and prescribed amoxicillin-clavulanate. At the time of this presentation, he had a fever of 40°C and a blood pressure of 50/30 mm Hg. His overall condition was poor, with drowsiness but responsiveness. Physical examination revealed mild oropharyngeal erythema and diffuse abdominal tenderness but no guarding or rebound tenderness.

His epidemiological history revealed that he worked in livestock farming but had no history of animal or arthropod bites. He was admitted to the internal intensive care unit, and blood and urine cultures were taken. Empirical treatment with meropenem was started. Testing included serology for *Brucella*, hepatitis, and human immunodeficiency virus; serology and PCR testing for Crimean-Congo hemorrhagic fever virus; and PCR testing for leptospirosis in urine and serum. A peripheral blood smear was conducted to rule out acute hematological malignancy, and a consultation with the hematology department was requested.

Laboratory results indicated elevated HSTI levels (normal range, 0 – 58 ng/L), prompting a cardiology consultation. A 12-lead EKG performed at the bedside in the intensive care unit showed no significant ST-segment changes, T-wave abnormalities, or other pathological findings (Figures 1A and B). His heart rate was recorded at 92 beats/min. Bedside transthoracic ECHO revealed hypokinesia in the anteroseptal wall of the left ventricle (Figures 2A and B). The cardiac valves appeared normal, with no significant stenosis, regurgitation, vegetation, or intracardiac thrombus. Anti-ischemic treatment was started based on a preliminary diagnosis of acute coronary syndrome, and inotropic support was provided for the patient's hypotension. The patient was closely monitored for further differential diagnoses.

On the 8th day of intensive care unit admission, the patient's condition improved and he was transferred to the infectious diseases ward for continued treatment. On the 11th day of treatment, PCR analysis of the serum sample confirmed the presence of *Leptospira*, confirming the diagnosis of leptospirosis. The urine *Leptospira* PCR test was negative. Given the patient's initial signs of septic shock, severe hypotension, and elevated cardiac biomarkers, and with the re-evaluation of EKG and ECHO findings, we reconsidered the diagnosis of acute coronary syndrome. Instead, based on the clinical and laboratory findings, we suspected myocardial involvement (myocarditis) due to leptospirosis.

The patient completed 14 days of inpatient treatment and was discharged in good health with follow-up recommendations for infectious diseases and cardiology clinics. Laboratory test results from admission and subsequent days are summarized in Table 1.

3. Discussion

Leptospirosis is a contagious disease that affects both animals and humans and is the most common zoonotic

Table 1. Various laboratory parameters observed during the patient's admission and follow-up

	Application day	3rd day	7th day	14th day
WBC (mm³)	1600	6770	11210	7580
Hemoglobin	14.3	13.8	13	13
Neutrophil	65	74	73	75
Platelet (mm³)	95	43	110	254
Aspartate aminotransferase (U/L)	89	98	61	44
Alanine aminotransferase (U/L)	28	68	63	46
Total bilirubin (mg/dL)	1.47	1.16	0.9	1.1
Alkalen fosfataz (U/L)	38	59	49	59
Gama glutamil transferaz (U/L)	13	37	54	39
Creatine kinase (U/L)	4555	1162	292	61
Creatine kinase-MB (U/L)	68	46	12	24
Troponin (ng/mL)	6415	549	6	6
Urea	112	65	58	41
Creatinine	2.14	0.95	0.7	0.57
C-reaktive protein (mg/l)	194	31	20	7
Procalcitonin (ng/mL)	100	4.6	0.7	0.2
Erythrocyte sedimentation rate (mm/h)	18	19	13	36
Urine leukocyte	6	1	8	2
Urine protein	+	++	-	-

Abbreviation: WBC: White blood cell.

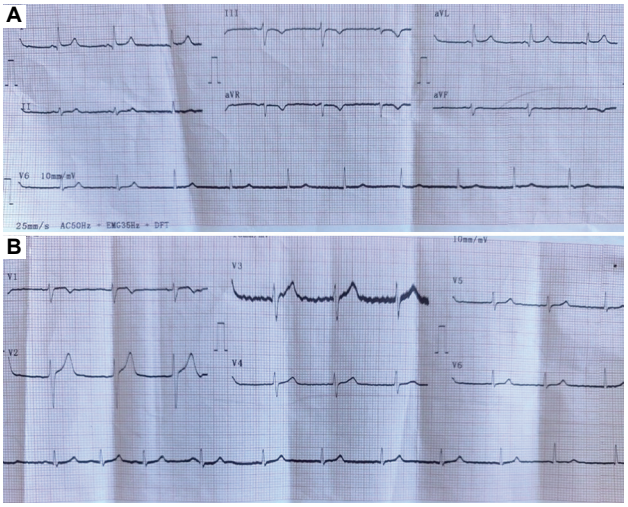

Figure 1. Electrocardiogram image of the patient. (A) Extremity derivations (limb leads). (B) Chest leads (precordial leads).

infection worldwide.[1-3] It is caused by a motile, obligate aerobic, non-spore-forming, and non-capsulated microorganism.[10]

Leptospirosis is estimated to cause one million cases and 58,900 deaths annually, with a case fatality rate of 6.85%.[11] Although its overall incidence has remained stable worldwide, major outbreaks often occur after floods and natural disasters.[11]

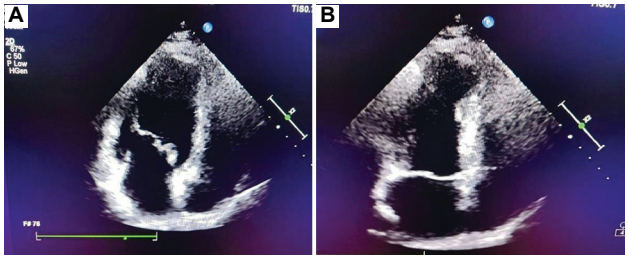

Figure 2. Echocardiogram image of the patient (A) Apical four-chamber view (left ventricular [LV] diastole). (B) Apical four-chamber view (LV systole).

Urban outbreaks are frequent in areas with poor hygiene and high rodent populations.[12] Leptospirosis predominantly affects economically disadvantaged groups and results in significant morbidity and mortality (5% – 15%).[11,13]

Leptospirosis is typically transmitted through direct contact with infected animal urine or exposure to soil or water contaminated with this urine.[14] High-risk individuals include farmers, those who work closely with animals, those exposed to rodents, those living in areas with poor sanitation, and individuals engaged in water sports.[11,13]

The incubation period for leptospirosis is 2 – 20 days, with an average of 7 – 12 days. Some patients experience a biphasic course of the disease: An initial acute or septicemic phase lasting about a week, followed by an immune phase

characterized by antibody production and the excretion of leptospires in the urine.[15] During the leptospiremic phase, the pathogen can be isolated from the blood and cerebrospinal fluid (CSF). Conversely, in the immune phase, it cannot be isolated from the blood or CSF owing to the presence of IgM-type antibodies, but it can still be isolated from the kidneys, urine, and aqueous humor.

Leptospirosis can manifest in two clinical forms: icteric or anicteric. The anicteric form typically begins with a sudden onset of fever and may include symptoms such as chills, myalgia, abdominal pain, conjunctivitis, and occasionally, a skin rash. Severe headaches and aseptic meningitis can also occur. This form is usually self-limiting and accounts for about 90% of cases. In contrast, the icteric form can range from severe illness with multiorgan dysfunction to a life-threatening condition.[1,2,16]

Cardiac involvement in leptospirosis may cause symptoms such as shortness of breath, chest pain, palpitations, tachycardia, hypotension, EKG abnormalities, arrhythmias, ST/T changes, conduction abnormalities, and ECHO wall motion abnormalities. Furthermore, it can lead to conditions such as endocarditis, myocarditis, pericarditis, and cardiogenic shock. EKG or clinical evidence of cardiac involvement is often associated with a poor prognosis.[17]

In our case, the patient presented with hypotension that was managed with inotropic support while in septic shock. After 48 h of monitoring in the intensive care unit, liver dysfunction also emerged. The patient did not show clear EKG abnormalities, but laboratory tests revealed elevated levels of cardiac biomarkers, including troponin, CK, CK-MB, and HSTI. ECHO revealed hypokinesia in the anteroseptal wall of the left ventricle. Although the initial cardiological assessment suggested acute coronary syndrome, clinical follow-up and a positive *Leptospira* PCR result confirmed myocardial involvement due to leptospirosis. In the literature, myocardial involvement has been documented through case studies and case series.[17,18]

LV dysfunction is usually not detected in clinical follow-ups of leptospirosis, leading to frequent oversight of cardiac involvement.[18] In our case, ECHO revealed hypokinesia in the LV anteroseptal wall, and elevated CK, CK-MB, and HSTI levels were supportive of myocardial involvement in leptospirosis.

Myocarditis is a fatal condition. Patients showing clinical and laboratory findings suggestive of cardiac involvement in leptospirosis should be evaluated for myocarditis using imaging techniques such as ECHO and cardiac magnetic resonance imaging.

The diagnosis is confirmed by a positive PCR result of blood or urine or by a positive serology result. Rarely, a diagnosis is made by a positive culture of blood or urine. Negative test results do not rule out the diagnosis because of the suboptimal sensitivity of leptospirosis tests. Molecular tests, such as PCR, offer a rapid and accurate diagnosis, especially in the early stages of illness (i.e., the 1st week).[19] A single positive PCR result is diagnostic for leptospirosis. Although the organism may be intermittently detected in urine during the 1st week of illness, it is more reliably identified after that period.[20] PCR tests typically have a sensitivity of 40% – 60% and a specificity above 95% in blood samples.[19]

4. Conclusion

Leptospirosis is a relatively underdiagnosed infectious disease, despite its frequent occurrence, and cardiac involvement is even less frequently reported. This could be due to insufficient documentation of the frequency and extent of cardiac involvement in leptospirosis. Diagnostic challenges arise when clinical symptoms suggest cardiac involvement, particularly in patients with a septic presentation where no clear source of infection is found. A comprehensive epidemiological history is essential in these cases. This case highlights the importance of recognizing cardiac involvement in leptospirosis.

Acknowledgments

None.

Funding

None.

Conflict of interest

The authors declare they have no competing interests.

Author contributions

Conceptualization: Ayşe Sağmak Tartar, Mehmet Ali Aşan
Investigation: Ayşe Sağmak Tartar, Mehmet Ali Aşan, Murat Harman
Writing–original draft: Ayşe Sağmak Tartar, Mehmet Ali Aşan, Murat Harman
Writing–review & editing: Ayşe Sağmak Tartar, Türkkan Öztürk Kaygusuz

Ethics approval and consent to participate

Consent was obtained from the patient.

Consent for publication

Consent was obtained from the patient.

Availability of data

Not applicable.

References

1. Wang S, Stobart Gallagher MA, Dunn N. Leptospirosis. In: *StatPearls*. Treasure Island, FL: StatPearls Publishing; 2022.
2. Haake DA, Levett PN. Leptospirosis in humans. *Curr Top Microbiol Immunol*. 2015;387:65-97.
   doi: 10.1007/978-3-662-45059-8_5
3. Mathew A, Shanks M, Punnoose E, *et al*. Cardiac involvement in critically ill patients with leptospirosis: A prospective study using myocardial deformation imaging. *Eur Heart J Acute Cardiovasc Care*. 2020;9(8):975-983.
   doi: 10.1177/2048872618809319
4. Jayathilaka PGNS, Mendis ASV, Perera MHMTS, Damsiri HMT, Gunaratne AVC, Agampodi SB. An outbreak of leptospirosis with predominant cardiac involvement: A case series. *BMC Infect Dis*. 2019;19(1):265.
   doi: 10.1186/s12879-019-3905-7
5. Shah K, Amonkar GP, Kamat RN, Deshpande JR. Cardiac findings in leptospirosis. *J Clin Pathol*. 2010;63(2):119-123.
   doi: 10.1136/jcp.2009.069575
6. Swarath S, Maharaj N, Seecheran R, *et al*. Leptospirosis-ınduced myocarditis and arrhythmias. *J Investig Med High Impact Case Rep*. 2023;11.
   doi: 10.1177/23247096231179450
7. Mehdaoui H, Caffiot E, Theodose R, *et al*. Characteristics of leptospirosis patients admitted to a tropical university hospital during the 2000 to 2010 period. *Crit Care*. 2012;16(Suppl 1):P40.
   doi: 10.1186/cc10647
8. Machado ES, Feres JG, Feijó LA, Andrade J, Nogueira SA. Is CK-MB isoenzyme useful for diagnosis of cardiac involvement in icteric leptospirosis? *Rev Inst Med Trop Sao Paulo*. 1995;37(5):461-465.
   doi: 10.1590/s0036-46651995000500013
9. Lashkarbolouk N, Mazandarani M. Leptospirosis in a patient with cardiac manifestation: A case report study and literature review. *Clin Case Rep*. 2024;12(5):e8883.
   doi: 10.1002/ccr3.8883
10. Guerra MA. Leptospirosis. *J Am Vet Med Assoc*. 2009;234(4):472-430.
    doi: 10.2460/javma.234.4.472
11. Costa F, Hagan JE, Calcagno J, *et al*. Global morbidity and mortality of leptospirosis: A systematic review. *PLoS Negl Trop Dis*. 2015;9(9):e0003898.
    doi: 10.1371/journal.pntd.0003898
12. Felzemburgh RD, Ribeiro GS, Costa F, *et al*. Prospective study of leptospirosis transmission in an urban slum community: Role of poor environment in repeated exposures to the *Leptospira* agent. *PLoS Negl Trop Dis*. 2014;8(5):e2927.
    doi: 10.1371/journal.pntd.0002927
13. Agampodi SB, Karunarathna D, Jayathilala N, Rathnayaka H, Agampodi TC, Karunanayaka L. Outbreak of leptospirosis after white-water rafting: Sign of a shift from rural to recreational leptospirosis in Sri Lanka? *Epidemiol Infect*. 2014;142(4):843-846.
    doi: 10.1017/S0950268813001465
14. Lokida D, Budiman A, Pawitro UE, *et al*. Case report: Weil's disease with multiple organ failure in a child living in dengue endemic area. *BMC Res Notes*. 2016;9(1):407.
    doi: 10.1186/s13104-016-2210-4
15. Rajapakse S. Leptospirosis: Clinical aspects. *Clin Med* (*Lond*). 2022;22(1):14-17.
    doi: 10.7861/clinmed.2021-0784
16. Adler B, de la Peña Moctezuma A. *Leptospira* and leptospirosis. *Vet Microbiol*. 2010;140(3-4):287-296.
    doi: 10.1016/j.vetmic.2009.03.012
17. Pushpakumara J, Prasath T, Samarajiwa G, Priyadarshani S, Perera N, Indrakumar J. Myocarditis causing severe heart failure--an unusual early manifestation of leptospirosis: A case report. *BMC Res Notes*. 2015;8:80.
    doi: 10.1186/s13104-015-1031-1
18. Kragholm KH, Lindgren FL, Zaremba T, *et al*. Mortality and ventricular arrhythmia after acute myocarditis: A nationwide registry-based follow-up study. *Open Heart*. 2021;8(2):e001806.
    doi: 10.1136/openhrt-2021-001806
19. Yang B, de Vries SG, Ahmed A, *et al*. Nucleic acid and antigen detection tests for leptospirosis. *Cochrane Database Syst Rev*. 2019;8(8):CD011871.
    doi: 10.1002/14651858.CD011871.pub2
20. Available from: https://www.cdc.gov/leptospirosis/pdf/fs-leptospirosis-clinicians-eng-508.pdf [Last accessed on 2024 Jun 24].

Our Journals

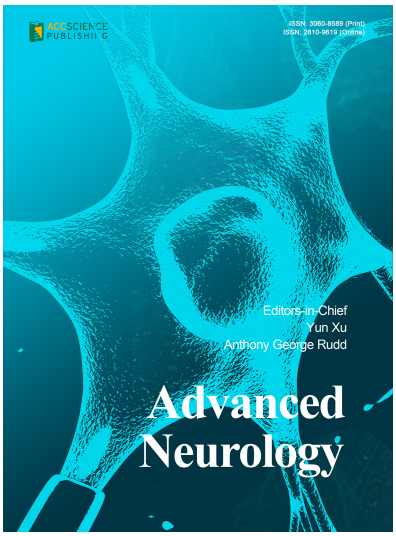

Advanced Neurology is a peer-reviewed and open-access journal that aims to publish and disseminate novel research in the breadth of neurology and neuroscience. The journal aims to advance our understanding in the nervous system and provide a platform to neuroscientists and physicians to showcase their findings in original fundamental and clinical research as well as to present new ideas that highlight the changes in the neurological clinical practice.

Advanced Neurology covers subject areas, including but not limited to the following:

- Neurological disorders
- Neurodegenerative disease
- Cerebrovascular disease
- Epilepsy and movement disorders
- Neuroimmune disease
- Neurological infections
- Muscle disease
- Molecular and cellular neuroscience
- Systems neuroscience
- Cognitive neuroscience
- Computational modeling of nervous system

Global Translational Medicine is a quarterly journal that focuses on medicine, biological sciences, and biomaterials engineering. The goal of *Global Translational Medicine* is to provide a platform to researchers for showcasing their latest research works in translational medicine so as to advance the field towards the betterment of human health. Despite the advancement of omics and new technologies, the process of transforming these technologies and scientific research results into effective therapies and putting them into clinical use still has a long way to go. *Global Translational Medicine* provides a platform to fill the gaps in preclinical and inter-disciplinary research, to promote clinical translation of scientific research results, and to contribute to the conception of new and improved preventive measures as well as diagnostic and therapeutic techniques of diseases.

Global Translational Medicine covers the following themes: cardiovascular disease, metabolism/diabetes/obesity, neuroscience/neurology, cancer, biomaterials and their applications in medicine, proteomics/metabolomics, pharmacogenomics, biomarkers, bioinformatics and data mining, animal and clinical research, and medical methods arising from interdisciplinary crossover.

Start a new journal

Write to us via email if you are interested to start a new journal with AccScience Publishing. Please attach your CV, professional profile page and a brief pitch proposal in your email. We shall inform you of our decision whether we are interested to collaborate in starting a new journal.

Contact: info@accscience.com

https://accscience.com/journal/BH

Contact

www.accscience.com

8 Burn Road, #15-03 Trivex, Singapore 369977

E-mail: editorial@accscience.com

Phone: +65 8182 1586